이학박사 학위논문

Development of New Synthetic Methodologies Based on the Functionalization of Carbon–Hydrogen and Carbon–Halogen Bonds

탄소−수소 및 탄소−할로겐 결합 기능화에 기반한 새로운 합성 방법론의 개발

2023 년 2 월

서울대학교 대학원

화학부 유기화학전공

구 장 우

탄소-수소 및 탄소-할로겐 결합 기능화에 기반한 새로운 합성 방법론의 개발

지도 교수 이 홍 근

이 논문을 이학박사 학위논문으로 제출함
23 년 2 월

서울대학교 대학원
화학부 유기화학전공
구 장 우

구장우의 이학박사 학위논문을 인준함
23 년 2 월

위 원 장 홍 종 인 (인)

부위원장 이 홍 근 (인)

위 원 김 병 문 (인)

위 원 이 동 환 (인)

위 원 조 은 진 (인)

Abstract

Development of New Synthetic Methodologies Based on the Functionalization of Carbon–Hydrogen and Carbon–Halogen Bonds

Jangwoo Koo

Department of Chemistry

The Graduate School

Seoul National University

The expansion of chemical diversity is one of the most significant approaches in synthetic organic chemistry. Radical chemistry might be the key answer to the question "how to achieve chemical diversity." Considering the tremendous reactivity of radicals, applying reactive species to selectively obtain the desired product has been in high demand. Thus, Chapter 1 describes the representative strategies of carbon-centered radical formation and the utilization of the corresponding radical for

a new bond-forming method, especially through the cleavage of carbon–hydrogen (Part I) and carbon–halogen (Part II) bonds.

Part 1 covers the functionalization of carbon–hydrogen bonds and activation of the benzylic C(sp^3)–H bonds of indoles using the dual catalytic strategy of photocatalysis and nickel catalysis (Chapter 2). The developed reaction undergoes sequential indole oxidation/deprotonation to form a radical in the benzylic position with the most acidic proton. Various aryl and acyl groups were introduced by nickel-catalyzed cross-coupling reactions. The initial step of radical formation was investigated through a mechanistic investigation and supported the high selectivity of benzylic position among other C–H bonds possessing a similar bond dissociation energy.

In Part 2, which handles carbon–halogen bond functionalization, light-mediated carbon radicals from alkyl (Chapter 3) or aryl iodides (Chapter 4) undergo radical borylation to establish new carbon–boron bonds. The products formed in Chapters 3 and 4 have pharmaceutical activity due to the peculiar nature of the boron group. Since the developed reaction does not require metal catalysis or external additives, it is considered eco-friendly and atom-economic process. The key point of the developed reaction is that various chemicals react sequentially to provide the desired product in the reaction media. Moreover, a radical-based carbon–fluorine bond activation with preliminary results will be briefly introduced in Chapter 5. Further mechanistic studies on the exact process of the carbon–fluorine bond cleavage step and the application of this reactivity to other classes of substrates are ongoing in our laboratory.

Keywords: carbon, hydrogen, halogen, radical, photochemistry, indole, aziridine, aminoboronic acid, heterocyclic compound, cross-coupling, borylation, hydrodefluorination, fluorine atom transfer

Student Number: 2017-21595

Table of Contents

Part I. Visible-light-induced carbon–hydrogen bond cleavage for radical generation

Chapter 2. Benzylic C(sp^3)–C(sp^2) cross-coupling of indoles enabled by oxidative radical generation and nickel catalysis

Part II. Visible-light-induced carbon–halogen bond cleavage for radical generation

Chapter 3. A tandem process for the synthesis of β-aminoboronic acids from aziridines with haloamine intermediates

List of Tables

Chapter 2

Chapter 3

Chapter 4

Chapter 5

List of Schemes

Chapter 1

Chapter 2

Chapter 3

Chapter 4

Chapter 5

List of Figures

Chapter 2

Chapter 3

Chapter 4

Chapter 5

Preface

Parts of this thesis have been adapted from the following published articles co-written by the author and are the result of extensive collaborations between the author and other researchers. The specific contributions of the author are outlined below.

Chapter 2

Weonjeong Kim,‡ Jangwoo Koo‡ and Hong Geun Lee, "Benzylic C(sp^3)–C(sp^2) cross-coupling of indoles enabled by oxidative radical generation and nickel catalysis." *Chem. Sci.*, 2021, **12**, 4119-4125.
‡These authors contributed equally to this work.

Respective contributions

J.K. conceptualized the research, and W.K. performed the reaction optimization for the preliminary results. W.K. and J.K. carried out the synthetic experiments (especially for arylation and acylation, respectively) and all mechanistic investigations. W.K. conducted the spectroscopic analysis. W.K., J.K., and H.G.L. wrote the manuscript with contributions from all authors, and H.G.L. supervised the project.

Chapter 3

Subin Park,‡ Jangwoo Koo,‡ Weonjeong Kim and Hong Geun Lee, "A tandem process for the synthesis of β-aminoboronic acids from aziridines with haloamine intermediates." *Chem. Commun.*, 2022, **58**, 3767-3770.
‡These authors contributed equally to this work.

Respective contributions

J.K. conceived the research and performed the reaction optimization for the preliminary results. S.P. and J.K. carried out the synthetic experiments and mechanistic investigations. S.P., J.K., W.K., and H.G.L. wrote the manuscript with contributions from all authors, and H.G.L. supervised the project.

Chapter 1. Functionalization of carbon–hydrogen and carbon–halogen bonds through a radical pathway under light irradiation

1.1 Introduction

Carbon is a significant atom that constructs the basic skeleton of a chemical compound. Therefore, organic chemists have focused on developing reactions that expand structure through the formation of carbon–carbon bond. One of the fundamental building blocks of the carbon frame is the carbon-centered radical, which can be easily generated from chemical feedstock, such as hydrocarbons, amines, alcohols, carbonyl compounds, and their derivatives. Furthermore, the chemical process involving carbon-centered radicals provides orthogonal reactivity to other carbon-based intermediates (e.g., carbanion, carbocation, and carbene), enabling various bonding modes to organize carbon backbone complexity.

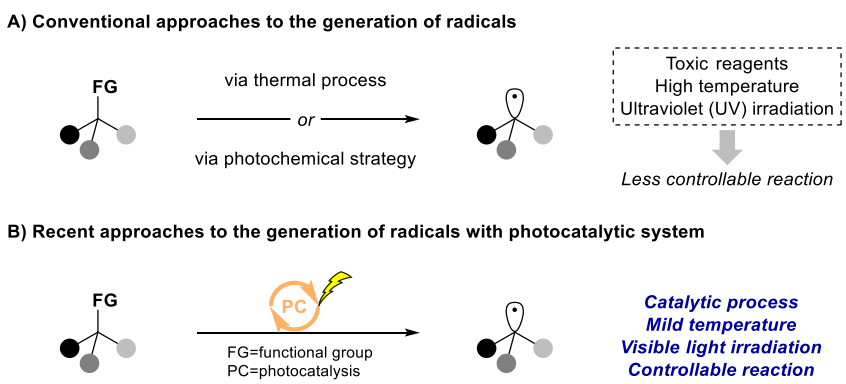

Scheme 1.1 General protocols for the generation of radical species

There have been several limitations to radical-based chemical reactions (Scheme 1.1A). For example, the radical generation step often requires highly toxic metal reagents (e.g., organotin compounds) or an energy-intensive process (e.g., high temperature or ultraviolet light irradiation). However, the major problem was that despite the harsh reaction conditions, off-target processes, such as dimerization and disproportionation, could not be avoided due to the high reactivity of the radicals.

In this context, methods for developing controllable radical reactions through green and mild procedures have been sought for a long time (Scheme 1.1B). In the 21st century, a visible-light-mediated radical reaction pioneered by many researchers overcame the limitations of conventional approaches and achieved historical development in the synthetic organic chemistry field.[1] Therefore, this chapter mainly covers representative visible-light-driven strategies for preparing alkyl or aryl radicals, especially the cleavage methods for carbon–hydrogen and carbon–halogen bonds in the last decade.

1.2 Visible-light-mediated C–H bond activation enabling radical generation

1.2.1 Hydrogen atom transfer (HAT) strategies

C–H bond activation, which does not require pre-functionalization, is an extremely fascinating approach to carbon-centered radical formation. However, given the high strength of the chemical bond between carbon and hydrogen ($BDE_{C–H}$ = 85 to 105 kcal/mol), HAT faces a great thermodynamic barrier to overcome, whether indirect or direct method (Scheme 1.2).[2] From the polarity matching process, $C(sp^3)$–H bonds

are generally cleaved homolytically by electrophilic radicals (**X**), which requires the formation of stronger bonds ($BDE_{X–H} > BDE_{C–H}$).

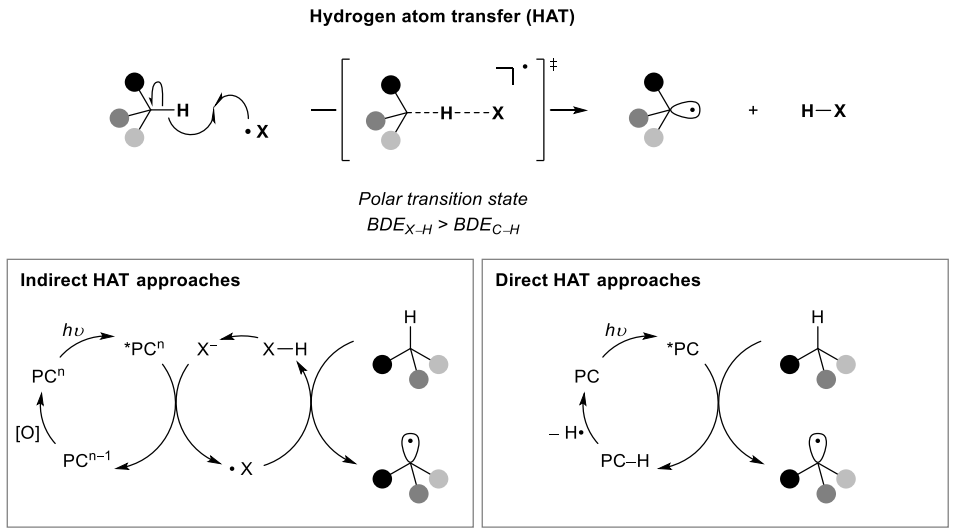

Scheme 1.2 Introduction of the HAT process

To consider the innate instability of electrophilic radicals and selective reactivity among the similar C–H bond energies in a complex system, the establishment of effective reaction conditions has been encouraged. Due to outstanding advances, the photoredox system suggests state-of-the-art solutions in that it produces electrophilic radicals under mild conditions and conducts the HAT process.[3] Therefore, the following examples will be classified according to the types of HAT reagents.

1.2.1.1 Indirect HAT approaches

1.2.1.1.1 HAT with oxygen-centered radicals

The oxygen-centered radical might be a potent candidate for the HAT mediator toward C(sp^3)–H bond activation regarding the strong oxygen–hydrogen bond and high electronegativity of the oxygen atom. Furthermore, there are many possibilities to use oxygen-centered radical precursors due to their abundance. Among them, persulfate, peroxide, carboxylates, alkoxides, molecular oxygen, and inorganic oxides have been potential hydrogen atom abstractors as oxygen-centered radical precursors in the photoredox system in recent years.

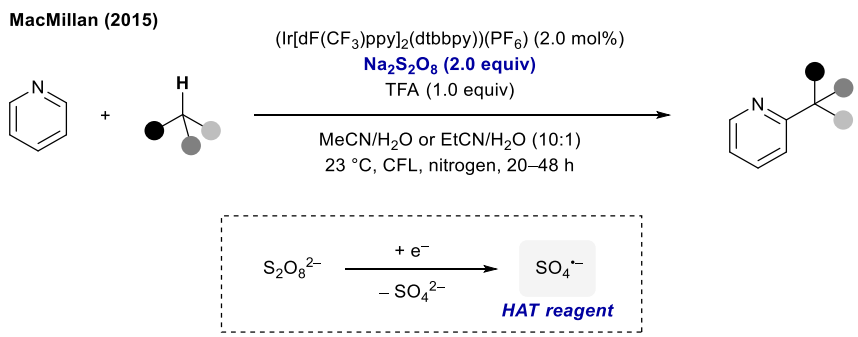

Scheme 1.3 Persulfate-mediated indirect HAT process

The combination of photoredox catalysis and peroxides/persulfates containing weak oxygen–oxygen bonds enables the release of the oxygen-centered radical for HAT, inducing the C(sp^3) radical in the photocatalytic system. In 2015, the MacMillan group reported the Minisci-type reaction with ether and heteroarene using iridium(III) photocatalysis and persulfate as the HAT source (Scheme 1.3).[4]

Based on their photocatalyzed cross-dehydrogenative coupling (CDC) reaction,[5] photoexcited iridium(III) releases an electron to $K_2S_2O_8$, producing the radical sulfate anions for the abstraction of the α-C(sp^3)–H bond of ethers. The generated C(sp^3) radical could be added to the heteroarene, followed by aromatization to provide the desired addition product.

In 2016, the Glorius group disclosed the site-selective trifluoromethylthiolation of the C(sp^3)–H bond using organic benzoate as a precursor to oxygen-centered radicals in the photoredox system (Scheme 1.4).[6] The resulting C(sp^3) radical built the carbon–sulfur bond with *N*-trifluoromethylthiophthalimide to give the desired product. Their developed HAT showed remarkable site selectivity. For example, the abstraction of the tertiary C(sp^3)–H bond was preferred over that of the primary or secondary bond (ratio >19:1), and the C(sp^3)–H bond adjacent to a heteroatom was more reactive than unactivated C(sp^3)–H bonds. Stern–Volmer analysis displayed the redox relationship between iridium photocatalysis and benzoate for the possibility of electron transfer.

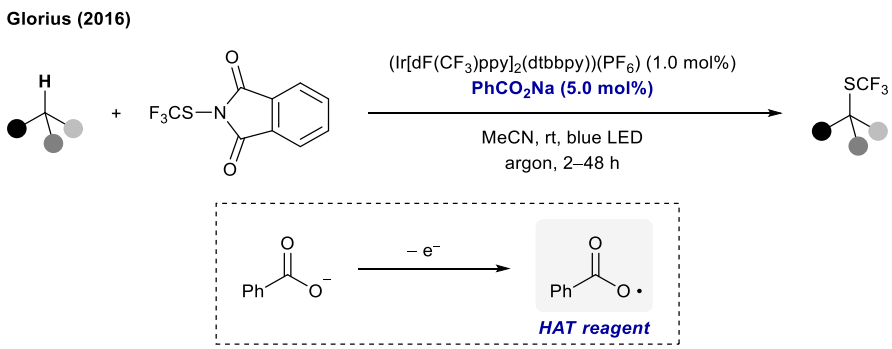

Scheme 1.4 Benzoate-mediated indirect HAT process

The ligand-to-metal charge transfer (LMCT) protocol is another powerful method for generating an oxygen-centered radical from the cerium-alkoxide complex. In 2018, the Zuo group demonstrated a new chemical methodology for generating oxygen-centered radicals using the LMCT strategy. This method can functionalize the alkane C–H bond even with gaseous hydrocarbon compounds (e.g., methane, ethane, propane, butane, etc.) to produce value-added products (Scheme 1.5).[7] The developed reaction was also scalable and applicable with continuous-flow reactors for multigram synthesis. Despite the controversial reaction mechanism,[8] the plausible reaction mechanism was expected to start from ligand exchange with alcohol substrates, followed by photolytic cleavage of the excited cerium-alkoxide complex to generate the alkoxy radical.

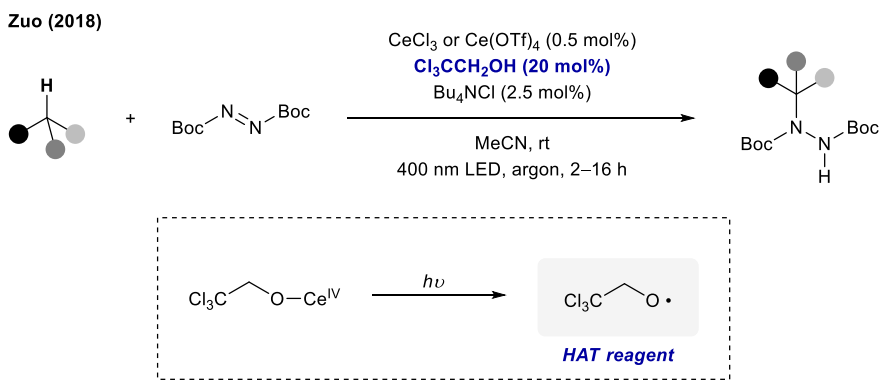

Scheme 1.5 Alkoxide-mediated indirect HAT process

Interestingly, although some common inorganic salts have remained underutilized, converting them to oxygen-centered radicals with strong oxidants is possible. Since organophotoredox catalysis (OPC) showed extensive redox potential,

it has sufficient oxidizing capacity to convert inorganic salts to oxygen-centered radicals under light irradiation. In 2018, the Nicewicz and Alexanian groups' collaborative project on the azidation of unactivated C(sp^3)–H bond was exhibited (Scheme 1.6).[9] Potassium phosphate (K_3PO_4) was converted to phosphate radicals using acridinium-based organic photocatalysis [Mes-Acr^+-Ph]* (E^*_{red} = +2.08 V vs. SCE in MeCN), performing the HAT to provide the key radical intermediate for azidation. The reaction was applicable to azidation, halogenation, trifluoromethylation, and alkylation.

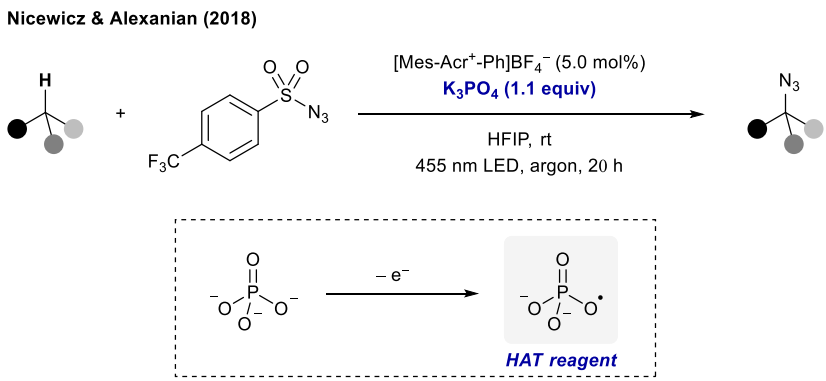

Scheme 1.6 Phosphate-mediated indirect HAT process

Similar to the previous report, the Nicewicz group described the homobenzylic oxygenation of alkyl-substituted arenes using the nitrate radical for the oxygen-centered radical precursor (Scheme 1.7).[10] Due to the relatively weak bond dissociation energy of the benzylic C(sp^3)–H bond (ca. 85 kcal/mol), the site-selective HAT process occurred first at the benzylic position, followed by oxidation and deprotonation processes that produced the styrene intermediate. The final

product, benzyl ketone, was then produced through cobaloxime-catalyzed Wacker-type olefin hydration in an anti-Markovnikov manner.

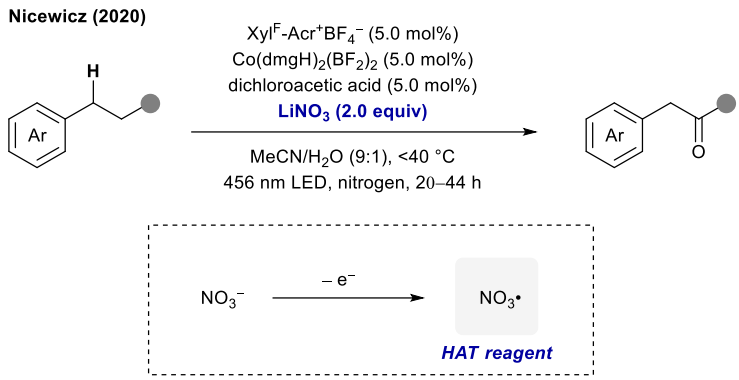

Scheme 1.7 Nitrate-mediated indirect HAT process

1.2.1.1.2 HAT with nitrogen-centered radicals

Nitrogen, which is less electronegative than oxygen, is still an electrophilic atom and is sufficient to accomplish the HAT to the C(sp^3)–H bond. Compared to the oxygen-centered radical, the nitrogen-centered radical is an attractive HAT reagent because its electronic and steric natures can be easily designed by varying the substituents of the nitrogen atom. The Hofmann–Löffler–Freytag (HLF) reaction is an early example of the use of nitrogen-centered radicals as an intramolecular HAT reaction (Scheme 1.8).[11]

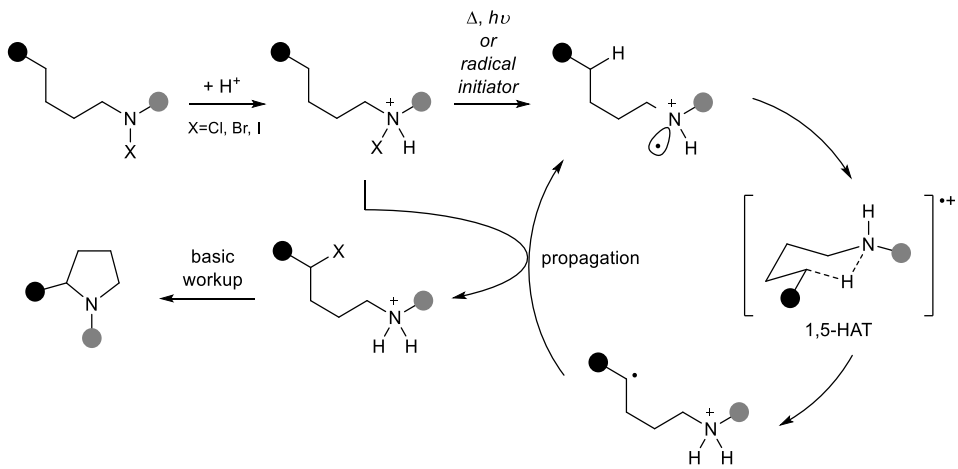

Scheme 1.8 Hofmann–Löffler–Freytag reaction

In 2015, the MacMillan group reported activating the alcoholic α-C(sp^3)–H bond through the iridium/quinuclidine/phosphate multicatalyzed photoreaction (Scheme 1.9).[12] The corresponding α-ethereal radical proceeded to a Giese-type addition reaction with electron-deficient alkenes. According to their mechanistic

investigation, the nitrogen-centered radical is made from the oxidation of quinuclidine (E_{red} = +1.10 V vs. SCE in MeCN) by an excited-iridium photocatalysis (E^*_{red} = +1.21 V vs. SCE in MeCN) and acts as a HAT reagent. Due to the proton-coupled activation mode with the hydroxyl group of the alcohol, only the adjacent C(sp^3)–H bond of the polar functional group was selectively activated, even if weak C(sp^3)–H bonds (e.g., allylic, benzylic, etc.) were present in the same molecule.

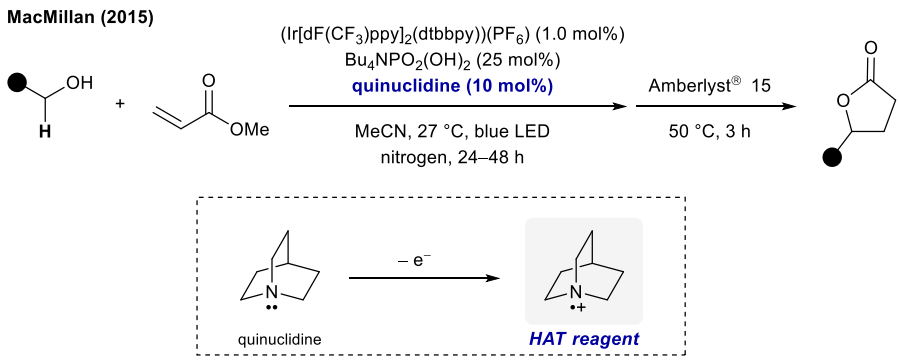

Scheme 1.9 Quinuclidine-mediated indirect HAT process

Similar to the nitrogen-centered radical preparation method reported by the MacMillan group, the Cresswell group generated azide radicals through the oxidative process, enabling the HAT of unprotected amines in 2020 (Scheme 1.10).[13] The anionic azide was directly converted to the azide radical by the photoexcited 1,2,3,5-tetrakis(carbazol-9-yl)-4,6-dicyanobenzene (4CzIPN), an organic photocatalyst. The resulting nitrogen-centered radical selectively abstracts C(sp^3)–H from the α-position of secondary amines and produces an α-amino radical. After the

alkene addition reaction of the corresponding radicals, the resulting amine could be cyclized from the subsequent basic workup to give lactam as the final product.

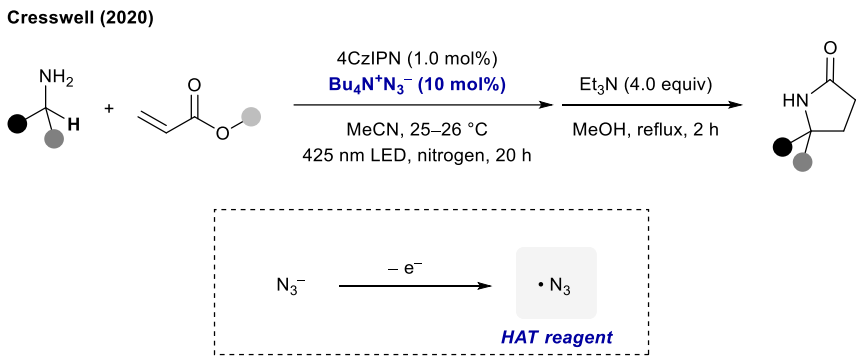

Scheme 1.10 Azide-mediated indirect HAT process

1.2.1.1.3 HAT with sulfur-centered radicals

Moving down the chalcogen column, the sulfur-centered radical has a less electrophilic character than the oxygen-centered radical but can perform the HAT successfully for some C(sp^3)–H bonds. Compared to the oxygen-centered radical, making sulfur-centered radicals is easy since sulfur has a more polarizable and less electronegative character. Like oxygen-centered radicals, sulfur-centered radicals could be prepared from thiophosphoric acids, thiocarboxylic acids, and thiols.

In 2015, the MacMillan group reported dehydrative Minisci alkylation through the dual catalytic approach of thiol and iridium photocatalysis (Scheme 1.11).[14] Mechanistically, elucidating that the thiyl radical is prepared from thiol (E_{red} = +0.85 V vs. SCE in MeCN for cysteine) using the electron transfer process of excited-

iridium photocatalysis (E^*_{red} = +1.21 V vs. SCE in MeCN) is possible. The alcoholic α-C(sp^3)–H bond was activated by the sulfur-centered radical with the assistance of the polar effect since the HAT step was thermodynamically unfavorable ($BDE_{C–H}$ for MeOH = 96 kcal/mol; $BDE_{S–H}$ for thiol = ca. 87 kcal/mol). After the addition reaction of the generated C(sp^3) radical to the proton-activated heteroarene, followed by spin-center shift and dehydration, an alkylated Minisci product was the final product. Additionally, introducing a methyl group into the aromatic ring using methanol as the alkylation source was viable, representing a remarkable advance in the field.

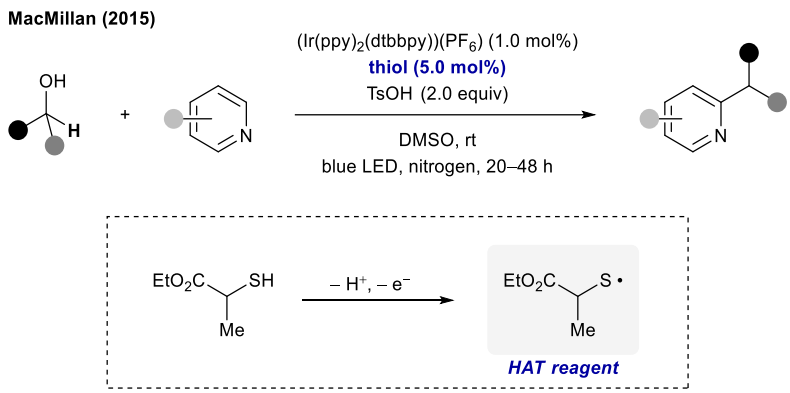

Scheme 1.11 Thiol-mediated indirect HAT process

In 2018, the Hamashima group discovered C(sp^3)–C(sp^2) cross-coupling using thiobenzoate as a HAT reagent (Scheme 1.12).[15] The oxidation of the excited-iridium photocatalysis by dicyanoarene was the initial step of the photocatalytic cycle. Oxidized photocatalysis can readily oxidize thiobenzoate, generating sulfur-centered radicals, which can activate the benzylic C(sp^3)–H bond of the benzylamine through

HAT. Due to the persistent radical effect, benzyl radicals and pre-formed cyanoaryl radicals build new carbon–carbon bonds through radical–radical cross-coupling.

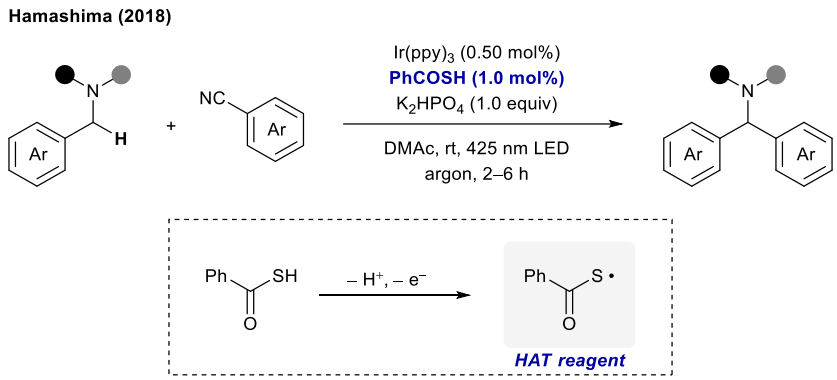

Scheme 1.12 Thiobenzoic acid-mediated indirect HAT process

In 2020, the Mitsunuma and Kanai groups developed an alcohol dehydrogenation reaction using acridinium, nickel, and thiophosphoric acid (Scheme 1.13).[16] The developed reaction was a multicatalytic process of three catalysts (photocatalysis, transition metal catalysis, and HAT catalysis).[17] The thiophosphoric acid formed through oxidation by exciting acridinium was converted to the sulfur-centered radical for HAT to activate the alcoholic α-C–H bond. The nickel catalyst intercepts the alkyl radical generated through the preceding process to make the enol product using β-hydride elimination. Subsequently, the equilibrium is shifted to a keto isomer with enhanced stability through tautomerization. The developed reaction did not require the terminal oxidant since the evolution of H_2 gas by the nickel catalyst established redox neutralization.

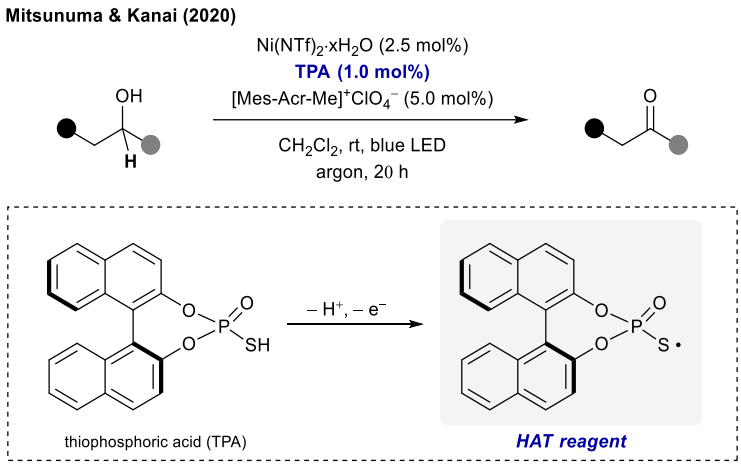

Scheme 1.13 Thiophosphoric acid (TPA)-mediated indirect HAT process

1.2.1.1.4 HAT with halogen radicals

Regnault discovered the first use of halogen radicals in chemical reactions over 180 years ago.[18] The dichloromethane conversion method was found by exposing chloroform and chloromethane to sunlight. Although the chlorine radical was used to synthesize alkyl chloride, modern organic chemistry has introduced various photoredox systems using the chlorine radical in the radical reaction. This section mainly focuses on the activation modes of the C(sp^3)–H bond using halogen radicals.

Inorganic chloride is useful as a source of chlorine radicals in laboratory-level synthesis. However, strong oxidizing agents are required to convert chloride (E_{red} = +2.03 V vs. SCE in MeCN) to chlorine radicals[19] and controlling the high reactivity of chlorine radicals remains challenging. In 2018, the Barriault group proposed a delicate solution to the two issues mentioned above through the iridium-catalyzed Giese addition (Scheme 1.14).[20] Since generating chlorine radicals by oxidation of

chloride through photocatalysis (E^*_{red} = +1.21 V vs. SCE in MeCN), is unfavorable thermal energy is required. Interestingly, the chlorine radical formed in the developed reaction was unusually highly selective for the tertiary C(sp^3)–H bond.

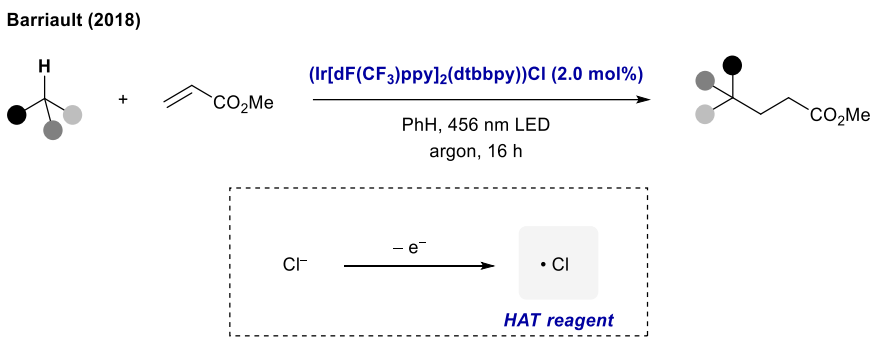

Scheme 1.14 Chloride-mediated indirect HAT process

Complementary to SET, LMCT is an efficient reaction pathway for producing chlorine radicals. In 2016, the Doyle group was inspired by the discovery of Nocera's photoinduced LMCT[21] and developed a cross-coupling reaction using aryl chloride and ether (Scheme 1.15).[19] The key step of the reaction is that LMCT occurs from the excited nickel(III) (Ni–Cl) complex formed by the iridium photocatalysis to generate the chlorine radical. The resulting chlorine radical leads the HAT process to produce an α-ethereal radical that could be trapped by nickel catalysis to build new carbon–carbon bonds. Notably, the developed method was also applicable with chemical feedstocks (e.g., cyclohexane, toluene, etc.) as reagents, despite its low reactivity.

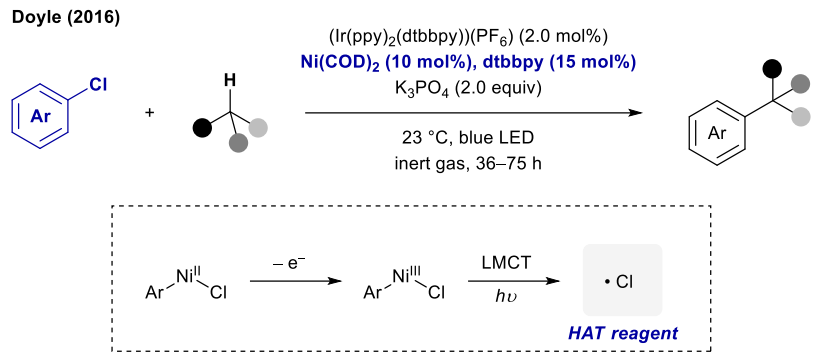

Scheme 1.15 Excited nickel(III) complex-mediated indirect HAT process

Unlike other heteroatoms mentioned previously, bromide has a low electronegativity, a weak H–Br bond dissociation energy (BDE_{H-Br} = 87 kcal/mol), and a manageable reduction potential (E_{red} = +1.60 V vs. SCE in MeCN). Accordingly, the bromine radical is the readily obtainable alternative HAT reagent in theory.[22] Ishida and Murakami, based on the aforementioned properties of bromine radicals, realized the coupling reaction under a dual iridium/nickel catalytic approach (Scheme 1.16).[23] With the bromine radical produced by the SET from the bromide anion to iridium(III), the dehydrogenative coupling reaction of aldehyde and toluene was feasible.

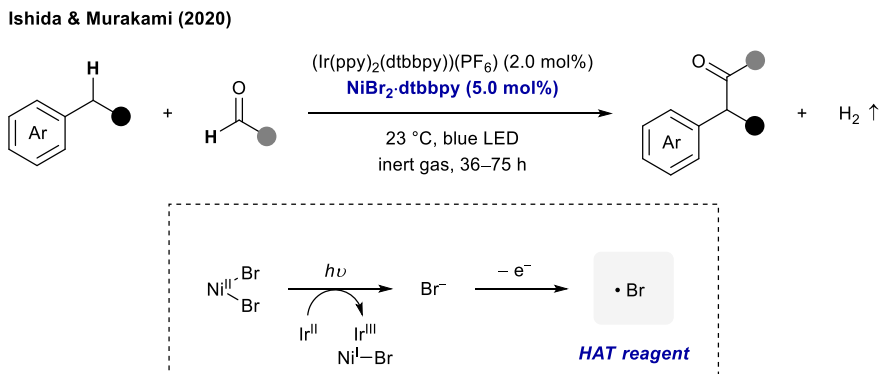

Scheme 1.16 Bromide-mediated indirect HAT process

1.2.1.1.5 HAT with carbon-centered radicals

Compared to the radicals based on heteroatoms, the carbon-centered radical has a nucleophilic character. Regarding the strength of the C–H bond and the polarity of the carbon-centered radicals, the elements on both sides of the HAT equation will be almost identical. Therefore, this process will have a very low energy barrier and a non-selective reaction pathway. Therefore, a reaction using a carbon-centered radical as a radical mediator has been a rare example of an intermolecular reaction, and selectivity remains the main issue of the HAT process. However, with the considerable development of photoreaction, the carbon-centered radical-mediated HAT protocol has also been used in various fields, representatively transition metal-catalyzed or metal-free reactions.[24]

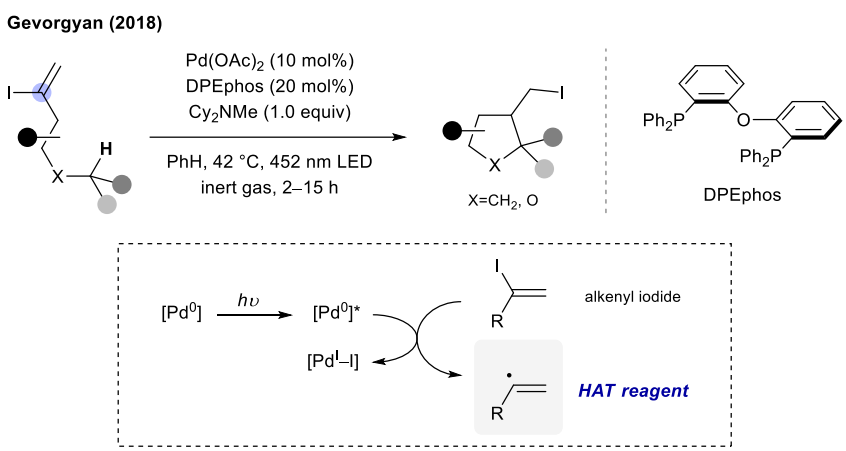

Scheme 1.17 Alkenyl iodide-mediated indirect HAT process

In 2018, the Gevorgyan group published the atom transfer radical cyclization (ATRC) with photoinduced palladium catalysis that produces pentacyclic compounds with high selectivity (Scheme 1.17).[25] The initial process of the developed reaction was the formation of vinyl/Pd(I) radical intermediates through an unprecedented electron transfer between vinyl iodide and photoexcited Pd (0). The formation of the thermodynamically favored tertiary C(sp^3) radical by the vinyl radical was conducted efficiently using the intramolecular HAT fashion. The resulting alkyl radical provides a final compound through iodocylization.

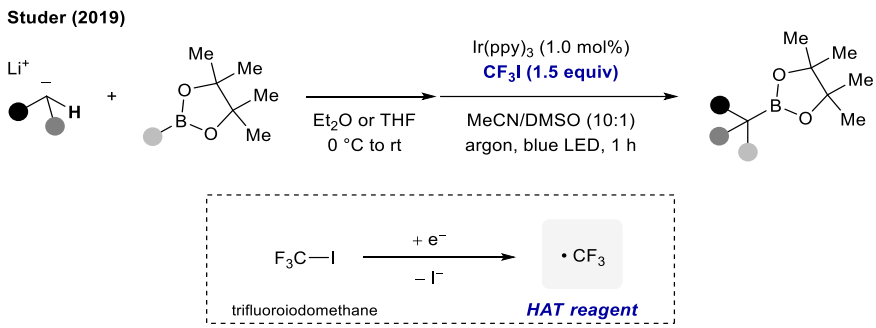

Scheme 1.18 Trifluoroiodomethane-mediated indirect HAT process

The Studer group reported the versatility of the C(sp^3) radical and the C(sp^2)-centered radical in 2019 (Scheme 1.18).[26] The published reaction was the synthesis of α-substituted boronate through a modified process of the Matteson reaction. The trifluoromethyl radical formed using SET between CF_3I (E_{red} = –1.22 V vs. SCE in MeCN) and iridium photocatalysis (E^*_{red} = –1.73 V vs. SCE in MeCN) reacts with the previously generated boronate complex made of alkyl lithium and boronic ester

to provide a radical anion intermediate. The resulting intermediate is oxidized by photocatalysis or trifluoromethyl iodide to generate a carbocation followed by 1,2-migration of an alkyl or aryl group to give the desired product. Based on the quantum yield measurement (Φ = 8.8), the radical chain process was found to be significantly involved.

In 2021, the Doyle group disclosed a C(sp^3)–H fluorination using methyl radicals as HAT mediators (Scheme 1.19).[27] The methyl radical produced from the reduction of *N*-acetyloxyphthalimide by photocatalysis activated the benzylic C(sp^3)–H bond, giving rise to the benzyl radical. Subsequently, the given alkyl radical was converted to a carbocation by donating an electron to photocatalysis, ending the catalytic cycle redox. Later, various nucleophiles (e.g., fluoride, azide, water, thiol, electron-rich arene, etc.) were introduced to produce numerous types of carbon–heteroatom bonds. Unlike the heteroatom-based strategy, the carbon-centered radical-based HAT is a differential methodology, as it can activate electron-deficient C(sp^3)–H bonds.

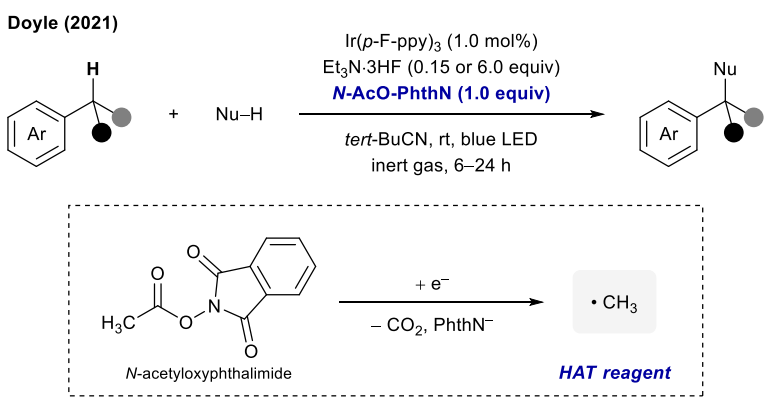

Scheme 1.19 *N*-Acetyloxyphthalimide-mediated indirect HAT process

1.2.1.2 Direct HAT approaches

Complementing the abovementioned examples that used photocatalysis and HAT reagents as each function, some photocatalysis or redox systems can perform HAT independently. Considering the great chemical achievements of Norrish, a representative example is the carbonyl compound. In 2013, Chen's group discovered a photocatalytic approach using 9-fluorenone as a dual function of a photosensitizer and HAT reagent (Scheme 1.20).[28] The triplet state of diaryl ketone formed using compact fluorescent lamp (CFL) as a light source could be a good candidate as a hydrogen abstractor. The formed radical successfully provided the fluorinated product by Selectfluor. Moreover, the protocol described tolerable reactivity not only in the benzylic C(sp^3)–H bond but also in the C(sp^3)–H bond of the cyclic and acyclic alkane.

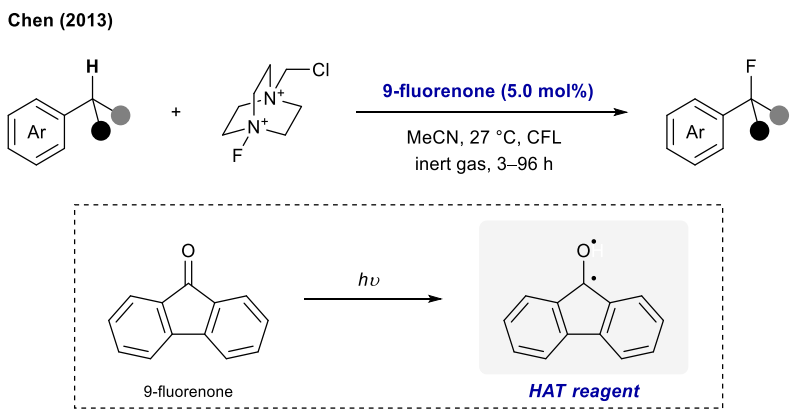

Scheme 1.20 9-Fluorenone-mediated direct HAT process

Eosin Y, an organic dye, also belongs to this photocatalytic class and can catalyze due to the captodative and steric effect of the reduced form of Eosin Y. The Giese-type reaction catalyzed by Eosin Y reported by the Wu group in 2018 is a typical example of the HAT ability of Eosin Y (Scheme 1.21).[29] The diradical formed in the para-quinone methide moiety by light irradiation enabled HAT for the ethereal α-C–H bond. The corresponding alkyl radical was added to the electron-deficient alkene. Furthermore, amide, alcohol, and cyclohexane could be applied as precursors of alkyl radicals.

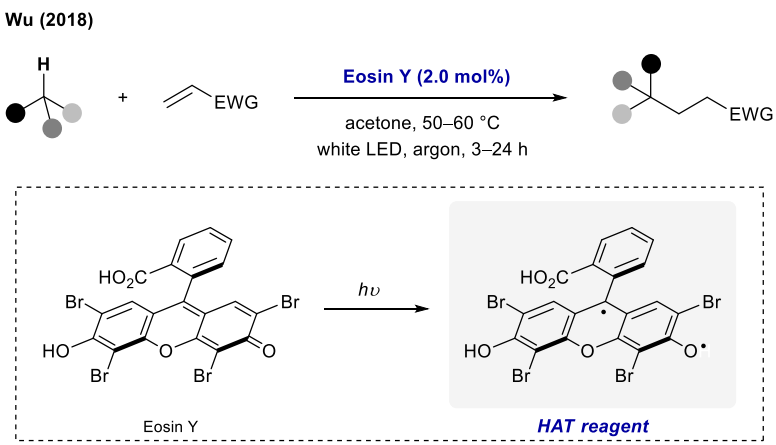

Scheme 1.21 Eosin Y-mediated direct HAT process

Like oxygen-based organic catalysis, organic photocatalysis directly serving as a nitrogen-centered radical precursor has been discovered with few examples. The trisaminocyclopropenium (TAC) ion widely used by Lambert's group performs ether site-selective heteroarylation (Scheme 1.22).[30] Using their specialized

photoelectrochemical tool as a redox system, TAC is oxidized by anodic oxidation, and an aminyl radical is formed through photoexcitation. The HAT of the ethereal α-C–H bond is achieved through the pregenerated aminyl radical cation, and the resulting alkyl radical is inserted into the heteroarene to provide a Minisci product. Simultaneously, the cathodic reduction of H^+ generates hydrogen gas (H_2).

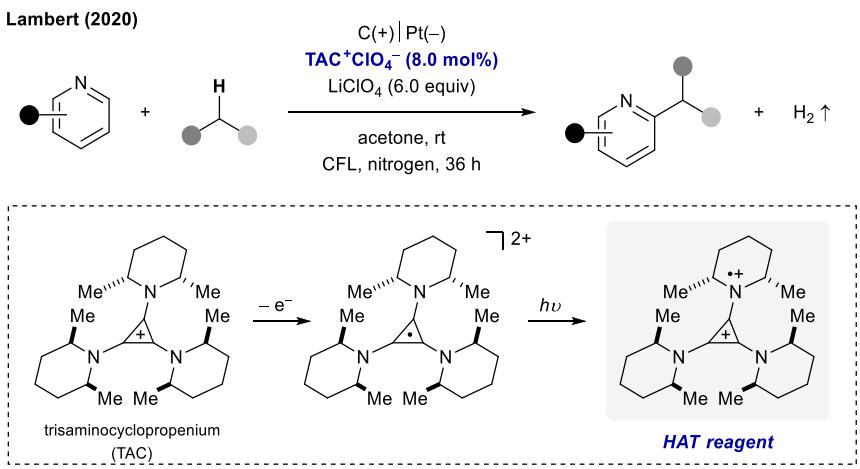

Scheme 1.22 Trisaminocyclopropenium (TAC)-mediated direct HAT process

Metal oxides such as decatungstate ($W_{10}O_{32}^{4-}$), uranyl dication (UO_2^{2+}),[31] and antimony porphyrin complexes (SbTPP)[32] acted like the organocatalysis above under near-ultraviolet (UVA) light irradiation. In 2020, the Wu group successfully implemented a CDC reaction by merging cobalt and tungsten catalysis (Scheme 1.23).[33] In the reaction system, the tungsten catalyst was responsible for the HAT step, and cobalt performed the net oxidative coupling through H_2 evolution. The

alkenyl product generated by the cobalt-mediated reductive Heck-type reaction showed high *E/Z* selectivity.

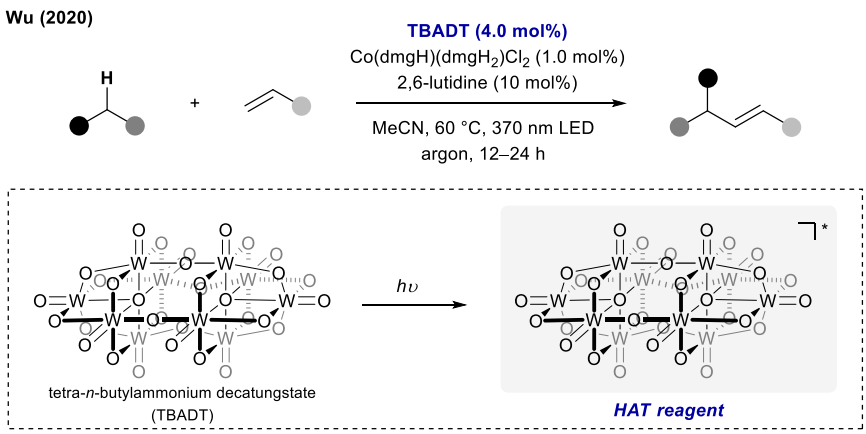

Scheme 1.23 TBADT-mediated direct HAT process

1.2.2 Electron transfer–proton transfer (ET/PT) strategies

A possible alternative to HAT for the selective functionalization of a C(sp^3)–H bond to generate the alkyl radical is the sequential electron transfer–proton transfer (ET/PT). Unlike the traditional HAT protocol, where the HAT reagent is required in the reaction, this method requires chemical oxidants or an oxidative environment to generate alkyl radicals.

Considering the low pK_a value of the benzylic C(sp^3)–H bond among other C–H bonds, easily producing benzylic radicals is possible using the following sequence: 1) oxidation of the arene ring and 2) deprotonation of the benzylic position. Despite the energetically uphill SET of the arene ring, activating the C–H bond is

significantly accelerated since the acidity is significantly increased after the arene ring oxidation. Consequently, the Chen and Wu groups reported the Giese addition of benzyl radical (E_{red} = +2.36 V vs. SCE in MeCN for toluene) to enone by acridinium photocatalysis (E^*_{red} = +2.06 V vs. SCE in MeCN) as the strong oxidizing agent (Scheme 1.24).[34]

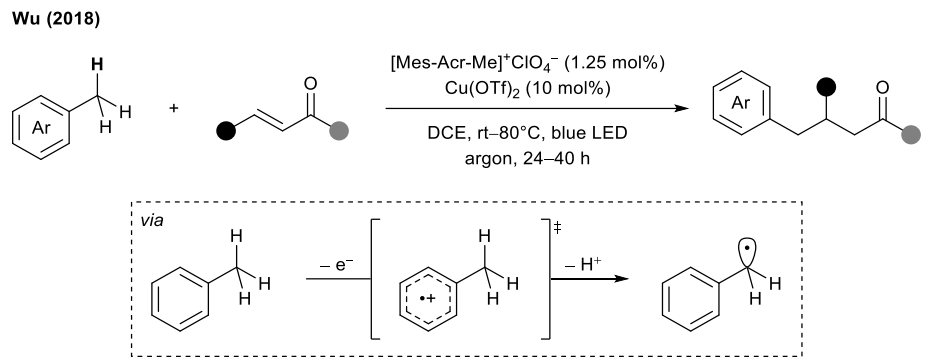

Scheme 1.24 Benzylic C(sp^3)–H bond activation via ET/PT strategy

A report in 2021 revealed that the Wu group directly activated the C(sp^3)–H bonds using the heterogeneous cadmium selenide quantum dots (CdSe QDs) under blue light irradiation (Scheme 1.25).[35] Since the described reaction used a heterogeneous catalyst with a wide surface area, the reactive species are simultaneously generated from the hole (h^+s) oxidation on quantum dots. Subsequently, the new chemical bond formation occurs by radical–radical cross-coupling. Simultaneously, the electrons scattered on the CdSe reacted with proton (H^+) to convert hydrogen gas (H_2) to equalize the redox property of the entire

reaction. Following the developed method, the same group has explored numerous radical transformations such as radical thiolation,[36] Minisci alkylation,[37] etc.

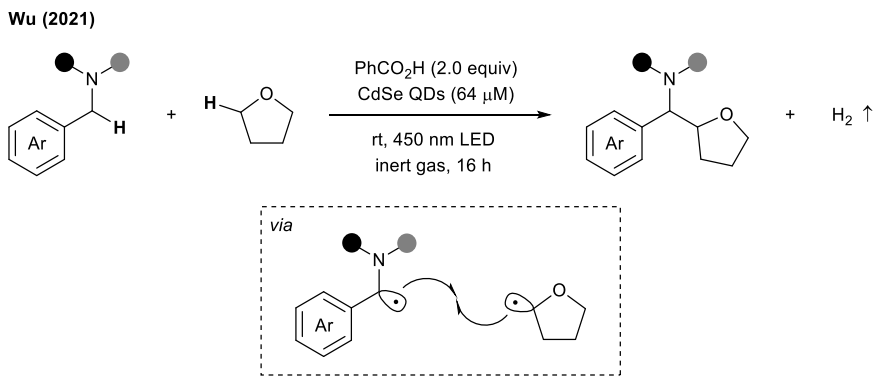

Scheme 1.25 Radical–radical cross-coupling via ET/PT strategy

1.3 Visible-light-mediated C–I bond activation enabling radical generation

Regarding user-friendly radical sources, halide-containing substrates will be the best option for synthetic organic chemists due to their commercial availability, chemical stability, and synthesizability. Among them, aryl/alkyl iodides possessing relatively weak carbon–iodide bonds are more easily accessible than the other corresponding halides. Although the homolytic cleavage of weak C–I bonds using strong light as the energy source has been pioneered, a method for forming radicals under mild conditions has emerged through recent achievements. In this context, representative aryl or alkyl radical generation methods from the corresponding iodide-containing molecules during the past decades will be described in this section.

1.3.1 Light-induced homolysis strategies

In 2015, the Ryu group reported an aryl radical generation method without a catalyst or reducing reagent (Scheme 1.26).[38] According to their postulated reaction mechanism, the pregenerated aryl radical by the photon reacts with carbon monoxide to form an acyl radical as a reaction intermediate. The final product is provided through amination with the corresponding amine. Furthermore, they explored the possibility of radical chain processes, which can be highly evaluated regarding reaction efficiency. The reported reaction has limitations, as it requires high-pressure carbon monoxide (ca. 70 atm). However, it graces a page in radical chemistry since it does not require additional chemical reagents and can form aryl radicals directly through high-energy input.

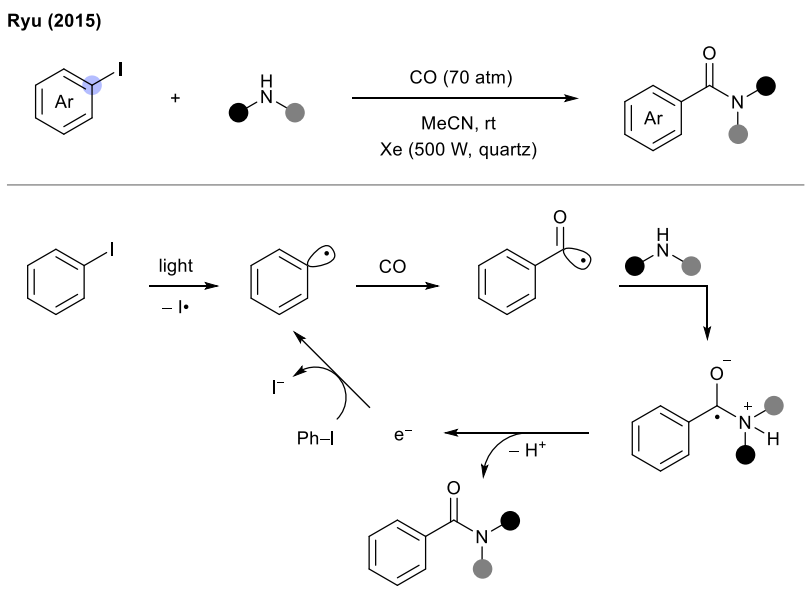

Scheme 1.26 Photoinduced aminocarbonylation

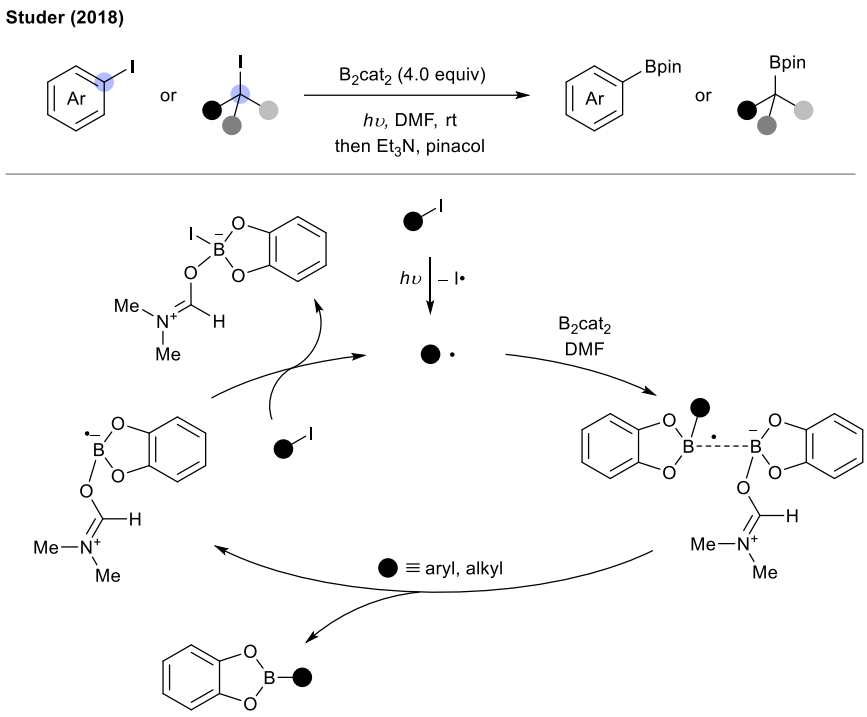

Scheme 1.27 Metal-free radical borylation of aryl and alkyl iodides

In 2018, the Studer group reported radical borylation using near-blue LED as the light energy source (Scheme 1.27).[39] A radical is produced from an aryl or alkyl iodide. The corresponding borylation product is formed through a reaction between bis(catecholato)diboron (B_2cat_2) complexes with DMF and the light-induced radical species generated from the corresponding aryl/alkyl iodide. Due to the instability of catechol boronates regarding their difficult handling, transesterification with triethylamine (Et_3N) and pinacol should be necessary. After publication, the developed method received significant attention because it was a transformation that used only light without any transition metals or additives. According to radical clock experiments, the kinetic rate of borylation was measured (7.4×10^7 M^{-1} S^{-1} for aryl

radical; 3.8×10^6 M^{-1} S^{-1} for primary C-radical), and the second-order rate constant between radical species and diboron complexes was revealed, meaning that the developed transformation was quite fast. They also revealed that reactive radical species are generated through chain propagation, signifying the high efficiency of their developed reaction.

1.3.2 Photocatalytic strategies

In 2012, the Stephenson group reported a reduction reaction of aryl, alkyl, and vinyl iodide using photocatalysis (Scheme 1.28).[40] The halide compounds exposed to the photocatalysis provided the corresponding carbon-centered radical and iodide anion through the electron transfer process of the excited photocatalysis. Subsequently, the proto-deiodinated product was finally obtained through the HAT of amine (BDE =

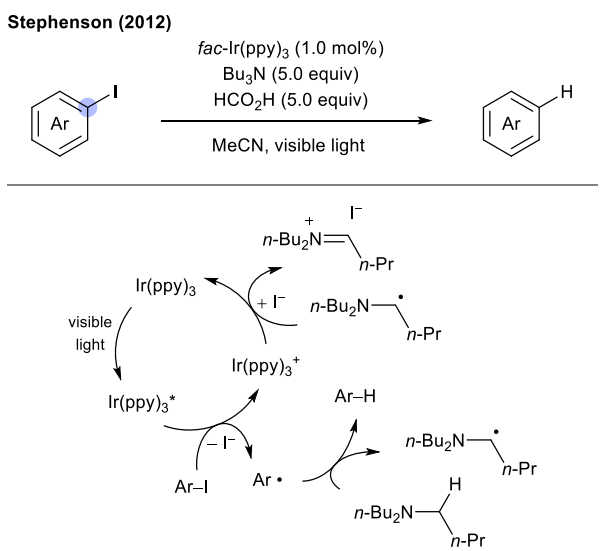

Scheme 1.28 Photocatalyzed electron transfer for the C(sp^2)–I bond activation

91 kcal/mol for α-amino C(sp^3)–H bond). Iridium-based photocatalysis, *fac*-Ir(ppy)$_3$, is a catalysis with a highly negative reduction potential (E^*_{red} = –1.73 V vs. SCE) known as the appropriate candidate for the initial step of radical generation. Substrates containing various functional groups, such as amines, amides, esters, and other halides, chemoselectively proceeded to the desired reaction pathway. However, with other halide-containing compounds (e.g., bromide and chloride), activation with the developed method was difficult, so developing a photocatalyst with greater reducing power is necessary.

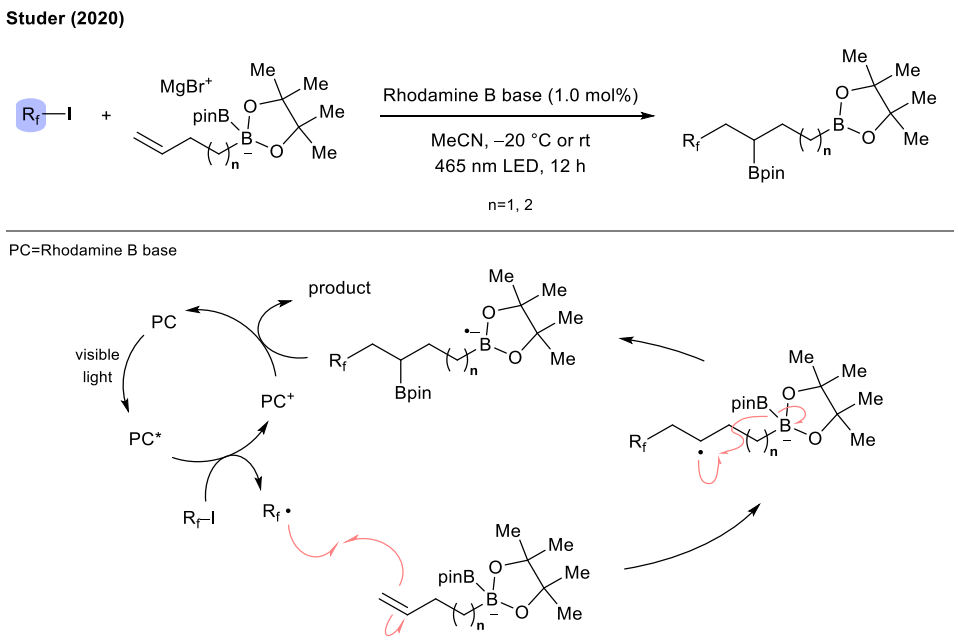

Scheme 1.29 Photocatalyzed electron transfer for the C(sp^3)–I bond activation

In 2020, the perfluoroalkylation of alkenes reported by the Studer group underwent a radical initiation through the oxidative quenching cycle of

organophotocatalysis (Scheme 1.29).[41] The organic photocatalyst used in the developed reaction, Rhodamine B, has sufficient reducing power for perfluoroalkyl iodide (E_{red} = –1.22 V vs. SCE in MeCN). Following the addition of the perfluoroalkyl group to the terminal alkene, the distal boron migration of the anionic diboron complexes pregenerated by *in situ* mixing of bis(pinacolato)diboron and the Grignard reagent yielded the final product, 1,n-bisborylalkane (n=3 or 4).

1.3.3 Halogen atom transfer (XAT) strategies

In addition to photolytic cleavage and single electron transfer, another method for activating carbon–iodide bonds is halogen atom transfer (XAT). Historically, XAT was made possible using metal radicals (e.g., chromium, tin, gold, cerium, etc.). Due to the emerging advances in photocatalysis and the great interest in this field, several new XAT reagents based on organic compounds are now available in mild conditions.

Tris(trimethylsilyl)silane (TTMSS) in XAT chemistry is one of the first synthetic applications to induce reactions through direct light irradiation on organic molecules. In 2015, the Paixão group reported a method for synthesizing heterocyclic compounds through cyclization after forming an aryl radical by utilizing TTMSS as an XAT agent (Scheme 1.30).[42] According to the mechanistic investigation, the reported reaction is rationalized that electron transfer occurs through electron donor–acceptor (EDA) complexation between the aryl halide and the TTMSS. The reaction is propagated through the HAT of TTMSS with a new C(sp^3) radical formed after cyclization ($\Phi > 28$).

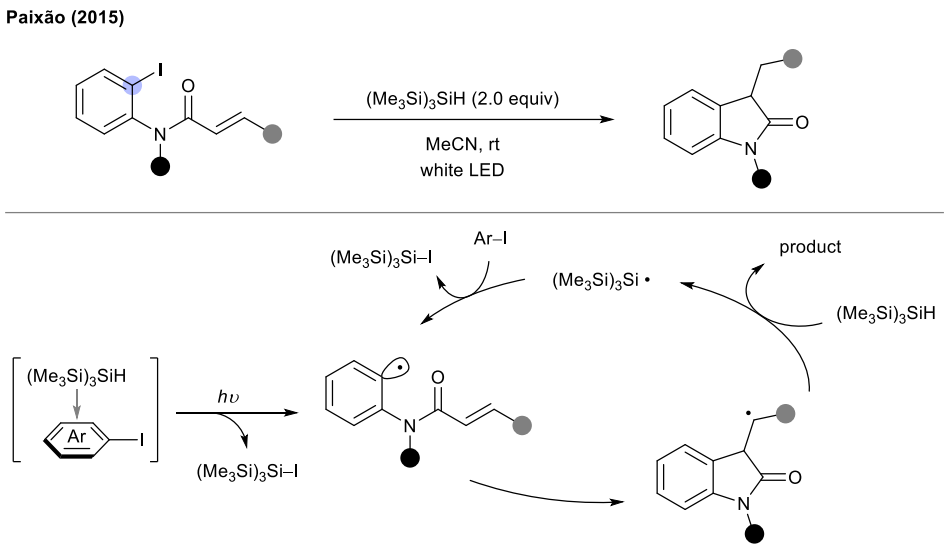

Scheme 1.30 XAT of the TTMSS radical

In 2020, the Leonori group reported an XAT protocol using an organic photocatalyst, 4CzIPN.[43] The XAT reagent, a key element of the described reaction, is an α-aminoalkyl radical generated from the electron transfer of 4CzIPN (Scheme 1.31). Since the radical species described has a strong nucleophilicity, it stabilizes the XAT polar transition state and strongly promotes the corresponding step. Through the process mentioned above, the alkyl radical formed from XAT is reacted with an alkene, and the Giese reaction is carried out. The back halogen atom transfer is the most important design principle when choosing the XAT reagent. The α-aminoalkyl radical selected as the XAT reagent by the Leonori group is a well-designed model because it degrades to iminium halide after XAT, which prevents the back halogen atom transfer.

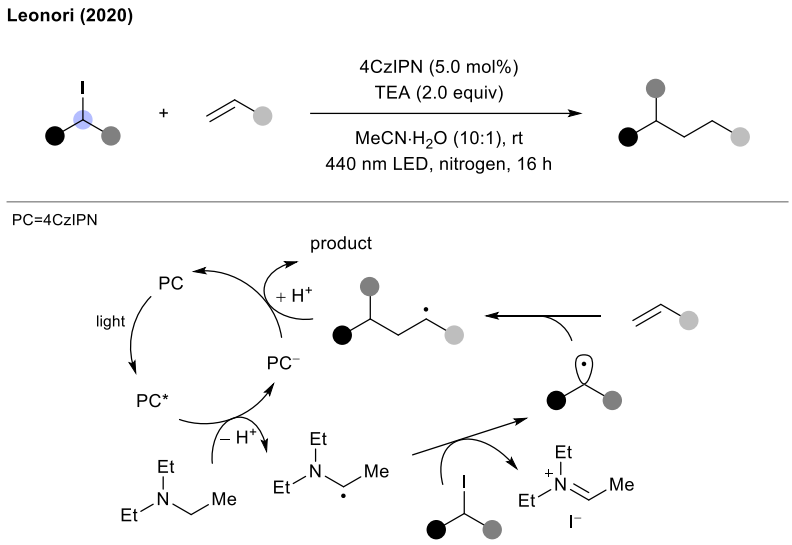

Scheme 1.31 XAT of the α-aminoalkyl radical

1.3.4 EDA interaction strategies

Simultaneously, with many advances in photoredox systems, the EDA approach has also achieved much prosperity.[44] Notably, an efficient SET through EDA complexation is possible because it does not need a third substance (e.g., photocatalysis or light-induced transition metal catalysis) in the electron transport system. The basic principle of EDA complexation is the electronic interactions between the donor and the acceptors facing each other directly (Scheme 1.32). The resulting molecular aggregate formed by EDA complexation exhibits a new absorption band (e.g., visible light) not found in the donor or acceptor. Electrons are transferred from the donor to the acceptor upon light irradiation, and the corresponding pairs of radical cations and anions are formed.

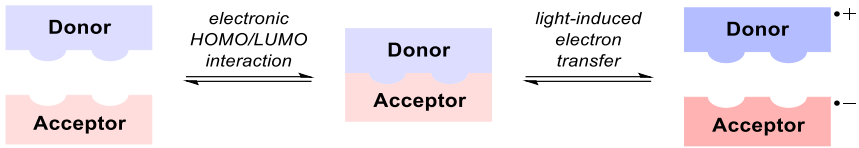

Scheme 1.32 Concept of the EDA complex formation

Most of the EDA complexation was performed well in the conjugated π-system. Therefore, it was used for aromatic compound functionalization. Additionally, by introducing various functional groups as substituents, the orbital energy can be adjusted. Predictably, this strategy attempts the formation of aryl radicals. However, a limitation is that the orbital energies of the donors and acceptors must match, and it should be noted regarding reaction efficiency and atom economy.

In 2019, the Xia group unveiled the α-arylation of oxyindole through the charge transfer pathway (Scheme 1.33).[45] According to the reported reaction, when aromatization by deprotonation of oxyindole occurs, the EDA complex is formed with the corresponding aryl iodide. The resulting radical pairs provided through direct electron transfer between two substrates resulted in new $C(sp^3)$–$C(sp^2)$ bonds. During the reaction, the complexation between the donor and the acceptor could be observed by the color change of the reaction mixture in the presence of a base. Expectedly, the reaction proceeds well when the electron-donating and electron-withdrawing groups are attached to the oxyindole (donor) and the aryl iodide (acceptor), respectively.

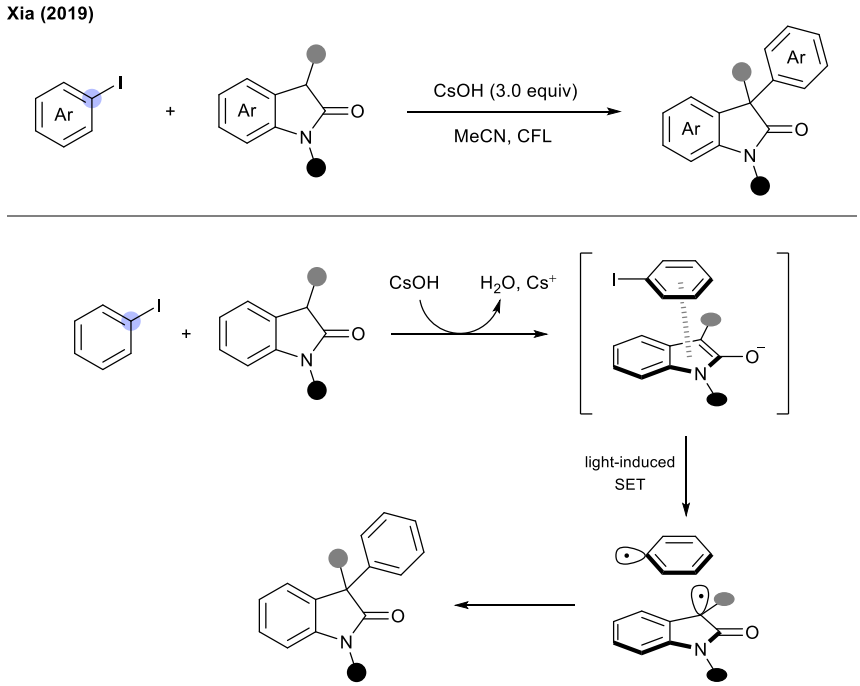

Scheme 1.33 Light-induced electron transfer through the EDA complex

1.4 Visible-light-mediated C–F bond activation enabling radical generation

The carbon–fluorine bond is one of the significant bonds in pharmaceuticals, pesticides, and high-value-added compounds due to the unique properties of the fluorine atom. However, activating the carbon–fluorine bond is difficult due to its low activity and high bond dissociation energy. Therefore, direct activation of carbon–fluorine bonds under mild, metal-free conditions is considered a challenging topic. Furthermore, it can be hailed as an important tool in organic synthesis. Recently, various activation modes of carbon–fluorine bonds by photochemical conditions have been studied to overcome limited classical methods. This section

will cover the rapidly growing field of carbon–fluorine bond functionalization with a special focus on reaction mechanisms and design.

1.4.1 Defluorinative functionalization of C(sp^2)–F bond

Fluoroarene derivatives are significant raw materials widely used in synthesizing bioactive molecules, pesticides, photosensitive materials, pharmaceuticals, or organic solvents.[46] Therefore, various synthetic methods using fluoroarene derivatives are in high demand since high-value-added substrates can be easily prepared by the C(sp^2)–F bond cleavage method.

Recently, organic chemists have been dedicated to developing photocatalytic systems capable of activating substances with high reduction potentials. In 2014, the Weaver group developed a hydrodefluorination reaction of fluoroarene ($E_{red} = -2.81$ vs. SCE for C_6F_6) with a photoreaction using an $Ir(ppy)_3$ catalyst under light irradiation (Scheme 1.34).[47] In the developed reaction, inexpensive and safe amines were used as reducing agents. Furthermore, two or more reduced hydrodefluorination products were found under optimized conditions, which are difficult to access by other previous methods. The flow method using the flow reactor is possible through the developed method.

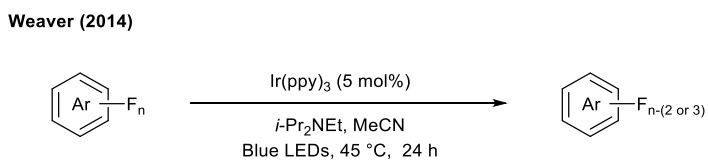

Scheme 1.34 Hydrodefluorination of perfluoroarenes

The Xia group published a methodology to obtain a defluoroalkylative product by activating the C(sp^2)–F bond of perfluoroarene (Scheme 1.35).[48] Excited Ir(III) photocatalysts under light irradiation oxidized quinuclidine to provide radical cation, which will generate α-heteroatom radical from ether or amine through HAT. The corresponding radical produced the final product through radical–radical coupling with the perfluoroaryl radical, and the developed reaction showed a wide range of substrates and efficiency.

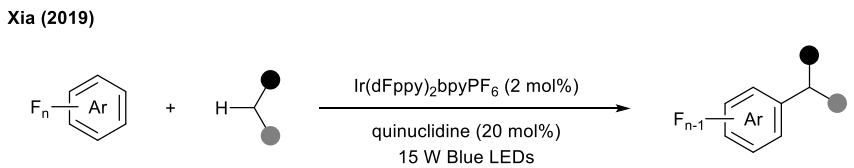

Scheme 1.35 Photocatalytic C(sp^2)–F alkylation via radical–radical cross-coupling

Monofluoroalkene, produced through gem-difluoroalkene defluorination, is in great demand for synthesis as an important backbone in materials and medicines (Scheme 1.36). Although the synthetic method through transition metal catalysis is well known,[49] the activation of C(sp^2)–F bonds through the electrochemical and photochemical method was first reported in 2016 by the Hashimi group.[50] Among them, monofluoroalkenes can be easily accessible from various radical precursors (e.g., tertiary amines, NHC–boranes, heterocyclic compounds, carboxylic acids, 1,4-dihydropyridine, etc.) using a radical–radical cross-coupling strategy.[50,51] The final product is formed through radical–radical cross-coupling between radicals produced

from radical precursors and fluoroalkenyl radicals through oxidation and reduction of light-excited photocatalysts.

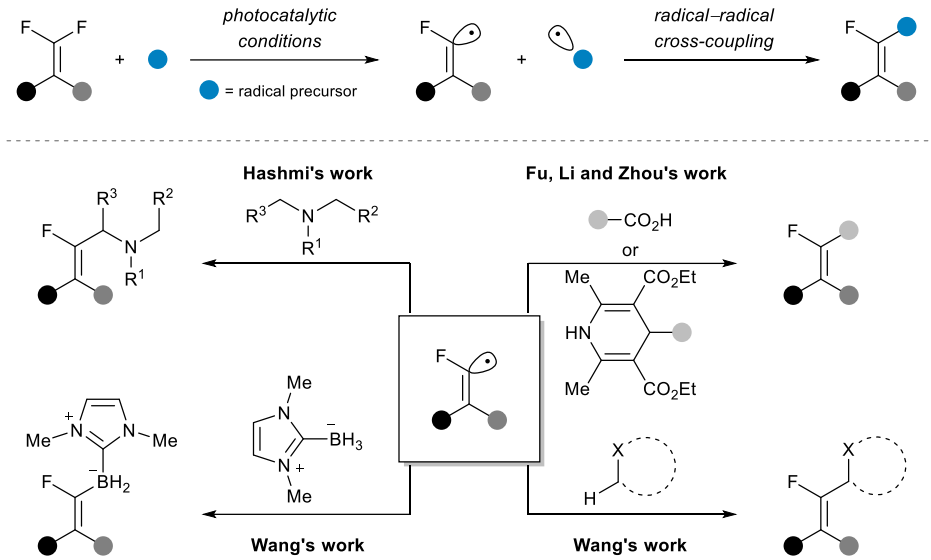

Scheme 1.36 Defluorination of *gem*-difluoroalkenes

In 2016, the Weaver group reported a photocatalytic alkenylation reaction by activating the C(sp^2)–F bond of perfluoroarene (Scheme 1.37).[52] This reaction is the first example of control to electron and energy transfer during the defluorination reaction using a photocatalyst under light irradiation. Consequently, implementing high *E/Z* selectivity was possible.

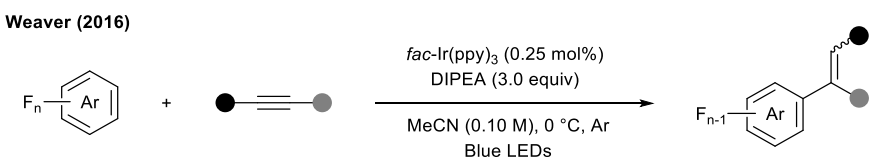

Scheme 1.37 Photocatalytic C(sp^2)–F alkenylation

1.4.2 Defluorinative functionalization of C(sp^3)–F bond

The development of an efficient synthetic method of aryldifluoromethyl ($ArCF_2R$) is significant to chemists due to its high value as a chemical scaffold in agricultural and medical chemistry.[53] This section describes the synthetic routes for preparing derivatives by selective activation of the C(sp^3)–F bonds of trifluoromethyl arene ($ArCF_3$), which is abundant in nature.

The hydrodefluorination reaction of trifluoromethyl arene mediated by 1,3-dicyano-2,4,5,6-tetrakis(diphenylamino)-benzene (4-DPA-IPN), an organic photocatalyst, was reported by the Gouverneur group in 2020 (Scheme 1.38).[54] Using developed methods, various valuable compounds can be synthesized. Furthermore, combining multi grams of products could be feasible using a flow reactor.

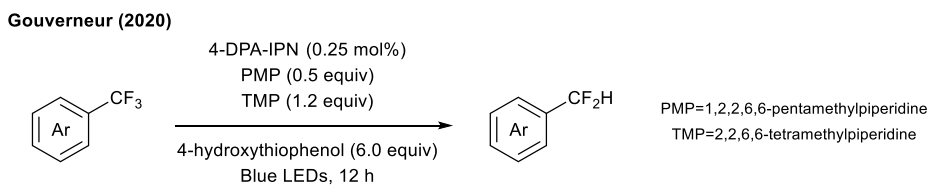

Scheme 1.38 Hydrodefluorination of trifluoromethyl arenes

The hydrodefluorination reaction can be applied not only to trifluoromethyl arene but also to trifluoromethyl ketone, and difluoromethyl ketone (DFMK) is a valuable functional group obtained as a product. In 2021, the Lennox group, for the first time, successfully electrically activated trifluoromethyl ketone without

additives or metal catalysts[55], and trimethylsilyl chloride (TMSCl) acted as a protecting group for the radical anion and promoted the hydrodefluorination reaction (Scheme 1.39).

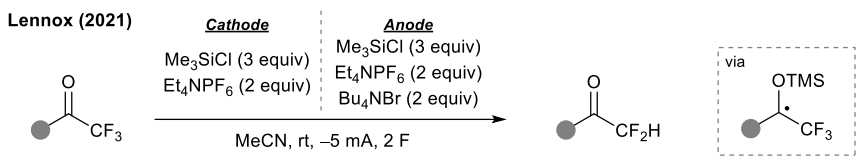

Scheme 1.39 Hydrodefluorination of trifluoromethy ketones

In 2018, the Jui group activated the benzyl C(sp^3)–F bond through trifluoromethyl arene reduction (E_{red} = −2.07 V vs. SCE for 1,3-bis(trifluoromethyl)benzene) using the photocatalyst *N*-phenylphenothiazine (PTH), which is the strong reductant under light irradiation (Scheme 1.40).[56] The benzyl radical formed from the release of the fluoride anion reacts with an alkene to form an alkylated product. The reaction was terminated with thiol, an HAT catalyst. Furthermore, sodium formate added to the reaction aids the regeneration of thiol catalysts and photocatalysts through HAT and electron transfer.

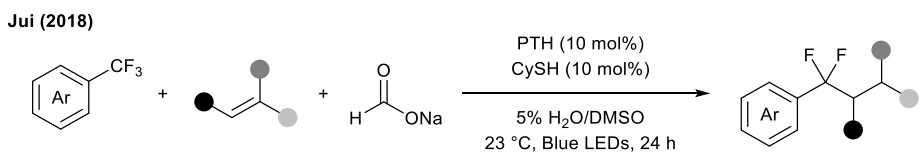

Scheme 1.40 Defluoroalkylation of trifluoromethyl arenes

The reactions used a reductive process to activate C–F bonds and generate radicals as intermediates. Therefore, the reactivity depended mainly on the reactivity of the radical itself, and a new strategy has been in high demand to overcome this. In 2021, Zhang's group revealed the cross-coupling reaction between trifluoromethyl arene (E_{red} = −2.07 V vs. SCE for 1,3-bis(trifluoromethyl)benzene) and arylboronic acid using an excited palladium species (Scheme 1.41).[57] Remarkably, this research showed the potential of cross-coupling reactions for constructing various bonding modes throughout the reaction.

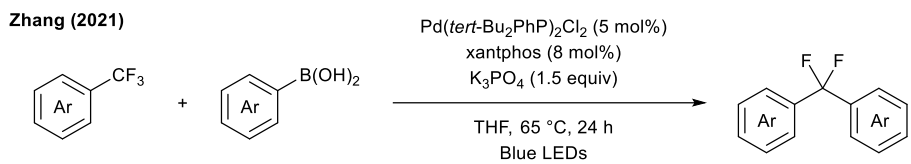

Scheme 1.41 Transition metal-catalyzed defluoroarylation of trifluoromethyl arenes

1.5 Conclusion

Since radicals are highly reactive intermediates, they can provide various bonding modes without requiring much energy. With the help of the transition metal, building various C–C/C–heteroatom bonds and introducing new functional groups through the well-known cross-coupling reaction is possible. Furthermore, it is highly attractive that the user can selectively provide the desired chirality by introducing the chiral ligand. Additionally, carbocation or carbanion can be produced through the oxidation or reduction of radical species. Consequently, the radical species can be easily converted into electrophiles or nucleophiles in the reaction system to design selective and sequential processes.

Through the development of modern organic chemistry, radical chemistry has overcome many known problems and has pursued an efficient reaction system. Particularly, it promotes chemical reactions under milder conditions by converting visible light into chemical energy by developing a photocatalytic system. The industrial field introduces flow chemistry to enable bulk synthesis, offering a cost-effective solution that simplifies the multistep process. Radical chemistry, which organic chemists will continue to develop in the future, will provide a method to perform various chemical reactions previously difficult to implement due to a high-energy barrier. Finally, it will suggest various activation modes once considered impossible.

1.6 References

1. (a) N. A. Romero and D. A. Nicewicz, *Chem. Rev.*, 2016, **116**, 10075-10166; (b) J. D. Bell and J. A. Murphy, *Chem. Soc. Rev.*, 2021, **50**, 9540-9685.

2. (a) L. Capaldo, D. Ravelli and M. Fagnoni, *Chem. Rev.*, 2022, **122**, 1875-1924; (b) H. Cao, X. Tang, H. Tang, Y. Yuan and J. Wu, *Chem Catal.*, 2021, **1**, 523-598.

3. L. Capaldo and D. Ravelli, *Eur. J. Org. Chem.*, 2017, 2056-2071.

4. J. Jin and D. W. C. MacMillan, *Angew. Chem. Int. Ed.*, 2015, **54**, 1565-1569.

5. C.-J. Li, *Acc. Chem. Res.*, 2009, **42**, 335-344.

6. S. Mukherjee, B. Maji, A. Tlahuext-Aca and F. Glorius, *J. Am. Chem. Soc.*, 2016, **138**, 16200-16203.

7. A. Hu, J.-J. Guo, H. Pan and Z. Zuo, *Science*, 2018, **361**, 668-672.

8. Q. Yang, Y.-H. Wang, Y. Qiao, M. Gau, P. J. Carroll, P. J. Walsh and E. J. Schelter, *Science*, 2021, **372**, 847-852.

9. K. A. Margrey, W. L. Czaplyski, D. A. Nicewicz and E. J. Alexanian, *J. Am. Chem. Soc.*, 2018, **140**, 4213-4217.

10. J. B. McManus, J. D. Griffin, A. R. White and D. A. Nicewicz, *J. Am. Chem. Soc.*, 2020, **142**, 10325-10330.

11. G. Majetich and K. Wheless, *Tetrahedron*, 1995, **51**, 7095-7129.

12. J. L. Jeffrey, J. A. Terrett and D. W. C. MacMillan, *Science*, 2015, **349**, 1532-1536.

13. A. S. H. Ryder, W. B. Cunningham, G. Ballantyne, T. Mules, A. G. Kinsella, J. Turner-Dore, C. M. Alder, L. J. Edwards, B. S. J. McKay, M. N. Grayson and A. J. Cresswell, *Angew. Chem. Int. Ed.*, 2020, **59**, 14986-14991.

14. J. Jin and D. W. C. MacMillan, *Nature*, 2015, **525**, 87-90.

15. T. Ide, J. P. Barham, M. Fujita, Y. Kawato, H. Egami and Y. Hamashima, *Chem. Sci.*, 2018, **9**, 8453-8460.

16. H. Fuse, H. Mitsunuma and M. Kanai, *J. Am. Chem. Soc.*, 2020, **142**, 4493-4499.

17. S. Kato, Y. Saga, M. Kojima, H. Fuse, S. Matsunaga, A. Fukatsu, M. Kondo, S. Masaoka and M. Kanai, *J. Am. Chem. Soc.*, 2017, **139**, 2204-2207.

18. V. Regnault, *J. Prakt. Chem.*, 1840, **19**, 193-218.

19. B. J. Shields and A. G. Doyle, *J. Am. Chem. Soc.*, 2016, **138**, 12719-12722.

20. S. Rohe, A. O. Morris, T. McCallum and L. Barriault, *Angew. Chem. Int. Ed.*, 2018, **57**, 15664-15669.

21. S. J. Hwang, D. C. Powers, A. G. Maher, B. L. Anderson, R. G. Hadt, S.-L. Zheng, Y.-S. Chen and D. G. Nocera, *J. Am. Chem. Soc.*, 2015, **137**, 6472-6475.

22. L. Troian-Gautier, M. D. Turlington, S. A. M. Wehlin, A. B. Maurer, M. D. Brady, W. B. Swords and G. J. Meyer, *Chem. Rev.*, 2019, **119**, 4628-4683.

23. T. Kawasaki, N. Ishida and M. Murakami, *J. Am. Chem. Soc.*, 2020, **142**, 3366-3370.

24. S. Sarkar, K. P. S. Cheung and V. Gevorgyan, *Chem. Sci.*, 2020, **11**, 12974-12993.

25. M. Ratushnyy, M. Parasram, Y. Wang and V. Gevorgyan, *Angew. Chem. Int. Ed.*, 2018, **57**, 2712-2715.

26. D. Wang, C. Mück-Lichtenfeld and A. Studer, *J. Am. Chem. Soc.*, 2019, **141**, 14126-14130.

27. I. N.-M. Leibler, M. A. Tekle-Smith and A. G. Doyle, *Nat. Commun.*, 2021, **12**, 6950.

28. J.-B. Xia, C. Zhu and C. Chen, *J. Am. Chem. Soc.*, 2013, **135**, 17494-17500.

29. X.-Z. Fan, J.-W. Rong, H.-L. Wu, Q. Zhou, H.-P. Deng, J. D. Tan, C.-W. Xue, L.-Z. Wu, H.-R. Tao and J. Wu, *Angew. Chem. Int. Ed.*, 2018, **57**, 8514-8518.

30. H. Huang, Z. M. Strater and T. H. Lambert, *J. Am. Chem. Soc.*, 2020, **142**, 1698-1703.

31. Y. Li, J. Su, E. Mitchell, G. Zhang and J. Li, *Sci. China Chem.*, 2013, **56**, 1671-1681.

32. T. Shiragami, J. Matsumoto, H. Inoue and M. Yasuda, *J. Photochem. Photobiol. C: Photochem. Rev.*, 2005, **6**, 227-248.

33. H. Cao, Y. Kuang, X. Shi, K. L. Wong, B. B. Tan, J. M. C. Kwan, X. Liu and J. Wu, *Nat. Commun.*, 2020, **11**, 1956.

34. H. Liu, L. Ma, R. Zhou, X. Chen, W. Fang and J. Wu, *ACS Catal.*, 2018, **8**, 6224-6229.

35. J. Qiao, Z.-Q. Song, C. Huang, R.-N. Ci, Z. Liu, B. Chen, C.-H. Tung and L.-Z. Wu, *Angew. Chem. Int. Ed.*, 2021, **60**, 27201-27205.

36. C. Huang, J. Qiao, R.-N. Ci, X.-Z. Wang, Y. Wang, J.-H. Wang, B. Chen, C.-H. Tung and L.-Z. Wu, *Chem*, 2021, **7**, 1244-1257.

37. C. Huang, R.-N. Ci, J. Qiao, X.-Z. Wang, K. Feng, B. Chen, C.-H. Tung and L.-Z. Wu, *Angew. Chem. Int. Ed.*, 2021, **60**, 11779-11783.

38. T. Kawamoto, A. Sato and I. Ryu, *Chem. Eur. J.*, 2015, **21**, 14764-14767.

39. Y. Cheng, C. Mück-Lichtenfeld and A. Studer, *Angew. Chem. Int. Ed.*, 2018, **57**, 16832-16836.

40. J. D. Nguyen, E. M. D'Amato, J. M. R. Narayanam and C. R. J. Stephenson, *Nat. Chem.*, 2012, **4**, 854-859.

41. D. Wang, C. Mück-Lichtenfeld and A. Studer, *J. Am. Chem. Soc.*, 2020, **142**, 9119-9123.

42. G. P. da Silva, A. Ali, R. C. da Silva, H. Jiang and M. W. Paixão, *Chem. Commun.*, 2015, **51**, 15110-15113.

43. T. Constantin, M. Zanini, A. Regni, N. S. Sheikh, F. Juliá and D. Leonori, *Science*, 2020, **367**, 1021-1026.

44. G. E. M. Crisenza, D. Mazzarella and P. Melchiorre, *J. Am. Chem. Soc.*, 2020, **142**, 5461-5476.

45. K. Liang, N. Li, Y. Zhang, T. Li and C. Xia, *Chem. Sci.*, 2019, **10**, 3049-3053.

46. (a) A. Facchetti, M.-H. Yoon, C. L. Stern, H. E. Katz and T. J. Marks, *Angew. Chem. Int. Ed.*, 2003, **42**, 3900-3903; (b) P. Jeschke, *ChemBioChem*, 2004, **5**, 570-589; (c) P. Jeschke, *Pest Manag. Sci.*, 2017, **73**, 1053-1066.

47. S. M. Senaweera, A. Singh and J. D. Weaver, *J. Am. Chem. Soc.*, 2014, **136**, 3002-3005.

48. J. Wang, B. Huang, Y. Gao, C. Yang and W. Xia, *J. Org. Chem.*, 2019, **84**, 6895-6903.

49. (a) P. Tian, C. Feng and T.-P. Loh, *Nat. Commun.*, 2015, **6**, 7472; (b) J. Hu, Y. Zhao and Z. Shi, *Nat. Catal.*, 2018, **1**, 860-869; (c) R. T. Thornbury and F. D. Toste, *Angew. Chem. Int. Ed.*, 2016, **55**, 11629-11632; (d) S. Morand, P. Jubault, J.-P. Bouillon and S. Couve-Bonnaire, *Chem. Eur. J.*, 2021, **27**, 17273-17292.

50. J. Xie, J. Yu, M. Rudolph, F. Rominger and A. S. K. Hashmi, *Angew. Chem. Int. Ed.*, 2016, **55**, 9416-9421.

51. (a) J. Li, Q. Lefebvre, H. Yang, Y. Zhao and H. Fu, *Chem. Commun.*, 2017, **53**, 10299-10302; (b) H. Tian, Q. Xia, Q. Wang, J. Dong, Y. Liu and Q. Wang, *Org. Lett.*, 2019, **21**, 4585-4589; (c) H. Yang, C. Tian, D. Qiu, H. Tian, G. An and G. Li, *Org. Chem. Front.*, 2019, **6**, 2365-2370; (d) Q. Wang, Y. Qu, H. Tian, Y. Liu, H. Song and Q. Wang, *Chem. Eur. J.*, 2019, **25**, 8686-8690; (e) H.-W. Du, J. Sun, Q.-S. Gao, J.-Y. Wang, H. Wang, Z. Xu and M.-D. Zhou, *Org. Lett.*, 2020, **22**, 1542-1546; (f) W. Xu, H. Jiang, J. Leng, H.-W. Ong and J. Wu, *Angew. Chem. Int. Ed.*, 2020, **59**, 4009-4016.

52. A. Singh, C. J. Fennell and J. D. Weaver, *Chem. Sci.*, 2016, **7**, 6796-6802.

53. (a) N. A. Meanwell, *J. Med. Chem.*, 2011, **54**, 2529-2591; (b) J. Boyer, E. Arnoult, M. Médebielle, J. Guillemont, J. Unge and D. Jochmans, *J. Med. Chem.*, 2011, **54**, 7974-7985.

54. J. B. I. Sap, N. J. W. Straathof, T. Knauber, C. F. Meyer, M. Médebielle, L. Buglioni, C. Genicot, A. A. Trabanco, T. Noël, C. W. am Ende and V. Gouverneur, *J. Am. Chem. Soc.*, 2020, **142**, 9181-9187.

55. J. R. Box, A. P. Atkins and A. J. J. Lennox, *Chem. Sci.*, 2021, **12**, 10252-10258.

56. H. Wang and N. T. Jui, *J. Am. Chem. Soc.*, 2018, **140**, 163-166.

57. Y.-C. Luo, F.-F. Tong, Y. Zhang, C.-Y. He and X. Zhang, *J. Am. Chem. Soc.*, 2021, **143**, 13971-13979.

Part I. Visible-light-induced carbon–hydrogen bond cleavage for radical generation

Chapter 2. Benzylic C(sp^3)–C(sp^2) cross-coupling of indoles enabled by oxidative radical generation and nickel catalysis*

2.1 Introduction

The development of synthetic strategies that allow direct functionalization of C–H bonds has received considerable attention from organic chemists because such methods are cost-effective and environmentally benign.[1] Among the various modes of hydrocarbon modification, the activation of benzylic C(sp^3)–H bonds is of increasing interest because of the abundance and popularity of arene-based building blocks in organic synthesis.[2] Recently, the scope of this transformation has been dramatically expanded by the advent of transition metal catalysis (Scheme 2.1a).[3] Despite significant advances in this area, major challenges associated with reactivity and/or selectivity are encountered regularly and remain an active target of investigation.[4]

Recently emerging radical-based technologies for benzylic C–H bond activation have contributed significantly to solving many of these problems (Scheme 2.1b). The expeditious introduction of benzylic radical intermediates to a metal center allows for the efficient generation of metal alkyl species, forming the foundation for

* The majority of this work has been published (*Chem. Sci.* **2021**, *12*, 4119-4125).

subsequent functionalization.[5] Conventionally, radical formation events at the benzylic position have been realized by hydrogen atom transfer (HAT),[6] with recent advances in photoredox catalysis (PC) having greatly broadened the applicability of this method.[7] However, the HAT process generally requires the use of a large excess of substrate due to its insufficient reactivity. Most importantly, selectivity problems can arise in complicated systems, as the discrimination of C–H bonds with comparable bond strength is difficult.[8] A potential alternative to HAT towards selective functionalization of a benzylic C–H bond is the employment of the sequential electron transfer-proton transfer (ET/PT) activity of arenes.[9] This process involves chemoselective one-electron oxidation followed by deprotonation, and can preferentially generate a benzylic radical on the periphery of the arene ring. Although the ET/PT-based radical formation strategy has found a multitude of applications for organic synthesis,[10,11] a synergistical merger with transition metal catalysis which can dramatically broaden the scope of benzylic C–H bond functionalization is underdeveloped.[12,13]

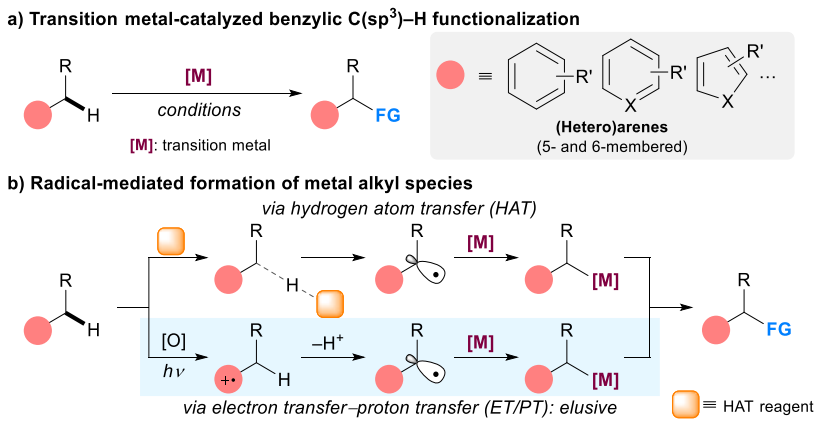

Scheme 2.1 Strategies for benzylic C(sp^3)–H functionalization

Herein, we present the successful interfacing of the ET/PT-driven indole-derived benzylic radical formation strategy with a Ni-catalyzed cross-coupling reaction for the construction of C(sp^3)–C(sp^2) bonds (Scheme 2.2a). This method exploits the facile oxidation of indoles by photoredox catalysis,[14] and has thus been applied to selective radical generation at the benzylic position of the indole ring without the involvement of any HAT. Eventually, a convenient preparation of indole derivatives containing an aryl or an acyl group at the C-3 alkyl group, common structural motifs with important bioactivity, could be realized (Scheme 2.2b).

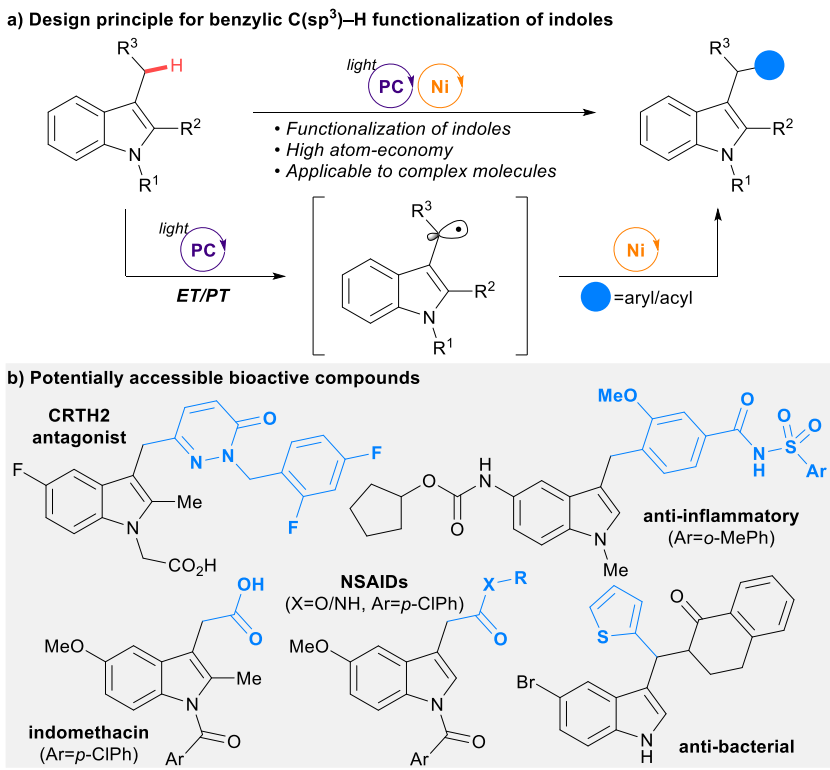

Scheme 2.2 Benzylic C(sp^3)–H functionalization of indoles by dual catalysis

2.2 Results and discussion

2.2.1 Optimization of reaction conditions

The reactivity of the combined catalytic systems was evaluated using 1,3-dimethyl-1*H*-indole (**1a**) and *p*-bromoacetophenone (**2a**) as substrates (Table 2.1).[15] In the presence of an Ir-based photocatalyst, visible-light irradiation, and a $NiCl_2$·glyme precatalyst with a 1,10-phenanthroline ligand, the desired benzylic arylation product (**3aa**) was formed in 83% yield (entry 1). The reaction was set up with the aid of a glovebox for the optimal results. However, it is noteworthy that the reactivity could be preserved even when the reaction was set up outside of a glovebox by using a standard Schlenk technique, or when the reaction was run under air (76% and 73%, respectively). These results demonstrate the robustness of the developed method. In contrast to the HAT-based dual catalytic systems, the use of excess radical precursor was not required, demonstrating the efficiency of the transformation. Control experiments indicated that the presence of both the photoredox system and the Ni catalyst was crucial for successful reaction (entries 2–4). In addition, the use of a non-nucleophilic organic base, viz. 1,8-diazabicyclo[5.4.0]undec-7-ene (DBU), and the incorporation of LiCl additive were also important for optimum performance (entries 5 and 6).[16,17] In agreement with the mechanistic postulate involving radical generation, no arylation product was detected when a radical scavenger was present (entry 7).[18] Finally, the reactivity could be extended to arylation with other types of aryl (pseudo)halides, among which aryl bromides and chlorides are the best substrates (entries 8–10).

Table 2.1 Optimization of reaction conditions[a]

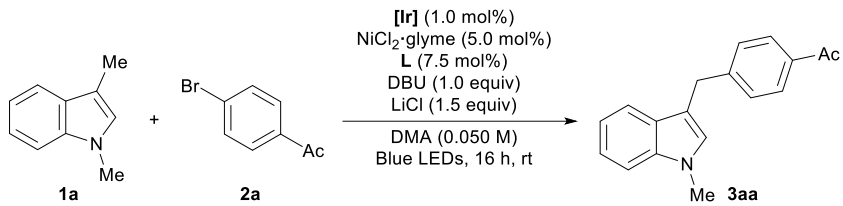

Entry	Conditions	Yield (%)
1	as shown	83 (76[b]/73[c])
2	no photocatalyst	N.D.
3	no light	N.D.
4	no $NiCl_2$·glyme	N.D.
5	no DBU	10
6	no LiCl	54
7	with TEMPO (3.0 equiv)	N.D.
8	ArCl instead of ArBr	76
9	ArI instead of ArBr	16
10[d]	ArOTf instead of ArBr	36

[a] Reaction conditions: **1a** (0.15 mmol), **2a** (0.10 mmol), **[Ir]** (1.0 mol%), $NiCl_2$·glyme (5.0 mol%), **L** (7.5 mol%), DBU (0.10 mmol), LiCl (0.15 mmol), and DMA (0.050 M) irradiated with 34 W blue LEDs. Yields were determined by ^{1}H NMR analysis using 1,1,2,2-tetrachloroethane as an internal standard. [b] The reaction was set up using standard Schlenk technique on the benchtop. [c] The reaction was carried out under ambient conditions. [d] Without LiCl. **[Ir]**=$Ir(dFCF_3ppy)_2(dtbbpy)PF_6$. dtbbpy=4,4'-di-*tert*-butyl-2,2'-bipyridine. **L**=1,10-phenanthroline. DMA=*N*,*N*-dimethylacetamide. TEMPO=(2,2,6,6-tetramethylpiperidin-1-yl)oxyl. N.D.=not detected.

2.2.2 Substrate scope of indoles

The generality of the reaction was examined under optimized conditions (Table 2.2). Initially, the effect of varying the N^1-substituent was assessed. Although an unmasked 3-methyl indole furnished the desired product in slightly reduced yield (**3ba**), indole derivatives with a variety of N^1-alkyl substituents underwent the desired arylation smoothly (**3aa**, **3ca**–**3ea**). Importantly, the placement of Si-based substituents, groups that can be conveniently removed after the targeted reaction, did not affect reactivity (**3fa** and **3ga**). However, the presence of an electron-withdrawing group at N^1 reduced reactivity, indicating the importance of the indole oxidation event (**3ha** and **3ia**). Next, the substituent effects at other positions on the indole skeleton were explored. Various electron-donating (**3ja**–**3na**) and electron-withdrawing functional groups (**3oa**–**3ra**) at the C4–C8 positions of indole were found to be compatible with the optimized conditions. Moreover, halogen substituents, which can be utilized as handles for further functionalization via cross-coupling reactions, were tolerated (**3pa**–**3ra**). The sterically encumbered 2-(hetero)aryl indole derivatives could also be arylated at the 3-methyl group in synthetically useful yields (**3sa**–**3ua**). Finally, the protocol was applicable to the arylation of a 2-methyl indole derivative (**3va**). It should be noted that numerous functional groups that are highly susceptible to HAT-based activation remained intact, indicating the orthogonality of the discovered reactivity (**3ca**, **3ea**, **3ka**, **3ma**, and **3ta**). Substrates based on other types of heterocycles, such as benzofuran, thiophene or pyrrole, were not suitable substrates for the transformation due to the inefficient oxidation process.[14]

Table 2.2 Substrate scope of indoles[a]

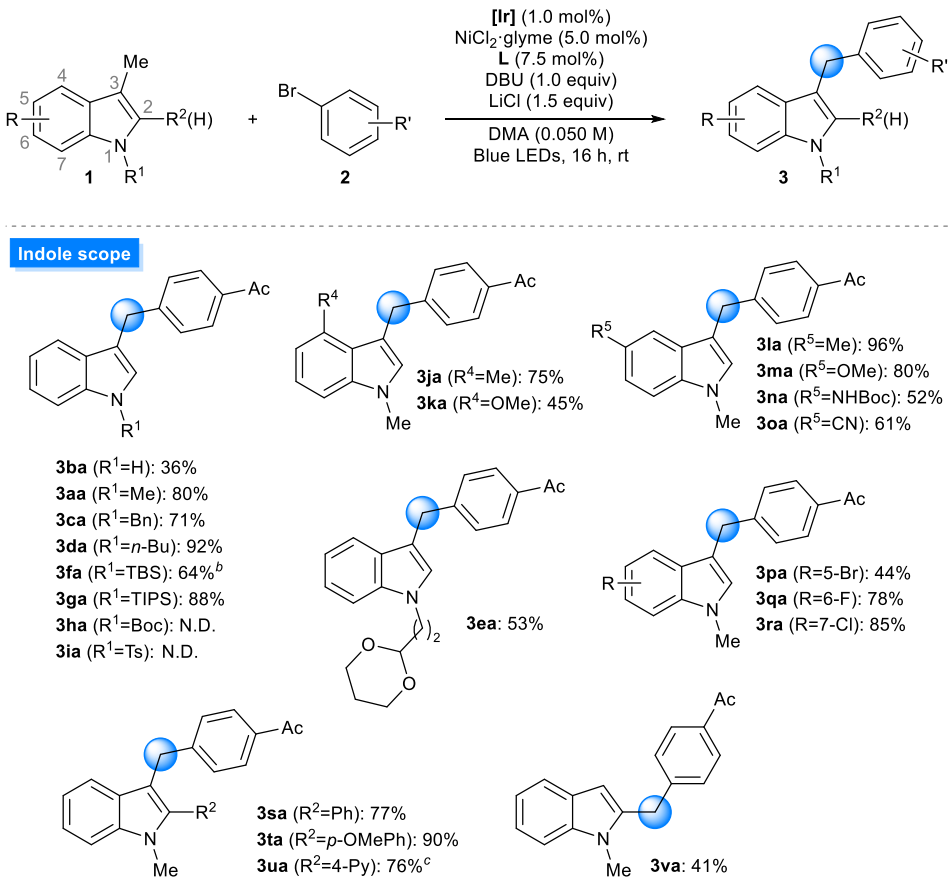

[a] Reaction conditions: **1** (0.30 mmol), **2** (0.20 mmol), **[Ir]** (1.0 mol%), $NiCl_2$·glyme (5.0 mol%), **L** (7.5 mol%), DBU (0.20 mmol), LiCl (0.30 mmol), and DMA (0.050 M) irradiated with 34 W blue LEDs. All yields are isolated yields. [b] 18% of the desilylated product was obtained during the course of the reaction. [c] The reaction was performed with 1,2,3,5-tetrakis(carbazol-9-yl)-4,6-dicyanobenzene (4CzIPN) instead of **[Ir]** for 23 h. **[Ir]**=$Ir(dFCF_3ppy)_2(dtbbpy)PF_6$. dtbbpy= 4,4'-di-*tert*-butyl-2,2'-bipyridine. **L**=1,10-phenanthroline. DMA=*N*,*N*-dimethylacetamide. N.D.=not detected.

2.2.3 Substrate scope of (hetero)aryl halides

Subsequently, the extent of the aryl (pseudo)halide coupling partners was investigated (Table 2.3). Although highly electron-rich or sterically congested aryl

halides underwent the targeted transformation with somewhat reduced productivity, a wide range of electron-neutral and electron-deficient arenes could be successfully used with minor modifications to the reaction conditions (**3ab**–**3ai**). In addition, coupling counterparts derived from an extended π-system (**3aj**), an alkenyl group (**3ak**), or heterocycles (**3al**–**3ao**) were also viable substrates.

Table 2.3 Substrate scope of (hetero)aryl halides[a]

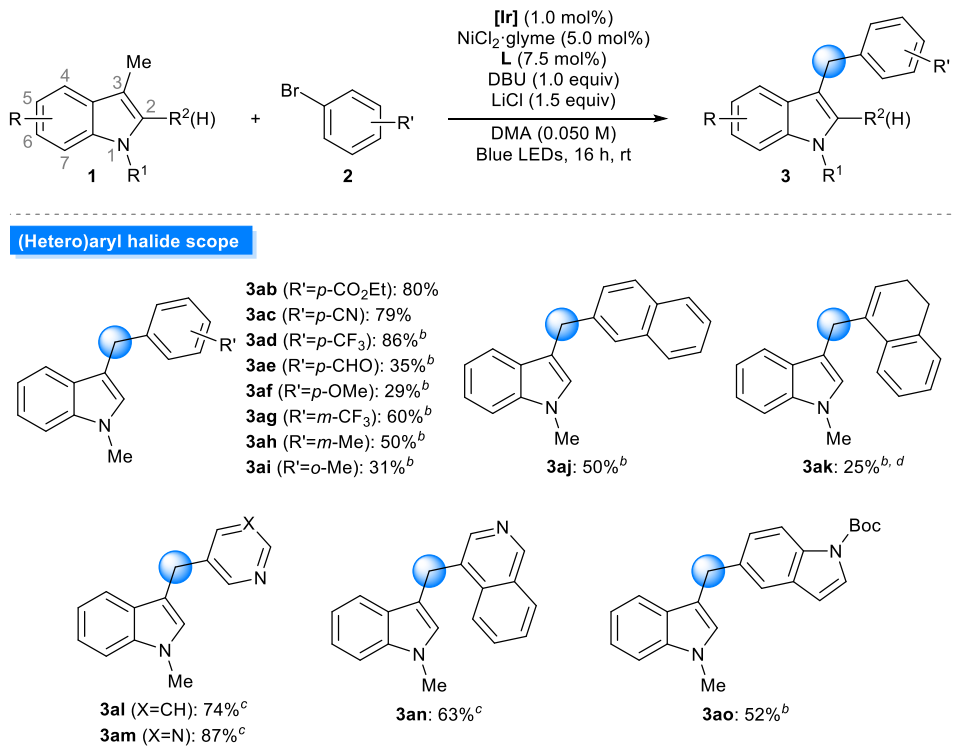

[a] Reaction conditions: **1** (0.30 mmol), **2** (0.20 mmol), **[Ir]** (1.0 mol%), $NiCl_2$·glyme (5.0 mol%), **L** (7.5 mol%), DBU (0.20 mmol), LiCl (0.30 mmol), and DMA (0.050 M) irradiated with 34 W blue LEDs. All yields are isolated yields. [b] 4,4'-dimethoxy-2,2'-bipyridine instead of **L**. [c] The reaction was conducted at 53 °C. [d] The corresponding vinyl triflate was used as substrate **[Ir]**=$Ir(dFCF_3ppy)_2(dtbbpy)PF_6$. dtbbpy= 4,4'-di-*tert*-butyl-2,2'-bipyridine. **L**=1,10-phenanthroline. DMA=*N*,*N*-dimethylacetamide. N.D.=not detected.

2.2.4 Substrate scope of bioactive molecules

Table 2.4 Substrate scope of bioactive molecules[a]

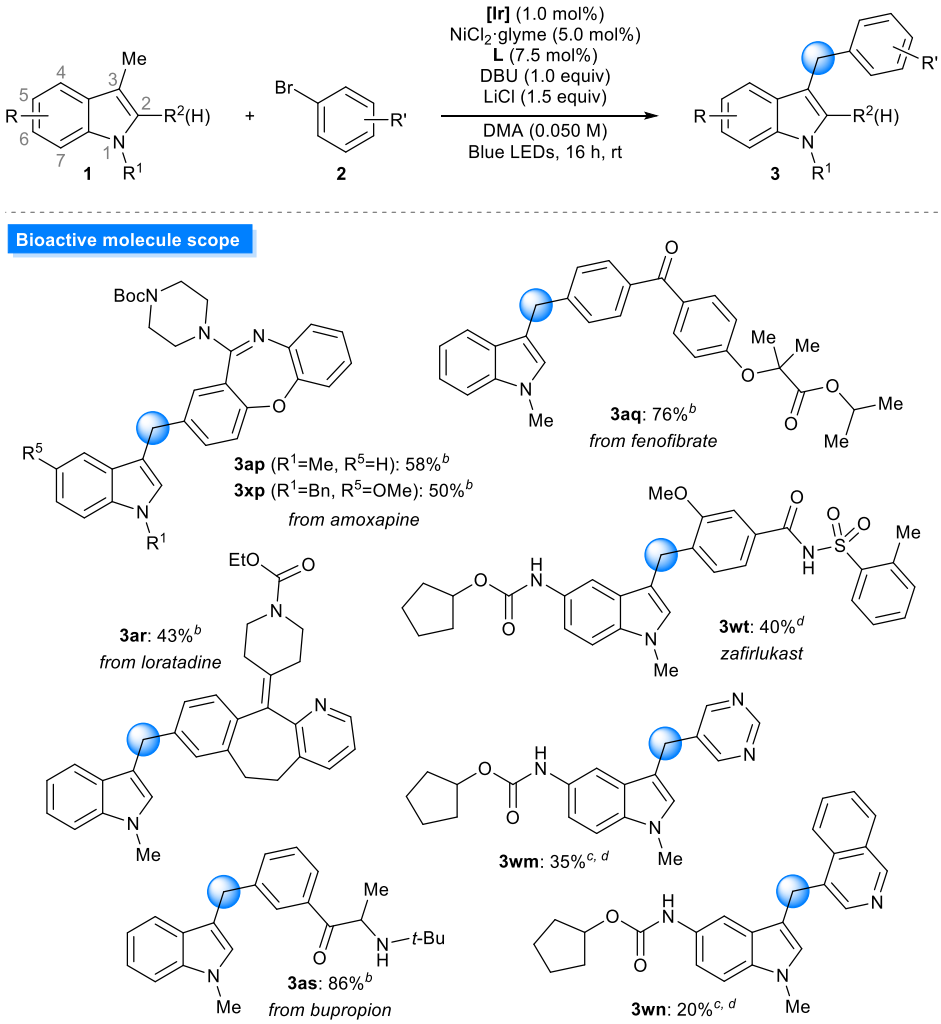

[a] Reaction conditions: **1** (0.30 mmol), **2** (0.20 mmol), **[Ir]** (1.0 mol%), $NiCl_2$·glyme (5.0 mol%), **L** (7.5 mol%), DBU (0.20 mmol), LiCl (0.30 mmol), and DMA (0.050 M) irradiated with 34 W blue LEDs. All yields are isolated yields. [b] $NiCl_2$·glyme (10.0 mol%), 4,4'-dimethoxy-2,2'-bipyridine (15.0 mol%), DMA (0.033 M), and ArCl instead of ArBr. [c] The reaction was conducted at 53 °C. [d] $NiCl_2$·glyme (10.0 mol%), **L** (15.0 mol%), and DMA (0.033 M). **[Ir]**=$Ir(dFCF_3ppy)_2(dtbbpy)PF_6$. dtbbpy= 4,4'-di-*tert*-butyl-2,2'-bipyridine. **L**=1,10-phenanthroline. DMA=*N*,*N*-dimethylacetamide. N.D.=not detected.

The strength of the developed strategy was further illustrated by applying this method to the preparation of derivatives of bioactive molecules (Table 2.4). Commercial drug molecules, containing a C-halogen bond, could be successfully employed as an aryl donor, demonstrating the robustness of the protocol (**3ap**–**3as**, **3xp**). In addition, a novel synthetic pathway could be devised for the preparation of the complex drug molecule zafirlukast, which enabled late-stage unification of two parts of comparable complexity (**3wt**).[19] Indeed, this strategy could be extended further to the facile preparation of zafirlukast derivatives using readily available aryl halides (**3wm**–**3wn**).

2.2.5 Mechanistic investigations

We then examined the mechanistic aspects of the transformation to investigate the potential involvement of HAT processes based on the generation of halogen radicals. First, the contribution of metal halide additive (*i.e.*, LiCl) was examined by a Giese addition experiment (Scheme 2.3A).[20] When the radical generation was attempted in the presence of a radical acceptor, the efficiency of the addition process was not affected by the presence of LiCl. Also, a fluorescence quenching study of the reaction system showed that LiCl is not the major electron transfer partner of the photocatalyst.[21] Thus, it was concluded that LiCl was not involved in radical formation. Second, the possibility of the Ni-halide complex initiating radical formation was analyzed (Scheme 2.3B).[7b,7c,22] Upon exposure to the indole substrate and the photoredox system, an independently prepared Ni(II) aryl halide complex (**[Ni-1]**) failed to deliver the expected arylation product (**3ad**). This result indicated

that potential radical generation via HAT from the Ni complex did not lead to the desired pathway of product formation.

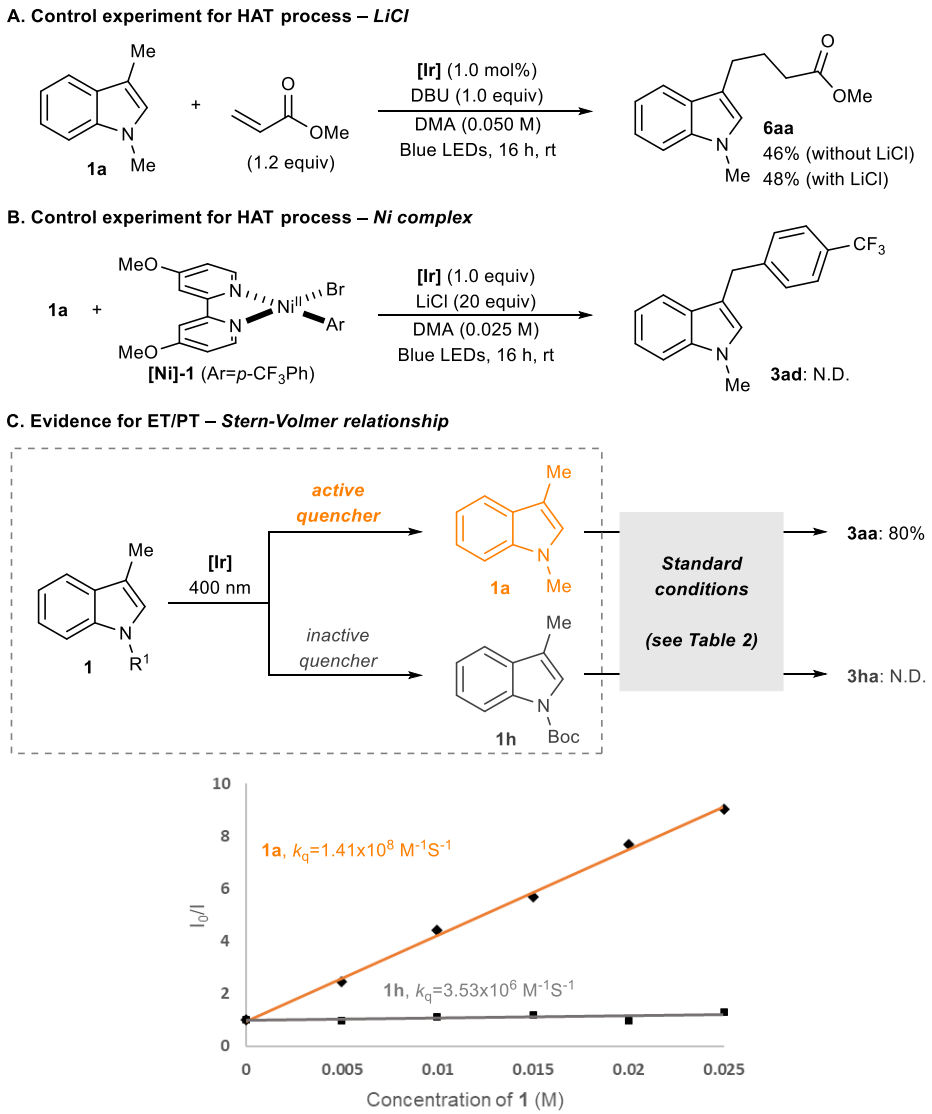

Scheme 2.3 Mechanistic studies

Further insight could be gained from the dependence of the reaction outcome on the electronic nature of the substrates (Scheme 2.3C). Under the standard conditions, an electron-deficient indole substrate (**1h**), in stark contrast to the case of an electron-rich substrate (**1a**), showed virtually no reactivity towards arylation. In case a HAT process is operating, a comparable product yield should be observed, since the cross-coupling step is not significantly sensitive to the electronic properties of the arene substrate.[23] Therefore, it is concluded that a HAT-driven radical generation is not predominantly involved in the overall transformation. This hypothesis was corroborated by a Stern–Volmer analysis of the indole substrates. The strong correlation between product yield and degree of fluorescence quenching suggested the involvement of the ET/PT-based process.

2.2.6 Proposed reaction mechanism

Based on the assembled information, a plausible catalytic cycle was proposed (Figure 2.1). Initially, visible-light irradiation of the **[Ir^{III}]** photocatalyst generates a potent excited-state oxidant **[Ir^{III}]*** (E^*_{red} = +1.25 V vs. Ag/AgCl in MeCN), which can oxidize the indole **1a** (E_{ox} = +1.00 V vs. Ag/AgCl in MeCN). The resulting radical cation (**I**) can be rapidly deprotonated to form the key benzylic radical intermediate (**II**). At this point, two possible downstream sequences of the radical intermediate to engage the Ni-based catalytic cycle were considered.[24] In the path A, radical **II** can be intercepted by the ligand-bound Ni^0 species (**III**) to generate an alkyl-Ni intermediate (**IV**), which in turn can afford a Ni^{III} complex (**V**) via oxidative addition with an aryl halide. In the alternative route (path B), the radical addition is taking place to a Ni^{II} intermediate (**VII**), which is formed by direct oxidative addition

of ligand-bound Ni^0 species (**III**). Our mechanistic experiment suggests that a Ni^{II} complex, such as **VII**, is unlikely to be involved in the catalytic cycle: an independently prepared Ni^{II} oxidative addition complex (**[Ni]-1**, Scheme 2.3B) does not provide any of the desired cross-coupling product under the radical-generating conditions.[25] Furthermore, it has been shown that the $Ni^0/Ni^I/Ni^{III}$ pathway (path A) is energetically more favored over the $Ni^0/Ni^{II}/Ni^{III}$ pathway (path B) in related systems.[26] Therefore, path B was excluded from further considerations. Finally, subsequent reductive elimination from the Ni^{III} complex (**V**) should furnish the desired product and a Ni^I–Br species (**VI**, $E_{red} = -1.10$ V vs. Ag/AgCl in DMF)[27] which after single electron transfer by **[Ir^{II}]** ($E_{red} = -1.32$ V vs. Ag/AgCl in MeCN) will resume the dual catalytic cycle.

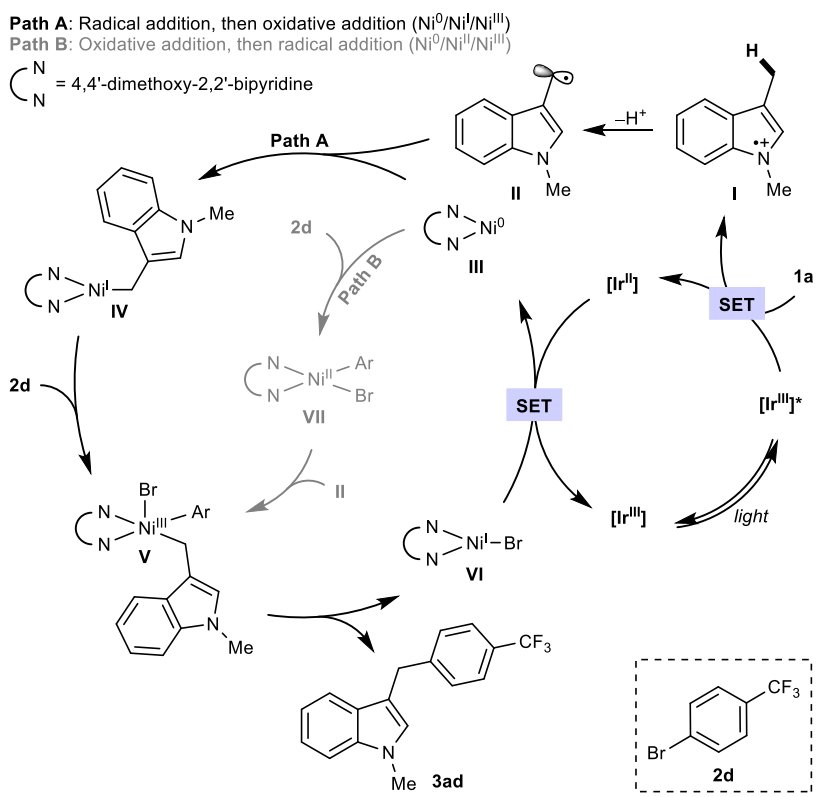

Figure 2.1 Proposed reaction mechanism

2.2.7 Substrate scope of symmetric acid anhydrides

The developed reactivity could be further extended to the Ni-catalyzed acylation reaction using a symmetric acid anhydride as the acyl source (Table 2.5).[28] Under slightly modified conditions involving the photocatalytic system, a Ni source, a bidentate ligand, and an inorganic base, *N*-alkyl indole derivatives underwent facile acylation reactions at the benzylic position.[29] The strictly halide-free conditions further supported the involvement of the ET/PT process instead of HAT during radical generation. Acyl groups based on a variety of alkyl (**5ca**–**5cd**), aryl (**5ce** and **5cf**), and alkenyl (**5cg**) groups were successfully installed. Analogously to the arylation reaction, synthetically useful yields could be obtained without the use of a glovebox when the standard Schlenk technique was applied or even when the reaction was carried out under ambient conditions (93% and 76% yield for **5cb**, respectively). Moreover, the addition of an aryl substituent at the C2 position, which can pose significant steric congestion at the reaction center, did not affect reaction efficiency (**5sb**). Interestingly, a 3-ethyl indole derivative also underwent a facile acylation, furnishing a methine moiety at C3 (**5yb**). Furthermore, substrates containing a heteroatom-based substituent (**5zb**) or an allyl group (**5zab**) exhibited excellent reactivities towards the acylation reaction, demonstrating the pronounced robustness and chemoselectivity of the developed method, respectively.[30] The protocol was also applied to the acylation of a 2-methyl indole derivative (**5zbb**). Finally, when multiple positions were available for acylation, a mixture of regioisomeric products was obtained (**5zcb**).[31]

Table 2.5 Substrate scope of symmetric acid anhydrides[a]

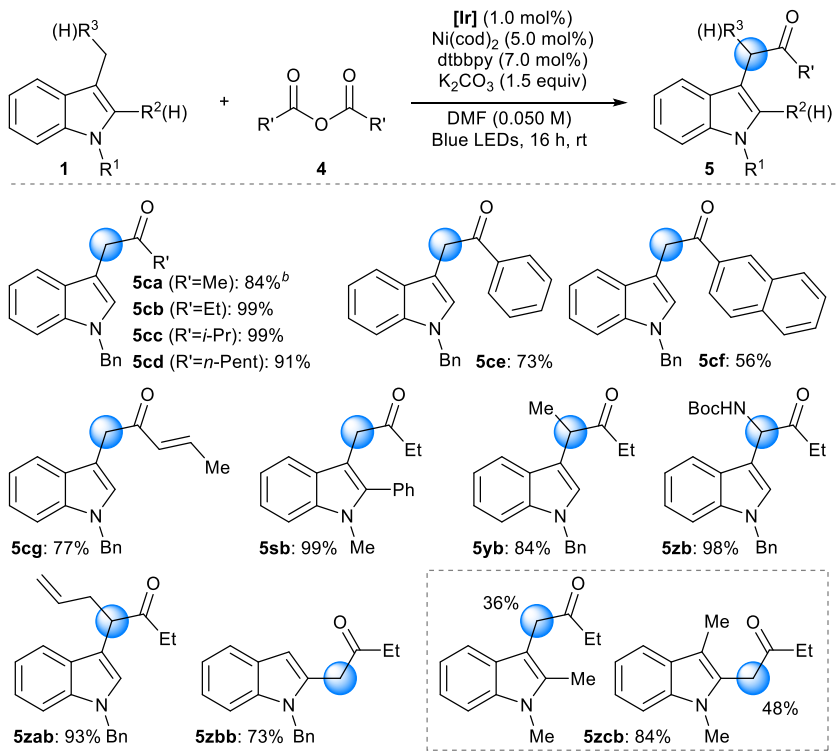

[a] Reaction conditions: **1** (0.20 mmol), **4** (0.24 mmol), **[Ir]** (1.0 mol%), $Ni(cod)_2$ (5.0 mol%), dtbbpy (7.0 mol%), K_2CO_3 (0.30 mmol), and DMF (0.050 M) irradiated with 34 W blue LEDs. All yields are isolated yields. [b] The reaction was conducted in the absence of K_2CO_3. **[Ir]**=$Ir(dFCF_3ppy)_2(dtbbpy)PF_6$. dtbbpy= 4,4'-di-*tert*-butyl-2,2'-bipyridine. DMF=*N*,*N*-dimethylformamide.

2.3 Conclusion

In conclusion, a novel benzylic C(sp^3)–H functionalization method for indoles, introducing C(sp^2)-based functional groups, has been developed. This process is an outcome of the unprecedented combination of Ni catalysis and ET/PT-driven radical generation under photoredox conditions. The reaction exhibited extremely high efficiency under mild conditions, and was therefore applicable to the preparation of

a wide range of indole products including complex drug molecule derivatives. Based on mechanistic investigations, it is evident that a conventionally employed HAT process was not involved in product formation. Rather, only the ET/PT process functioned as the major pathway. This distinct mechanistic pathway provides remarkable selectivity towards the activation of indole-derived benzylic C–H bonds over others. It is believed that the underdeveloped orchestration of ET/PT-controlled radical generation and other types of transition metal catalysis should provide a mild, robust, and efficient activation strategy for inert benzylic C(sp^3)–H bonds. Moreover, the scope of the applicability should be expanded to other settings with the development of more efficient and selective arene oxidation protocols.

2.4 Experimental section

2.4.1 General experimental details

Unless otherwise noted, all reactions were performed under inert conditions. Analytical TLC was performed on a Merck 60 F254 silica gel plates (0.25mm thickness), and visualized either using UV light (254 nm) or by staining with potassium permanganate and heating. Column chromatography was performed on Merck 60 silica gel (230–400 mesh). NMR spectroscopy experiments were conducted with a Varian 400 and 500 MHz or a Bruker 300 MHz system. Gas chromatography (GC) was carried out using a GC-2030 (Shimadzu) equipped with an Rxi® -5Sil MS column and a flame ionization detector (FID). Liquid chromatography-mass spectrometry (LC-MS) spectra were obtained on an Agilent 6120 Quadrupole LC/MS. NMR spectra were processed with ACD NMR Processor

or MestReNova. Chemical shifts are reported in ppm and referenced to residual solvent peaks ($CHCl_3$ in $CDCl_3$: 7.26 ppm for ^1H, 77.16 ppm for ^{13}C; CH_2Cl_2 in CD_2Cl_2: 5.32 ppm for ^1H, 53.84 ppm for ^{13}C; $(CH_3)_2SO$ in $(CD_3)_2SO$: 2.50 ppm for ^1H, 39.52 ppm for ^{13}C). ^{19}F NMR spectra were calibrated to an external standard of neat $CFCl_3$ (0.0 ppm for ^{19}F). Coupling constants are reported in Hertz. Deuterated compounds were purchased from Cambridge Isotope Laboratories, Inc. All anhydrous solvents and chemicals were purchased from commercial sources (Sigma-Aldrich, Acros, Alfa Aesar, TCI, or Strem) and used without further purification. The iridum-based photocatalyst $Ir[dF(CF_3)ppy]_2(dtbbpy)PF_6$ was synthesized according to literature procedure.[32] 34 W Blue LED lamps purchased from Kessil (Kessil H150 Grow Light-Blue) were used for all the visible light photocatalytic reactions. Cyclic voltammetry was measured using a CH Instruments, CHI620E potentiostat using a three-electrode-cell assembly. High resolution mass spectroscopy (HRMS) analyses were performed by the ultrahigh resolution ESI Q-TOF mass spectrometer at the Organic Chemistry Research Center in Sogang University and the Mass Spectrometry Laboratory of National Instrumentation Center for Environmental Management (NICEM) in Seoul National University. UV–Vis spectra were recorded on an Agilent 8453 UV–Vis spectrophotometer with ChemStation software. Fluorescence spectra were recorded on a Photon Technology International (PTI) QM-400 spectrofluorometer with FelixGX software. The quenching constant (k_q) was determined following the Stern–Volmer relationship.[33]

2.4.2 Substrate preparations

General procedure A[34]

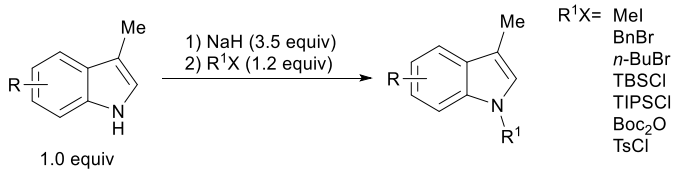

To a stirred solution of NaH (454 mg, 11.3 mmol, 3.5 equiv, 60% suspension in mineral oil) in dry DMF (10 mL), 3-methylindole (425 mg, 3.2 mmol, 1.0 equiv) in DMF (5 mL) was added dropwise at 0℃. The mixture was allowed to warm up to room temperature and stirred for 30 min. After cooling down to 0 ℃, R^1X (3.9 mmol, 1.2 equiv) was added dropwise. The reaction mixture was stirred at room temperature for another 6 h, then quenched by addition of water and extracted with ethyl acetate (10 mL, 3 times). The combined organic layer was washed with brine, dried over anhydrous Na_2SO_4, and concentrated under reduced pressure. The residue was purified by column chromatography on silica gel to give the corresponding compounds.

General procedure B[35]

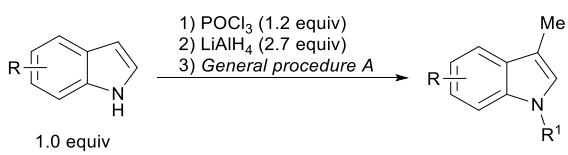

1) Phosphorus oxychloride (0.56 mL, 6.0 mmol, 1.2 equiv) was added dropwise to DMF (20 mL) with an ice-bath. The mixture was stirred for 5 min then added to a

solution of *1H*-indole (5.0 mmol, 1.0 equiv) in DMF (10 mL) at 0 ℃. The mixture was then warm to room temperature and stirred for 30 min. The reaction became a heavy suspension that required vigorous stirring. 5.0 M aqueous potassium hydroxide was added until pH>9 and the mixture was heated at 100 ℃ for 2 h. The resulting suspension was cooled down to 0 ℃, the precipitate was filtered off, washed with water then dried under vacuum overnight and used in the next step without further purification.

2) To a suspension of $LiAlH_4$ (0.50 g, 13 mmol, 2.7 equiv) in THF (55 mL) at 0 ℃ under the argon atmosphere was added previously synthesized 3-formyl-*1H*-indole (5.0 mmol, 1.0 equiv) over a spatula. The suspension was then warm to room temperature and stirred for 4 h. The reaction was cooled down to 0 ℃, distilled water (0.5 mL) was added dropwise, then 10% aqueous solution of NaOH (0.5 mL) then again H_2O (1.0 mL). The resulting slurry was strirred vigorously for 30 min, diluted with Et_2O and anhydrous $MgSO_4$ was added. The white precipitate was filtered through Celite and then washed with Et_2O. The solvent was removed in vacuo and the product used in the next step without further purification.

3) The crude 3-methyl-*1H*-indole was protected following *General procedure A*. Purification by flash column chromatography led to indoles as the starting materials.

General procedure C[36]

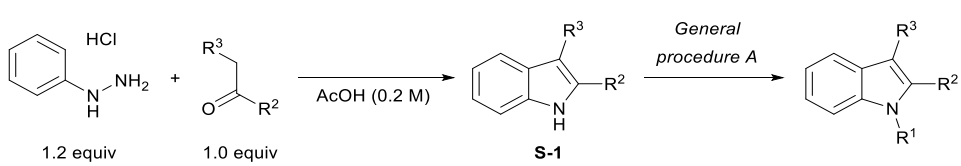

1.2 equiv 1.0 equiv **S-1**

1) The suspension of phenylhydrazine hydrochloride (0.87g, 6.0 mmol, 1.2 equiv) in AcOH (25 mL) was heated at 50 ℃ for 30 min, then the corresponding ketone (5.0 mmol, 1.0 equiv) was added in one portion and the reaction mixture was refluxed for 3 h. After cooling to room temperature, AcOH was removed in vacuo and the residue was dissolved in ethyl acetate. The organic phase was washed with water and brine, dried over anhydrous Na_2SO_4, and concentrated in vacuo to give grey residue, which was purified by flash chromatography on silica gel to afford the **S-1**.

2) Synthesized indole, in the previous step, was protected according to *General procedure A*. Purification by flash column chromatography led to indoles as the starting materials.

2.4.3 Characterization data of substrates

Previously reported *N*-protected indoles (**1a**,[37] **1c**,[37] **1d**,[38] **1f**,[39] **1g**,[40] **1h**,[41] **1i**,[42] **1j**,[43] **1l**,[44] **1m**,[45] **1p**,[37] **1r**,[37] **1s**,[46] **1t**,[47] **1v**,[48] **1x**,[49] **1y**,[38] **1za**,[50] **1zb**,[51] **1zc**,[48] **6aa**[52]) were characterized by spectral comparison with literature data. New *N*-protected indoles (**1e**, **1k**, **1n**, **1o**, **1q**, **1u**, **1w**, **1z**, **D-1a**) and aryl halides (**2t**) were characterized by ^{1}H NMR, ^{13}C NMR, ^{19}F NMR. The **[Ni]-1**,[53] **3wt**[54] was confirmed by ^{1}H NMR and ^{19}F NMR spectral comparison with literature data, while the new products were characterized by ^{1}H NMR, ^{13}C NMR, ^{19}F NMR and HRMS-ESI.

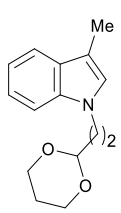

1-(2-(1,3-Dioxan-2-yl)ethyl)-3-methyl-1*H*-indole (**1e**)

Following the general procedure A, compound **1e** was prepared from 3-methylindole and 2-(2-bromoethyl)-1,3-dioxane as R^1X.

^{1}H NMR (500 MHz, $CDCl_3$) δ 7.80 (1H, d, *J* 7.8), 7.53 (1H, d, *J* 8.2), 7.42 (1H, t, *J* 7.6), 7.33 (1H, t, *J* 7.4), 7.01 (1H, s), 4.52 (1H, t, *J* 5.2), 4.35 (2H, t, *J* 6.9), 4.23 (2H, dd, *J* 11.8, 4.9), 3.76 (2H, t, *J* 12.1), 2.56 (3H, s), 2.30 – 2.15 (3H, m), 1.38 (1H, d, *J* 13.5) ppm. ^{13}C NMR (126 MHz, $CDCl_3$) δ 136.28, 128.64, 125.32, 121.32, 118.84, 118.45, 110.17, 109.17, 99.45, 66.57, 40.75, 35.67, 25.63, 9.55 ppm.

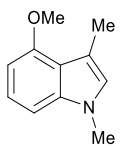

4-Methoxy-1,3-dimethyl-1*H*-indole (**1k**)

Following the general procedure B, compound **1k** was prepared from 4-methoxyindole and iodomethane as R^1X.

^{1}H NMR (400 MHz, $CDCl_3$) δ 7.12 (1H, t, *J* 8.0), 6.89 (1H, d, *J* 8.2), 6.68 (1H, s), 6.48 (1H, d, *J* 7.7), 3.93 (3H, s), 3.69 (3H, s), 2.49 (3H, s) ppm. ^{13}C NMR (101 MHz, $CDCl_3$) δ 155.39, 138.93, 125.35, 122.35, 118.36, 110.75, 102.64, 98.95, 55.33, 32.77, 12.13 ppm.

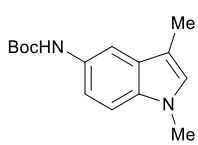

tert-Butyl (1,3-dimethyl-1*H*-indol-5-yl)carbamate (**1n**)

Compound **1n** was prepared following slightly modified literature procedures using 5-nitro-1*H*-indole.[35, 55]

^{1}H NMR (500 MHz, $CDCl_3$) δ 7.64 (1H, s), 7.17 (1H, d, *J* 8.7), 7.09 (1H, d, *J* 8.2), 6.80 (1H, s), 6.50 (1H, s), 3.69 (3H, s), 2.29 (3H, s), 1.55 (9H, s) ppm. ^{13}C NMR (126 MHz, $CDCl_3$) δ 153.70, 134.24, 130.13, 128.93, 127.45, 115.18, 110.15, 109.88, 109.21, 79.97, 32.68, 28.60, 9.67 ppm.

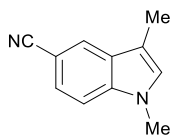

1,3-Dimethyl-1*H*-indole-5-carbonitrile (**1o**)

Compound **1o** was prepared following slightly modified literature procedures using 5-bromo-1,3-dimethyl-1*H*-indole (**1p**).[54]

^{1}H NMR (500 MHz, $CDCl_3$) δ 7.87 (1H, s), 7.40 (1H, dd, *J* 8.5, 1.2), 7.28 (1H, d, *J* 8.5), 6.93 (1H, s), 3.75 (3H, s), 2.31 (3H, s) ppm. ^{13}C NMR (126 MHz, $CDCl_3$) δ 138.45, 128.81, 128.51, 124.67, 124.36, 121.19, 111.50, 109.88, 101.44, 32.79, 9.36 ppm.

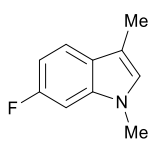

6-Fluoro-1,3-dimethyl-1*H*-indole (**1q**)

Following the general procedure B, compound **1q** was prepared from 6-fluoroindole and iodomethane as R^1X.

^{1}H NMR (500 MHz, $CDCl_3$) δ 7.50 (1H, dd, *J* 8.6, 5.3), 6.98 (1H, dd, *J* 10.0, 2.2), 6.91 (1H, ddd, *J* 9.7, 8.7, 2.3), 6.83 – 6.79 (1H, m), 3.69 (3H, s), 2.35 (3H, s) ppm. ^{13}C NMR (126 MHz, $CDCl_3$) δ 160.13 (d, $J_{C–F}$ 237.0), 137.14 (d, $J_{C–F}$ 12.2), 126.89 (dd, $J_{C–F}$ 3.5), 125.39, 119.77 (d, $J_{C–F}$ 10.3), 110.52, 107.25 (d, $J_{C–F}$ 24.6), 95.47 (d, $J_{C–F}$ 26.1), 32.62, 9.60 ppm. ^{19}F NMR (376 MHz, $CDCl_3$) δ –121.59 ppm.

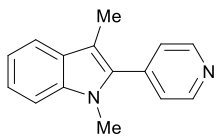

1,3-Dimethyl-2-(pyridin-4-yl)-1*H*-indole (**1u**)

Following the general procedure C, compound **1u** was prepared from phenylhydrazine hydrochloride, 4-propionylpyridine, and iodomethane as R^1X.

^{1}H NMR (500 MHz, $CDCl_3$) δ 8.75 (2H, d, *J* 5.7), 7.65 (1H, d, *J* 7.9), 7.38 – 7.30 (4H, m), 7.20 (1H, t, *J* 7.3), 3.66 (3H, s), 2.36 (3H, s) ppm. ^{13}C NMR (126 MHz, $CDCl_3$) δ 149.85, 140.18, 138.00, 134.60, 128.36, 125.04, 122.90, 119.65, 119.35, 110.73, 109.57, 31.27, 9.49 ppm.

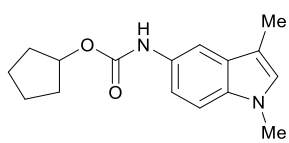

Cyclopentyl (1,3-dimethyl-1*H*-indol-5-yl)carbamate (**1w**)

Compound **1w** was prepared following slightly modified literature procedures using 5-nitro-1*H*-indole.[35, 57]

^{1}H NMR (500 MHz, $CDCl_3$) δ 7.67 (1H, s), 7.17 (1H, d, *J* 8.6), 7.11 (1H, d, *J* 7.9), 6.80 (1H, s), 6.60 (1H, s), 5.33 – 5.18 (1H, m), 3.69 (3H, s), 2.29 (3H, s), 1.96 – 1.87

(2H, m), 1.84 – 1.71 (4H, m), 1.68 – 1.58 (2H, m) ppm. ^{13}C NMR (126 MHz, $CDCl_3$) δ 154.40, 134.30, 129.87, 128.90, 127.49, 115.10, 110.14, 109.80, 109.22, 77.81, 32.95, 32.65, 23.82, 9.60 ppm.

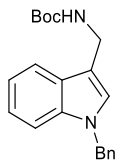

tert-Butyl ((1-benzyl-1*H*-indol-3-yl)methyl)carbamate (**1z**)

Compound **1z** was prepared following slightly modified literature procedures using Indole-3-carboxaldehyde.[58-59]

^{1}H NMR (500 MHz, $CDCl_3$) δ 7.67 (1H, d, *J* 7.8), 7.33 – 7.25 (4H, m), 7.24 – 7.17 (1H, m), 7.17 – 7.09 (3H, m), 7.07 (1H, s), 5.28 (2H, s), 4.49 (2H, s), 1.47 (9H, s) ppm. ^{13}C NMR (126 MHz, DMSO-d_6) δ 155.61, 138.31, 136.11, 128.47, 127.29, 127.22, 127.09, 126.99, 121.29, 119.15, 118.68, 113.13, 110.06, 77.46, 48.88, 35.19, 28.29 ppm.

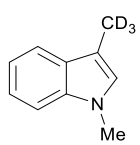

1-Methyl-3-(methyl-*d*$_3$)-1*H*-indole (**D-1a**)

Following the general procedure B, compound **D-1a** was prepared from indole, DMF-d_7 instead of DMF, $LiAlD_4$ instead of $LiAlH_4$, and iodomethane as R^1X.

^{1}H NMR (400 MHz, $CDCl_3$) δ 7.66 (1H, d, *J* 8.6), 7.33 (2H, dt, *J* 14.2, 7.7), 7.22 – 7.17 (1H, m), 6.88 (1H, s), 3.78 (3H, s) ppm. ^{13}C NMR (101 MHz, $CDCl_3$) δ 137.10,

128.78, 126.63, 121.50, 119.04, 118.59, 110.05, 109.09, 32.53, 8.88 (hept, *J* 19.4) ppm.

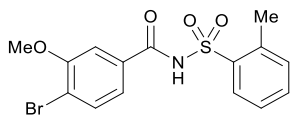

4-Bromo-3-methoxy-*N*-(*o*-tolylsulfonyl)benzamide (**2t**)

Compound **2t** was prepared following slightly modified literature procedures using methyl 4-bromo-3-hydroxybenzoate.[54, 60]

^{1}H NMR (500 MHz, DMSO-d$_6$) δ 8.00 (1H, dd, *J* 7.9, 1.4), 7.63 (1H, d, *J* 8.2), 7.58 (1H, d, *J* 1.9), 7.49 – 7.41 (2H, m), 7.36 (1H, td, *J* 7.7, 1.4), 7.31 (1H, d, *J* 7.5), 3.88 (3H, s), 2.59 (3H, s) ppm. ^{13}C NMR (126 MHz, DMSO-d$_6$) δ 165.92, 155.09, 140.23, 136.46, 135.40, 132.60, 131.99, 131.75, 129.56, 125.57, 121.89, 114.85, 111.90, 56.25, 19.75 ppm.

2.4.4 General procedure for arylation and acylation

General procedure D: Arylation of indole

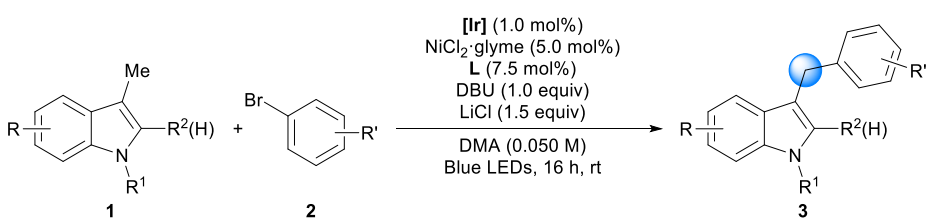

The reaction was set up in a nitrogen-filled glove box. To an 8 mL vial equipped with a PTFE-coated stirrer bar was added the corresponding indole **1** (0.30 mmol, 1.5 equiv), Ir[dF(CF$_3$)ppy]$_2$(dtbbpy)PF$_6$ (2.2 mg, 0.0020 mmol, 1.0 mol%),

$NiCl_2$·glyme (2.2 mg, 0.010 mmol, 5.0 mol%), 1,10-phenanthroline (2.7 mg, 0.015 mmol, 7.5 mol%), DBU (30 µL, 0.20 mmol, 1.0 equiv), LiCl (12.7 mg, 0.30 mmol, 1.5 equiv), aryl halide **2** (0.20 mmol, 1.0 equiv), and DMA (4.0 mL). The reaction vial was removed from the glove box, stirred for 16 h under 34 W blue LED irradiation with fan cooling. At the end of the reaction, the resulting solution was transferred to a separatory funnel and partitioned between water (7 mL) and Et_2O (20 mL). The organic extract was washed with water (7 mL x 2) and brine (7 mL), dried over $MgSO_4$, filtered and concentrated under reduced pressure. Purification by flash column chromatography provided the arylated indoles as the desired products.

General procedure E: Acylation of indole

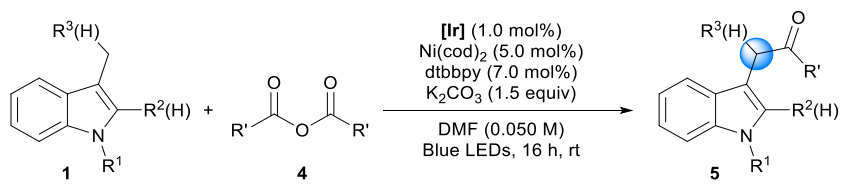

The reaction was set up in a nitrogen-filled glove box. To an 8 mL vial equipped with a PTFE-coated stirring bar was added the corresponding indole **1** (0.20 mmol, 1.0 equiv), $Ir[dF(CF_3)ppy]_2(dtbbpy)PF_6$ (2.2 mg, 0.0020 mmol, 1.0 mol%), $Ni(cod)_2$ (2.8 mg, 0.010 mmol, 5.0 mol%), 4,4'-di-tert-butyl-2,2'-bipyridine (3.8 mg, 0.014 mmol, 7.0 mol%), K_2CO_3 (42 mg, 0.30 mmol, 1.5 equiv), acid anhydride **4** (0.24 mmol, 1.2 equiv) and DMF (4.0 mL). The reaction vial was removed from the glove box, stirred for 16 h under 34 W blue LED irradiation with fan cooling. At the end of the reaction, the resulting solution was transferred to a separatory funnel and partitioned between water (7 mL) and Et_2O (20 mL). The organic extract was washed

with water (7 mL x 2) and brine (7 mL), dried over $MgSO_4$, filtered and concentrated under reduced pressure. Purification by flash column chromatography provided the acylated indoles as the desired products.

2.4.5 Characterization data

Characterization data of arylation products

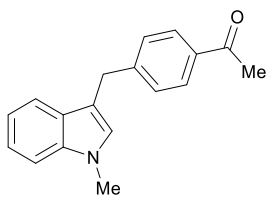

1-(4-((1-Methyl-1*H*-indol-3-yl)methyl)phenyl)ethan-1-one (**3aa**)

^{1}H NMR (400 MHz, $CDCl_3$) δ 7.89 (2H, d, *J* 8.2), 7.49 (1H, d, *J* 7.9), 7.39 (2H, d, *J* 8.1), 7.32 (1H, d, *J* 8.2), 7.25 (1H, t, *J* 7.3), 7.10 (1H, t, *J* 7.2), 6.80 (1H, s), 4.18 (2H, s), 3.76 (3H, s), 2.59 (3H, s) ppm. ^{13}C NMR (101 MHz, $CDCl_3$) δ 197.97, 147.39, 137.29, 135.23, 128.93, 128.64, 127.75, 127.33, 121.86, 119.14, 119.06, 113.21, 109.37, 32.73, 31.70, 26.66 ppm. HRMS (ESI): m/z $[M+Na]^+$ calcd for $C_{18}H_{17}NNaO$: 286.1202, found: 286.1202.

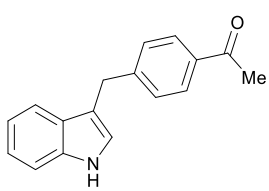

1-(4-((1*H*-Indol-3-yl)methyl)phenyl)ethan-1-one (**3ba**)

^{1}H NMR (500 MHz, DMSO-d_6) δ 10.89 (1H, s), 7.88 – 7.82 (2H, m), 7.37 (4H, m), 7.20 (1H, s), 7.04 (1H, t, *J* 7.5), 6.92 (1H, t, *J* 7.5), 4.11 (2H, s), 2.52 (3H, s) ppm. ^{13}C NMR (126 MHz, DMSO-d_6) δ 197.44, 147.59, 136.40, 134.63, 128.62, 128.27, 126.85, 123.35, 121.00, 118.42, 118.35, 112.93, 111.43, 31.02, 26.58 ppm. HRMS (ESI): m/z $[M+Na]^+$ calcd for $C_{17}H_{15}NNaO$: 272.1046, found: 272.1046.

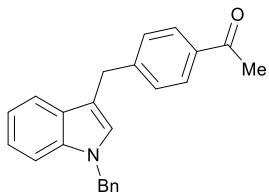

1-(4-((1-Benzyl-1*H*-indol-3-yl)methyl)phenyl)ethan-1-one (**3ca**)

^{1}H NMR (400 MHz, $CDCl_3$) δ 7.91 – 7.83 (2H, m), 7.51 – 7.44 (1H, m), 7.36 (2H, d, *J* 8.0), 7.34 – 7.23 (4H, m), 7.17 (1H, ddd, *J* 8.3, 6.9, 1.2), 7.12 – 7.02 (3H, m), 6.87 (1H, s), 5.25 (2H, s), 4.16 (2H, s), 2.55 (3H, s) ppm. ^{13}C NMR (126 MHz, $CDCl_3$) δ 197.95, 147.23, 137.68, 136.96, 135.22, 128.91, 128.84, 128.64, 128.02, 127.67, 126.81, 126.73, 122.07, 119.33, 119.28, 113.85, 109.87, 49.99, 31.73, 26.64 ppm. HRMS (ESI): m/z $[M+Na]^+$ calcd for $C_{24}H_{21}NNaO$: 362.1515, found: 362.1515.

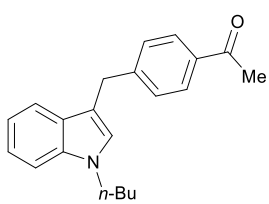

1-(4-((1-Butyl-1*H*-indol-3-yl)methyl)phenyl)ethan-1-one (**3da**)

^{1}H NMR (500 MHz, $CDCl_3$) δ 7.89 (2H, d, *J* 8.1), 7.48 (1H, d, *J* 7.9), 7.39 (2H, d, *J* 8.1), 7.35 (1H, d, *J* 8.2), 7.22 (1H, t, *J* 7.6), 7.08 (1H, t, *J* 7.4), 6.86 (1H, s), 4.18 (2H,

s), 4.08 (2H, t, *J* 7.1), 2.59 (3H, s), 1.82 (2H, p, *J* 7.3), 1.36 (2H, h, *J* 7.5), 0.96 (3H, t, *J* 7.4) ppm. ^{13}C NMR (126 MHz, $CDCl_3$) δ 197.94, 147.46, 136.68, 135.29, 128.95, 128.64, 127.89, 126.32, 121.69, 119.23, 118.98, 113.10, 109.57, 46.09, 32.49, 31.77, 26.61, 20.32, 13.81 ppm. HRMS (ESI): m/z $[M+Na]^+$ calcd for $C_{21}H_{23}NNaO$: 328.1672, found: 328.1672.

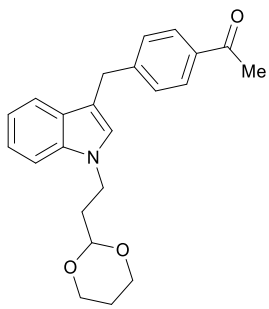

1-(4-((1-(2-(1,3-Dioxan-2-yl)ethyl)-1*H*-indol-3-yl)methyl)phenyl)ethan-1-one (**3ea**)

^{1}H NMR (400 MHz, $CDCl_3$) δ 7.88 (2H, d, *J* 8.2), 7.47 (1H, d, *J* 7.9), 7.40 – 7.33 (3H, m), 7.21 (1H, t, *J* 7.6), 7.07 (1H, t, *J* 7.5), 6.81 (1H, s), 4.37 (1H, t, *J* 5.2), 4.21 (2H, t, *J* 6.9), 4.16 (2H, s), 4.09 (2H, dd, *J* 10.8, 5.0), 3.66 (2H, td, *J* 12.4, 2.3), 2.58 (3H, s), 2.07 (2H, q, *J* 7.0), 1.33 (1H, d, *J* 13.5), 1.26 (1H, s) ppm. ^{13}C NMR (101 MHz, $CDCl_3$) δ 198.02, 147.39, 136.64, 135.25, 128.98, 128.67, 127.82, 126.38, 121.88, 119.18, 119.09, 113.56, 109.66, 99.68, 66.95, 41.20, 35.72, 31.77, 26.71, 25.83 ppm. HRMS (ESI): m/z $[M+Na]^+$ calcd for $C_{23}H_{25}NNaO_3$: 386.1727, found: 386.1727.

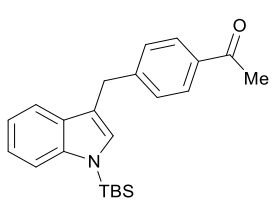

1-(4-((1-(*tert*-Butyldimethylsilyl)-1*H*-indol-3-yl)methyl)phenyl)ethan-1-one (**3fa**)

^{1}H NMR (400 MHz, $CDCl_3$) δ 7.87 (2H, d, *J* 8.2), 7.50 (1H, d, *J* 8.3), 7.41 (1H, d, *J* 7.8), 7.36 (2H, d, *J* 8.3), 7.15 (1H, t, *J* 7.6), 7.06 (1H, t, *J* 7.4), 6.96 (1H, s), 4.16 (2H, s), 2.57 (3H, s), 0.93 (9H, s), 0.59 (6H, s) ppm. ^{13}C NMR (101 MHz, $CDCl_3$) δ 198.08, 147.27, 141.81, 135.24, 130.81, 129.35, 128.89, 128.65, 121.74, 119.65, 119.07, 116.33, 114.14, 31.83, 26.70, 26.46, 19.65, –3.78 ppm. HRMS (ESI): m/z $[M+Na]^+$ calcd for $C_{23}H_{29}NNaOSi$: 386.1911, found: 386.1911.

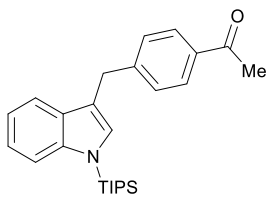

1-(4-((1-(Triisopropylsilyl)-1*H*-indol-3-yl)methyl)phenyl)ethan-1-one (**3ga**)

^{1}H NMR (400 MHz, $CDCl_3$) δ 7.89 (2H, d, *J* 8.1), 7.51 (1H, d, *J* 8.3), 7.43 (1H, d, *J* 7.7), 7.36 (2H, d, *J* 8.0), 7.16 (1H, t, *J* 7.5), 7.07 (1H, t, *J* 7.4), 7.03 (1H, s), 4.19 (2H, s), 2.58 (3H, s), 1.70 (3H, p, *J* 7.5), 1.16 (18H, d, *J* 7.5) ppm. ^{13}C NMR (101 MHz, $CDCl_3$) δ 198.08, 147.36, 141.65, 135.18, 130.85, 129.58, 128.86, 128.63, 121.71, 119.59, 118.93, 116.19, 114.15, 31.82, 26.69, 18.26, 12.93 ppm. HRMS (ESI): m/z $[M+Na]^+$ calcd for $C_{26}H_{35}NNaOSi$: 428.2380, found: 428.2380.

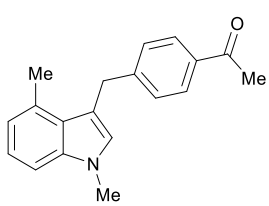

1-(4-((1,4-Dimethyl-1*H*-indol-3-yl)methyl)phenyl)ethan-1-one (**3ja**)

^{1}H NMR (500 MHz, $CDCl_3$) δ 7.89 (2H, d, *J* 8.2), 7.31 (2H, d, *J* 8.1), 7.19 – 7.10 (2H, m), 6.83 (1H, d, *J* 6.8), 6.68 (1H, s), 4.35 (2H, s), 3.73 (3H, s), 2.59 (3H, s), 2.53 (3H, s) ppm. ^{13}C NMR (126 MHz, $CDCl_3$) δ 197.99, 148.22, 137.90, 135.29, 131.09, 128.87, 128.65, 128.19, 126.50, 122.02, 120.76, 113.35, 107.30, 33.41, 32.82, 26.64, 20.19 ppm. HRMS (ESI): m/z $[M+Na]^+$ calcd for $C_{19}H_{19}NNaO$: 300.1359, found: 300.1359.

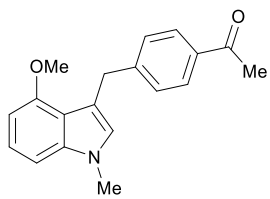

1-(4-((4-Methoxy-1-methyl-1*H*-indol-3-yl)methyl)phenyl)ethan-1-one (**3ka**)

^{1}H NMR (500 MHz, $CDCl_3$) δ 7.88 (2H, d, *J* 8.2), 7.38 (2H, d, *J* 8.2), 7.13 (1H, t, *J* 8.0), 6.90 (1H, d, *J* 8.2), 6.58 (1H, s), 6.48 (1H, d, *J* 7.8,), 4.32 (2H, s), 3.84 (3H, s), 3.69 (3H, s), 2.58 (3H, s) ppm. ^{13}C NMR (126 MHz, $CDCl_3$) δ 198.10, 155.01, 148.92, 138.98, 134.93, 129.06, 128.45, 126.03, 122.68, 117.71, 113.90, 102.72, 99.37, 55.14, 33.12, 32.90, 26.62 ppm. HRMS (ESI): m/z $[M+Na]^+$ calcd for $C_{19}H_{19}NNaO_2$: 316.1308, found: 316.1308.

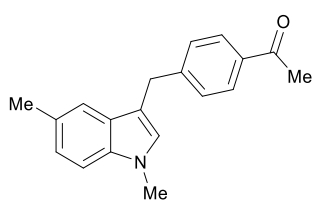

1-(4-((1,5-Dimethyl-1*H*-indol-3-yl)methyl)phenyl)ethan-1-one (**3la**)

^{1}H NMR (400 MHz, $CDCl_3$) δ 7.89 (2H, d, *J* 8.2), 7.38 (2H, d, *J* 8.2), 7.27 (1H, s), 7.21 (1H, d, *J* 8.3), 7.07 (1H, d, *J* 8.3), 6.75 (1H, s), 4.14 (2H, s), 3.72 (3H, s), 2.59

(3H, s), 2.44 (3H, s) ppm. ^{13}C NMR (101 MHz, $CDCl_3$) δ 198.02, 147.55, 135.74, 135.19, 128.91, 128.65, 128.30, 127.98, 127.44, 123.49, 118.73, 112.57, 109.10, 32.78, 31.65, 26.68, 21.59 ppm. HRMS (ESI): m/z $[M+Na]^+$ calcd for $C_{19}H_{19}NNaO$: 300.1359, found: 300.1359.

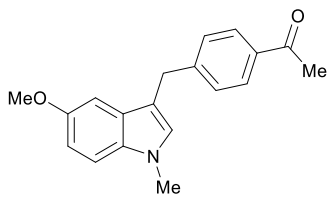

1-(4-((5-Methoxy-1-methyl-1*H*-indol-3-yl)methyl)phenyl)ethan-1-one (**3ma**)

^{1}H NMR (500 MHz, $CDCl_3$) δ 7.89 (2H, d, *J* 8.1), 7.38 (2H, d, *J* 8.1), 7.20 (1H, d, *J* 8.5), 6.90 (2H, d, *J* 8.9), 6.75 (1H, s), 4.12 (2H, s), 3.81 (3H, s), 3.71 (3H, s), 2.58 (3H, s) ppm. ^{13}C NMR (126 MHz, $CDCl_3$) δ 198.02, 153.90, 147.36, 135.22, 132.71, 128.92, 128.66, 128.05, 127.98, 112.61, 111.89, 110.15, 101.14, 56.05, 32.91, 31.70, 26.67 ppm. HRMS (ESI): m/z $[M+Na]^+$ calcd for $C_{19}H_{19}NNaO_2$: 316.1308, found: 316.1308.

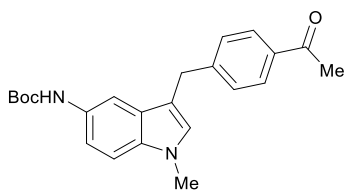

tert-Butyl (3-(4-acetylbenzyl)-1-methyl-1*H*-indol-5-yl)carbamate (**3na**)

^{1}H NMR (500 MHz, $CDCl_3$) δ 7.87 (2H, d, *J* 8.1), 7.49 (1H, s), 7.35 (2H, d, *J* 8.1), 7.20 (2H, d, *J* 8.3), 6.72 (1H, s), 6.48 (1H, s), 4.10 (2H, s), 3.70 (3H, s), 2.57 (3H, s), 1.51 (9H, s) ppm. ^{13}C NMR (126 MHz, $CDCl_3$) δ 197.97, 153.65, 147.35, 135.26, 134.36, 130.57, 128.93, 128.66, 128.11, 127.92, 115.61, 113.12, 109.65, 109.52,

80.04, 32.86, 31.58, 28.54, 26.63 ppm. HRMS (ESI): m/z $[M+Na]^+$ calcd for $C_{23}H_{26}N_2NaO_3$: 401.1836, found: 401.1836.

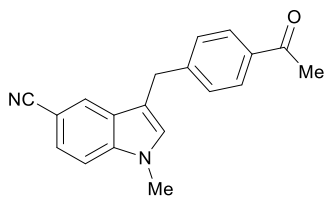

3-(4-Acetylbenzyl)-1-methyl-1*H*-indole-5-carbonitrile (**3oa**)

^1H NMR (500 MHz, $CDCl_3$) δ 7.88 (2H, d, *J* 8.3), 7.77 (1H, s), 7.41 (1H, dd, *J* 8.5, 1.4), 7.33 (3H, d, *J* 8.4), 6.93 (1H, s), 4.12 (2H, s), 3.78 (3H, s), 2.57 (3H, s) ppm. ^{13}C NMR (126 MHz, $CDCl_3$) δ 197.75, 146.12, 138.79, 135.61, 129.56, 128.83, 128.81, 127.53, 124.81, 124.79, 114.61, 110.27, 102.18, 33.00, 31.37, 26.62 ppm. HRMS (ESI): m/z $[M+Na]^+$ calcd for $C_{19}H_{16}N_2NaO$: 311.1155, found: 311.1155.

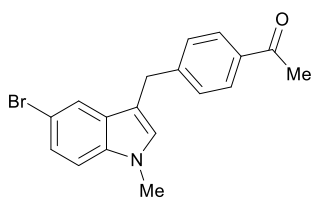

1-(4-((5-Bromo-1-methyl-1*H*-indol-3-yl)methyl)phenyl)ethan-1-one (**3pa**)

^1H NMR (400 MHz, $CDCl_3$) δ 7.88 (2H, d, *J* 8.2), 7.58 (1H, d, *J* 1.8), 7.34 (2H, d, *J* 8.1), 7.29 (1H, dd, *J* 8.7, 1.8), 7.16 (1H, d, *J* 8.7), 6.78 (1H, s), 4.09 (2H, s), 3.72 (3H, s), 2.58 (3H, s) ppm. ^{13}C NMR (101 MHz, $CDCl_3$) δ 198.03, 146.82, 135.95, 135.35, 129.40, 128.86, 128.76, 128.53, 124.70, 121.65, 112.88, 112.54, 110.93, 32.96, 31.46, 26.72 ppm. HRMS (ESI): m/z $[M+Na]^+$ calcd for $C_{18}H_{16}BrNNaO$: 364.0308, found: 364.0307.

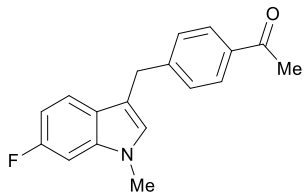

1-(4-((6-Fluoro-1-methyl-1*H*-indol-3-yl)methyl)phenyl)ethan-1-one (**3qa**)

^{1}H NMR (400 MHz, $CDCl_3$) δ 7.89 (2H, d, *J* 8.2), 7.36 (3H, d, *J* 7.9), 6.97 (1H, dd, *J* 9.9, 2.2), 6.84 (1H, td, *J* 9.3, 2.2), 6.78 (1H, s), 4.13 (2H, s), 3.68 (3H, s), 2.58 (3H, s) ppm. ^{13}C NMR (126 MHz, $CDCl_3$) δ 197.84, 160.11 (d, $J_{C–F}$ 237.8), 147.02, 137.43, 137.38 (d, $J_{C–F}$ 12.3), 128.86, 128.64, 127.60 (d, $J_{C–F}$ 3.5), 124.31, 119.90 (d, $J_{C–F}$ 10.3), 113.51, 107.73 (d, $J_{C–F}$ 24.7), 95.75 (d, $J_{C–F}$ 26.1), 32.74, 31.63, 26.56 ppm. ^{19}F NMR (376 MHz, $CDCl_3$) δ –120.79 ppm. HRMS (ESI): m/z $[M+Na]^+$ calcd for $C_{18}H_{16}FNNaO$: 304.1108, found: 304.1108.

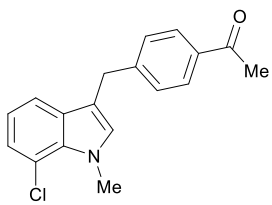

1-(4-((7-Chloro-1-methyl-1*H*-indol-3-yl)methyl)phenyl)ethan-1-one (**3ra**)

^{1}H NMR (400 MHz, $CDCl_3$) δ 7.88 (2H, d, *J* 8.0), 7.33 (3H, t, *J* 7.5), 7.14 (1H, d, *J* 7.6), 6.94 (1H, t, *J* 7.7), 6.73 (1H, s), 4.11 (2H, s), 4.09 (3H, s), 2.58 (3H, s) ppm. ^{13}C NMR (101 MHz, $CDCl_3$) δ 197.90, 146.81, 135.37, 132.57, 130.87, 130.12, 128.87, 128.69, 123.39, 119.90, 117.92, 117.14, 113.31, 36.55, 31.47, 26.65 ppm. HRMS (ESI): m/z $[M+Na]^+$ calcd for $C_{18}H_{16}ClNNaO$: 320.0813, found: 320.0813.

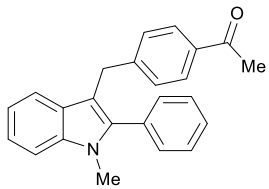

1-(4-((1-Methyl-2-phenyl-1*H*-indol-3-yl)methyl)phenyl)ethan-1-one (**3sa**)

^{1}H NMR (500 MHz, $CDCl_3$) δ 7.86 (2H, d, *J* 8.1), 7.49 (4H, dt, *J* 20.5, 7.4), 7.41 (3H, t, *J* 6.7), 7.30 (3H, dd, *J* 13.9, 7.7), 7.14 (1H, t, *J* 7.4), 4.18 (2H, s), 3.69 (3H, s), 2.58 (3H, s) ppm. ^{13}C NMR (126 MHz, $CDCl_3$) δ 197.86, 147.95, 139.03, 137.48, 135.06, 131.77, 130.60, 128.59, 128.53, 128.49, 128.36, 127.78, 122.03, 119.63, 119.28, 110.64, 109.55, 31.00, 30.92, 26.54 ppm. HRMS (ESI): m/z $[M+Na]^+$ calcd for $C_{24}H_{21}NNaO$: 362.1515, found: 362.1515.

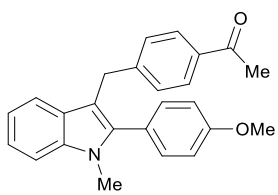

1-(4-((2-(4-Methoxyphenyl)-1-methyl-1*H*-indol-3-yl)methyl)phenyl)ethan-1-one (**3ta**)

^{1}H NMR (500 MHz, $CDCl_3$) δ 7.84 (2H, d, *J* 8.3), 7.43 (1H, d, *J* 7.9), 7.39 (1H, d, *J* 8.2), 7.28 (5H, dd, *J* 13.3, 8.5), 7.11 (1H, t, *J* 7.5), 7.02 (2H, d, *J* 8.7), 4.14 (2H, s), 3.89 (3H, s), 3.65 (3H, s), 2.57 (3H, s) ppm. ^{13}C NMR (126 MHz, $CDCl_3$) δ 197.92, 159.76, 148.10, 138.93, 137.33, 135.04, 131.81, 128.54, 128.51, 127.79, 123.93, 121.83, 119.55, 119.13, 114.11, 110.39, 109.49, 55.42, 30.98, 30.91, 26.57 ppm. HRMS (ESI): m/z $[M+Na]^+$ calcd for $C_{25}H_{23}NNaO_2$: 392.1621, found: 392.1621.

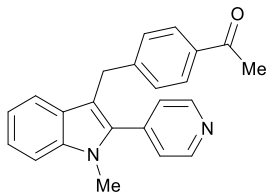

1-(4-((1-Methyl-2-(pyridin-4-yl)-1*H*-indol-3-yl)methyl)phenyl)ethan-1-one (**3ua**)

3ua was prepared according to the general procedure D *with the following modifications*: The reaction was conducted for 23 h with 4CzIPN instead of $Ir[dF(CF_3)ppy]_2(dtbbpy)PF_6$.

^{1}H NMR (400 MHz, $CDCl_3$) δ 8.72 (2H, s), 7.82 (2H, d, *J* 8.2), 7.42 (2H, dd, *J* 11.7, 8.1), 7.35 – 7.28 (3H, m), 7.22 (2H, d, *J* 8.1), 7.12 (1H, t, *J* 7.4), 4.16 (2H, s), 3.70 (3H, s), 2.55 (3H, s) ppm. ^{13}C NMR (101 MHz, $CDCl_3$) δ 197.89, 149.78, 147.15, 140.15, 138.16, 135.75, 135.30, 128.73, 128.39, 127.72, 125.14, 123.20, 120.22, 119.76, 112.48, 109.89, 31.41, 30.72, 26.66 ppm. HRMS (ESI): m/z $[M+H]^+$ calcd $C_{23}H_{21}N_2O$: 341.1648, found: 341.1648.

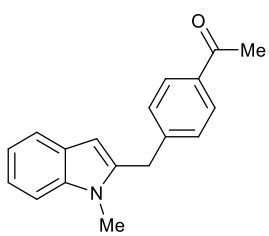

1-(4-((1-Methyl-1*H*-indol-2-yl)methyl)phenyl)ethan-1-one (**3va**)

^{1}H NMR (500 MHz, $CDCl_3$) δ 7.90 (2H, d, *J* 7.1), 7.57 (1H, d, *J* 7.8), 7.31 – 7.25 (3H, m), 7.19 (1H, t, *J* 7.5), 7.10 (1H, t, *J* 7.4), 6.29 (1H, s), 4.20 (2H, s), 3.55 (3H, s), 2.58 (3H, s) ppm. ^{13}C NMR (126 MHz, $CDCl_3$) δ 197.88, 144.22, 138.05, 137.81, 135.77, 128.92, 128.85, 127.79, 121.28, 120.24, 119.64, 109.05, 101.64, 33.56,

29.87, 26.72 ppm. HRMS (ESI): m/z $[M+H]^+$ calcd $C_{18}H_{18}NO$: 264.1383, found: 264.1379.

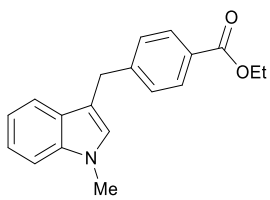

Ethyl 4-((1-methyl-1*H*-indol-3-yl)methyl)benzoate (**3ab**)

^{1}H NMR (400 MHz, $CDCl_3$) δ 7.98 (2H, d, *J* 8.2), 7.49 (1H, d, *J* 7.9), 7.36 (2H, d, *J* 8.1), 7.31 (1H, d, *J* 8.2), 7.23 (1H, d, *J* 7.6), 7.09 (1H, t, *J* 7.4), 6.78 (1H, s), 4.38 (2H, q, *J* 7.1), 4.17 (2H, s), 3.75 (3H, s), 1.40 (3H, t, *J* 7.1) ppm. ^{13}C NMR (101 MHz, $CDCl_3$) δ 166.81, 146.95, 137.30, 129.79, 128.77, 128.36, 127.78, 127.34, 121.84, 119.19, 119.04, 113.41, 109.35, 60.88, 32.76, 31.75, 14.48 ppm. HRMS (ESI): m/z $[M+Na]^+$ calcd for $C_{19}H_{19}NNaO_2$: 316.1308, found: 316.1308.

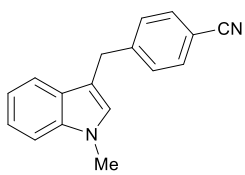

4-((1-Methyl-1*H*-indol-3-yl)methyl)benzonitrile (**3ac**)

^{1}H NMR (300 MHz, $CDCl_3$) δ 7.59 (2H, d, *J* 8.0), 7.50 – 7.33 (4H, m), 7.30 (1H, d, *J* 6.9), 7.13 (1H, t, *J* 7.3), 6.86 (1H, s), 4.20 (2H, s), 3.80 (3H, s) ppm. ^{13}C NMR (126 MHz, $CDCl_3$) δ 147.22, 137.23, 132.18, 129.36, 127.52, 127.33, 121.90, 119.17, 119.11, 118.92, 112.38, 109.75, 109.37, 32.68, 31.70 ppm. HRMS (ESI): m/z $[M+Na]^+$ calcd for $C_{17}H_{14}N_2Na$: 269.1049, found: 269.1049.

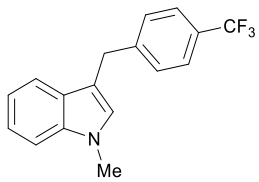

1-Methyl-3-(4-(trifluoromethyl)benzyl)-1*H*-indole (**3ad**)

3ad was prepared according to the general procedure D *with the following modifications*: The reaction was conducted with 4,4‘-dimethoxy-2,2‘-bipyridine instead of 1,10-phenanthroline.

^{1}H NMR (500 MHz, $CDCl_3$) δ 7.56 (2H, d, *J* 8.0), 7.51 (1H, dt, *J* 7.9, 0.9), 7.42 (2H, d, *J* 7.9), 7.35 (1H, dt, *J* 8.3, 0.8), 7.28 (1H, ddd, *J* 8.3, 7.0, 1.2), 7.13 (1H, ddd, *J* 8.0, 7.0, 1.0), 6.81 (1H, s), 4.19 (2H, s), 3.77 (3H, s) ppm. ^{13}C NMR (126 MHz, $CDCl_3$) δ 145.76, 137.34, 129.04, 128.34 (q, $J_{C–F}$ 32.0), 127.76, 127.37, 125.38 (q, $J_{C–F}$ 3.8), 124.55 (q, $J_{C–F}$ 271.8), 121.93, 119.14, 119.13, 113.23, 109.42, 32.75, 31.52 ppm. ^{19}F NMR (376 MHz, $CDCl_3$) δ –62.24 ppm. HRMS (ESI): m/z $[M+Na]^+$ calcd for $C_{17}H_{14}F_3NNa$: 312.0971, found: 312.0971.

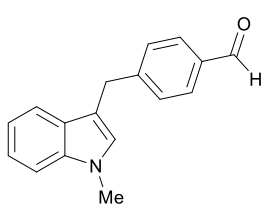

4-((1-Methyl-1*H*-indol-3-yl)methyl)benzaldehyde (**3ae**)

3ae was prepared according to the general procedure D *with the following modifications*: The reaction was conducted with 4,4‘-dimethoxy-2,2‘-bipyridine instead of 1,10-phenanthroline.

^{1}H NMR (500 MHz, $CDCl_3$) δ 9.97 (1H, s), 7.79 (2H, d, *J* 8.0), 7.45 (3H, t, *J* 8.5), 7.32 (1H, d, *J* 8.2), 7.24 (1H, t, *J* 7.6), 7.08 (1H, t, *J* 7.4), 6.81 (1H, s), 4.19 (2H, s), 3.76 (3H, s) ppm. ^{13}C NMR (126 MHz, $CDCl_3$) δ 192.20, 149.09, 137.31, 134.70, 130.11, 129.43, 129.39, 127.74, 127.41, 121.91, 119.15, 112.94, 109.45, 32.84, 31.93 ppm. HRMS (ESI): m/z $[M+Na]^+$ calcd for $C_{17}H_{15}NNaO$: 272.1046, found: 272.1046.

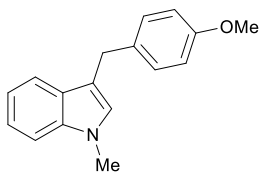

3-(4-Methoxybenzyl)-1-methyl-1*H*-indole (**3af**)

3af was prepared according to the general procedure D *with the following modifications*: The reaction was conducted with 4,4‘-dimethoxy-2,2‘-bipyridine instead of 1,10-phenanthroline.

^{1}H NMR (400 MHz, $CDCl_3$) δ 7.51 (1H, d, *J* 7.9), 7.29 (1H, d, *J* 8.2), 7.20 (3H, d, *J* 8.3), 7.07 (1H, t, *J* 7.9), 6.83 (2H, d, *J* 8.6), 6.74 (1H, s), 4.04 (2H, s), 3.78 (3H, s), 3.73 (3H, s) ppm. ^{13}C NMR (101 MHz, $CDCl_3$) δ 157.91, 137.31, 133.64, 129.70, 127.92, 127.14, 121.67, 119.34, 118.85, 114.89, 113.86, 109.25, 55.39, 32.72, 30.74 ppm. HRMS (ESI): m/z $[M+Na]^+$ calcd for $C_{17}H_{17}NNaO$: 274.1202, found: 274.1202.

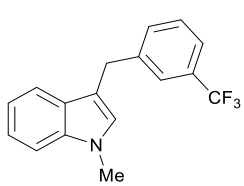

1-Methyl-3-(3-(trifluoromethyl)benzyl)-1*H*-indole (**3ag**)

3ag was prepared according to the general procedure D *with the following modifications*: The reaction was conducted with 4,4‘-dimethoxy-2,2‘-bipyridine instead of 1,10-phenanthroline.

^{1}H NMR (400 MHz, $CDCl_3$) δ 7.57 (1H, s), 7.47 (3H, dd, *J* 11.5, 8.0), 7.42 – 7.36 (1H, m), 7.32 (1H, d, *J* 8.2), 7.23 (1H, d, *J* 8.1), 7.09 (1H, t, *J* 7.4), 6.78 (1H, s), 4.16 (2H, s), 3.76 (3H, s) ppm. ^{13}C NMR (126 MHz, $CDCl_3$) δ 142.56, 137.41, 132.19, 130.78 (q, $J_{C–F}$ 31.9), 128.87, 127.81, 127.35, 125.50 (q, $J_{C–F}$ 3.9), 122.94 (q, $J_{C–F}$ 3.8), 122.30 (q, $J_{C–F}$ 272.2), 121.93, 119.15, 119.13, 113.39, 109.41, 32.75, 31.54 ppm. ^{19}F NMR (376 MHz, $CDCl_3$) δ –62.48 ppm. HRMS (ESI): m/z $[M+Na]^+$ calcd for $C_{17}H_{14}F_3NNa$: 312.0971, found: 312.0971.

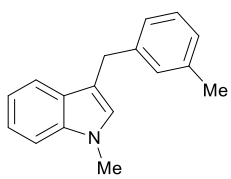

1-Methyl-3-(3-methylbenzyl)-1*H*-indole (**3ah**)

3ah was prepared according to the general procedure D *with the following modifications*: The reaction was conducted with 4,4‘-dimethoxy-2,2‘-bipyridine instead of 1,10-phenanthroline.

^{1}H NMR (400 MHz, $CDCl_3$) δ 7.56 (1H, d, *J* 8.7), 7.31 (1H, d, *J* 8.2), 7.26 – 7.21 (1H, m), 7.18 (1H, d, *J* 7.4), 7.15 – 7.07 (3H, m), 7.03 (1H, d, *J* 7.4), 6.77 (1H, s), 4.08 (2H, s), 3.75 (3H, s), 2.33 (3H, s) ppm. ^{13}C NMR (101 MHz, $CDCl_3$) δ 141.49, 137.98, 137.28, 129.61, 128.34, 128.01, 127.23, 127.21, 126.72, 125.86, 121.66,

119.34, 118.87, 114.55, 109.24, 32.74, 31.56, 21.57 ppm. HRMS (ESI): m/z $[M+Na]^+$ calcd for $C_{17}H_{17}NNa$: 258.1253, found: 258.1253.

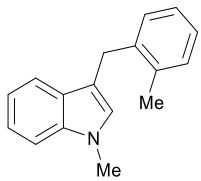

1-Methyl-3-(2-methylbenzyl)-1*H*-indole (**3ai**)

3ai was prepared according to the general procedure D *with the following modifications*: The reaction was conducted with 4,4‘-dimethoxy-2,2‘-bipyridine instead of 1,10-phenanthroline.

^{1}H NMR (400 MHz, $CDCl_3$) δ 7.58 (1H, d, *J* 7.9), 7.31 (1H, d, *J* 8.2), 7.25 – 7.06 (6H, m), 6.57 (1H, s), 4.08 (2H, s), 3.71 (3H, s), 2.34 (3H, s) ppm. ^{13}C NMR (101 MHz, $CDCl_3$) δ 139.24, 137.14, 136.41, 130.09, 129.41, 127.89, 127.12, 127.10, 126.11, 125.90, 121.53, 119.08, 118.69, 113.58, 109.11, 32.59, 29.13, 19.49 ppm. HRMS (ESI): m/z $[M+Na]^+$ calcd for $C_{17}H_{17}NNa$: 258.1253, found: 258.1253.

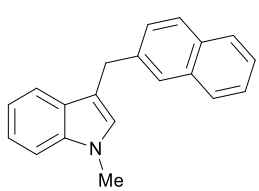

1-Methyl-3-(naphthalen-2-ylmethyl)-1*H*-indole (**3aj**)

3aj was prepared according to the general procedure D *with the following modifications*: The reaction was conducted with 4,4‘-dimethoxy-2,2‘-bipyridine instead of 1,10-phenanthroline.

^{1}H NMR (500 MHz, $CDCl_3$) δ 7.86 – 7.76 (4H, m), 7.59 (1H, d, *J* 7.9), 7.50 – 7.41 (3H, m), 7.33 (1H, d, *J* 8.2), 7.29 – 7.23 (1H, m), 7.11 (1H, t, *J* 7.8), 6.79 (1H, s), 4.30 (2H, s), 3.75 (3H, s) ppm. ^{13}C NMR (126 MHz, $CDCl_3$) δ 139.10, 137.38, 133.83, 132.26, 128.06, 128.01, 127.80, 127.75, 127.69, 127.43, 126.79, 125.95, 125.28, 121.75, 119.36, 118.98, 114.37, 109.29, 32.72, 31.90 ppm. HRMS (ESI): m/z $[M+Na]^+$ calcd for $C_{20}H_{17}NNa$: 294.1253, found: 294.1253.

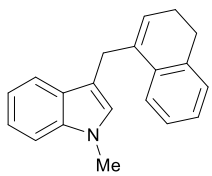

3-((3,4-Dihydronaphthalen-1-yl)methyl)-1-methyl-1*H*-indole (**3ak**)

3ak was prepared according to the general procedure D *with the following modifications*: The reaction was conducted using alkenyl triflate with 4,4‘-dimethoxy-2,2‘-bipyridine instead of 1,10-phenanthroline.

^{1}H NMR (500 MHz, $CDCl_3$) δ 7.64 (1H, d, *J* 7.9), 7.35 – 7.32 (1H, m), 7.30 (1H, d, *J* 8.2), 7.23 (1H, t, *J* 7.6), 7.18 – 7.09 (4H, m), 6.80 (1H, s), 5.90 (1H, t, *J* 4.5), 3.90 (2H, s), 3.72 (3H, s), 2.80 (2H, t, *J* 8.0), 2.33 – 2.26 (2H, m) ppm. ^{13}C NMR (126 MHz, $CDCl_3$) δ 137.33, 136.82, 135.39, 135.22, 128.27, 127.58, 127.44, 127.43, 126.70, 126.45, 123.31, 121.58, 119.39, 118.80, 113.06, 109.24, 32.75, 28.86, 28.60, 23.41 ppm. HRMS (ESI): m/z $[M+Na]^+$ calcd for $C_{20}H_{19}NNa$: 296.1410, found: 296.1410.

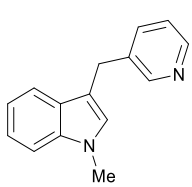

1-Methyl-3-(pyridin-3-ylmethyl)-1*H*-indole (**3al**)

3al was prepared according to the general procedure D *with the following modifications*: The reaction was conducted with the reaction temperature reaching 53 ℃ (without fan-cooling).

^{1}H NMR (500 MHz, $CDCl_3$) δ 8.61 (1H, s), 8.46 (1H, d, *J* 3.9), 7.57 (1H, d, *J* 7.7), 7.48 (1H, d, *J* 7.9), 7.31 (1H, d, *J* 8.2), 7.26 – 7.18 (2H, m), 7.09 (1H, t, *J* 7.4), 6.78 (1H, s), 4.11 (2H, s), 3.75 (3H, s) ppm. ^{13}C NMR (126 MHz, $CDCl_3$) δ 149.94, 147.28, 137.36, 137.07, 136.50, 127.64, 127.33, 123.54, 121.97, 119.17, 119.06, 113.04, 109.42, 32.76, 28.89 ppm. HRMS (ESI): m/z $[M+H]^+$ calcd for $C_{15}H_{15}N_2$: 223.1230, found: 223.1230.

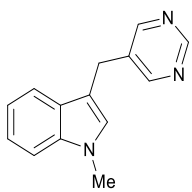

1-Methyl-3-(pyrimidin-5-ylmethyl)-1*H*-indole (**3am**)

3am was prepared according to the general procedure D *with the following modifications*: The reaction was conducted with the reaction temperature reaching 53 ℃ (without fan-cooling).

^{1}H NMR (500 MHz, $CDCl_3$) δ 9.08 (1H, s), 8.66 (2H, s), 7.46 (1H, d, *J* 7.9), 7.32 (1H, d, *J* 8.2), 7.25 (1H, t, *J* 7.5), 7.10 (1H, t, *J* 7.4), 6.80 (1H, s), 4.09 (2H, s), 3.76 (3H, s) ppm. ^{13}C NMR (126 MHz, $CDCl_3$) δ 157.00, 156.85, 156.83, 137.38, 134.64, 127.33, 122.20, 119.42, 118.77, 111.66, 109.56, 32.81, 26.48 ppm. HRMS (ESI): m/z $[M+H]^+$ calcd for $C_{14}H_{14}N_3$: 224.1182, found: 224.1182.

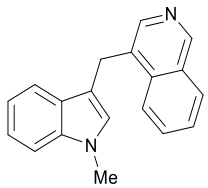

4-((1-Methyl-1*H*-indol-3-yl)methyl)isoquinoline (**3an**)

3an was prepared according to the general procedure D *with the following modifications*: The reaction was conducted with the reaction temperature reaching 53 °C (without fan-cooling).

^{1}H NMR (500 MHz, $CDCl_3$) δ 9.22 (1H, s), 8.53 (1H, s), 8.02 (2H, dd, *J* 19.5, 8.2), 7.70 (1H, d, *J* 7.9), 7.62 (2H, dt, *J* 25.6, 7.2), 7.35 – 7.25 (2H, m), 7.17 (1H, t, *J* 7.2), 6.52 (1H, s), 4.50 (2H, s), 3.64 (3H, s) ppm. ^{13}C NMR (126 MHz, $CDCl_3$) δ 151.62, 143.22, 137.11, 135.04, 130.32, 130.17, 128.58, 128.21, 127.60, 127.41, 126.95, 123.70, 121.83, 119.05, 118.94, 113.12, 109.33, 32.65, 26.24 ppm. HRMS (ESI): m/z $[M+H]^+$ calcd for $C_{19}H_{17}N_2$: 273.1386, found: 273.1386.

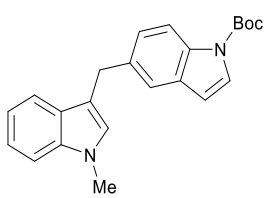

tert-Butyl 5-((1-methyl-1*H*-indol-3-yl)methyl)-1*H*-indole-1-carboxylate (**3ao**)

3ao was prepared according to the general procedure D *with the following modifications*: The reaction was conducted with 4,4‘-dimethoxy-2,2‘-bipyridine instead of 1,10-phenanthroline.

^{1}H NMR (500 MHz, $CDCl_3$) δ 8.04 (1H, s), 7.58 – 7.56 (1H, m), 7.54 (1H, d, *J* 7.9), 7.46 (1H, s), 7.32 – 7.25 (2H, m), 7.22 (1H, t, *J* 8.0), 7.07 (1H, t, *J* 7.8), 6.75 (1H, s),

6.49 (1H, d, *J* 3.7), 4.20 (2H, s), 3.73 (3H, s), 1.67 (9H, s) ppm. ^{13}C NMR (126 MHz, $CDCl_3$) δ 150.00, 137.36, 135.91, 130.94, 128.01, 127.29, 127.28, 126.08, 125.44, 121.67, 120.78, 119.41, 118.87, 115.10, 115.03, 109.23, 107.39, 83.61, 32.72, 31.54, 28.35 ppm. HRMS (ESI): m/z $[M+Na]^+$ calcd for $C_{23}H_{24}N_2NaO_2$: 383.1730, found: 383.1730.

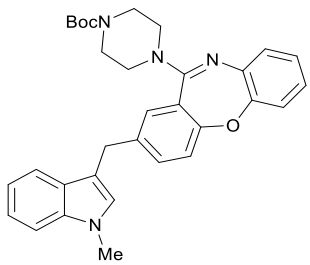

tert-Butyl 4-(2-((1-methyl-1*H*-indol-3-yl)methyl)dibenzo[*b,f*][1,4]oxazepin-11-yl) piperazine-1-carboxylate (**3ap**)

3ap was prepared according to the general procedure D *with the following modifications*: The reaction was conducted with $NiCl_2$·glyme (10.0 mol%), 4,4'-dimethoxy-2,2'-bipyridine (15.0 mol%), DMA (0.033 M) and corresponding aryl chloride instead of aryl bromide.

^{1}H NMR (500 MHz, $CDCl_3$) δ 7.41 (1H, d, *J* 6.9), 7.36 (1H, d, *J* 7.9), 7.32 (1H, d, *J* 8.2), 7.23 (1H, t, *J* 7.6), 7.19 – 7.09 (4H, m), 7.06 (2H, q, *J* 7.2, 6.7), 6.99 (1H, t, *J* 7.6), 6.82 (1H, s), 4.07 (2H, s), 3.76 (3H, s), 3.26 (8H, s), 1.50 (9H, s) ppm. ^{13}C NMR (126 MHz, $CDCl_3$) δ 160.62, 159.43, 154.87, 152.47, 140.37, 138.50, 137.43, 133.09, 129.38, 127.54, 127.29, 127.04, 125.58, 124.56, 123.00, 121.97, 121.06, 120.32, 119.12, 119.10, 113.38, 109.50, 80.01, 47.29, 43.47, 32.78, 30.83, 28.56 ppm. HRMS (ESI): m/z $[M+H]^+$ calcd for $C_{32}H_{35}N_4O_3$: 523.2704, found: 524.2704.

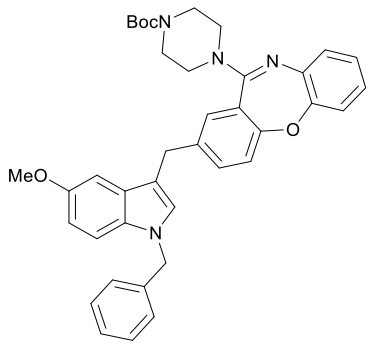

tert-Butyl -(2-((1-benzyl-5-methoxy-1*H*-indol-3-yl)methyl)dibenzo[*b,f*][1,4] oxazepin-11-yl)piperazine-1-carboxylate (**3xp**)

3xp was prepared according to the general procedure D *with the following modifications*: The reaction was conducted with $NiCl_2$·glyme (10.0 mol%), 4,4'-dimethoxy-2,2'-bipyridine (15.0 mol%), DMA (0.033 M) and corresponding aryl chloride instead of aryl bromide.

^{1}H NMR (500 MHz, $CDCl_3$) δ 7.43 (1H, d, *J* 8.1), 7.29 (3H, m), 7.23 – 7.05 (8H, m), 6.98 (1H, t, *J* 7.5), 6.91 (1H, s), 6.84 (1H, dd, *J* 8.8, 1.9), 6.73 (1H, s), 5.24 (2H, s), 4.06 (2H, s), 3.71 (3H, s), 3.25 (8H, s), 1.49 (9H, s) ppm. ^{13}C NMR (126 MHz, $CDCl_3$) δ 160.57, 159.47, 154.80, 154.06, 152.45, 138.23, 137.73, 133.03, 132.52, 129.37, 128.89, 128.20, 127.81, 127.42, 127.08, 126.87, 125.56, 124.50, 123.15, 121.05, 120.29, 113.38, 112.01, 110.75, 101.63, 79.94, 55.98, 50.27, 47.37, 43.17, 30.94, 28.57 ppm. HRMS (ESI): m/z $[M+H]^+$ calcd for $C_{39}H_{41}N_4O_4$: 629.3122, found: 629.3122.

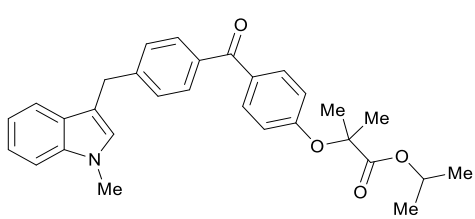

Isopropyl 2-methyl-2-(4-(4-((1-methyl-1*H*-indol-3-yl)methyl)benzoyl)phenoxy) propanoate (**3aq**)

3aq was prepared according to the general procedure D *with the following modifications*: The reaction was conducted with $NiCl_2$·glyme (10.0 mol%), 4,4'-dimethoxy-2,2'-bipyridine (15.0 mol%), DMA (0.033 M) and corresponding aryl chloride instead of aryl bromide.

^{1}H NMR (400 MHz, $CDCl_3$) δ 7.77 (2H, d, *J* 8.2), 7.70 (2H, d, *J* 7.5), 7.52 (1H, d, *J* 7.7), 7.39 (2H, d, *J* 7.5), 7.32 (1H, d, *J* 8.0), 7.27 – 7.21 (1H, m), 7.10 (1H, t, *J* 7.1), 6.87 (2H, d, *J* 8.2), 6.82 (1H, s), 5.13 – 5.04 (1H, m), 4.19 (2H, s), 3.76 (3H, s), 1.67 (6H, s), 1.21 (6H, d, *J* 6.0) ppm. ^{13}C NMR (126 MHz, $CDCl_3$) δ 195.44, 173.30, 159.47, 146.23, 137.28, 135.91, 132.07, 130.98, 130.18, 128.58, 127.79, 127.37, 121.82, 119.19, 119.03, 117.23, 113.37, 109.36, 79.44, 69.37, 32.73, 31.67, 25.48, 21.62 ppm. HRMS (ESI): m/z $[M+Na]^+$ calcd for $C_{30}H_{31}NNaO_4$: 492.2145, found: 492.2145.

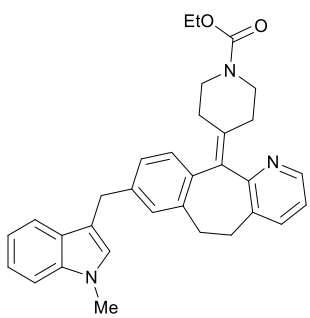

Ethyl 4-(8-((1-methyl-1*H*-indol-3-yl)methyl)-5,6-dihydro-11*H*-benzo[5,6] cyclohepta[1,2-*b*]pyridin-11-ylidene)piperidine-1-carboxylate (**3ar**)

3ar was prepared according to the general procedure D *with the following modifications*: The reaction was conducted with $NiCl_2$·glyme (10.0 mol%), 4,4'-

dimethoxy-2,2'-bipyridine (15.0 mol%), DMA (0.033 M) and corresponding aryl chloride instead of aryl bromide.

^{1}H NMR (500 MHz, $CDCl_3$) δ 8.39 (1H, dd, *J* 4.8, 1.6), 7.53 (1H, dt, *J* 7.9, 0.9), 7.44 (1H, d, *J* 7.5), 7.28 (1H, dt, *J* 8.2, 0.8), 7.21 (1H, ddd, *J* 8.1, 7.1, 1.0), 7.14 – 7.03 (5H, m), 6.78 (1H, s), 4.13 (2H, q, *J* 7.5), 4.04 (2H, s), 3.82 (2H, s), 3.73 (3H, s), 3.43 – 3.26 (2H, m), 3.20 – 3.06 (2H, m), 2.88 – 2.72 (2H, m), 2.53 – 2.22 (4H, m), 1.25 (3H, t, *J* 7.2) ppm. ^{13}C NMR (126 MHz, $CDCl_3$) δ 157.76, 155.64, 146.18, 140.87, 137.80, 137.48, 137.24, 136.93, 136.56, 134.95, 134.14, 129.51, 129.41, 127.98, 127.23, 126.45, 122.23, 121.68, 119.28, 118.88, 114.10, 109.26, 61.38, 45.01, 44.92, 32.73, 32.00, 31.83, 31.18, 30.84, 30.71, 14.81 ppm. HRMS (ESI): m/z $[M+H]^+$ calcd for $C_{32}H_{34}N_3O_2$: 492.2646, found: 492.2646.

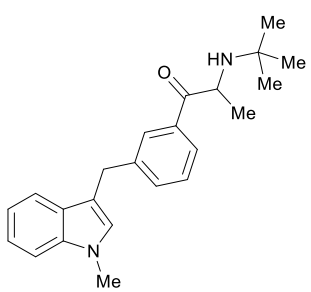

2-(*tert*-Butylamino)-1-(3-((1-methyl-1*H*-indol-3-yl)methyl)phenyl)propan-1-one (**3as**)

3as was prepared according to the general procedure D *with the following modifications*: The reaction was conducted with $NiCl_2$·glyme (10.0 mol%), 4,4'-dimethoxy-2,2'-bipyridine (15.0 mol%), DMA (0.033 M) and corresponding aryl chloride instead of aryl bromide.

^{1}H NMR (500 MHz, $CDCl_3$) δ 7.95 (1H, s), 7.82 (1H, d, *J* 7.7), 7.52 – 7.48 (2H, m), 7.39 (1H, t, *J* 7.7), 7.30 (1H, d, *J* 8.2), 7.25 – 7.21 (1H, m), 7.08 (1H, ddd, *J* 7.9, 7.1, 0.9), 6.79 (1H, d, *J* 1.0), 4.33 (1H, q, *J* 7.1), 4.18 (2H, s), 3.75 (3H, s), 2.75 (1H, d, *J* 6.9), 1.24 (3H, d, *J* 7.1), 1.04 (9H, s) ppm. ^{13}C NMR (126 MHz, $CDCl_3$) δ 205.29, 142.43, 137.36, 135.25, 133.80, 128.88, 128.69, 127.78, 127.30, 126.12, 121.87, 119.15, 119.06, 113.60, 109.38, 52.06, 50.89, 32.74, 31.58, 29.88, 22.85 ppm. HRMS (ESI): m/z $[M+H]^+$ calcd for $C_{23}H_{29}N_2O$: 349.2274, found: 349.2274.

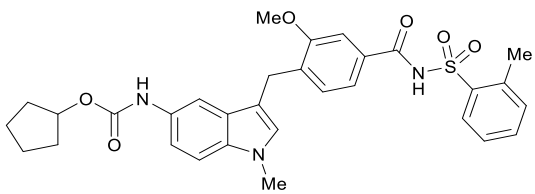

Cyclopentyl (3-(2-methoxy-4-((*o*-tolylsulfonyl)carbamoyl)benzyl)-1-methyl-1*H*-indol-5-yl)carbamate (**3wt**)

3wt was prepared according to the general procedure D *with the following modifications*: The reaction was conducted with $NiCl_2$·glyme (10.0 mol%), 1,10-phenanthroline (15.0 mol%) and DMA (0.033 M).

^{1}H NMR (500 MHz, $CDCl_3$) δ 9.12 (1H, s), 8.25 (1H, d, *J* 7.8), 7.55 – 7.46 (2H, m), 7.40 (1H, t, *J* 7.6), 7.33 – 7.27 (2H, m), 7.17 (2H, dd, *J* 12.7, 8.5), 7.10 (2H, t, *J* 10.0), 6.77 (1H, s), 6.52 (1H, s), 5.24 – 5.16 (1H, m), 4.03 (2H, s), 3.84 (3H, s), 3.70 (3H, s), 2.68 (3H, s), 1.86 (2H, s), 1.75 (4H, m), 1.60 (2H, s) ppm.

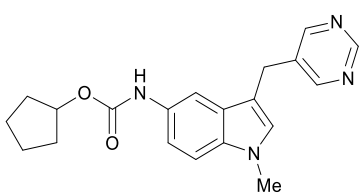

Cyclopentyl (1-methyl-3-(pyrimidin-5-ylmethyl)-1*H*-indol-5-yl)carbamate (**3wm**)

3wm was prepared according to the general procedure D *with the following modifications*: The reaction was conducted with $NiCl_2$·glyme (10.0 mol%), 1,10-phenanthroline (15.0 mol%) and DMA (0.033 M) and the reaction temperature reaching 53 °C (without fan-cooling).

^{1}H NMR (500 MHz, $CDCl_3$) δ 9.06 (1H, s), 8.64 (2H, s), 7.59 (1H, s), 7.21 (1H, d, *J* 8.6), 7.14 (1H, d, *J* 7.1), 6.75 (1H, s), 6.68 (1H, s), 5.19 (1H, s), 4.03 (2H, s), 3.71 (3H, s), 1.92 – 1.83 (2H, m), 1.75 (4H, m), 1.65 – 1.54 (2H, m) ppm. ^{13}C NMR (126 MHz, $CDCl_3$) δ 156.98, 156.78, 154.26, 134.62, 134.42, 130.72, 128.16, 127.54, 115.71, 111.55, 109.79, 109.26, 77.94, 32.94, 26.34, 23.80 ppm. HRMS (ESI): m/z $[M+Na]^+$ calcd for $C_{20}H_{22}N_4NaO_2$: 373.1635, found: 373.1635.

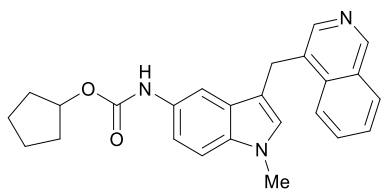

Cyclopentyl (3-(isoquinolin-4-ylmethyl)-1-methyl-1*H*-indol-5-yl)carbamate (**3wn**)

3wn was prepared according to the general procedure D *with the following modifications*: The reaction was conducted with $NiCl_2$·glyme (10.0 mol%), 1,10-phenanthroline (15.0 mol%) and DMA (0.033 M) and the reaction temperature reaching 53 °C (without fan-cooling).

^{1}H NMR (400 MHz, $CDCl_3$) δ 9.19 (1H, s), 8.42 (1H, s), 8.02 (2H, dd, *J* 7.9, 3.6), 7.75 (1H, s), 7.68 (1H, t, *J* 7.6), 7.61 (1H, t, *J* 7.4), 7.22 – 7.13 (2H, m), 6.64 (1H, s), 6.49 (1H, s), 5.27 – 5.17 (1H, m), 4.44 (2H, s), 3.62 (3H, s), 1.95 – 1.83 (2H, m),

1.83 – 1.67 (4H, m), 1.67 – 1.53 (2H, m) ppm. ^{13}C NMR (101 MHz, $CDCl_3$) δ 154.35, 150.92, 141.90, 135.40, 134.30, 131.03, 130.90, 130.45, 128.53, 128.41, 128.39, 127.76, 127.40, 123.82, 115.48, 112.63, 109.66, 109.38, 77.90, 32.96, 32.89, 26.21, 23.82 ppm. HRMS (ESI): m/z $[M+H]^+$ calcd for $C_{25}H_{26}N_3O_2$: 400.2020, found: 400.2020.

Characterization data of acylation products

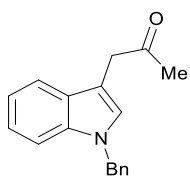

1-(1-Benzyl-1*H*-indol-3-yl)propan-2-one (**5ca**)

5ca was prepared according to the general procedure E *with the following modifications*: The reaction was conducted in the absence of K_2CO_3.

^{1}H NMR (500 MHz, $CDCl_3$) δ 7.54 (1H, d, *J* 7.9), 7.31 – 7.22 (4H, m), 7.21 – 7.15 (1H, m), 7.15 – 7.08 (3H, m), 7.07 (1H, s), 5.29 (2H, s), 3.80 (2H, s), 2.16 (3H, s) ppm. ^{13}C NMR (126 MHz, $CDCl_3$) δ 207.43, 137.50, 136.77, 128.92, 128.10, 127.80, 127.32, 126.94, 122.22, 119.71, 119.05, 109.97, 108.09, 50.15, 40.92, 29.01 ppm. HRMS (ESI): m/z $[M+Na]^+$ calcd for $C_{18}H_{17}NNaO$: 286.1202, found: 286.1202.

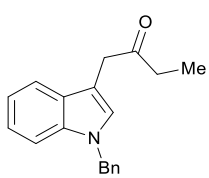

1-(1-Benzyl-1*H*-indol-3-yl)butan-2-one (**5cb**)

^{1}H NMR (500 MHz, $CDCl_3$) δ 7.56 (1H, d, *J* 7.8), 7.33 – 7.22 (4H, m), 7.18 (1H, t, *J* 7.2), 7.16 – 7.09 (3H, m), 7.07 (1H, s), 5.28 (2H, s), 3.80 (2H, s), 2.51 (2H, q, *J* 7.3), 1.01 (3H, t, *J* 7.3) ppm. ^{13}C NMR (126 MHz, $CDCl_3$) δ 207.43, 137.50, 136.77, 128.92, 127.80, 127.32, 126.94, 122.22, 119.71, 119.05, 109.97, 108.09, 50.15, 40.92, 29.01 ppm. HRMS (ESI): m/z $[M+Na]^+$ calcd for $C_{19}H_{19}NNaO$: 300.1359, found: 300.1359.

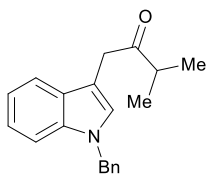

1-(1-Benzyl-1*H*-indol-3-yl)-3-methylbutan-2-one (**5cc**)

^{1}H NMR (500 MHz, $CDCl_3$) δ 7.57 (1H, d, *J* 7.9), 7.34 – 7.24 (4H, m), 7.20 (1H, t, *J* 7.6), 7.14 (3H, dd, *J* 11.3, 7.3), 7.12 (1H, s), 5.31 (2H, s), 3.90 (2H, s), 2.93 – 2.68 (1H, m), 1.13 (6H, d, *J* 6.9) ppm. ^{13}C NMR (126 MHz, $CDCl_3$) δ 212.63, 137.61, 136.71, 128.87, 128.28, 127.73, 127.36, 126.93, 122.09, 119.57, 119.01, 109.90, 108.06, 50.13, 39.66, 37.67, 18.69 ppm. HRMS (ESI): m/z $[M+Na]^+$ calcd for $C_{20}H_{21}NNaO$: 314.1515, found: 314.1515.

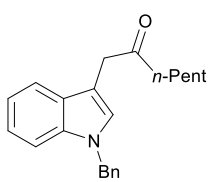

1-(1-Benzyl-1*H*-indol-3-yl)heptan-2-one (**5cd**)

^{1}H NMR (500 MHz, $CDCl_3$) δ 7.57 (1H, d, *J* 7.5), 7.33 – 7.23 (4H, m), 7.22 – 7.16 (1H, m), 7.16 – 7.09 (3H, m), 7.08 (1H, s), 5.29 (2H, s), 3.81 (2H, s), 2.48 (2H, t, *J*

7.4), 1.62 – 1.50 (2H, m), 1.29 – 1.14 (4H, m), 0.85 (3H, t, *J* 7.0) ppm. ^{13}C NMR (126 MHz, $CDCl_3$) δ 209.49, 137.55, 136.72, 128.86, 128.18, 127.73, 127.28, 126.90, 122.12, 119.61, 119.06, 109.90, 108.14, 50.09, 41.52, 39.99, 31.43, 23.69, 22.52, 14.00 ppm. HRMS (ESI): m/z $[M+Na]^+$ calcd for $C_{22}H_{25}NNaO$: 342.1828, found: 342.1828.

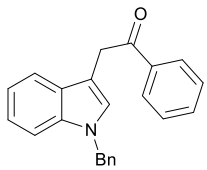

2-(1-Benzyl-1*H*-indol-3-yl)-1-phenylethan-1-one (**5ce**)

^{1}H NMR (500 MHz, $CDCl_3$) δ 8.09 – 8.02 (2H, m), 7.67 – 7.62 (1H, m), 7.56 – 7.49 (1H, m), 7.43 (2H, t, *J* 7.7), 7.28 – 7.22 (4H, m), 7.20 – 7.12 (2H, m), 7.08 (1H, s), 7.06 (2H, dd, *J* 7.9, 1.5), 5.24 (2H, s), 4.41 (2H, s) ppm. ^{13}C NMR (126 MHz, $CDCl_3$) δ 197.91, 137.57, 136.78, 136.66, 133.05, 128.81, 128.69, 128.65, 128.17, 127.65, 127.44, 126.84, 122.09, 119.58, 119.11, 109.91, 108.17, 50.07, 35.70 ppm. HRMS (ESI): m/z $[M+Na]^+$ calcd for $C_{23}H_{19}NNaO$: 348.1359, found: 348.1359.

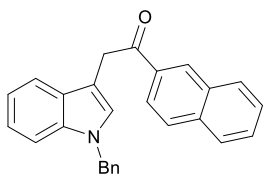

2-(1-Benzyl-1*H*-indol-3-yl)-1-(naphthalen-2-yl)ethan-1-one (**5cf**)

^{1}H NMR (500 MHz, $CDCl_3$) δ 8.61 (1H, s), 8.10 (1H, dd, *J* 8.6, 1.8), 7.93 (1H, d, *J* 8.1), 7.87 (2H, dd, *J* 8.4, 4.4), 7.70 (1H, dd, *J* 6.8, 1.0), 7.57 (2H, dtd, *J* 16.2, 6.9, 1.2), 7.29 – 7.22 (4H, m), 7.18 (2H, ddd, *J* 14.4, 8.2, 2.6), 7.13 (1H, s), 7.06 (2H, dd,

J 6.4, 2.9), 5.27 (2H, s), 4.55 (2H, s) ppm. ^{13}C NMR (126 MHz, $CDCl_3$) δ 197.99, 137.56, 136.68, 135.65, 134.09, 132.62, 130.41, 129.75, 128.83, 128.55, 128.51, 128.19, 127.86, 127.67, 127.46, 126.85, 126.82, 124.51, 122.14, 119.63, 119.15, 109.95, 108.37, 50.11, 35.89 ppm. HRMS (ESI): m/z $[M+Na]^+$ calcd for $C_{27}H_{21}NNaO$: 398.1515, found: 398.1515.

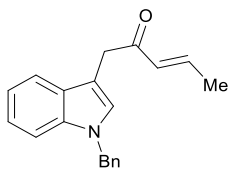

(*E*)-1-(1-Benzyl-1*H*-indol-3-yl)pent-3-en-2-one (**5cg**)

^{1}H NMR (500 MHz, $CDCl_3$) δ 7.59 (1H, d, *J* 7.8), 7.38 – 7.23 (4H, m), 7.20 (1H, t, *J* 7.1), 7.14 (3H, dd, *J* 12.3, 7.3), 7.08 (1H, s), 6.98 (1H, dq, *J* 18.2, 6.9), 6.25 (1H, dd, *J* 15.6, 1.6), 5.31 (2H, s), 3.94 (2H, s), 1.86 (3H, dd, *J* 6.9, 1.6) ppm. ^{13}C NMR (126 MHz, $CDCl_3$) δ 197.77, 143.19, 137.60, 136.75, 130.68, 128.88, 128.27, 127.74, 127.36, 126.95, 122.12, 119.60, 119.14, 109.91, 108.15, 50.15, 37.86, 18.37 ppm. HRMS (ESI): m/z $[M+Na]^+$ calcd for $C_{20}H_{19}NNaO$: 312.1359, found: 312.1359.

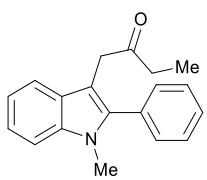

1-(1-Methyl-2-phenyl-1*H*-indol-3-yl)butan-2-one (**5sb**)

^{1}H NMR (500 MHz, $CDCl_3$) δ 7.57 – 7.50 (3H, m), 7.48 (1H, dd, *J* 10.3, 4.4), 7.44 – 7.35 (3H, m), 7.32 – 7.27 (1H, m), 7.18 (1H, td, *J* 7.5, 0.8), 3.75 (2H, s), 3.64 (3H, s), 2.40 (2H, q, *J* 7.3), 0.97 (3H, t, *J* 7.3) ppm. ^{13}C NMR (126 MHz, $CDCl_3$) δ 210.28,

139.38, 137.38, 131.57, 130.66, 128.72, 128.54, 127.77, 122.19, 119.93, 119.04, 109.62, 106.44, 39.57, 34.76, 31.03, 7.95 ppm. HRMS (ESI): m/z $[M+Na]^+$ calcd for $C_{19}H_{19}NNaO$: 300.1359, found: 300.1359.

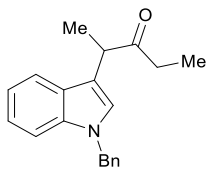

2-(1-Benzyl-1*H*-indol-3-yl)pentan-3-one (**5yb**)

^{1}H NMR (500 MHz, $CDCl_3$) δ 7.60 (1H, d, *J* 7.9), 7.36 – 7.23 (4H, m), 7.19 (1H, t, *J* 7.3), 7.12 (3H, dd, *J* 16.3, 7.9), 7.00 (1H, s), 5.29 (2H, s), 4.04 (1H, q, *J* 7.0), 2.58 – 2.30 (2H, m), 1.49 (3H, d, *J* 7.0), 0.96 (3H, t, *J* 7.3) ppm. ^{13}C NMR (126 MHz, $CDCl_3$) δ 212.53, 137.51, 136.93, 128.92, 127.79, 127.37, 126.90, 126.04, 122.22, 119.66, 119.28, 115.16, 110.03, 50.21, 43.97, 33.53, 17.13, 8.28 ppm. HRMS (ESI): m/z $[M+Na]^+$ calcd for $C_{20}H_{21}NNaO$: 314.1515, found: 314.1515.

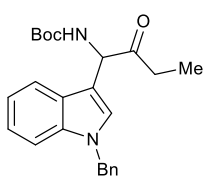

tert-Butyl (1-(1-benzyl-1*H*-indol-3-yl)-2-oxobutyl)carbamate (**5zb**)

^{1}H NMR (500 MHz, $CDCl_3$) δ 7.60 (1H, d, *J* 7.9), 7.32 – 7.22 (4H, m), 7.18 (1H, t, *J* 7.5), 7.14 (1H, s), 7.12 (1H, d, *J* 6.6), 7.07 (2H, d, *J* 6.7), 5.64 (2H, m), 5.26 (2H, s), 2.60 – 2.38 (2H, m), 1.40 (9H, s), 0.99 (3H, t, *J* 7.3) ppm. ^{13}C NMR (126 MHz, $CDCl_3$) δ 207.69, 155.30, 137.00, 136.97, 128.93, 127.90, 127.90, 126.91, 126.51,

122.59, 120.29, 119.35, 110.55, 110.21, 79.74, 56.39, 50.28, 32.96, 28.46, 8.01 ppm. HRMS (ESI): m/z $[M+H]^+$ calcd for $C_{24}H_{29}N_2O_3$: 393.2173, found: 393.2167.

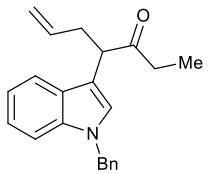

4-(1-Benzyl-1*H*-indol-3-yl)hept-6-en-3-one (**5zab**)

^{1}H NMR (500 MHz, $CDCl_3$) δ 7.66 (1H, d, *J* 7.7), 7.29 (4H, t, *J* 8.0), 7.18 (2H, dt, *J* 14.7, 7.1), 7.09 (2H, d, *J* 6.8), 7.03 (1H, s), 5.79 (1H, dt, *J* 24.0, 12.0), 5.31 (2H, s), 5.06 (1H, d, *J* 17.0), 4.98 (1H, d, *J* 10.2), 4.03 (1H, t, *J* 7.5), 2.89 (1H, dt, *J* 14.5, 7.3), 2.65 – 2.34 (3H, m), 0.98 (3H, t, *J* 7.3) ppm. ^{13}C NMR (126 MHz, $CDCl_3$) δ 211.12, 137.46, 136.85, 136.56, 128.89, 127.77, 127.52, 126.79, 126.65, 122.21, 119.70, 119.28, 116.41, 112.85, 110.04, 50.17, 49.55, 36.14, 34.60, 8.13 ppm. HRMS (ESI): m/z $[M+H]^+$ calcd for $C_{22}H_{24}NO$: 318.1852, found: 318.1853.

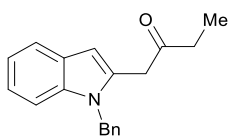

1-(1-Benzyl-1*H*-indol-2-yl)butan-2-one (**5zbb**)

^{1}H NMR (500 MHz, $CDCl_3$) δ 7.62 (1H, d, *J* 7.6), 7.34 – 7.19 (4H, m), 7.15 (2H, dt, *J* 14.7, 7.0), 6.95 (2H, d, *J* 7.0), 6.49 (1H, s), 5.33 (2H, s), 3.77 (2H, s), 2.45 (2H, q, *J* 7.3), 0.97 (3H, t, *J* 7.3) ppm. ^{13}C NMR (126 MHz, $CDCl_3$) δ 207.64, 137.73, 137.63, 133.34, 128.91, 128.01, 127.53, 126.11, 121.83, 120.42, 119.99, 109.77, 102.94, 46.86, 41.77, 35.03, 7.72 ppm. HRMS (ESI): m/z $[M+Na]^+$ calcd for $C_{19}H_{19}NNaO$: 300.1359, found: 300.1359.

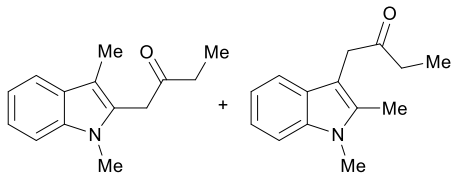

5zb-C2 **5zb-C3**

1-(1,3-Dimethyl-1*H*-indol-2-yl)butan-2-one(**5zcb-C2**) & 1-(1,2-Dimethyl-1*H*-indol-3-yl)butan-2-one (**5zcb-C3**)

Regioisomers were obtained in **5zcb-C2** and **5zcb-C3** at a ratio of 4:3, respectively.

^{1}H NMR (500 MHz, $CDCl_3$) δ 7.56 (1H, d, *J* 7.9, **5zcb-C2**), 7.49 (0.72H, d, *J* 6.9, **5zcb-C3**), 7.28 (1.81H, d, *J* 7.7), 7.25 – 7.16 (1.70H, m), 7.16 – 7.08 (1.66H, m), 3.84 (2H, s, **5zcb-C2**), 3.75 (1.45H, s, **5zcb-C3**), 3.68 (2.15H, s, **5zcb-C3**), 3.64 (3H, s, **5zcb-C2**), 2.45 (3.44H, qd, *J* 7.3, 1.6), 2.39 (2.15H, s, **5zcb-C3**), 2.34 (3H, s, **5zcb-C2**), 1.01 (5.17H, dt, *J* 16.6, 7.3) ppm. ^{13}C NMR (126 MHz, $CDCl_3$) δ 210.03, 207.96, 137.15, 136.79, 134.58, 129.63, 128.28, 127.72, 121.63, 121.02, 119.41, 119.04, 118.61, 117.89, 108.98, 108.85, 108.72, 104.28, 39.71, 39.35, 34.83, 34.38, 30.02, 29.72, 10.49, 9.16, 7.92, 7.73 ppm. HRMS (ESI): m/z $[M+Na]^+$ calcd for $C_{14}H_{17}NNaO$: 238.1202, found: 238.1202.

2.4.6 Optimization of reaction conditions

Table 2.6 Optimization of the reaction with **1a** and **2a**[a]

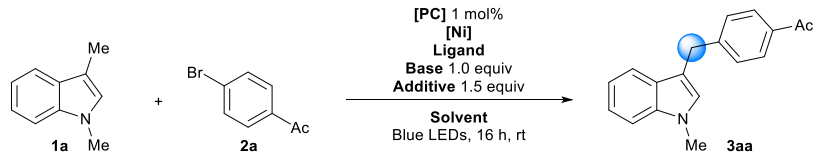

entry	[PC]	[Ni] (mol%)	ligand (mol%)	base	additive	solvent (M)	result (%)
1	$Ir(dFCF_3ppy)_2(dtbbpy)PF_6$	$NiCl_2$ glyme (10)	dtbbpy (15)	DABCO	-	DMF (0.1M)	29
2	$Ir(ppy)_3$	$NiCl_2$ glyme (10)	dtbbpy (15)	DABCO	-	DMF (0.1M)	0
3	$Ru(bpy)_3Cl_2$	$NiCl_2$ glyme (10)	dtbbpy (15)	DABCO	-	DMF (0.1M)	0
4	4-CzIPN	$NiCl_2$ glyme (10)	dtbbpy (15)	DABCO	-	DMF (0.1M)	4
5	2,4,6-triphenylpyrylium BF_4	$NiCl_2$ glyme (10)	dtbbpy (15)	DABCO	-	DMF (0.1M)	0
6	$Ir(dFCF_3ppy)_2(dtbbpy)PF_6$	$NiBr_2$ glyme (10)	dtbbpy (15)	DABCO	-	DMF (0.1M)	29
7	$Ir(dFCF_3ppy)_2(dtbbpy)PF_6$	$Ni(cod)_2$ (10)	dtbbpy (15)	DABCO	-	DMF (0.1M)	20
8	$Ir(dFCF_3ppy)_2(dtbbpy)PF_6$	$Ni(acac)_2$ (10)	dtbbpy (15)	DABCO	-	DMF (0.1M)	trace
9	$Ir(dFCF_3ppy)_2(dtbbpy)PF_6$	$NiBr_2$ glyme (10)	dtbbpy (15)	K_3PO_4	-	DMF (0.1M)	0
10	$Ir(dFCF_3ppy)_2(dtbbpy)PF_6$	$NiBr_2$ glyme (10)	dtbbpy (15)	K_2CO_3	-	DMF (0.1M)	13
11	$Ir(dFCF_3ppy)_2(dtbbpy)PF_6$	$NiBr_2$ glyme (10)	dtbbpy (15)	DBU	-	DMF (0.1M)	35
12	$Ir(dFCF_3ppy)_2(dtbbpy)PF_6$	$NiBr_2$ glyme (10)	dtbbpy (15)	2,4,6-collidine	-	DMF (0.1M)	0
13	$Ir(dFCF_3ppy)_2(dtbbpy)PF_6$	$NiBr_2$ glyme (10)	dtbbpy (15)	BTMG	-	DMF (0.1M)	31
14	$Ir(dFCF_3ppy)_2(dtbbpy)PF_6$	$NiBr_2$ glyme (10)	dtbbpy (15)	DBU	-	DMA (0.1M)	40
15	$Ir(dFCF_3ppy)_2(dtbbpy)PF_6$	$NiBr_2$ glyme (10)	dtbbpy (15)	DBU	-	DMSO (0.1M)	21
16	$Ir(dFCF_3ppy)_2(dtbbpy)PF_6$	$NiBr_2$ glyme (10)	dtbbpy (15)	DBU	-	CH_3CN (0.1M)	30
17	$Ir(dFCF_3ppy)_2(dtbbpy)PF_6$	$NiBr_2$ glyme (10)	dtbbpy (15)	DBU	-	CH_2Cl_2 (0.1M)	trace
18	$Ir(dFCF_3ppy)_2(dtbbpy)PF_6$	$NiBr_2$ glyme (10)	dtbbpy (15)	DBU	-	toluene (0.1M)	27
19	$Ir(dFCF_3ppy)_2(dtbbpy)PF_6$	$NiBr_2$ glyme (10)	2,2'-bipyridine (15)	DBU	-	DMA (0.1M)	27
20	$Ir(dFCF_3ppy)_2(dtbbpy)PF_6$	$NiBr_2$ glyme (10)	2,2-bisoxazole (15)	DBU	-	DMA (0.1M)	14
21	$Ir(dFCF_3ppy)_2(dtbbpy)PF_6$	$NiBr_2$ glyme (10)	Terpyridine (15)	DBU	-	DMA (0.1M)	35
22	$Ir(dFCF_3ppy)_2(dtbbpy)PF_6$	$NiBr_2$ glyme (10)	1,10-phenanthroline (15)	DBU	-	DMA (0.1M)	44
23[b]	$Ir(dFCF_3ppy)_2(dtbbpy)PF_6$	$NiBr_2$ glyme (10)	1,10-phenanthroline (15)	DBU	$ZnBr_2$	DMA (0.1M)	12
24[b]	$Ir(dFCF_3ppy)_2(dtbbpy)PF_6$	$NiBr_2$ glyme (10)	1,10-phenanthroline (15)	DBU	$MgBr_2$	DMA (0.1M)	trace
25[b]	$Ir(dFCF_3ppy)_2(dtbbpy)PF_6$	$NiBr_2$ glyme (10)	1,10-phenanthroline (15)	DBU	LiCl	DMA (0.1M)	73
26[b]	$Ir(dFCF_3ppy)_2(dtbbpy)PF_6$	$NiBr_2$ glyme (10)	1,10-phenanthroline (15)	DBU	LiBr	DMA (0.1M)	22
27[b]	$Ir(dFCF_3ppy)_2(dtbbpy)PF_6$	$NiBr_2$ glyme (10)	1,10-phenanthroline (15)	DBU	TBACl	DMA (0.1M)	70
28[b]	$Ir(dFCF_3ppy)_2(dtbbpy)PF_6$	$NiBr_2$ glyme (10)	1,10-phenanthroline (15)	DBU	TBABr	DMA (0.1M)	38
29[b]	$Ir(dFCF_3ppy)_2(dtbbpy)PF_6$	$NiBr_2$ glyme (5)	1,10-phenanthroline (7.5)	DBU	LiCl	DMA (0.05M)	78
30[b]	$Ir(dFCF_3ppy)_2(dtbbpy)PF_6$	$NiCl_2$ glyme (5)	1,10-phenanthroline (7.5)	DBU	LiCl	DMA (0.05M)	83 (73)[c]

[a] Reaction condition: **1a** (0.13 mmol), **2a** (0.10 mmol), **[PC]** (1.0 mol%), **[Ni]**, **ligand**, **base** (0.10 mmol), **additive** (0.15 mmol) and **solvent** irradiated with 34W blue LEDs. Yields are determined by gas chromatography using dodecane as an internal standard. [b] **1a** (0.15 mmol). [c] The reaction was carried out under air conditions. glyme=1,2-dimethoxyethane. dtbbpy=4,4'-di-*tert*-butyl-2,2'-bipyridine. DBU=1,8-diazabicyclo[5.4.0]undec-7-ene. DABCO=1,4-diazabicyclo[2.2.2]octane. DMF=*N,N*-dimethylformamide. 4CzIPN=1,2,3,5-tetrakis(carbazol-9-yl)-4,6-dicyanobenzene. DMA=*N,N*-dimethylacetamide. BTMG=2-*tert*-butyl-1,1,3,3-tetramethyl-guanidine. DMSO=dimethyl sulfoxide.

Table 2.7 Evaluation of other Ni sources[a]

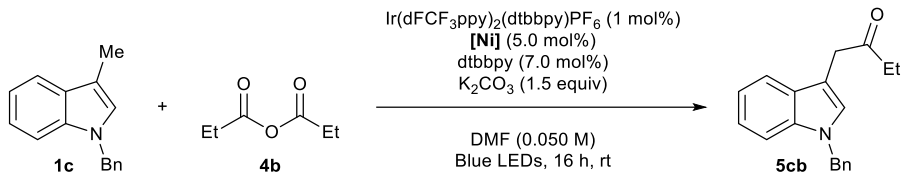

[Ni]	yield (%)
$NiCl_2$·glyme	76
$NiBr_2$·glyme	73
$NiSO_4·6H_2O$	87
$Ni(acac)_2$	77
$Ni(TMHD)_2$	80
$Ni(cod)_2$	99

[a] The reaction was carried out with the *General procedure E*.

Table 2.8 Attempted enantioselective arylation with chiral ligands

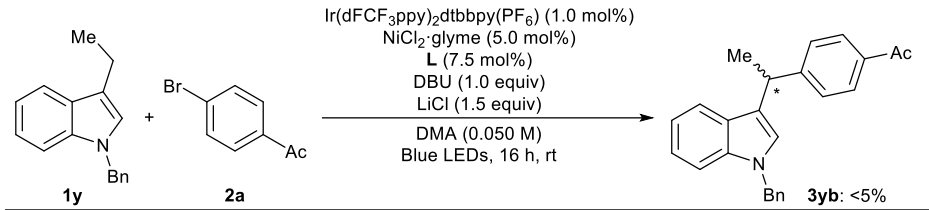

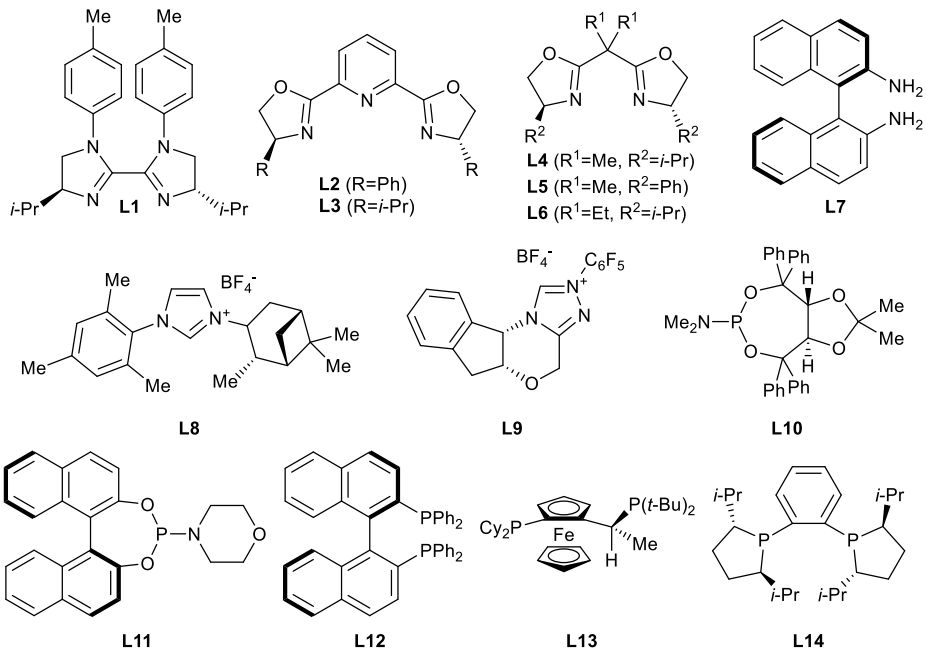

All reactions performed in the presence of a chiral ligand did not show the required level of reactivity in the first place. Hence, the enantioselective benzylic functionalization has been excluded from the scope of the current study.

Table 2.9 Attempted enantioselective acylation with chiral ligands

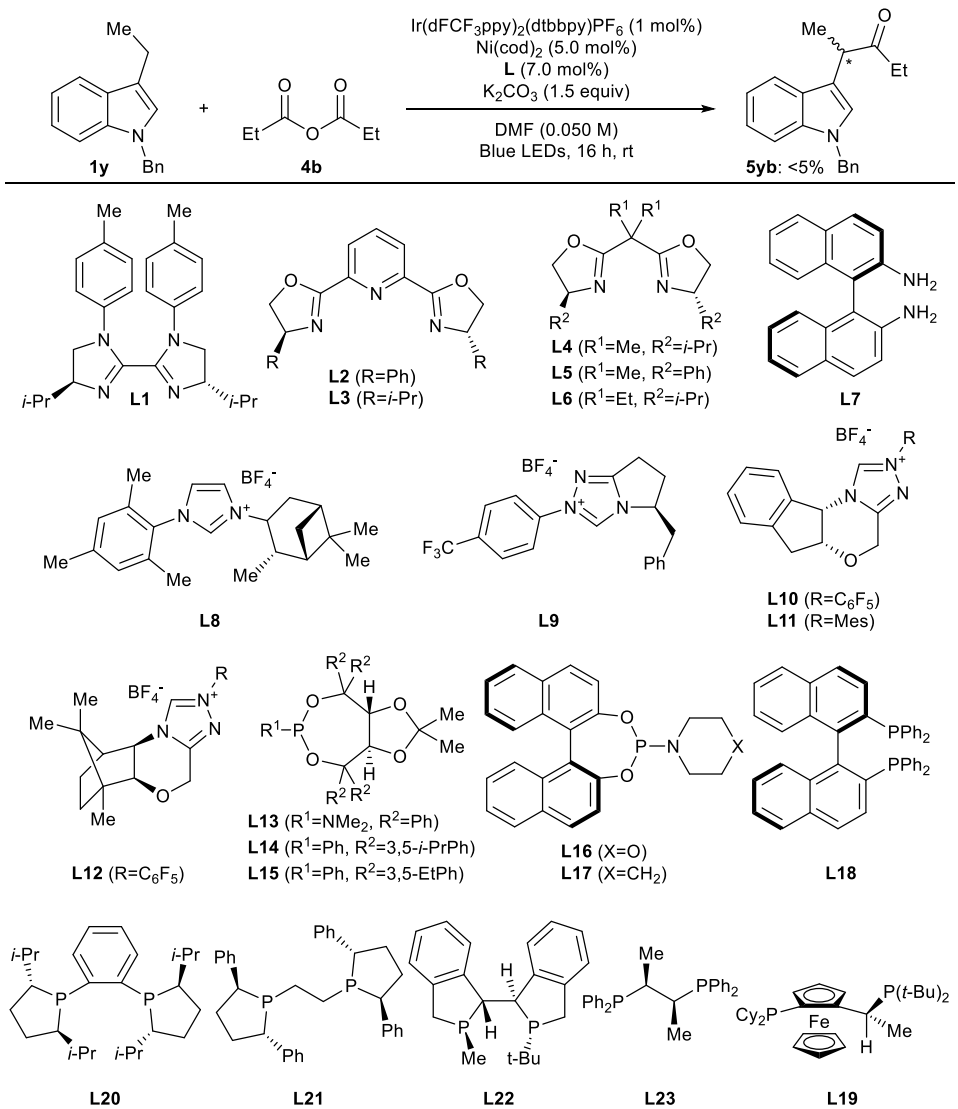

All reactions performed in the presence of a chiral ligand did not show the required level of reactivity in the first place. Hence, the enantioselective benzylic functionalization has been excluded from the scope of the current study.

Table 2.10 Unsuccessful substrates for the arylation reaction

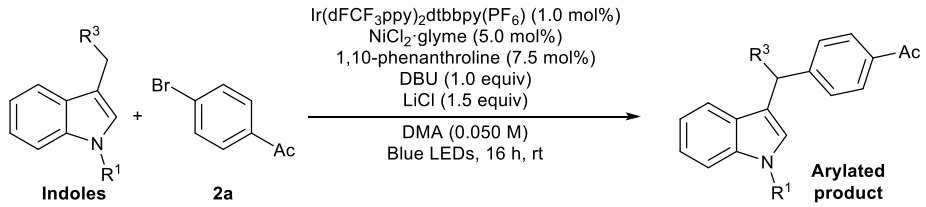

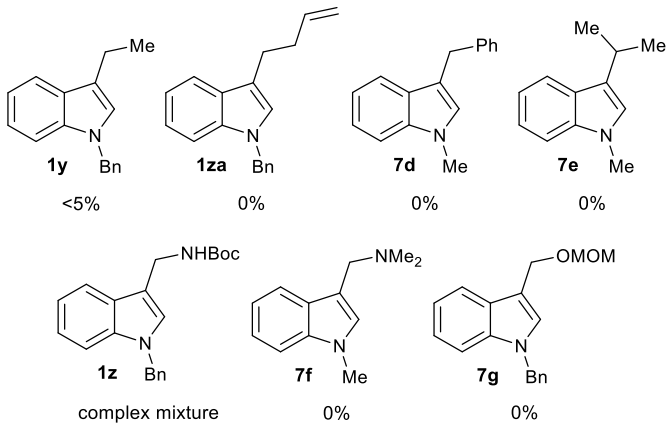

Table 2.11 Unsuccessful substrates for the acylation reaction

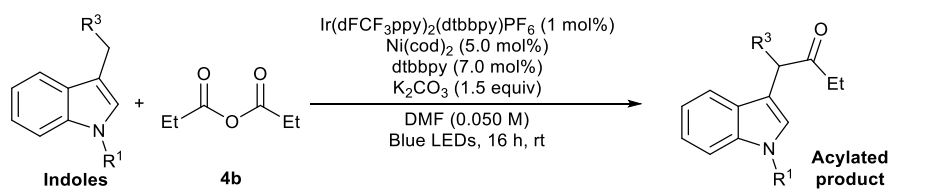

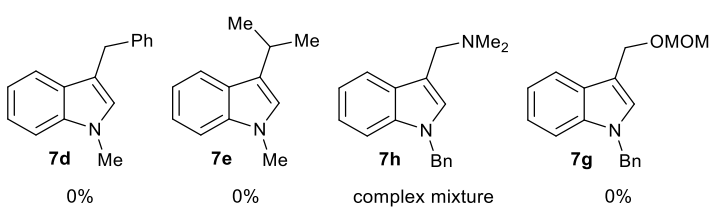

2.4.7 Radical trapping experiments

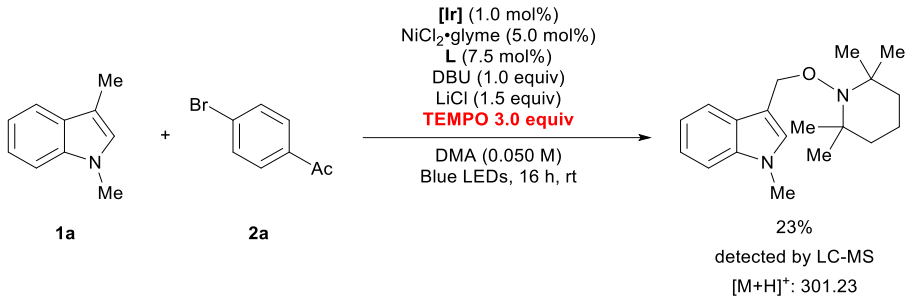

The reaction was set up in a nitrogen-filled glove box. To an 8 mL vial equipped with a PTFE-coated stirrer bar was added the corresponding indole **1a** (0.30 mmol, 1.5 equiv), $Ir[dF(CF_3)ppy]_2(dtbbpy)PF_6$ (2.2 mg, 0.0020 mmol, 1.0 mol%), $NiCl_2$·glyme (2.2 mg, 0.010 mmol, 5.0 mol%), 1,10-phenanthroline (2.7 mg, 0.015 mmol, 7.5 mol%), DBU (30 μL, 0.20 mmol, 1.0 equiv), LiCl (12.7 mg, 0.30 mmol, 1.5 equiv), aryl halide **2a** (0.20 mmol, 1.0 equiv), (2,2,6,6-tetramethylpiperidine-1-yl)oxy (93.7 mg, 0.60 mmol, 3.0 equiv) and DMA (4.0 mL). The reaction vial was removed from the glove box, stirred for 16 h under 34 W blue LED irradiation with fan cooling. At the end of the reaction, the resulting solution was transferred to a separatory funnel and partitioned between water (7 mL) and Et_2O (20 mL). The organic extract was washed with water (7 mL x 2) and brine (7 mL), dried over $MgSO_4$, filtered and concentrated under reduced pressure. The crude residue was analyzed by ^1H NMR relative to 1,1,2,2-tetrachloroethane(10 μL, 0.094 mmol) as an external standard to determine the existence of the product **3aa**.[61]

In the LC-MS analysis, the product **3aa** was not detected and the TEMPO-indole adduct was detected. This indicates that the reaction indeed proceeds through a radical pathway and that the indole radical is generated during the reaction. Figure 2.3 depicts the selective ion chromatogram with peaks showing molecular weight

values of 301.23. The peak eluting at 13.120 min was determined to be the TEMPO-indole adduct. The mass spectrum is shown in Figure 2.3.

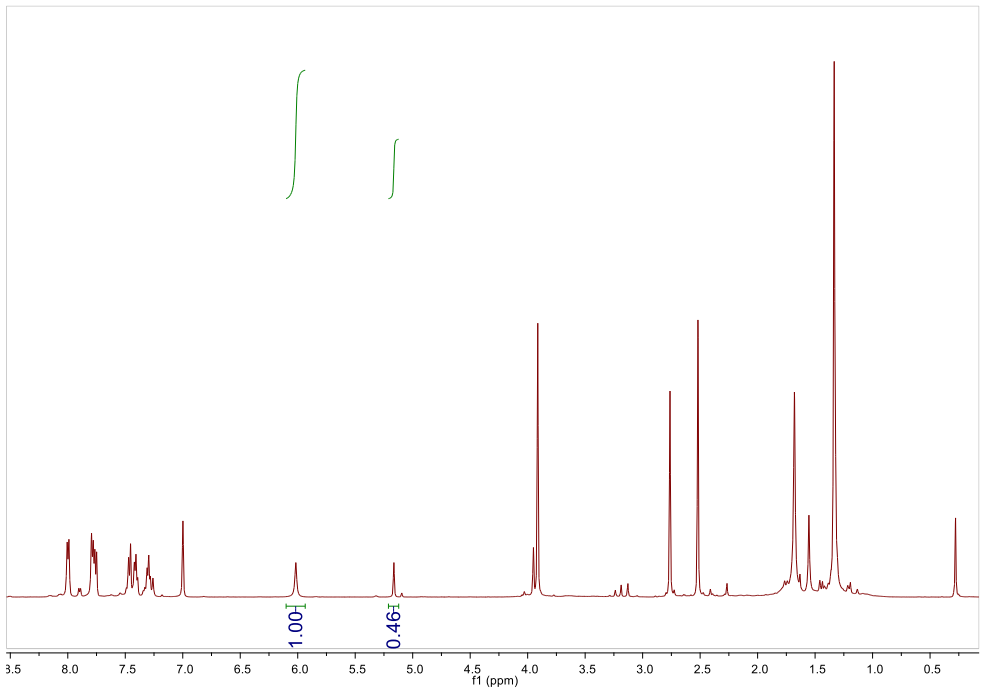

Figure 2.2 ^{1}H-NMR spectrum of the crude reaction mixture

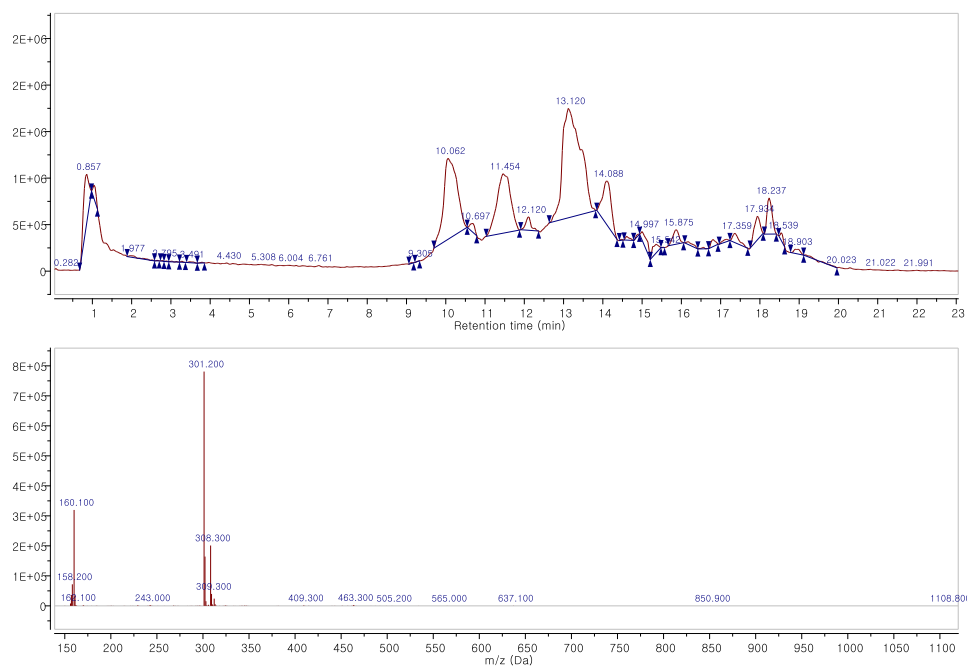

Figure 2.3 LC-MS spectrum of the crude mixture showing ions of mass 301.2

2.4.8 Control experiments to exclude the HAT process

Giese addition with LiCl

For the experiments shown in Scheme 2.3A, the following procedure was employed.

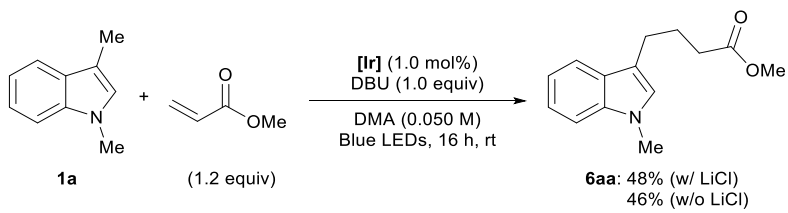

The reaction was set up in a nitrogen-filled glove box. To a 4 mL vial equipped with a PTFE-coated stirring bar was added the corresponding indole **1a** (14.6 mg, 0.10 mmol, 1.0 equiv), methyl acrylate (10.8 μL, 0.12 mmol, 1.2 equiv), $Ir[dF(CF_3)ppy]_2(dtbbpy)PF_6$ (1.1 mg, 0.0010 mmol, 1.0 mol%), DBU (15 μL, 0.10 mmol, 1.0 equiv), LiCl (6.3 mg, 0.15 mmol, 1.5 equiv), and DMF (2.0 mL). The reaction vial was removed from the glove box, stirred for 16 h under 34 W blue LED irradiation with fan cooling. At the end of the reaction, the resulting solution was transferred to a separatory funnel and partitioned between water (7 mL) and Et_2O (20 mL). The organic extract was washed with water (7 mL x 2) and brine (7 mL), dried over $MgSO_4$, filtered and concentrated under reduced pressure. The crude residue was analyzed by ^1H NMR relative to 1,1,2,2-tetrachloroethane as an external standard.

Stoichiometric experiment with [Ni]-1

The oxidative addition complex **[Ni]-1** was prepared following the literature procedure.[53] For the experiments shown in Scheme 2.3B, the following procedure was employed.

Table 2.12 Stoichiometric experiment result of nickel complex **[Ni]-1** with various oxidants and additives

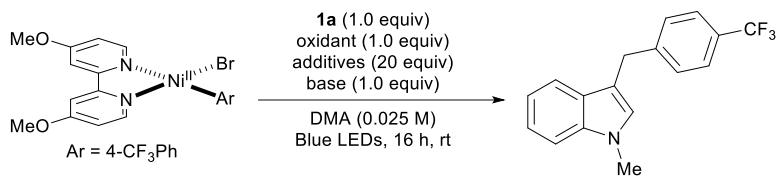

[Ni]-1 **3ad**: N.D.

entry	oxidant	additives	base	result
1	$(TBPA)SbCl_6$	-	-	N.D.
2	$(TBPA)SbCl_6$ (dark)	-	-	N.D.
3	$(TBPA)SbCl_6$	LiCl	-	N.D.
4	$Ir(dFCF_3ppy)_2(dtbbpy)PF_6$	-	-	N.D.
5	$Ir(dFCF_3ppy)_2(dtbbpy)PF_6$	LiCl	-	N.D.
6	$Ir(dFCF_3ppy)_2(dtbbpy)PF_6$	LiCl	DBU	N.D.

The reaction was set up in a nitrogen-filled glove box. To a 4 mL vial equipped with a PTFE-coated stirring bar was added the corresponding **[Ni]-1** (25 mg, 0.050 mmol, 1.0 equiv), indole **1a** (7.3 mg, 0.050 mmol, 1.0 equiv), oxidant (0.050 mmol, 1.0 equiv), LiCl (42.39 mg, 1.0 mmol, 20 equiv), DBU (7.5 μL, 0.050 mmol, 1.0 equiv), and DMF (2.0 mL). The reaction vial was removed from the glove box,

stirred for 16 h under 34 W blue LED irradiation with fan cooling. At the end of the reaction, the resulting solution was transferred to a separatory funnel and partitioned between water (7 mL) and Et_2O (20 mL). The organic extract was washed with water (7 mL x 2) and brine (7 mL), dried over $MgSO_4$, filtered and concentrated under reduced pressure. The crude residue was analyzed by ^1H NMR relative to 1,1,2,2-tetrachloroethane as an external standard.

2.4.9 Fluorescence quenching experiment (Stern–Volmer relationship)

Fluoresence quenching experiment was conducted with 25 μM $Ir[dF(CF_3)ppy]_2(dtbbpy)PF_6$ in DMA. Various substrates were used as quenchers (see below in more detail). Samples were excited at 400 nm and peak emissions were recorded at 500 nm to construct the Stern–Volmer regression.

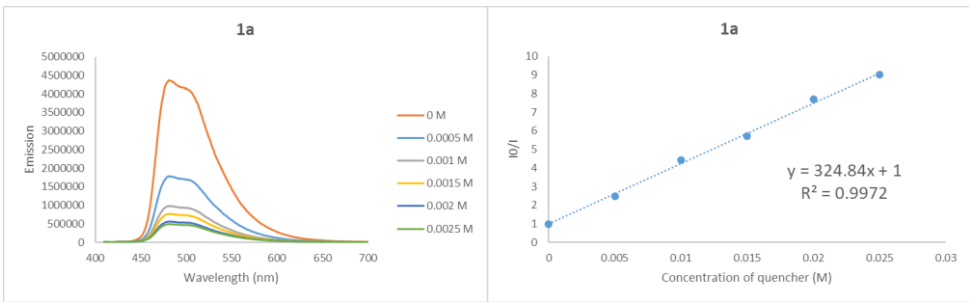

Figure 2.4 Stern–Volmer quenching study with 1,3-dimethyl-1*H*-indole, **1a**

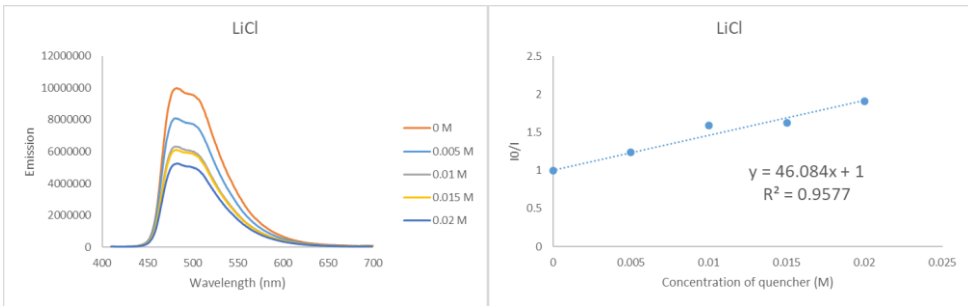

Figure 2.5 Stern–Volmer quenching study with LiCl

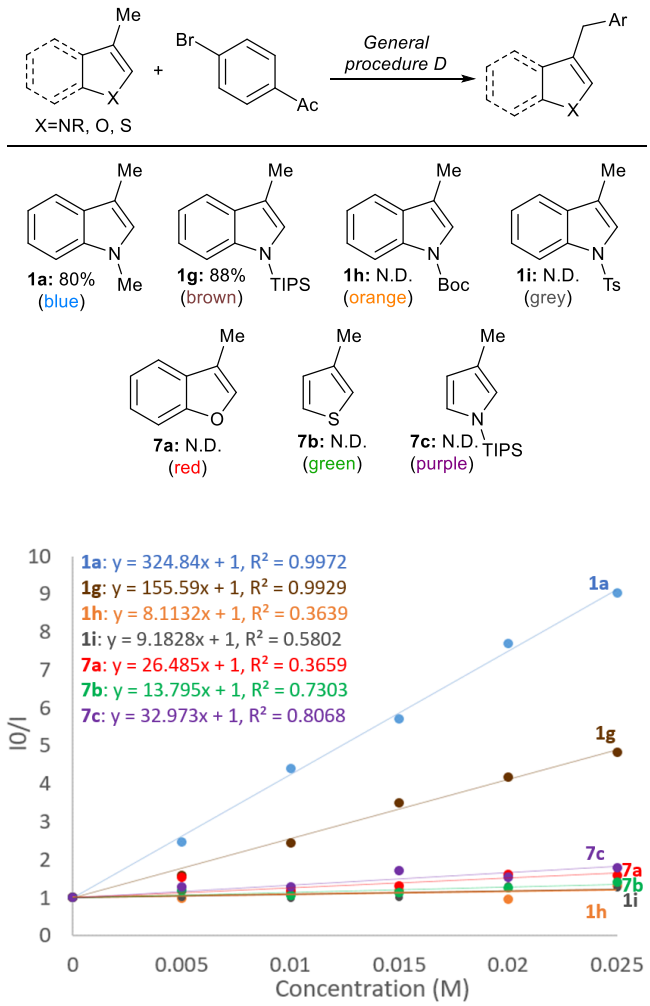

Figure 2.6 Stern–Volmer quenching studies with various indoles and other heterocyclic compounds

2.4.10 Electrochemical characterizations

The electrochemical properties of the substrates and the photocatalyst were characterized by standard cyclic voltammetry (CV) techniques. The samples were dissolved in Ar-saturated CH_3CN (10 mL) to a concentration of 10.0 mM photocatalyst and 5.0 mM other substrates. The solution contained 0.10 M $TBAPF_6$

supporting electrolyte. A three-electrode cell assembly consisting of a glassy carbon (GC) working electrode, a Pt coiled counter electrode, and Ag/AgCl pseudo reference electrode was employed for the voltammetric measurements. All cyclic voltammogram data (grey line) were obtained in Ar-saturated CH_3CN. The dotted line is an electrochemical response of a blank CH_3CN solution. The photoexcitation wavelength was 400 nm.

Procedure for Ir[dF(CF_3)ppy]$_2$(dtbbpy)PF_6

The cyclic voltammogram was acquired at a scan rate of 0.10 V s^{-1} and a scan range of –1.8 to 0.0 V. The excited-state reduction potential of Ir[dF(CF_3)ppy]$_2$(dtbbpy)PF_6 was calculated from the triplet state energy (2.57 eV) and ground-state redox potential. The cyclic voltammograms indicate that a reversible reduction has occurred at –1.32 V vs. Ag/AgCl. As a result, the excited-state reduction potential of Ir[dF(CF_3)ppy]$_2$(dtbbpy)PF_6 is +1.24 V vs. Ag/AgCl.

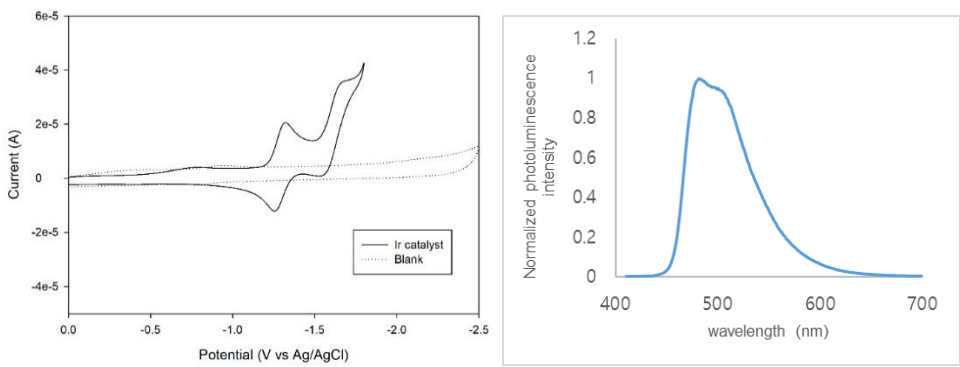

Figure 2.7 The cyclic voltammograms (left) and the phosphorescence spectrum (right) of 10.0 mM of **[Ir]**

Procedure for 1,3-dimethyl-1*H*-indole (1a)

The cyclic voltammogram was acquired at a scan rate of 0.10 V s^{-1} and a scan range of 0.0 to +2.0 V. The cyclic voltammograms indicates that an irreversible oxidation occurred at +1.00 V vs. Ag/AgCl.

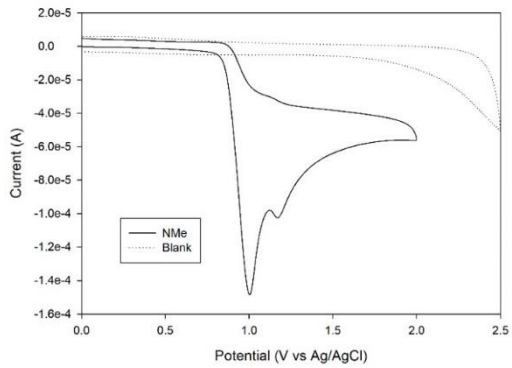

Figure 2.8 The cyclic voltammograms (grey line) of 5.0 mM of 1,3-dimethyl-1*H*-indole

Procedure for *tert*-butyl 3-methyl-1*H*-indole-1-carboxylate (1h)

The cyclic voltammogram was acquired at a scan rate of 0.10 V s^{-1} and a scan range of 0.0 to +2.0 V. The cyclic voltammograms indicates that an irreversible oxidation occurred at +1.49 V vs. Ag/AgCl.

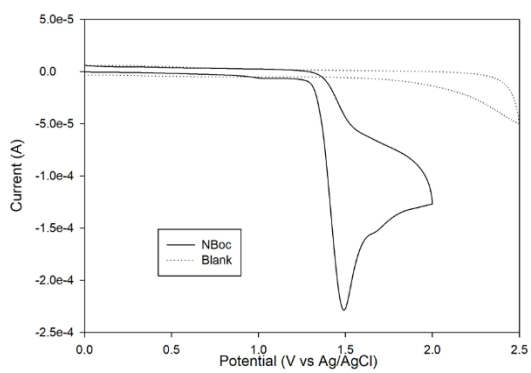

Figure 2.9 The cyclic voltammograms (grey line) of 5.0 mM of *tert*-butyl 3-methyl-1*H*-indole-1-carboxylate

Procedure for lithium chloride (LiCl)

The cyclic voltammogram was acquired at a scan rate of 0.10 V s^{-1} and a scan range of 0.0 to +2.5 V. The cyclic voltammograms indicates that an irreversible oxidation occurred at +1.31 V vs. Ag/AgCl.

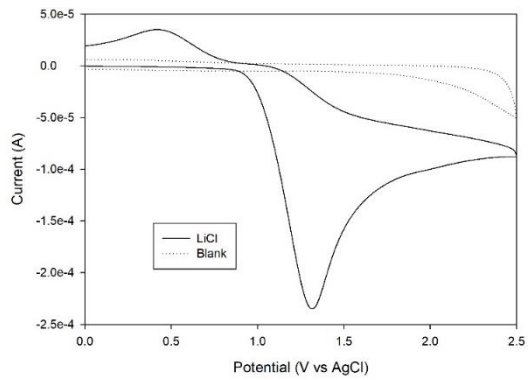

Figure 2.10 The cyclic voltammograms (grey line) of 5.0 mM of lithium chloride

Procedure for 3-methyl-1-(triisopropylsilyl)-1*H*-pyrrole (7c)

The cyclic voltammogram was acquired at a scan rate of 0.10 V s^{-1} and a scan range of 0.0 to +2.0 V. The cyclic voltammograms indicates that an irreversible oxidation occurred at +1.32 V vs. Ag/AgCl.

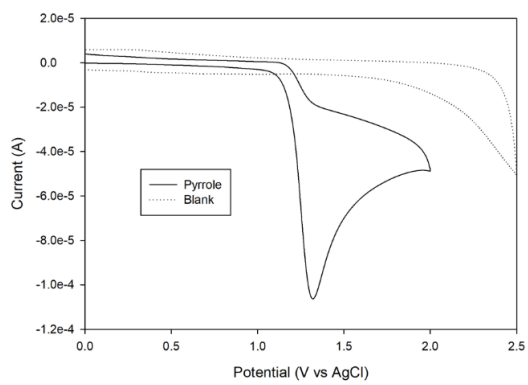

Figure 2.11 The cyclic voltammograms (grey line) of 5.0 mM of 3-methyl-1-(triisopropylsilyl)-1*H*-pyrrole

2.4.11 Kinetic isotope effect (KIE) experiment

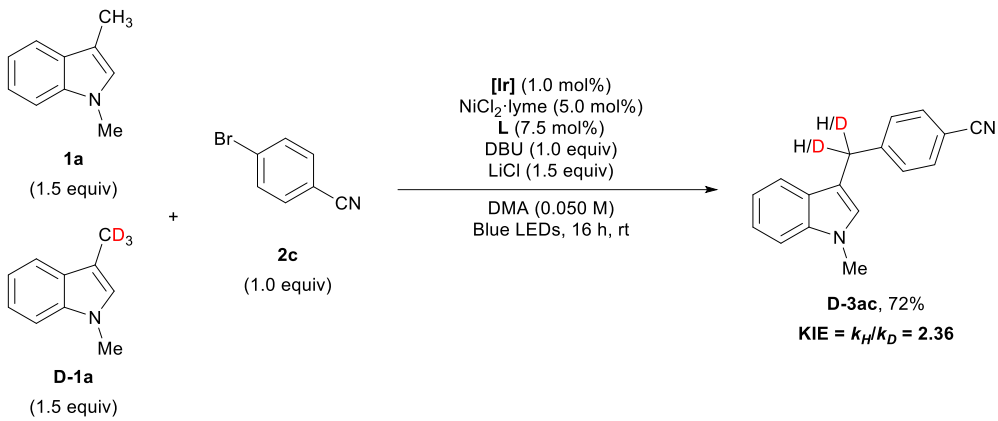

The reaction was set up in a nitrogen-filled glove box. To an 8 mL vial equipped with a PTFE-coated stirrer bar was added the corresponding indole **1a** (0.30 mmol, 1.5 equiv) deutrated indole **D-1a** (0.30 mmol, 1.5 equiv), $Ir[dF(CF_3)ppy]_2(dtbpy)PF_6$ (2.2 mg, 0.0020 mmol, 1.0 mol%), $NiCl_2$·glyme (2.2 mg, 0.010 mmol, 5.0 mol%), 1,10-phenanthroline (2.7 mg, 0.015 mmol, 7.5 mol%), DBU (30 μL, 0.20 mmol, 1.0 equiv), LiCl (12.7 mg, 0.30 mmol, 1.5 equiv) the corresponding aryl halide **2c** (0.20 mmol, 1.0 equiv), and DMA (4.0 mL). The reaction vial was removed from the glove box, stirred for 16 h under 34 W blue LED irradiation with fan cooling. At the end of the reaction, the resulting solution was transferred to a separatory funnel and partitioned between water (7 mL) and Et_2O (20 mL). The organic extract was washed with water (7 mL x 2) and brine (7 mL), dried over $MgSO_4$, filtered and concentrated under reduced pressure. Purification by flash column chromatography led to the 72% of the combined arylated products. The KIE value was k_H/k_D=2.36 determined by ^1H NMR spectrum (Figure 2.12).

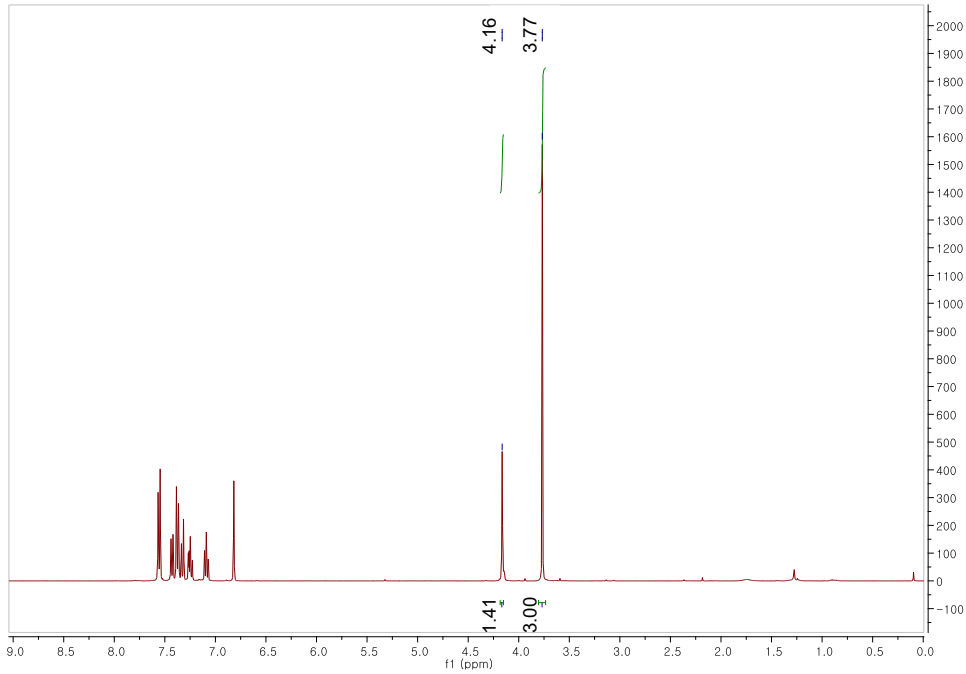

Figure 2.12 ^{1}H-NMR spectrum of KIE experiment, **D-3ac**

2.5 References

1. For selected reviews, see: (a) H. M. L. Davies, J. Du Bois and J.-Q. Yu, *Chem. Soc. Rev.*, 2011, **40**, 1855-1856; (b) P. Gandeepan, T. Müller, D. Zell, G. Cera, S. Warratz and L. Ackermann, *Chem. Rev.*, 2019, **119**, 2192-2452; (c) A. E. Shilov and G. B. Shul'pin, *Chem. Rev.*, 1997, **97**, 2879-2932.

2. For reviews, see: (a) R. Vanjari and K. N. Singh, *Chem. Soc. Rev.*, 2015, **44**, 8062-8096; (b) U. Gulati, R. Gandhi and J. K. Laha, *Chem. Asian. J.*, 2020, **15**, 3135-3161.

3. For a recent review, see: R. Yazaki and T. Ohshima, *Tetrahedron Lett.*, 2019, **60**, 151225.

4. For representative approaches, see: (a) M. Rosillo, G. Domínguez and J. Pérez-Castells, *Chem. Soc. Rev.*, 2007, **36**, 1589-1604; (b) G. Rouquet and N. Chatani, *Angew. Chem. Int. Ed.*, 2013, **52**, 11726-11743; (c) Y. Masuda, N. Ishida and M. Murakami, *Chem. Asian. J.*, 2019, **14**, 403-406; For recent examples, see: (d) M. A. Larsen, C. V. Wilson and J. F. Hartwig, *J. Am. Chem. Soc.*, 2015, **137**, 8633-8643; (e) S. Takemoto, E. Shibata, M. Nakajima, Y. Yumoto, M. Shimamoto and H. Matsuzaka, *J. Am. Chem. Soc.*, 2016, **138**, 14836-14839; (f) W. N. Palmer, J. V. Obligacion, I. Pappas and P. J. Chirik, *J. Am. Chem. Soc.*, 2016, **138**, 766-769; (g) S.-C. Sha, S. Tcyrulnikov, M. Li, B. Hu, Y. Fu, M. C. Kozlowski and P. J. Walsh, *J. Am. Chem. Soc.*, 2018, **140**, 12415-12423.

5. For reviews, see: (a) H. Yi, G. Zhang, H. Wang, Z. Huang, J. Wang, A. K. Singh and A. Lei, *Chem. Rev.*, 2017, **117**, 9016-9085; (b) I. Bosque, R.

Chinchilla, J. C. Gonzalez-Gomez, D. Guijarro and F. Alonso, *Org. Chem. Front.*, 2020, **7**, 1717-1742.

6. For a review of HAT, see: (a) J. M. Mayer, *Acc. Chem. Res.*, 2011, **44**, 36-46; For recent examples, see: (b) W. Zhang, L. Wu, P. Chen and G. Liu, *Angew. Chem. Int. Ed.*, 2019, **58**, 6425-6429; (c) H. Hu, S.-J. Chen, M. Mandal, S. M. Pratik, J. A. Buss, S. W. Krska, C. J. Cramer and S. S. Stahl, *Nat. Catal.*, 2020, **3**, 358-367.

7. For a recent review, see: (a) L. Capaldo and D. Ravelli, *Eur. J. Org. Chem.*, 2017, 2056-2071; For representative examples, see: (b) D. R. Heitz, J. C. Tellis and G. A. Molander, *J. Am. Chem. Soc.*, 2016, **138**, 12715-12718; (c) B. J. Shields and A. G. Doyle, *J. Am. Chem. Soc.*, 2016, **138**, 12719-12722; (d) Y. Shen, Y. Gu and R. Martin, *J. Am. Chem. Soc.*, 2018, **140**, 12200-12209; (e) A. Dewanji, P. E. Krach and M. Rueping, *Angew. Chem. Int. Ed.*, 2019, **58**, 3566-3570; (f) X. Cheng, H. Lu and Z. Lu, *Nat. Commun.*, 2019, **10**, 3549; (g) P. E. Krach, A. Dewanji, T. Yuan and M. Rueping, *Chem. Commun.*, 2020, **56**, 6082-6085; (h) N. Ishida, Y. Masuda, N. Ishikawa and M. Murakami, *Asian J. Org. Chem.*, 2017, **6**, 669-672; (i) T. Kawasaki, N. Ishida and M. Murakami, *J. Am. Chem. Soc.*, 2020, **142**, 3366-3370.

8. For selected examples of site-selectivity issues of HAT process, see: (a) T. Ide, J. P. Barham, M. Fujita, Y. Kawato, H. Egami and Y. Hamashima, *Chem. Sci.*, 2018, **9**, 8453-8460; (b) H.-P. Deng, Q. Zhou and J. Wu, *Angew. Chem. Int. Ed.*, 2018, **57**, 12661-12665; (c) K. A. Margrey, W. L. Czaplyski, D. A. Nicewicz and E. J. Alexanian, *J. Am. Chem. Soc.*, 2018, **140**, 4213-4217.

9. For a review, see: R. I. Cukier and D. G. Nocera, *Annu. Rev. Phys. Chem.*, 1998, **49**, 337-369.

10. For benzylic functionalizations based on ET/PT, see: (a) K. Ohkubo, K. Mizushima, R. Iwata, K. Souma, N. Suzuki and S. Fukuzumi, *Chem. Commun.*, 2010, **46**, 601-603; (b) G. Pandey, S. Pal and R. Laha, *Angew. Chem. Int. Ed.*, 2013, **52**, 5146-5149; (c) R. Zhou, H. Liu, H. Tao, X. Yu and J. Wu, *Chem. Sci.*, 2017, **8**, 4654-4659; (d) D. Mazzarella, G. E. M. Crisenza and P. Melchiorre, *J. Am. Chem. Soc.*, 2018, **140**, 8439-8443; (e) B. J. Lee, K. S. DeGlopper and T. P. Yoon, *Angew. Chem. Int. Ed.*, 2020, **59**, 197-202; (f) T. Duhamel and K. Muñiz, *Chem. Commun.*, 2019, **55**, 933-936; (g) R. C. Betori, C. M. May and K. A. Scheidt, *Angew. Chem. Int. Ed.*, 2019, **58**, 16490-16494; (h) S. Bloom, M. McCann and T. Lectka, *Org. Lett.*, 2014, **16**, 6338-6341; (i) W. Xu, W. Wang, T. Liu, J. Xie and C. Zhu, *Nat. Commun.*, 2019, **10**, 4867; (j) Y. Yu, L.-K. Zhang, A. V. Buevich, G. Li, H. Tang, P. Vachal, S. L. Colletti and Z.-C. Shi, *J. Am. Chem. Soc.*, 2018, **140**, 6797-6800; (k) L. Zhang and X. Hu, *Chem. Sci.*, 2020, **11**, 10786-10791.

11. For ET/PT-based transformations of other classes of compounds, see: (a) F. R. Petronijević, M. Nappi and D. W. C. MacMillan, *J. Am. Chem. Soc.*, 2013, **135**, 18323-18326; (b) C. L. Joe and A. G. Doyle, *Angew. Chem. Int. Ed.*, 2016, **55**, 4040-4043; (c) D. T. Ahneman and A. G. Doyle, *Chem. Sci.*, 2016, **7**, 7002-7006; (d) K. Ohmatsu, T. Nakashima, M. Sato and T. Ooi, *Nat. Commun.*, 2019, **10**, 2706.

12. For seminal publications on the synergistic combination of transition metal

catalysis and phtoredox-mediated radical generation, see: (a) J. C. Tellis, D. N. Primer and G. A. Molander, *Science*, 2014, **345**, 433; (b) Z. Zuo, D. T. Ahneman, L. Chu, J. A. Terrett, A. G. Doyle and D. W. C. MacMillan, *Science*, 2014, **345**, 437.

13. To our best knowledge, a recent report by Hu describes the only example of ET/PT-based Ni catalysis using noncatalytic convergent paired electrolysis (ref. 10k). Mechanistically, however, involvement of the HAT process could not be ruled out in this case.

14. H. G. Roth, N. A. Romero and D. A. Nicewicz, *Synlett*, 2016, **27**, 714-723.

15. See the Table 2.6 for full optimization data.

16. For additive effects in transition metal catalysis, see: L. Hong, W. Sun, D. Yang, G. Li and R. Wang, *Chem. Rev.*, 2016, **116**, 4006-4123.

17. For discussions on LiCl-mediated enhancement of catalytic activity in cross-coupling reaction, see: (a) J. Sherwood, J. H. Clark, I. J. S. Fairlamb and J. M. Slattery, *Green Chem.*, 2019, **21**, 2164-2213. Also see: (b) C. Zhang, R. Liu, J. Xiang, H. Kang, Z. Liu and Y. Huang, *J. Phys. Chem. B*, 2014, **118**, 9507-9514.

18. The corresponding TEMPO adduct was detected in 22% yield. See the Figure 2.2 and 2.3 for more details.

19. (a) G. Goverdhan, A. R. Reddy, V. Himabindu and G. M. Reddy, *Synth. Commun.*, 2013, **43**, 498-504; (b) S. Schierle, C. Flauaus, P. Heitel, S. Willems, J. Schmidt, A. Kaiser, L. Weizel, T. Goebel, A. S. Kahnt, G.

Geisslinger, D. Steinhilber, M. Wurglics, G. E. Rovati, A. Schmidtko, E. Proschak and D. Merk, *J. Med. Chem.*, 2018, **61**, 5758-5764; (c) S. Paladugu, P. S. Mainkar and S. Chandrasekhar, *ACS Omega*, 2018, **3**, 4289-4294.

20. For examples associated with HAT processes mediated by added halide ions, see: (a) S. Rohe, A. O. Morris, T. McCallum and L. Barriault, *Angew. Chem. Int. Ed.*, 2018, **57**, 15664-15669; (b) Z. Wang, X. Ji, T. Han, G.-J. Deng and H. Huang, *Adv. Synth. Catal.*, 2019, **361**, 5643-5647.

21. See the Figure 2.5 and 2.10.

22. (a) S. J. Hwang, B. L. Anderson, D. C. Powers, A. G. Maher, R. G. Hadt and D. G. Nocera, *Organometallics*, 2015, **34**, 4766-4774; (b) S. J. Hwang, D. C. Powers, A. G. Maher, B. L. Anderson, R. G. Hadt, S.-L. Zheng, Y.-S. Chen and D. G. Nocera, *J. Am. Chem. Soc.*, 2015, **137**, 6472-6475.

23. This is based on the nature of the benzylic HAT process, which is not significantly influenced by the electronics of the arene. See ref. [7f] for a related example.

24. For a general review on the mechanisms of Ni-catalysed coupling reactions, see: J. B. Diccianni and T. Diao, *Trends Chem.*, 2019, **1**, 830-844.

25. An analogous stoichiometric experiment was utilised to identify the operating mechanism of a related reaction, see: K. Nakajima, S. Nojima and Y. Nishibayashi, *Angew. Chem. Int. Ed.*, 2016, **55**, 14106-14110.

26. For related examples in support of our proposed reaction pathway, see: (a) G. S. Lee, J. Won, S. Choi, M.-H. Baik and S. H. Hong, *Angew. Chem. Int.*

Ed., 2020, **59**, 16933-16942; (b) M. Yuan, Z. Song, S. O. Badir, G. A. Molander and O. Gutierrez, *J. Am. Chem. Soc.*, 2020, **142**, 7225-7234; (c) B. Maity, C. Zhu, H. Yue, L. Huang, M. Harb, Y. Minenkov, M. Rueping and L. Cavallo, *J. Am. Chem. Soc.*, 2020, **142**, 16942-16952; (d) X. Tao, Y. Chen, J. Guo, X. Wang and H. Gong, *Chem. Sci.*, 2021, **12**, 220-226.

27. M. Börjesson, T. Moragas and R. Martin, *J. Am. Chem. Soc.*, 2016, **138**, 7504-7507.

28. For related examples of radical formation-based acylation reactions, see: (a) J. Amani, E. Sodagar and G. A. Molander, *Org. Lett.*, 2016, **18**, 732-735; (b) J. Amani and G. A. Molander, *Org. Lett.*, 2017, **19**, 3612-3615; (c) J. Amani, R. Alam, S. Badir and G. A. Molander, *Org. Lett.*, 2017, **19**, 2426-2429; (d) J. Amani and G. A. Molander, *J. Org. Chem.*, 2017, **82**, 1856-1863; (e) Z. Sun, N. Kumagai and M. Shibasaki, *Org. Lett.*, 2017, **19**, 3727-3730; (f) S. O. Badir, A. Dumoulin, J. K. Matsui and G. A. Molander, *Angew. Chem. Int. Ed.*, 2018, **57**, 6610-6613; (g) L. K. G. Ackerman, J. I. Martinez Alvarado and A. G. Doyle, *J. Am. Chem. Soc.*, 2018, **140**, 14059-14063; (h) E. Levernier, V. Corcé, L.-M. Rakotoarison, A. Smith, M. Zhang, S. Ognier, M. Tatoulian, C. Ollivier and L. Fensterbank, *Org. Chem. Front.*, 2019, **6**, 1378-1382. Also see ref. [7g] and [11b].

29. Other readily available and air-stable Ni(II) salts showed synthetically useful level of reactivity (5 cases, 79% on average). However, optimal performance of the system was observed with $Ni(cod)_2$. See the Table 2.7 for more details.

30. For related examples of preferred activation of an allylic C–H bond over a

benzylic C–H bond, see: (a) J. D. Cuthbertson and D. W. C. MacMillan, *Nature*, 2015, **519**, 74-77; (b) Y. Li, M. Lei and L. Gong, *Nat. Catal.*, 2019, **2**, 1016-1026.

31. It should be noted that the product ratio may not reflect the reactivity of each position due to potential 1,4-shift of a hydrogen atom. For a relevant review, see: M. Nechab, S. Mondal and M. P. Bertrand, *Chem. Eur. J.*, 2014, **20**, 16034-16059.

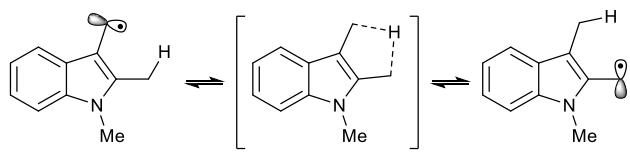

32. M. S. Lowry, J. I. Goldsmith, J. D. Slinker, R. Rohl, R. A. Pascal, G. G. Malliaras and S. Bernhard, *Chem. Mater.*, 2005, **17**, 5712-5719.

33. D. M. Arias-Rotondo and J. K. McCusker, *Chem. Soc. Rev.*, 2016, **45**, 5803-5820.

34. R. B. Bedford, N. Fey, M. F. Haddow and R. F. Sankey, *Chem. Commun.*, 2011, **47**, 3649-3651.

35. T. Tomakinian, R. Guillot, C. Kouklovsky and G. Vincent, *Angew. Chem. Int. Ed.*, 2014, **53**, 11881-11885.

36. L. Wang, J. Zhou, T.-M. Ding, Z.-Q. Yan, S.-H. Hou, G.-D. Zhu and S.-Y. Zhang, *Org. Lett.*, 2019, **21**, 2795-2799.

37. Y.-M. Su, Y. Hou, F. Yin, Y.-M. Xu, Y. Li, X. Zheng and X.-S. Wang, *Org. Lett.*, 2014, **16**, 2958-2961.

38. M. Taddei, M. G. Mura, S. Rajamäki, L. D. Luca and A. Porcheddu, *Adv. Synth. Catal.*, 2013, **355**, 3002-3013.

39. D. Dhanak and C. B. Reese, *J. Chem. Soc., Perkin Trans. 1*, 1986, 2181-2186.

40. Y. Feng, D. Holte, J. Zoller, S. Umemiya, L. R. Simke and P. S. Baran, *J. Am. Chem. Soc.*, 2015, **137**, 10160-10163.

41. S. Rohrbach, R. S. Shah, T. Tuttle and J. A. Murphy, *Angew. Chem. Int. Ed.*, 2019, **58**, 11454-11458.

42. Qiang-Liu, Y.-X. Liu, H.-J. Song and Q.-M. Wang, *Adv. Synth. Catal.*, 2020, **362**, 3110-3115.

43. J. Ni, H. Wang and S. E. Reisman, *Tetrahedron*, 2013, **69**, 5622-5633.

44. L. M. Repka, J. Ni and S. E. Reisman, *J. Am. Chem. Soc.*, 2010, **132**, 14418-14420.

45. J. J. Newsome, E. Swann, M. Hassani, K. C. Bray, A. M. Z. Slawin, H. D. Beall and C. J. Moody, *Org. Biomol. Chem.*, 2007, **5**, 1629-1640.

46. M. Peña-López, H. Neumann and M. Beller, *Chem. Eur. J.*, 2014, **20**, 1818-1824.

47. X. Zeng, R. Kinjo, B. Donnadieu and G. Bertrand, *Angew. Chem. Int. Ed.*, 2010, **49**, 942-945.

48. D. Zhang, T. Iwai and M. Sawamura, *Org. Lett.*, 2020, **22**, 5240-5245.

49. T. Mandal, G. Chakraborti and J. Dash, *Tetrahedron Lett.*, 2020, **61**, 152109.

50. B. E. Daniels, J. Ni and S. E. Reisman, *Angew. Chem. Int. Ed.*, 2016, **55**, 3398-3402.

51. A. J. Smith, A. Young, S. Rohrbach, E. F. O'Connor, M. Allison, H.-S. Wang, D. L. Poole, T. Tuttle and J. A. Murphy, *Angew. Chem. Int. Ed.*, 2017, **56**, 13747-13751.

52. C. L. Hansen, R. G. Ohm, L. B. Olsen, E. Ascic, D. Tanner and T. E. Nielsen, *Org. Lett.*, 2016, **18**, 5990-5993.

53. S.-Z. Sun and R. Martin, *Angew. Chem. Int. Ed.*, 2018, **57**, 3622-3625.

54. G. Goverdhan, A. R. Reddy, V. Himabindu and G. M. Reddy, *Synth. Commun.*, 2013, **43**, 498-504.

55. S. Laufer and F. Lehmann, *Bioorg. Med. Chem. Lett.*, 2009, **19**, 1461-1464.

56. T. Utsumi, K. Noda, D. Kawauchi, H. Ueda and H. Tokuyama, *Adv. Synth. Catal.*, 2020, **362**, 3583-3588.

57. A. A. Martinez, B. A. Espinosa, R. N. Adamek, B. A. Thomas, J. Chau, E. Gonzalez, N. Keppetipola and N. T. Salzameda, *Eur. J. Med. Chem.*, 2018, **157**, 1202-1213.

58. X. Zhong, N. Chen and J. Xu, *New J. Chem.*, 2018, **42**, 13549-13557.

59. M. Géraldy, M. Morgen, P. Sehr, R. R. Steimbach, D. Moi, J. Ridinger, I. Oehme, O. Witt, M. Malz, M. S. Nogueira, O. Koch, N. Gunkel and A. K. Miller, *J. Med. Chem.*, 2019, **62**, 4426-4443.

60. A. Klinkebiel, O. Beyer, B. Malawko and U. Lüning, *Beilstein J. Org. Chem.*,

2016, **12**, 2267-2273.

61. L. Buzzetti, A. Prieto, S. R. Roy and P. Melchiorre, *Angew. Chem. Int. Ed.*, 2017, **56**, 15039-15043.

Part II. Visible-light-induced carbon–halogen bond cleavage for radical generation

Chapter 3. A tandem process for the synthesis of β-aminoboronic acids from aziridines with haloamine intermediates*

3.1 Introduction

Organoboronic acids are important class of compounds in synthetic chemistry. They act as versatile building blocks for organic reactions, but also as important motifs in drug discovery because of the unique structural and electronic nature of the boron centre.[1] Among the subclasses of organoboronic acids, particular attention has been given to aminoboronic acids because of their potential use as bioisosteres of amino acids.[2] Moreover, growing interest in the chemistry and biology of metabolically inert amino acids has stimulated synthetic demands for β-aminoboronic acids, which are the bioisosteres of β-amino acids (Scheme 3.1A).[3]

Numerous strategies for synthesising β-aminoboronic acids have been developed to meet the pharmacological needs.[4] Conventionally, the classic 1,2-metallate rearrangement and its associated reactivity have played a central role in this field.[5] However, these approaches impose fundamental issues associated with the use of extremely basic organometallic reagents and generation of excessive metal

* The majority of this work has been published (*Chem. Commun.* **2022**, *58*, 3767-3770).

waste. Therefore, numerous alternatives have been introduced to overcome these shortcomings.[6] One of the influential turning points was the advent of transition-metal-catalysed methods for incorporating a boryl group into organic molecules (Scheme 3.1B).[7] Representatively, activated π-systems, such as a C=C double bond or an azomethine moiety could be utilised as handles for the installation of a boron-based functional group through transition-metal-catalysed hydroboration,[8] aminoboration,[9] or addition of boryl alkyl nucleophiles (Scheme 3.1B, a–c).[10] Another important class of functional handles that allows orthogonal access to β-

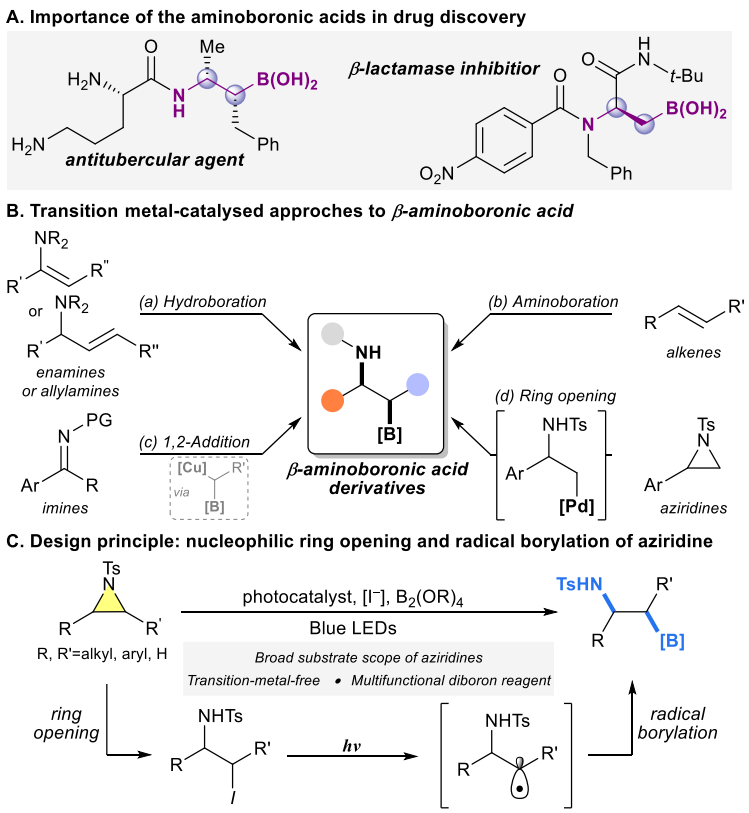

Scheme 3.1 Pharmaceutical importance and synthetic strategies of β-aminoboronic acids

aminoboronic acids via catalytic borylation is aziridine (Scheme 3.1B, d).[11] The strained azacycle can undergo regioselective borylation via nucleophilic palladium catalysis. However, the reactivity latitude of this method is severely limited by the fact that only electronically activated and sterically uncrowded aziridines can be empolyed as suitable substrates.

We envisaged that a more reactive mode of the ring-opening process would help overcome these limitations. Specifically, it was contemplated that a nucleophilic halide could serve as a transient handle for the subsequent transformation, that is, the introduction of a boryl group (Scheme 3.1C).[12, 13] As such, incorporation of iodide was exploited as a central strategy to (a) activate the aziridine precursors in a more general manner and (b) promote the generation of a radical intermediate that can mediate borylation via various established protocols. Among these, the recently emerging approach based on photochemical reactivity is believed to enable the construction of the desired C–B bond under environmentally friendly and mild conditions.[14] Herein, we present a novel synthetic strategy for β-aminoboronic acids from aziridines via a combination of nucleophilic ring-opening with iodide and visible-light-mediated radical borylation. The tandem process can be applied to prepare β-aminoboronic acid derivatives with unprecedented substitution patterns.

3.2 Results and discussion

3.2.1 Evaluation of reaction parameters

Table 3.1 Evaluation of reaction parameters[a]

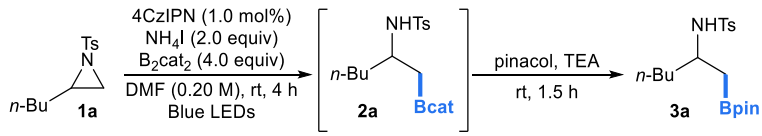

Entry	Conditions	Yield (%)[b]
1	As shown	80 (26)[c]
2	1.0, 2.0 or 3.0 equiv of B_2cat_2	45–69
3	TBAI, LiI, or NaI instead of NH_4I	42–59
4	No light	0
5	B_2pin_2, B_2neop_2, or $B_2(OH)_4$ instead of B_2cat_2	0

[a] Reaction conditions: **1a** (0.10 mmol), 4CzIPN (1.0 mol%), NH_4I (0.20 mmol), B_2cat_2 (0.40 mmol) and DMF (0.20 M) irradiated with 34 W blue LEDs (456 nm); pinacol (0.7 mmol), TEA (1.0 M). [b] Yields were determined by ^1H NMR analysis using 1,1,2,2-tetrachloroethane as an internal standard. [c] The reaction was performed without 4CzIPN. 4CzIPN=1,2,3,5-tetrakis(carbazol-9-yl)-4,6-dicyanobenzene, TBAI=tetrabutylammonium iodide.

At the outset of the investigation, we explored the reactivity of 2-*n*-butyl-1-tosylaziridine (**1a**) with bis(catecholato)diboron (B_2cat_2) to promote the formation of aminoboronic acid in the corresponding pinacol ester form (**3a**) (Table 3.1).[15] We noted that ammonium iodide in *N*,*N*-dimethylformamide (DMF) mediates the desired transformation upon light irradiation. It was shown that the use of a 4CzIPN

photocatalyst and 4 equivalents of the boron source is important for achieving the high efficiency of the reaction (entry 1 and 2). Other sources of iodide were not as competent as ammonium iodide (entry 3). In addition, a control experiment revealed that light irradiation was essential for the success of the developed method (entry 4). Significantly, the replacement of B_2cat_2 with other diboron reagents, such as bis(pinacolato)diboron (B_2pin_2), bis(neopentyl glycolato)diboron (B_2neop_2), or tetrahydroxy diboron ($B_2(OH)_4$), completely inhibited the desired reactivity, suggesting the unique contribution of B_2cat_2 (entry 5).[14a]

3.2.2 Sequential ring opening and radical borylation of aziridines

With the optimsed conditions in hand, we examined the applicability of the protocol to a variety of aziridines (Table 3.2). In addition to **3a**, the significantly more lipophilic 2-*n*-dodecylaziridine provided the desired product in a good yield (**3b**). Sterically demanding 2-isobutyl aziridine and 2-cyclohexyl aziridine also underwent borylation in practical yields (**3c** and **3d**). The C=C double bond was compatible with the optimised conditions (**3e**), and substrates containing ester or phenoxy substituents also provided the desired products (**3f** and **3g**). Products with aromatic substituents, such as benzyl or homobenzyl groups, were formed in useful yields (**3h** and **3i**). Interestingly, aziridines derived from styrene derivatives delivered the corresponding β-aminoboronic acids as a mixture of regioisomers (**3j'** – **3m'**). This process favoured the formation of branched products, presumably due to the preferential nucleophilic attack of iodide at the benzylic position of the aziridine. Furthermore, the modified reaction conditions without the photocatalytic system proved to be superior in terms of product formation for this class of substrates.[16]

Importantly, an extended π-system and halogen substituent on the arene were tolerated (**3l'** and **3m'**). Moreover, 2,3-disubstituted aziridines are compatible precursors capable of affording the 1,2-disubstituted β-aminoboronic acids, which are a class of products that are difficult to obtain using other methods. The bicyclic aziridines, containing either a cyclohexyl or a cyclopentyl moiety, could be selectively transformed into a single trans diastereomer (**3n** and **3o**).

Table 3.2 Sequential ring opening and radical borylation of aziridines[a]

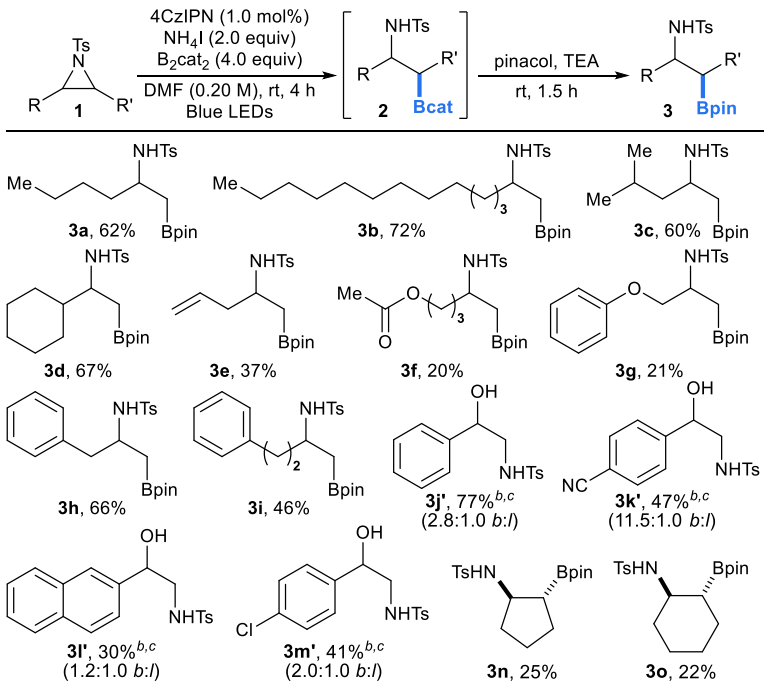

[a] Reaction conditions: **1a** (0.20 mmol), 4CzIPN (1.0 mol%), NH_4I (0.40 mmol), B_2cat_2 (0.80 mmol) and DMF (0.20 M) irradiated with 34 W blue LEDs (456 nm); pinacol (0.7 mmol), TEA (1.0 M). [b] The reaction was performed without 4CzIPN [c] The desired product was converted to the corresponding alcohol by reaction with sodium perborate tetrahydrate ($NaBO_3 \cdot 4H_2O$). All yields are the yield of the isolated products. *b*=branched isomer, *l*=linear isomer.

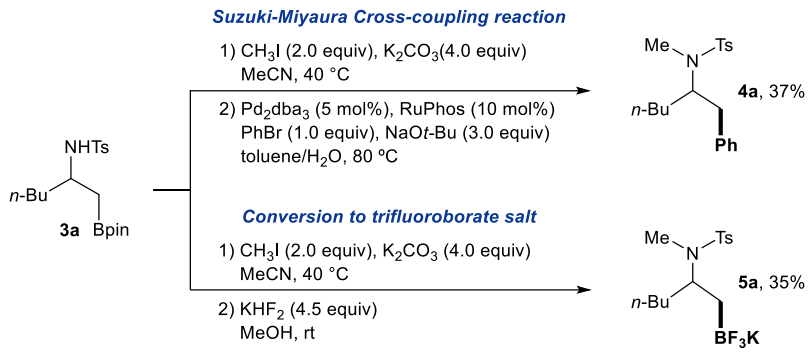

Scheme 3.2 Transformation of β-aminoboronic acid, **3a**

The synthetic utility of the developed method was demonstrated by functionalising the boronic acid moiety of the β-aminoboronic acid product (Scheme 3.2).[5c] After straightforward alkylation of the nitrogen atom, the product was successfully subjected to the Suzuki–Miyaura cross-coupling reaction with bromobenzene (**4a**). Moreover, the product could be conveniently converted to its trifluoroborate salt form, which is another class of versatile and bench-stable synthetic intermediates for organic reactions (**5a**).[17]

3.2.3 Mechanistic studies

Mechanistic studies were then conducted to analyse the reactive intermediates of the reaction (Scheme 3.3). First, we examined the nucleophilic ring-opening process of aziridines using iodide as a nucleophile (Scheme 3.3A-1). Contrary to our expectations, virtually no β-iodoamine intermediate was formed when the aziridine substrates were treated with ammonium iodide alone without light irradiation (eq. 1). Instead, most of the starting material remained intact. Control experiments showed

that the presence of B_2cat_2 was crucial for the successful formation of the iodide intermediate (eq. 2). It is speculated that the strongly Lewis acidic boron centre of B_2cat_2 helps activate the ring-opening step of the overall process.

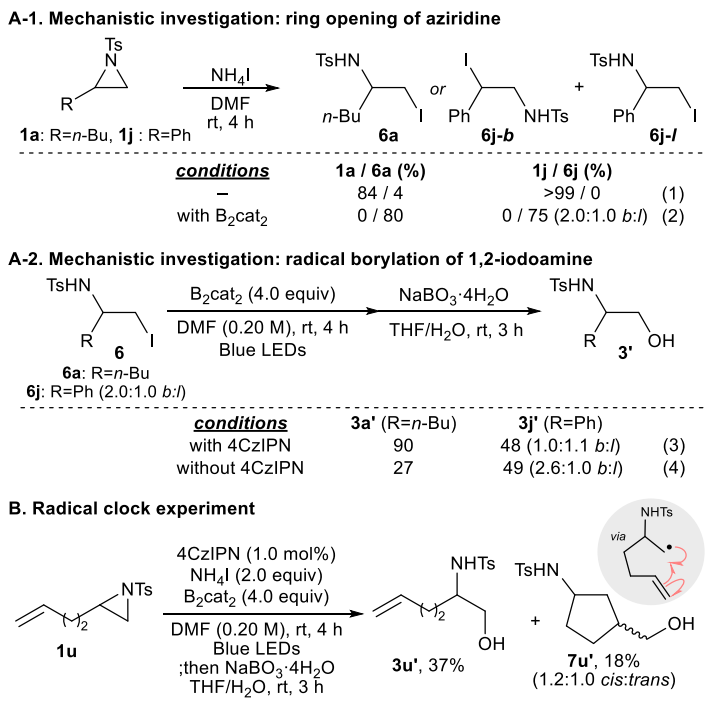

Scheme 3.3 Mechanistic studies

Next, the role of β-iodoamine as a direct precursor to provide the product was assessed by subjecting the intermediate to borylation conditions (Scheme 3.3A-2). Interestingly, although the use of photocatalyst improved the efficiency of the borylation process for the intermediate with an aliphatic substituent (**3a'**, eq. 3), it did not significantly affect the efficiency for the substrates with an aromatic substituent (**3j'**, eq. 4). Therefore, the photocatalytic system was excluded for the

transformation of 2-arylaziridine substrates. Finally, the radical clock experiment was performed to examine the involvement of the radical pathway in the transformation (Scheme 3.3B). The cyclised product (**7u'**) was formed under standard conditions, suggesting the formation of a radical intermediate. However, the substantial formation of **3u'** also indicates that the trapping of a primary carbon-centred radical with B_2cat_2 is a competitive process (3.8×10^6 M^{-1} s^{-1} for borylation vs. 2.3×10^5 s^{-1} for 5-exo-trig cyclisation).[14a]

3.2.4 Plausible mechanistic scenario

Based on these results and previous reports, a plausible reaction mechanism was proposed (Figure 3.1). First, the nucleophilic ring opening of aziridine, assisted by the Lewis acidity of the boron source, forms a β-iodoamine intermediate (**Int-1**). The generated **Int-1** is transformed to the corresponding radical intermediate (**Int-2**) via light-mediated C–I bond homolysis. The subsequent homolytic substitution of the B_2cat_2-DMF complex[14a, 18] provided the adduct radical (**Int-3**). Finally, the fragmentation of **Int-3** by cleavage of the B–B bond affords the desired β-aminoboronate product (**2**) and the DMF-complexed boryl radical (**Int-4**). This reactive radical intermediate, **Int-4**, could generate **Int-2** through iodine atom transfer from **Int-1**. Alternatively, **Int-4** can undergo electron transfer to the photocatalyst with concomitant iodide addition. The reduced photocatalyst ($PC^{\bullet-}$) could also generate the reactive intermediate **Int-2** *via* a single-electron transfer process, regenerating the previous state.[19]

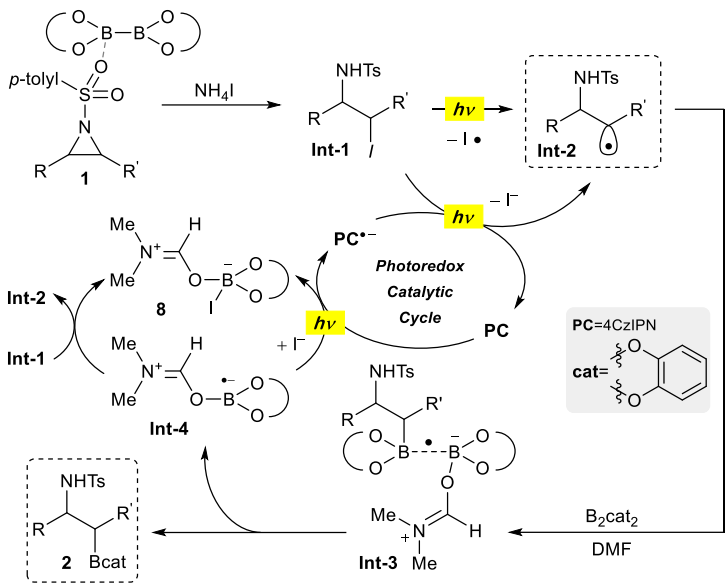

Figure 3.1 Plausible mechanistic scenario

3.3 Conclusion

In conclusion, we have developed a novel strategy for the synthesis of β-aminoboronic acids. The aziridine ring-opening reaction by using nucleophilic iodide sets off a cascade process, in which an *in situ*-generated haloamine intermediate serves as a precursor for subsequent radical borylation. The developed protocol enabled the preparation of β-aminoboronic acids from various types of substrates that were not suitable for previous approaches. Eventually, the method has successfully expanded the synthetic utility of aziridines compared to previous methods. During our investigation, an unexpected participation of B_2cat_2 in the aziridine opening step was identified, which critically facilitated the overall transformation. The finding will eventually contribute to drug design processes that are based on β-aminoboronic acids, a pharmaceutically important motif.

3.4 Experimental section

3.4.1 General experimental details

Unless otherwise noted, all reactions were performed under inert conditions. Analytical TLC was performed on a Merck 60 F254 silica gel plates (0.25mm thickness), and visualized either using UV light (254 nm) or by staining with potassium permanganate and heating. Column chromatography was performed on Merck 60 silica gel (230–400 mesh). NMR spectroscopy experiments were conducted with a Varian 400 and 500 MHz or a Bruker 300 MHz system. NMR spectra were processed with ACD NMR Processor or MestReNova. Chemical shifts are reported in ppm and referenced to residual solvent peaks ($CHCl_3$ in $CDCl_3$: 7.26 ppm for 1H, 77.16 ppm for 13C). Coupling constants are reported in Hertz. Deuterated compounds were purchased from Cambridge Isotope Laboratories, Inc. All anhydrous solvents and chemicals were purchased from commercial sources (Sigma-Aldrich, Acros, Alfa Aesar, TCI, or Strem) and used without further purification. 34 W Blue LED lamps purchased from Kessil (Kessil H150 Grow Light-Blue) were used for all the visible light photocatalytic reactions. High-resolution mass spectrometry (HRMS) was performed at the Organic Chemistry Research Center in Sogang University or at the Chemistry Core Facility in Seoul National University using the ESI method.

3.4.2 Optimisation of reaction conditions

Table 3.3 Optimisation of reaction conditions

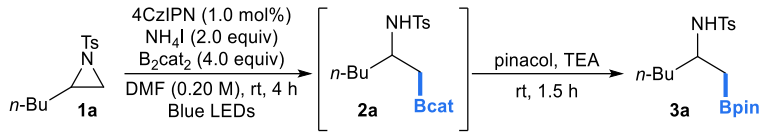

Entry	Conditions	Yield (%)
1	As shown	80 (26)
2	1.0 equiv of B_2cat_2	45
3	2.0 equiv of B_2cat_2	60
4	3.0 equiv of B_2cat_2	69
5	TBAI instead of NH_4I	52
6	KI instead of NH_4I	30
7	NaI instead of NH_4I	42
8	LiI instead of NH_4I	59
9	No light	N.D.
10	B_2pin_2, B_2neop_2, or $B_2(OH)_4$ instead of B_2cat_2	N.D.
11	NBoc instead of NTs	N.D.
12	NCbz instead of NTs	N.D.
13	NNs instead of NTs	N.D.

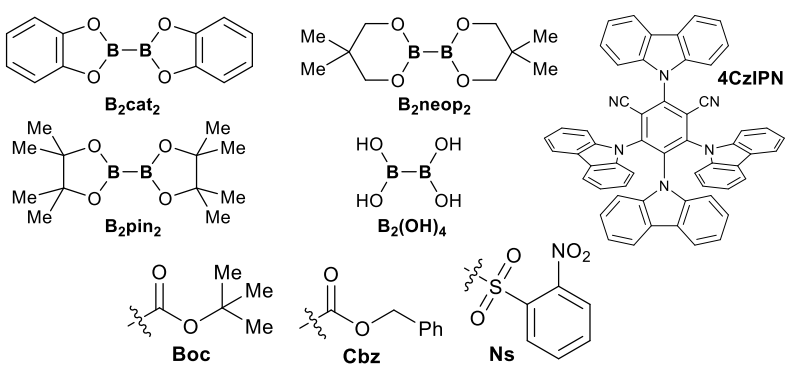

3.4.3 General procedure for synthesis of aziridines

General procedure A[20]

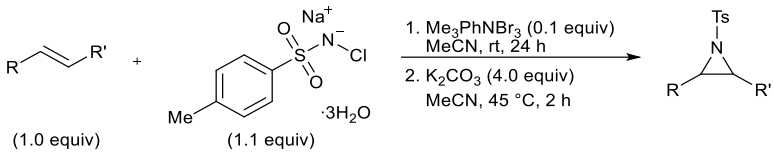

A flame-dried round bottom flask equipped with a stir bar was charged with chloramine-T trihydrate (5.0 g, 20 mmol, 1.1 equiv) and trimethylphenylammonium tribromide (0.75 g, 2.0 mmol, 0.1 equiv) and dissolved in MeCN (25 mL, 0.80 M). Alkene (20 mmol, 1.0 equiv) was added and the mixture was stirred at room temperature for 24 h. The reaction mixture was concentrated *in vauco,* dissolved in a minimal amount of DCM and filtered through a short silica gel colunm eluting with 1:9 EtOAc/hexane (150 mL). The solvent was removed and the reside was dissolved in MeCN (15 mL). Anhydrous potassium carbonate (11.0 g, 80 mmol, 4.0 equiv) was added and the mixture was stirred at 45 °C for 2 h. The reaction was concentrated to dryness and Et_2O was added. The solution was filtered through a pad of Celite eluting with Et_2O, and concentrated to dryness. The crude mixture was purified by flash column chromatography on silica gel, eluting with a mixture of EtOAc in hexanes to give the corresponding compounds.

General procedure B[21]

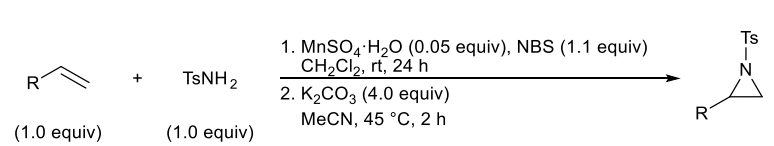

A flame-dried round bottom flask equipped with a stir bar was charged with manganese sulfate monohydrate (168 mg, 1.0 mmol, 0.05 equiv), *p*-toluenesulfonamide (3.42 g, 20 mmol, 1.0 equiv) and *N*-bromosuccinimide (3.92g, 1.1 equiv) and dissolved in CH_2Cl_2 (25 mL, 0.8 M). Alkene (20 mmol, 1.0 equiv) was added and the mixture was stirred at room temperature for 24 h. Anhydrous potassium carbonate (11.0 g, 80 mmol, 4.0 equiv) was added and the mixture was stirred at room temperature for 2 h. The reaction mixture was diluted with CH_2Cl_2 and H_2O, and the aqueous layer was extracted with CH_2Cl_2 (2 times). The combined organic layer was dried over anhydrous Na_2SO_4 and the filterate was concentrated to dryness. The crude mixture was purified by flash column chromatography on silica gel, eluting with a mixture of EtOAc in hexanes to give the corresponding compounds .

General procedure C[22]

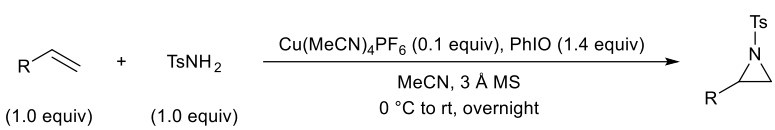

A flame-dried round bottom flask equipped with a stir bar was charged with tetrakis(acetonitrile)copper(I) hexafluorophosphate (372 mg, 1.0 mmol, 0.1 equiv), *p*-toluenesulfonamide (1.71 g, 10 mmol, 1.0 equiv) and activated 3 Å molecular sieves (1.0 g/mmol alkene) and dissolved in MeCN (20 mL, 0.5 M). Alkene (10 mmol, 1.0 equiv) was added and the mixture was cooled to 0 °C, then iodosylbenzene (3.08 g, 14 mmol, 1.4 equiv) was added in one portion. The mixture was allowed to warm to room temperature and stirred overnignt. The reaction mixture was filtered

through a pad of Celite and the filterate was concentrated to dryness. The crude mixture was purified by flash column chromatography on silica gel eluting with a mixture of EtOAc in hexanes to give the corresponding compounds .

General procedure D[23]

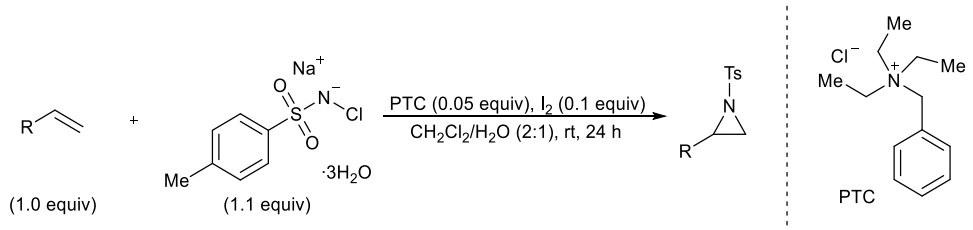

A flame-dried round bottom flask equipped with a stir bar was charged with benzyltriethylammonium chloride (228 mg, 1.0 mmol, 0.05 equiv), iodine (507 mg, 2.0 mmol, 0.1 equiv) and chloramine-T (5.0 g, 22 mmol, 1.1 equiv) and dissolved in 2:1 CH_2Cl_2/H_2O (25 mL, 0.8 M). Alkene (20 mmol, 1.0 equiv) was added and the mixture was stirred at room temperature for 24 h. The reaction mixture was treated with a saturated aq. $Na_2S_2O_3$ (10 mL) and the aqueous layer was extracted with CH_2Cl_2 (3 times). The combined organic layer was dried over anhydrous Na_2SO_4 and concentrated to dryness. The crude mixture was purified by flash column chromatography on silica gel eluting with a mixture of EtOAc in hexanes to give the corresponding compounds.

3.4.4 General procedure for photoinduced borylation of aziridines

General procedure E

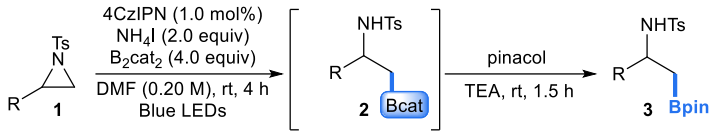

The reaction was set up in a nitrogen-filled glove box. To an 8 mL vial equipped with a PTFE-coated stirrer bar was added the corresponding aziridine **1** (0.20 mmol, 1.0 equiv), 4CzIPN (1.6 mg, 0.0020 mmol, 1.0 mol%), NH_4I (58 mg, 0.80 mmol, 2.0 equiv), B_2cat_2 (190 mg, 0.80 mmol, 4.0 equiv), and DMF (1.0 mL, 0.20 M). The reaction vial was removed from the glove box, stirred under 34 W blue LED irradiation. After 4 h, a solution of pinacol (0.70mmol., 3.5 equiv) in triethylamine (1.0 M) was added to the mixture and stirred for an additional 1.5 h. The reaction mixture was transferred to a separatory funnel and partitioned between water (7 mL) and Et_2O (20 mL). The organic layer was washed with water (7 mL x 3), dried over anhydrous Na_2SO_4 and concentrated to dryness. The crude mixture was purified by flash column chromatography on silica gel eluting with a mixture of EtOAc in hexanes to give the desired products.

General procedure F

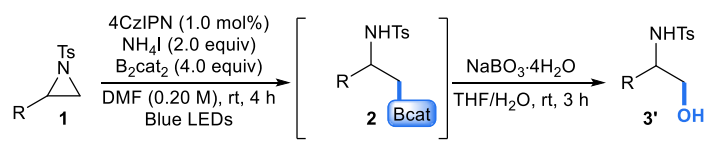

The reaction was set up in a nitrogen-filled glove box. To an 8 mL vial equipped with a PTFE-coated stirrer bar was added the corresponding aziridine **1** (0.20 mmol, 1.0 equiv), 4CzIPN (1.6 mg, 0.0020 mmol, 1.0 mol%), NH_4I (58 mg, 0.80 mmol, 2.0 equiv), B_2cat_2 (190 mg, 0.80 mmol, 4.0 equiv), and DMF (1.0 mL, 0.20 M). The

reaction vial was removed from the glove box, stirred under 34 W blue LED irradiation. After 4 h, $NaBO_3 \cdot 4H_2O$ in THF/H_2O (0.30M) was added to the mixture and stirred for an additional 3 h. The reaction mixture was transferred to a separatory funnel and partitioned between water (7 mL) and Et_2O (20 mL). The organic layer was washed with water (7 mL x 3), dried over anhydrous Na_2SO_4 and concentrated to dryness. The crude mixture was purified by flash column chromatography on silica gel eluting with a mixture of EtOAc in hexanes to give the desired products.

3.4.5 Instability evaluation of β-aminoboronate products

Table 3.4 Yield decreasing trend according to the number of isolations

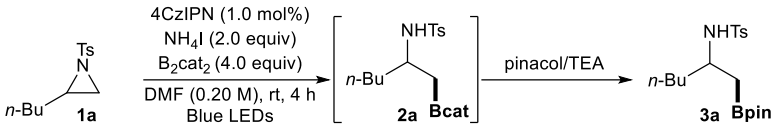

3a	yield	note
Crude mixture	80%*	
1st isolation	62% (47 mg)	
2nd isolation	45% (33 mg)	**73%** remaining after isolation step

* ^{1}H NMR yield

Table 3.5 Comparison of the yields of isolated products

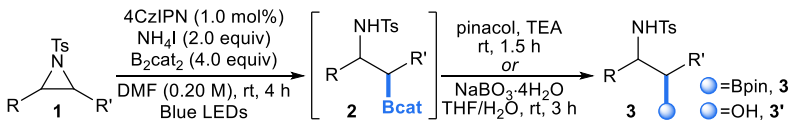

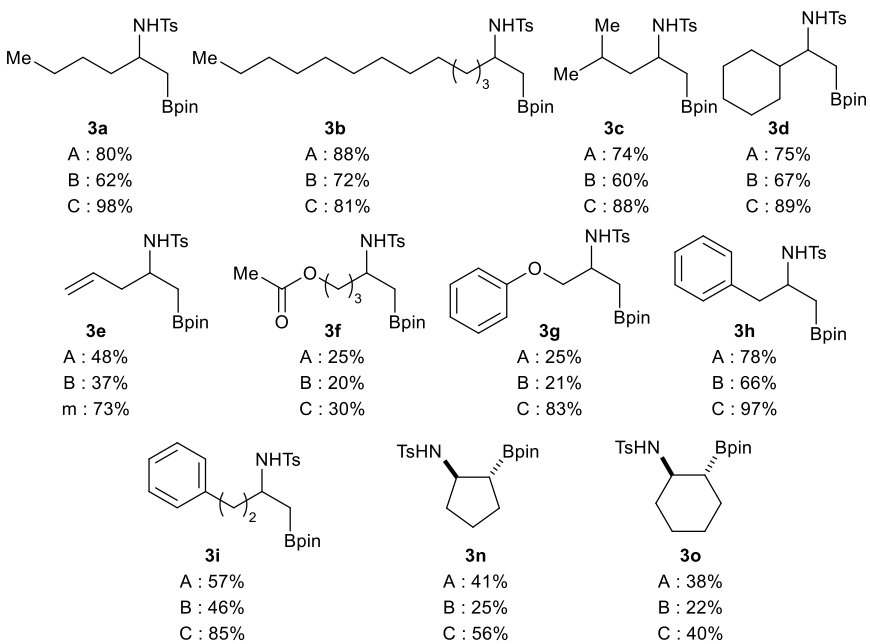

A : ^{1}H NMR yield of **3**
B : Yield of the isolated product **3**
C : Yield of the isolated amino alcohol product **3'**

3.4.6 Investigation of modified reaction conditions for aziridines derived from styrene

The reaction of styrene derived aziridine under photocatalytic conditions (General procedure F)

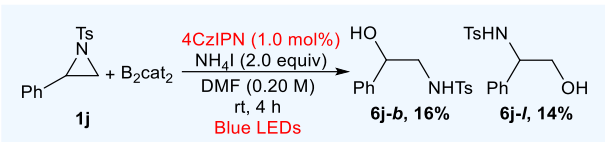

The reaction was set up in a nitrogen-filled glove box. To an 8 mL vial equipped with a PTFE-coated stirrer bar was added the corresponding aziridine **1** (0.20 mmol, 1.0 equiv), 4CzIPN (1.6 mg, 0.0020 mmol, 1.0 mol%), NH_4I (58 mg, 0.80 mmol, 2.0 equiv), B_2cat_2 (190 mg, 0.80 mmol, 4.0 equiv), and DMF (1.0 mL, 0.20 M). The reaction vial was removed from the glove box, stirred under 34 W blue LED irradiation. After 4 h, $NaBO_3{\cdot}4H_2O$ in THF/H_2O (0.30M) was added to the mixture and stirred for an additional 3 h. The reaction mixture was transferred to a separatory funnel and partitioned between water (7 mL) and Et_2O (20 mL). The organic layer was washed with water (7 mL x 3), dried over anhydrous Na_2SO_4 and concentrated to dryness. The crude residue was analyzed by ^1H NMR relative to 1,1,2,2-tetrachloroethane (10 μL, 0.094 mmol) as an external standard.

Control experiments of 1j with iodide salts and photocatalyst under blue light irradiation

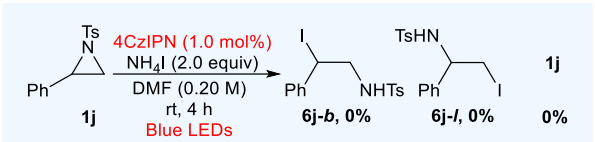

The reaction was set up in a nitrogen-filled glove box. To an 8 mL vial equipped with a PTFE-coated stirrer bar was added the corresponding aziridines (**1**) (0.20 mmol, 1.0 equiv), 4CzIPN (1.6 mg, 0.0020 mmol, 1.0 mol%), NH_4I (58 mg, 0.80 mmol, 2.0 equiv) and DMF (1.0 mL, 0.20 M). The reaction vial was removed from the glove box, stirred for 4 h under 34W blue LED irradiation. The reaction mixture was transferred to a separatory funnel and partitioned between water (7 mL) and Et_2O (20 mL). The organic layer was washed with water (7 mL x 3), dried over anhydrous Na_2SO_4 and concentrated to dryness. The crude residue was analyzed by ^1H NMR relative to 1,1,2,2-tetrachloroethane (10 μL, 0.094 mmol) as an external standard.

The result showed that virtually neither iodiamine intermediate nor **1j** remained. This observation suggested that the presence of the photocatalytic system not only prevented the generation of β-iodoamine intermediate, but also had a destructive effect on the entire system by decomposing the starting material.

3.4.7 A summary of reactions with challenging substrates

Table 3.6 A summary of experimental trials with challenging substrates

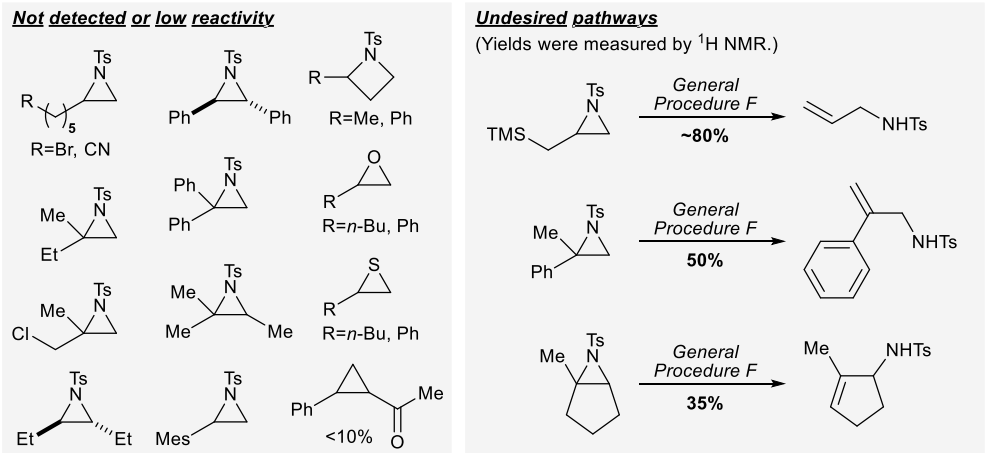

Table 3.7 Postulation of inhibition effect of alcohols and control experiments with alcohol additives

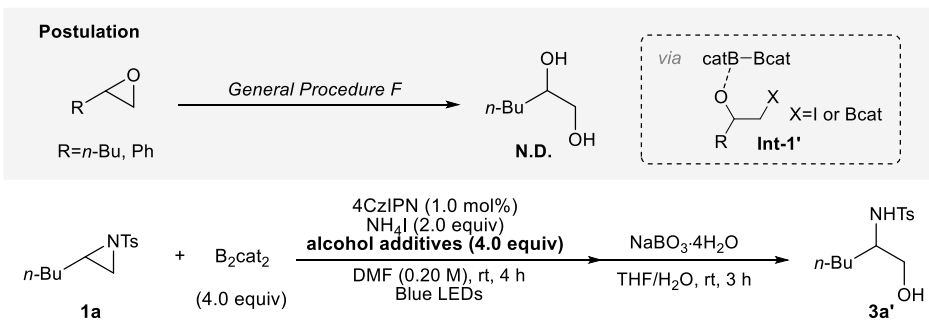

additives	result[a]
-	99%
2-pentanol	62%
CH_3OH	52%

[a]Yields were determined by ^{1}H NMR analysis using 1,1,2,2-tetrahcloroethane as an external standard.

In evaluating the reactivity of the developed conditions, we applied not only aziridines but also epoxides as the strained cyclic compounds. However, this class of compounds did not show the required level of reactivity in the first place. We hypothesized that the generation of the alcohol (or the alkoxide form thereof) during the reaction could inhibit the further process by coordination to a vacant p orbital of the boron reagent. To evaluate our postulation, control experiments were conducted on the modified reaction condition with **1a**. The yield of the corresponding β-amino alcohol, **3a'**, was diminished by treatment of additional alcohol additives. As a result, the postulated effect of alcohol may affect the efficiency of the reaction.

3.4.8 Mechanistic studies

Ring opening experiments with iodide salts

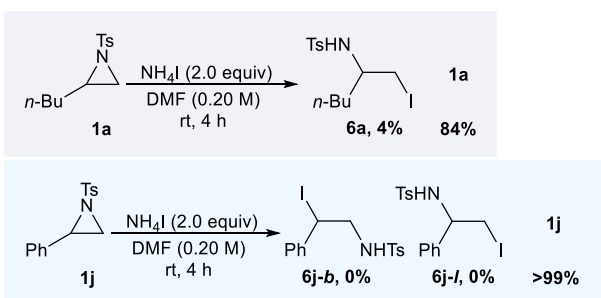

The reaction was set up in a nitrogen-filled glove box. To an 8 mL vial equipped with a PTFE-coated stirrer bar was added the corresponding aziridines (**1**) (0.20 mmol, 1.0 equiv), NH_4I (58 mg, 0.80 mmol, 2.0 equiv), and DMF (1.0 mL, 0.20 M). The reaction vial was removed from the glove box, stirred for 4 h at room temperature. The reaction mixture was transferred to a separatory funnel and partitioned between water (7 mL) and Et_2O (20 mL). The organic layer was washed with water (7 mL x

3), dried over anhydrous Na_2SO_4 and concentrated to dryness. The crude residue was analyzed by ^1H NMR relative to 1,1,2,2-tetrachloroethane (10 μL, 0.094 mmol) as an external standard.

Ring opening experiments with iodide salts and B_2cat_2

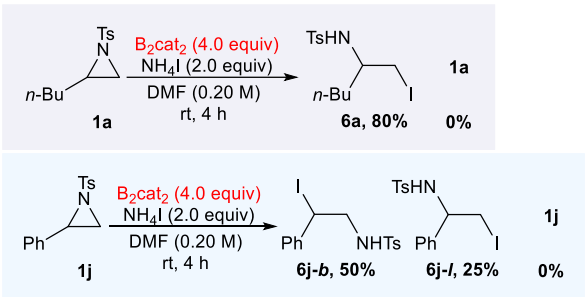

The reaction was set up in a nitrogen-filled glove box. To an 8 mL vial equipped with a PTFE-coated stirrer bar was added the corresponding aziridines (**1**) (0.20 mmol, 1.0 equiv), NH_4I (58 mg, 0.80 mmol, 2.0 equiv), B_2cat_2 (190 mg, 0.80 mmol, 4.0 equiv), and DMF (1.0 mL, 0.20 M). The reaction vial was removed from the glove box, stirred for 4 h at room temperature. The reaction mixture was transferred to a separatory funnel and partitioned between water (7 mL) and Et_2O (20 mL). The organic layer was washed with water (7 mL x 3), dried over anhydrous Na_2SO_4 and concentrated to dryness. The crude residue was analyzed by ^1H NMR relative to 1,1,2,2-tetrachloroethane (10 μL, 0.094 mmol) as an external standard.

Visible-light mediated radical borylation of *N*-(1-iodohexan-2-yl)-4-methylbenzenesulfonamide

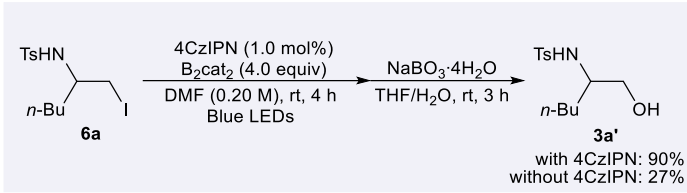

To an 8 mL vial equipped with a PTFE-coated stirrer bar was added **6a** (76.2 mg, 0.20 mmol, 1.0 equiv), 4CzIPN (1.6 mg, 0.0020 mmol, 1.0 mol%), B_2cat_2 (190 mg, 0.80 mmol, 4.0 equiv), and DMF (1.0 mL, 0.20 M). The reaction vial was removed from the glove box, stirred for 4 h under 34 W blue LED irradiation. The reaction mixture was transferred to a separatory funnel and partitioned between water (7 mL) and Et_2O (20 mL). The organic layer was washed with water (7 mL x 3), dried over anhydrous Na_2SO_4 and concentrated to dryness. The crude residue was analyzed by ^1H NMR relative to 1,1,2,2-tetrachloroethane (10 μL, 0.094 mmol) as an external standard.

Visible-light mediated radical borylation of *N*-(2-iodo-1 or 2-phenylethyl)-4-methylbenzenesulfonamide

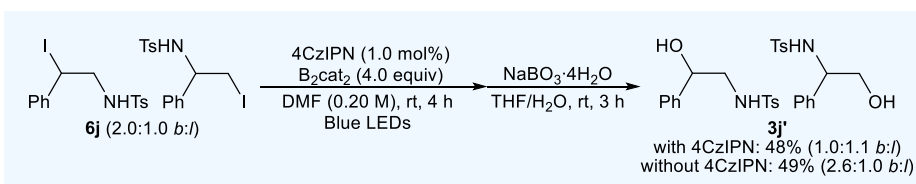

To an 8 mL vial equipped with a PTFE-coated stirrer bar was added **6j** (80.2 mg, 0.20 mmol, 1.0 equiv), 4CzIPN (1.6 mg, 0.0020 mmol, 1.0 mol%), B_2cat_2 (190 mg, 0.80 mmol, 4.0 equiv), and DMF (1.0 mL, 0.20 M). The reaction vial was removed from the glove box, stirred for 4 h under 34 W blue LED irradiation. After 4 h,

$NaBO_3{\cdot}4H_2O$ in THF/H_2O (0.30M) was added to the mixture and stirred for an additional 3 h. The reaction mixture was transferred to a separatory funnel and partitioned between water (7 mL) and Et_2O (20 mL). The organic layer was washed with water (7 mL x 3), dried over anhydrous Na_2SO_4 and concentrated to dryness. The crude residue was analyzed by ^1H NMR relative to 1,1,2,2-tetrachloroethane (10 μL, 0.094 mmol) as an external standard.

Radical cyclization experiments

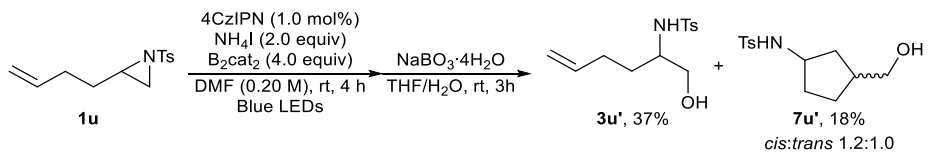

The reaction was set up in a nitrogen-filled glove box. To an 8 mL vial equipped with a PTFE-coated stirrer bar was added 2-(but-3-en-1-yl)-1-tosylaziridine **1u** (0.20 mmol, 1.0 equiv), 4CzIPN (1.6 mg, 0.0020 mmol, 1.0 mol%), NH_4I (58 mg, 0.80 mmol, 2.0 equiv), B_2cat_2 (190 mg, 0.80 mmol, 4.0 equiv), and DMF (1.0 mL, 0.20 M). The reaction vial was removed from the glove box, stirred for 4 h under 34 W blue LED irradiation. After 4 h, $NaBO_3{\cdot}4H_2O$ in THF/H_2O (0.30M) was added to the mixture and stirred for an additional 3 h. The reaction mixture was transferred to a separatory funnel and partitioned between water (7 mL) and Et_2O (20 mL). The organic layer was washed with water (7 mL x 3), dried over anhydrous Na_2SO_4 and concentrated to dryness. The crude mixture was purified by flash column chromatography on silica gel eluting with a mixture of EtOAc in hexanes to give the desired amino alcohol product (37%) and cyclized amino alcohol product (18%, *cis*:*trans* 1.2:1.0).

3.4.9 Miscellaneous experiments

Control experiment; an exclusion of aziridine to investigate what happens to the rest of B_2cat_2

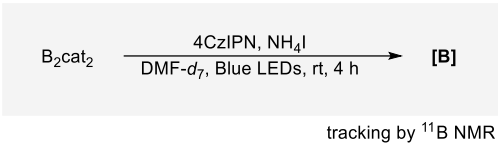

The reaction was set up in a nitrogen-filled glove box. To an 8 mL vial equipped with a PTFE-coated stirrer bar was added 4CzIPN (1.6 mg, 0.0020 mmol, 1.0 mol%), NH_4I (58 mg, 0.80 mmol, 2.0 equiv), B_2cat_2 (190 mg, 0.80 mmol, 4.0 equiv), and DMF-d_7 (1.0 mL, 0.20 M). The reaction vial was removed from the glove box, stirred under 34 W blue LED irradiation. The crude mixture was directly transferred to quartz-NMR tube after passing through a short silica filter for analysis.

Based on ^{11}B NMR analysis, the formation of bis(catecholato)boronate[24] was observed as the major boron species under our reaction conditions. The existence of competitive pathway that undesirably consumes the diboron reagent suggests the necessary use of 4 equivalents of the reagent.

B_2cat_2 in DMF-d_7

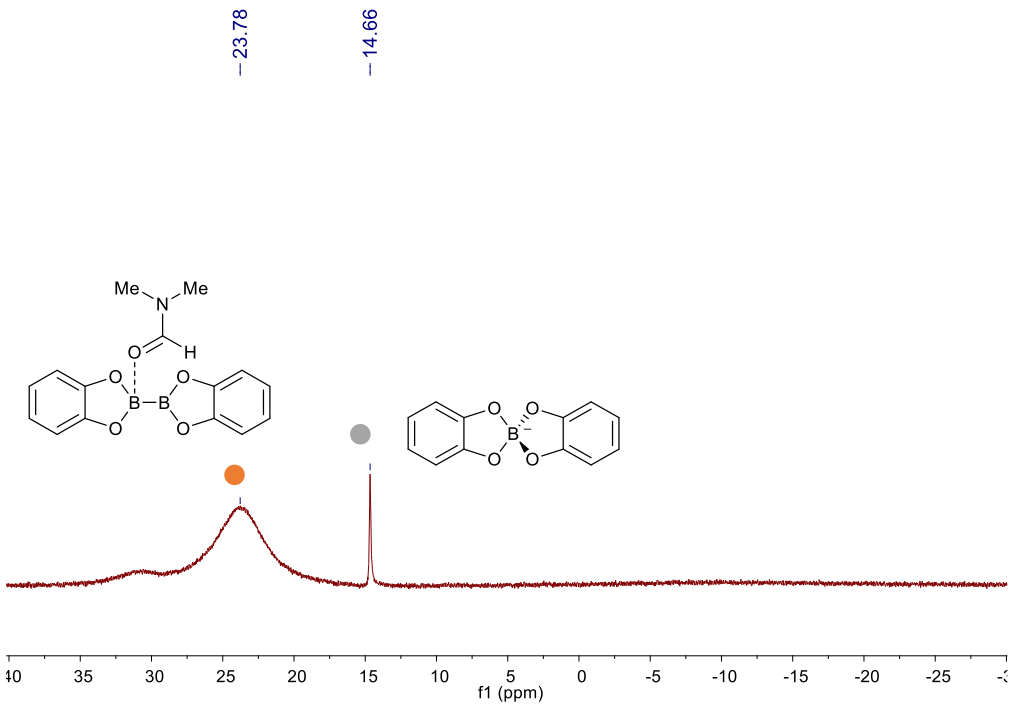

B_2cat_2 with 4CzIPN and NH_4I under light irradiation for 4 h in DMF-d_7

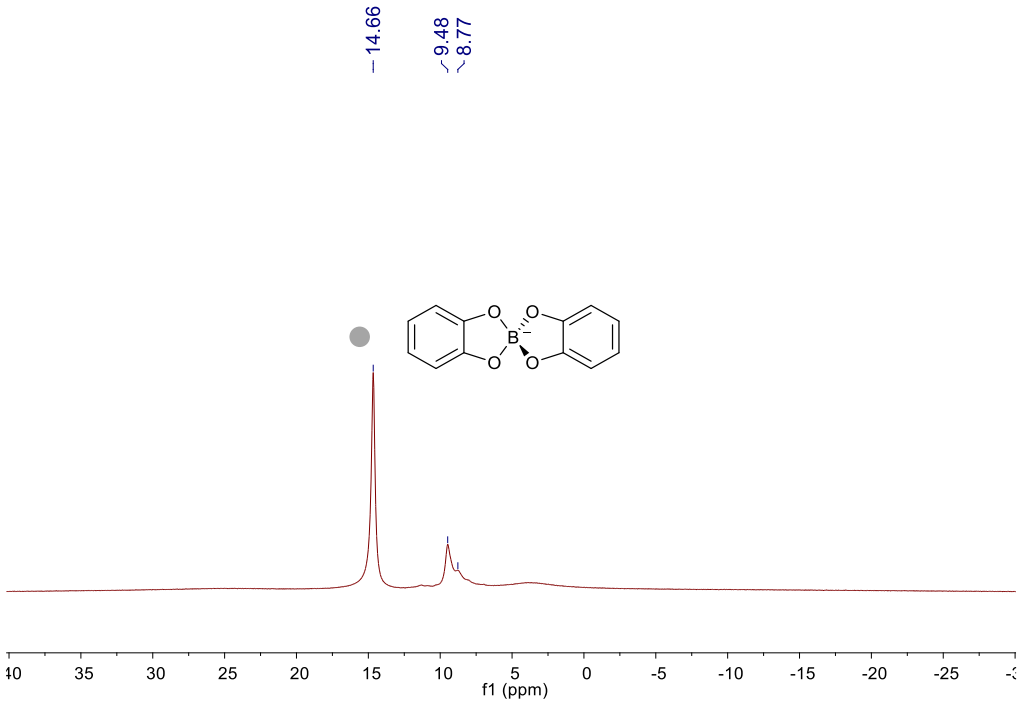

Figure 3.2 ^{11}B NMR studies

Attempts to use other protecting groups

Table 3.8 Attempts to use other protecting groups instead of the tosyl group

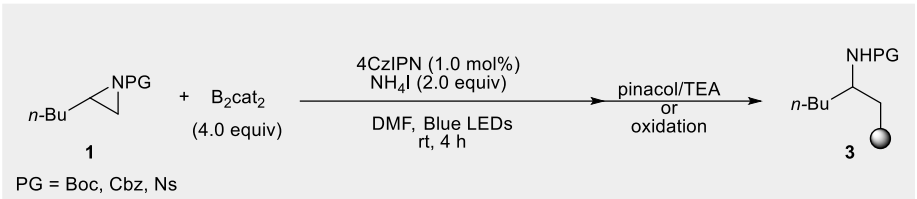

PG	Aziridine	Desired (3)[a]	Note
Boc	O	N.D.	Boc group seems to have disappeared.
Cbz	O	N.D.	Cbz group seems to have disappeared.
Ns	O	N.D.	100% conversion, a aziridine different from 1 was formed.

[a] Yields were determined by ^{1}H NMR analysis using 1,1,2,2-tetrachloroethane as an internal standard. N.D.=not detected.

Experiment for removing tosyl group of 3h[25]

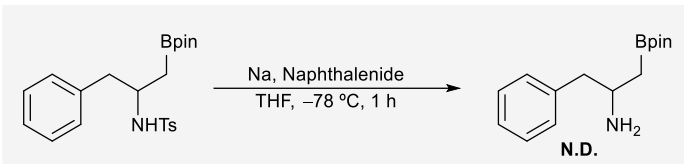

Naphthalene (256 mg, 2.0 mmol) was added to a vigorously stirred suspension of sodium (46 mg, 2.0 mmol; washed free of oil in hexanes) in tetrahydrofuran (4 mL) under nitrogen at 25 °C. The resulting green suspension was stirred for 1 h at 25 °C, then transferred to a solution of **3h** (40 mg, 0.1 mmol) in THF (4 mL) cooled at –78 °C. Portion-wise addition of this suspension to the reaction solution was ceased upon formation of a persistent dark-green reaction solution. The dark-green solution was stirred at –78 °C for 1 h. Water (1 mL) was added to the solution at –78 °C. The resulting suspension was stirred at –78 °C for 2 min, then warmed to ambient temperature. The organic layer was separated and the aqueous layer was extracted with CH_2Cl_2 (5 mL x 3), dried over anhydrous Na_2SO_4 and concentrated to dryness.

3.4.10 Characterization data of synthesized compounds

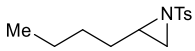

2-Butyl-1-tosylaziridine (**1a**)

Following the general procedure A, compound **1a** was prepared from 1-hexene (colorless oil, 60%).

δ_H (400 MHz, Chloroform-*d*) 7.82 (2 H, d, *J* 8.2), 7.33 (2 H, d, *J* 8.0), 2.75–2.62 (1 H, m), 2.63 (1 H, d, *J* 7.0), 2.44 (3 H, s), 2.05 (1 H, d, *J* 4.6), 1.58–1.50 (1 H, m), 1.38–1.28 (1 H, m), 1.27–1.18 (4 H, m), 0.81 (3 H, t, *J* 6.9). The identity of synthesized product was confirmed based on reported NMR spectra.[20]

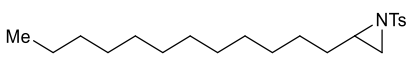

2-Dodecyl-1-tosylaziridine (**1b**)

Following the general procedure A, compound **1b** was prepared from 1-tetradecene (colorless oil, 51%).

δ_H (500 MHz, Chloroform-*d*) 7.83 (2 H, d, *J* 7.7), 7.33 (2 H, d, *J* 7.9), 2.74-2.66 (1 H, m), 2.62 (1 H, d, *J* 7.0), 2.43 (3 H, s), 2.05 (1 H, d, *J* 4.5), 1.62–1.47 (1 H, m), 1.44–1.07 (21 H, m), 0.91 (3 H, t, *J* 6.5). δ_c (126 MHz, Chloroform-*d*) 144.23, 135.30, 129.54, 127.94, 40.27, 33.56, 31.92, 31.28, 29.68, 29.66, 29.47, 29.45, 29.37, 29.01, 26.76, 22.68, 21.46, 14.10. HRMS (ESI): m/z $[M+Na]^+$ calcd for $C_{21}H_{35}NNaO_2S$: 388.2286, found: 388.2281

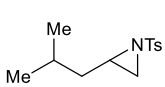

2-Isobutyl-1-tosylaziridine (**1c**)

Following the general procedure A, compound **1c** was prepared from 4-methylpent-1-ene (colorless oil, 37%).

δ_H (500 MHz, Chloroform-*d*) 7.83 (2 H, d, *J* 8.2), 7.33 (2 H, d, *J* 8.0), 2.82–2.76 (1 H, m), 2.63 (1 H, d, *J* 7.0), 2.45 (3 H, s), 2.02 (1 H, d, *J* 4.6), 1.67–1.54 (1 H, m), 1.39–1.28 (2 H, m), 0.88 (6 H, dd, *J* 6.7, 2.4). The identity of synthesized product was confirmed based on reported NMR spectra.[20]

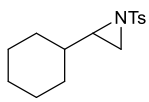

2-Cyclohexyl-1-tosylaziridine **(1d)**

Following the general procedure A, compound **1d** was prepared from vinylcyclohexene (white solid, 45%).

δ_H (500 MHz, Chloroform-*d*) 7.82 (2 H, d, *J* 8.3), 7.33 (2 H, d, *J* 7.9), 2.60 (1 H, d, *J* 7.0), 2.54 (1 H, td, *J* 7.2, 4.6), 2.45 (3 H, s), 2.10 (1 H, d, *J* 4.6), 1.73–1.59 (4 H, m), 1.53–1.46 (1 H, m), 1.25–0.83 (6 H, m). The identity of synthesized product was confirmed based on reported NMR spectra.[20]

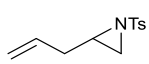

2-Allyl-1-tosylaziridine **(1e)**

Following the general procedure A, compound **1e** was prepared from 1,4-pentadiene (colorless oil, 30%).

δ_H (500 MHz, Chloroform-*d*) 7.81 (2 H, d, *J* 8.3), 7.33 (3 H, d, *J* 8.1), 5.63–5.55 (1

H, m), 5.11–4.93 (2 H, m), 2.82–2.77 (1 H, m), 2.63 (1 H, d, *J* 6.9), 2.44 (3 H, s), 2.32–2.13 (2 H, m), 2.09 (1 H, d, *J* 4.5). The identity of synthesized product was confirmed based on reported NMR spectra.[26]

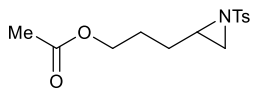

3-(1-Tosylaziridin-2-yl)propyl acetate **(1f)**

Following the general procedure A, compound **1f** was prepared from 4-pentenyl acetate (colorless oil, 40%).

δ_H (500 MHz, Chloroform-*d*) 7.82 (2 H, d, *J* 8.3), 7.34 (2 H, d, *J* 8.0), 4.01 (2 H, q, *J* 6.0), 2.79–2.74 (1 H, m), 2.63 (1 H, d, *J* 6.9), 2.45 (3 H, s), 2.08 (1 H, d, *J* 4.5), 2.02 (3 H, s), 1.73–1.65 (1 H, m), 1.65–1.58 (2 H, m), 1.40–1.34 (1 H, m). The identity of synthesized product was confirmed based on reported NMR spectra.[20]

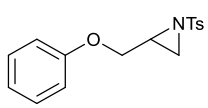

2-(Phenoxymethyl)-1-tosylaziridine **(1g)**

Following the general procedure A, compound **1g** was prepared from (allyloxy)benzene (white solid, 45%).

δ_H (500 MHz, Chloroform-*d*) 7.83 (2 H, d, *J* 8.3), 7.34–7.30 (2 H, m), 7.23 (2 H, dd, *J* 8.7, 7.3), 6.96–6.91 (1 H, m), 6.73 (2 H, d, *J* 7.8), 4.05 (1 H, dd, *J* 10.8, 4.4), 3.93 (1 H, dd, *J* 10.8, 6.1), 3.18–3.12 (1 H, m), 2.80 (1 H, d, *J* 7.1), 2.45 (3 H, s), 2.35 (1 H, d, *J* 4.4). The identity of synthesized product was confirmed based on reported NMR spectra.[27]

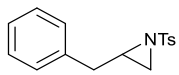

2-Benzyl-1-tosylaziridine **(1h)**

Following the general procedure A, compound **1h** was prepared from allylbenzene (white solid, 30%).

δ_H (500 MHz, Chloroform-*d*) 7.68 (2 H, d, *J* 8.4), 7.21 (2 H, d, *J* 8.0), 7.17–7.13 (3 H, m), 7.08–7.02 (2 H, m), 2.98–2.91 (1 H, m), 2.85–2.65 (3 H, m), 2.42 (3 H, s), 2.16 (1 H, d, *J* 4.5). The identity of synthesized product was confirmed based on reported NMR spectra.[20]

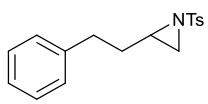

2-Phenethyl-1-tosylaziridine **(1i)**

Following the general procedure A, compound **1i** was prepared from 4-phenyl-1-butene (white solid, 60%).

δ_H (400 MHz, Chloroform-*d*) 7.83 (2 H, d, *J* 8.0), 7.34 (2 H, d, *J* 8.0), 7.30–7.23 (2 H, m), 7.19 (1 H, d, *J* 7.4), 7.11 (2 H, d, *J* 7.4), 2.77 (1 H, tt, *J* 7.5, 4.6), 2.64–2.56 (3 H, m), 2.45 (3 H, s), 2.05 (1 H, d, *J* 4.4), 1.93–1.82 (1 H, h, *J* 7.5), 1.74–1.61 (1 H, dq, *J* 14.6, 7.5). The identity of synthesized product was confirmed based on reported NMR spectra.[28]

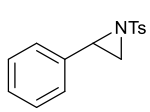

2-Phenyl-1-tosylaziridine **(1j)**

Following the general procedure B, compound **1j** was prepared from styrene (white solid, 50%).

δ_H (400 MHz, Chloroform-*d*) 7.85 (2 H, d, *J* 8.0), 7.31 (2 H, d, *J* 8.0), 7.28–7.16 (6 H, m), 3.76 (1 H, dd, *J* 7.2, 4.5), 2.96 (1 H, d, *J* 7.2), 2.41 (3 H, s), 2.37 (1 H, d, *J* 4.5). The identity of synthesized product was confirmed based on reported NMR spectra.[20]

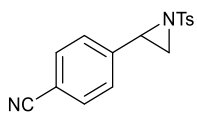

4-(1-Tosylaziridin-2-yl)benzonitrile **(1k)**

Following the general procedure C, compound **1k** was prepared from 4-cyanostyrene (white solid, 66%).

δ_H (400 MHz, Chloroform-*d*) 7.86 (2 H, d, *J* 8.3), 7.59 (2 H, d, *J* 8.3), 7.35 (4 H, dd, *J* 8.4, 2.8), 3.80 (1 H, dd, *J* 7.2, 4.3), 3.02 (1 H, d, *J* 7.2), 2.45 (3 H, s), 2.35 (1 H, d, *J* 4.3). The identity of synthesized product was confirmed based on reported NMR spectra.[20]

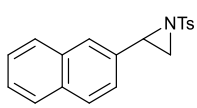

2-(Naphthalen-2-yl)-1-tosylaziridine **(1l)**

Following the general procedure D, compound **1l** was prepared from 2-vinylnaphthalene (white solid, 70%).

δ_H (400 MHz, Chloroform-*d*) 7.90 (2 H, d, *J* 8.1), 7.82–7.71 (4 H, m), 7.47 (2 H, td,

J 5.8, 5.4, 3.0), 7.33 (2 H, d, *J* 8.0), 7.27 (1 H, d, *J* 8.0), 3.93 (1 H, dd, *J* 7.2, 4.5), 3.07 (1 H, d, *J* 7.2), 2.50 (1 H, d, *J* 4.4), 2.42 (3 H, s). The identity of synthesized product was confirmed based on reported NMR spectra.[29]

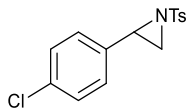

2-(4-Chlorophenyl)-1-tosylaziridine **(1m)**

Following the general procedure B, compound **1m** was prepared from 4-chlorostyrene (white solid, 60%).

δ_H (400 MHz, Chloroform-*d*) 7.85 (2 H, d, *J* 8.1), 7.34 (2 H, d, *J* 8.0), 7.29–7.24 (2 H, m), 7.15 (2 H, d, *J* 8.4), 3.73 (1 H, dd, *J* 7.2, 4.4), 2.98 (1 H, d, *J* 7.2), 2.44 (3 H, s), 2.34 (1 H, d, *J* 4.4). The identity of synthesized product was confirmed based on reported NMR spectra.[29]

6-Tosyl-6-azabicyclo[3.1.0]hexane **(1n)**

Following the general procedure B, compound **1n** was prepared from cyclopentene (white solid, 60%).

δ_H (400 MHz, Chloroform-*d*) 7.81 (2 H, d, *J* 8.2), 7.32 (2 H, d, *J* 7.9), 3.33 (2 H, d, *J* 1.6), 2.44 (3 H, s), 1.94 (2 H, dd, *J* 13.2, 7.8), 1.69–1.52 (3 H, m), 1.48–1.30 (1 H, m). The identity of synthesized product was confirmed based on reported NMR spectra.[20]

7-Tosyl-7-azabicyclo[4.1.0]heptane **(1o)**

Following the general procedure D, compound **1o** was prepared from cyclohexene (white solid, 80%).

δ $_H$ (400 MHz, Chloroform-*d*) 7.81 (2 H, d, *J* 8.3), 7.32 (2 H, d, *J* 7.9), 3.04–2.89 (2 H, m), 2.44 (4 H, s), 1.90–1.72 (5 H, m), 1.45–1.34 (3 H, m), 1.29–1.16 (3 H, m). The identity of synthesized product was confirmed based on reported NMR spectra.[29]

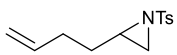

2-(But-3-en-1-yl)-1-tosylaziridine **(1u)**

Following the general procedure A, compound **1u** was prepared from 1,5-hexadiene (colorless liquid ,56%).

δ $_H$ (400 MHz, Chloroform-*d*) 7.82 (2 H, d, *J* 8.2), 7.34 (2 H, d, *J* 8.0), 5.72 (1 H, ddt, *J* 17.0, 10.3, 6.6), 5.00–4.91 (2 H, m), 2.81–2.72 (1 H, m), 2.63 (1 H, d, *J* 7.0), 2.45 (3 H, s), 2.08 (1 H, d, *J* 4.6), 2.06–1.98 (2 H, m), 1.70–1.62(1 H, m), 1.45 (1 H, td, *J* 14.5, 7.4). The identity of synthesized product was confirmed based on reported NMR spectra.[20]

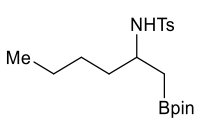

4-Methyl-*N*-(1-(4,4,5,5-tetramethyl-1,3,2-dioxaborolan-2-yl)hexan-2-yl)benzenesulfonamide (**3a**)

δ $_H$ (400 MHz, Chloroform-*d*) 7.75 (2 H, d, *J* 8.0), 7.26 (2 H, d, *J* 8.1), 5.06 (1 H, d, *J* 9.4), 3.48 – 3.37 (1 H, m), 2.40 (3 H, s), 1.45 – 1.26 (4 H, m), 1.21 (12 H, d, *J* 8.0), 1.19 – 1.12 (2 H, m), 0.88 – 0.73 (5 H, m). δ $_C$ (101 MHz, Chloroform-*d*) 143.05, 138.93, 129.63, 127.14, 83.64, 51.15, 37.16, 28.14, 24.96, 24.78, 22.44, 21.63, 14.04. δ $_B$ (161 MHz, Chloroform-*d*) 33.37. HRMS (ESI): m/z $[M+Na]^+$ calcd for $C_{19}H_{32}BNNaO_4S$: 404.20373, found: 404.2029

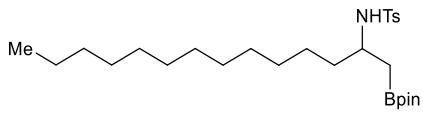

4-Methyl-*N*-(1-(4,4,5,5-tetramethyl-1,3,2-dioxaborolan-2-yl)tetradecan-2-yl)benzenesulfonamide (**3b**)

δ $_H$ (500 MHz, Chloroform-*d*) 7.75 (2 H, d, *J* 8.3), 7.26 (2 H, d, *J* 8.0), 5.06 (1 H, d, *J* 9.4), 3.42 (1 H, m), 2.40 (3 H, s), 1.33 – 1.11 (34 H, m), 0.86 (5 H, m). δ $_C$ (126 MHz, Chloroform-*d*) δ 143.01, 138.90, 129.61, 127.14, 83.62, 51.16, 37.44, 32.04, 29.80, 29.79, 29.78, 29.76, 29.69, 29.66, 29.60, 29.49, 29.37, 25.96, 24.95, 24.77, 22.82, 21.62, 14.26. δ $_B$ (161 MHz, Chloroform-*d*) 33.96. HRMS (ESI): m/z $[M+H]^+$ calcd for $C_{27}H_{49}BNO_4S$: 494.34699, found: 494.3459

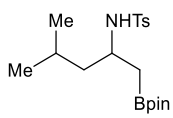

4-Methyl-*N*-(4-methyl-1-(4,4,5,5-tetramethyl-1,3,2-dioxaborolan-2-yl)pentan-2-yl)benzenesulfonamide (**3c**)

δ $_H$ (400 MHz, Chloroform-*d*) 7.75 (2 H, d, *J* 7.9), 7.26 (2 H, d, *J* 8.0), 5.05 (1 H, d, *J* 9.7), 3.51 (1 H, m), 2.40 (3 H, s), 1.63 (1 H, h, *J* 6.9), 1.33 (1 H, m), 1.21 (12 H, d,

J 8.5), 1.14 – 1.06 (1 H, m), 0.84 – 0.75 (8 H, m). δ_C (101 MHz, Chloroform-*d*) 143.06, 138.97, 129.63, 127.15, 83.62, 49.31, 46.87, 24.96, 24.77, 24.71, 22.86, 22.16, 21.63. δ_B (161 MHz, Chloroform-*d*) 33.45. HRMS (ESI): m/z $[M+H]^+$ calcd for $C_{19}H_{33}BNO_4S$: 382.22179, found: 382.2207

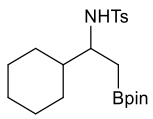

N-(1-Cyclohexyl-2-(4,4,5,5-tetramethyl-1,3,2-dioxaborolan-2-yl)ethyl)-4-methylbenzenesulfonamide (**3d**)

δ_H (400 MHz, Chloroform-*d*) 7.74 (2 H, d, *J* 8.0), 7.25 (2 H, d, *J* 8.0), 5.18 (1 H, d, *J* 9.7), 3.24 (1 H, dtd, *J* 10.1, 6.7, 3.5), 2.40 (3 H, s), 1.85 – 1.49 (6 H, m), 1.20 (12 H, d, *J* 8.3), 1.13 – 1.03 (3 H, m), 0.93 – 0.80 (3 H, m), 0.61 (1 H, dd, *J* 16.3, 6.6). δ_C (101 MHz, Chloroform-*d*) 142.97, 138.94, 129.59, 127.12, 83.62, 55.85, 43.80, 29.50, 29.41, 26.34, 26.25, 26.21, 24.86, 24.75, 21.63. δ_B (161 MHz, Chloroform-*d*) 33.11 HRMS (ESI): m/z $[M+H]^+$ calcd for $C_{21}H_{35}BNO_4S$: 408.23744, found: 408.2359

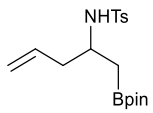

4-Methyl-*N*-(1-(4,4,5,5-tetramethyl-1,3,2-dioxaborolan-2-yl)pent-4-en-2-yl)benzenesulfonamide (**3e**)

δ_H (400 MHz, Chloroform-*d*) 7.73 (2 H, d, *J* 8.0), 7.25 (2 H, d, *J* 7.8), 5.61 (1 H, td, *J* 17.2, 7.2), 5.04 (1 H, d, *J* 8.8), 4.97 (2 H, t, *J* 12.9), 3.51 (1 H, dd, *J* 15.8, 9.8), 2.39 (4 H, s), 2.26 – 2.05 (2 H, m), 1.20 (12 H, d, *J* 5.3), 0.94 (1 H, dd, *J* 16.3, 4.1), 0.84

(1 H, dd, *J* 16.3, 6.7). δ_C (101 MHz, Chloroform-*d*) 143.17, 138.64, 134.23, 129.67, 127.19, 118.33, 83.69, 50.66, 41.65, 24.95, 24.84, 21.65. δ_B (161 MHz, Chloroform-*d*) 32.96. HRMS (ESI): m/z $[M+H]^+$ calcd for $C_{18}H_{29}BNO_4S$: 366.19049, found: 366.1895

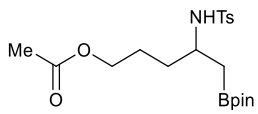

4-((4-Methylphenyl)sulfonamido)-5-(4,4,5,5-tetramethyl-1,3,2-dioxaborolan-2-yl)pentyl acetate (**3f**)

δ_H (400 MHz, Chloroform-*d*) 7.72 (2 H, d, *J* 8.2), 7.25 (2 H, d, *J* 6.7), 5.11 (1 H, d, *J* 9.5), 4.01 – 3.90 (2 H, m), 3.50 – 3.35 (1 H, m), 2.39 (3 H, s), 1.99 (3 H, s), 1.72 – 1.63 (1 H, m), 1.60 – 1.52 (1 H, m), 1.40 (2 H, ddd, *J* 15.6, 9.2, 5.9), 1.19 (12 H, d, *J* 8.2), 0.79 (2 H, qd, *J* 16.5, 5.2). δ_C (101 MHz, Chloroform-*d*) 171.22, 143.23, 138.69, 129.71, 127.08, 83.76, 64.15, 50.84, 33.79, 25.30, 24.94, 24.75, 21.66, 21.07. δ_B (161 MHz, Chloroform-*d*) 33.17. HRMS (ESI): m/z $[M+H]^+$ calcd for $C_{20}H_{33}BNO_6S$: 426.21162, found: 426.2103

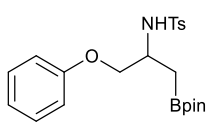

4-Methyl-*N*-(1-phenoxy-3-(4,4,5,5-tetramethyl-1,3,2-dioxaborolan-2-yl)propan-2-yl)benzenesulfonamide (**3g**)

δ_H (400 MHz, Chloroform-*d*) 7.76 (2 H, d, *J* 8.2), 7.27 – 7.20 (4 H, m), 6.93 (1 H, t, *J* 7.4), 6.75 (2 H, d, *J* 8.1), 5.33 (1 H, d, *J* 8.2), 3.92 (1 H, dd, *J* 8.8, 4.0), 3.87 – 3.76 (2 H, m), 2.39 (3 H, s), 1.21 (12 H, s), 1.11 (2 H, d, *J* 7.2). δ_C (101 MHz, Chloroform-

d) 158.44, 143.31, 138.27, 129.70, 129.50, 127.17, 121.22, 114.82, 83.78, 70.92, 50.26, 24.96, 24.90, 21.63. δ_B (161 MHz, Chloroform-*d*) 33.66. HRMS (ESI): m/z $[M+H]^+$ calcd for $C_{22}H_{31}BNO_5S$: 432.20105, found: 432.1997

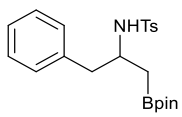

4-Methyl-*N*-(1-phenyl-3-(4,4,5,5-tetramethyl-1,3,2-dioxaborolan-2-yl)propan-2-yl)benzenesulfonamide (**3h**)

δ_H (400 MHz, Chloroform-*d*) 7.66 (2 H, d, *J* 8.2), 7.24 – 7.15 (5 H, m), 7.04 (2 H, d, *J* 6.7), 5.10 (1 H, d, *J* 8.7), 3.73 – 3.62 (1 H, m), 2.80 (1 H, dd, *J* 13.4, 6.0), 2.65 (1 H, dd, *J* 13.5, 7.7), 2.39 (3 H, s), 1.24 (12 H, d, *J* 6.3), 0.93 (2 H, dd, *J* 5.3, 2.5). δ_C (101 MHz, Chloroform-*d*) 143.02, 138.28, 137.85, 129.65, 129.55, 128.50, 127.11, 126.53, 83.70, 52.40, 43.50, 24.99, 24.94, 21.63, 21.56. δ_B (161 MHz, Chloroform-*d*) 33.16. HRMS (ESI): m/z $[M+H]^+$ calcd for $C_{22}H_{31}BNO_4S$: 416.20614, found: 416.2060

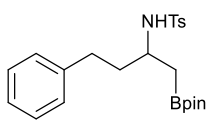

4-Methyl-*N*-(4-phenyl-1-(4,4,5,5-tetramethyl-1,3,2-dioxaborolan-2-yl)butan-2-yl)benzenesulfonamide (**3i**)

δ_H (400 MHz, Chloroform-*d*) 7.75 (2 H, d, *J* 7.8), 7.25 (5 H, dd, *J* 11.4, 7.5), 7.09 (2 H, d, *J* 7.5), 5.20 (1 H, d, *J* 9.5), 3.55 – 3.43 (1 H, m), 2.72 – 2.60 (1 H, m), 2.59 – 2.48 (1 H, m), 2.41 (3 H, s), 1.68 (2 H, ddd, *J* 15.1, 13.4, 7.2), 1.21 (11 H, d, *J* 8.3), 0.89 – 0.83 (2 H, m). δ_C (101 MHz, Chloroform-*d*) 143.16, 141.77, 138.74, 129.69,

128.50, 128.43, 127.14, 125.89, 83.72, 50.88, 39.21, 32.31, 24.96, 24.78, 21.63. δ_B (161 MHz, Chloroform-*d*) 33.02. HRMS (ESI): m/z $[M+H]^+$ calcd for $C_{23}H_{33}BNO_4S$: 430.22179, found: 430.2205

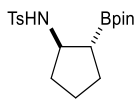

4-Methyl-*N*-(2-(4,4,5,5-tetramethyl-1,3,2-dioxaborolan-2-yl)cyclopentyl)benzenesulfonamide (**3n**)

δ_H (400 MHz, Chloroform-*d*) 7.77 (2 H, d, *J* 8.1), 7.28 (2 H, d, *J* 8.0), 4.64 (1 H, d, *J* 5.3), 3.43 (1 H, dt, *J* 14.3, 7.0), 2.41 (3 H, s), 1.93 – 1.73 (2 H, m), 1.42 (4 H, dd, *J* 11.7, 8.0), 1.16 (12 H, s), 1.14 – 1.08 (1 H, m). δ c (126 MHz, Chloroform-*d*) 143.18, 137.67, 129.64, 127.48, 83.53, 57.53, 34.74, 25.95, 24.81, 24.79, 24.25, 21.63. . δ_B (161 MHz, Chloroform-*d*) 33.17. HRMS (ESI): m/z $[M+Na]^+$ calcd for $C_{18}H_{28}BNNaO_4S$: 388.17243, found: 388.1711

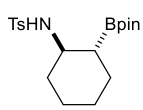

4-Methyl-*N*-(2-(4,4,5,5-tetramethyl-1,3,2-dioxaborolan-2-yl)cyclohexyl)benzenesulfonamide (**3o**)

δ_H (500 MHz, Chloroform-*d*) 7.76 (2 H, d, *J* 8.3), 7.27 (3 H, d, *J* 9.1), 4.72 (1 H, d, *J* 6.2), 3.23 (1 H, dq, *J* 13.8, 4.6, 3.9), 2.41 (3 H, s), 1.39 – 1.22 (5 H, m), 1.20 (13 H, d, *J* 5.5), 1.16 – 1.05 (1 H, m), 0.95 (1 H, td, *J* 10.5, 3.6). δ_C (126 MHz, Chloroform-*d*) 143.05, 138.88, 129.65, 127.23, 83.70, 54.19, 34.23, 29.85, 26.49, 25.81, 24.92, 24.84, 21.65. δ_B (161 MHz, Chloroform-*d*) 33.96. HRMS (ESI): m/z $[M+H]^+$ calcd for $C_{19}H_{31}BNO_4S$: 380.20614, found: 380.2050

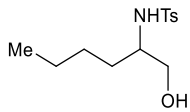

N-(1-Hydroxyhexan-2-yl)-4-methylbenzenesulfonamide (**3a'**)

δ_H (400 MHz, Chloroform-*d*) 7.78 (2 H, d, *J* 8.1), 7.30 (2 H, d, *J* 8.0), 4.98 (1 H, d, *J* 7.9), 3.57 (1 H, dd, *J* 11.3, 3.8), 3.47 (1 H, dd, *J* 11.3, 5.3), 3.21 (1 H, tt, *J* 8.0, 6.1, 2.8), 2.42 (3 H, s), 2.31 (1 H, s), 1.48 – 0.93 (6 H, m), 0.74 (3 H, t, *J* 6.9). The identity of synthesized product was confirmed based on reported NMR spectra.[30]

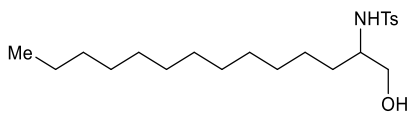

N-(1-Hydroxytetradecan-2-yl)-4-methylbenzenesulfonamide (**3b'**)

δ_H (500 MHz, Chloroform-*d*) 7.79 (2 H, d, *J* 8.0), 7.31 (2 H, d, *J* 8.0), 4.98 (1 H, d, *J* 7.7), 3.59 (1 H, dd, *J* 11.2, 3.7), 3.49 (1 H, dd, *J* 11.2, 5.3), 3.23 (1 H, s), 2.43 (3 H, s), 1.51 – 1.00 (22 H, m), 0.89 (3 H, t, *J* 6.9). δ_C (126 MHz, Chloroform-*d*) 143.63, 137.70, 129.82, 127.30, 65.10, 55.79, 32.05, 31.85, 29.80, 29.78, 29.77, 29.63, 29.53, 29.48, 29.31, 25.65, 22.82, 21.65, 14.25. HRMS (ESI): m/z $[M+Na]^+$ calcd for $C_{21}H_{37}NNaO_3S$: 406.2392, found: 406.2386

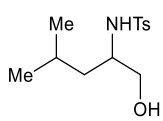

N-(1-Hydroxy-4-methylpentan-2-yl)-4-methylbenzenesulfonamide (**3c'**)

δ_H (400 MHz, Chloroform-*d*) 7.78 (2 H, d, *J* 8.1), 7.30 (2 H, d, *J* 8.0), 5.14 (1 H, d, *J* 8.0), 3.57 (1 H, dd, *J* 11.3, 3.6), 3.44 (1 H, dd, *J* 11.3, 5.0), 3.27 (1 H, dtd, *J* 14.4,

7.9, 4.2), 2.42 (3 H, s), 1.43 (1 H, dt, *J* 13.5, 6.7), 1.31 – 1.15 (2 H, m), 0.75 (3 H, d, *J* 6.6), 0.61 (3 H, d, *J* 6.5). The identity of synthesized product was confirmed based on reported NMR spectra.[31]

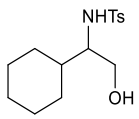

N-(1-Cyclohexyl-2-hydroxyethyl)-4-methylbenzenesulfonamide (**3d'**)

δ_H (400 MHz, Chloroform-*d*) 7.77 (2 H, d, *J* 8.0), 5.01 (1 H, d, *J* 8.4), 3.55 (2 H, qd, *J* 11.5, 4.3), 3.04 (1 H, tt, *J* 9.3, 5.3), 2.42 (3 H, s), 1.73 – 1.37 (6 H, m), 1.18 – 0.73 (6 H, m). δ_C (101 MHz, Chloroform-*d*) 143.55, 137.78, 129.75, 127.27, 62.76, 60.48, 39.21, 29.48, 29.07, 26.21, 26.12, 26.10, 21.67. HRMS (ESI): m/z $[M+Na]^+$ calcd for $C_{15}H_{23}NNaO_3S$: 320.1296, found: 320.1291

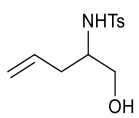

N-(1-Hydroxypent-4-en-2-yl)-4-methylbenzenesulfonamide (**3e'**)

δ_H (500 MHz, Chloroform-*d*) 7.76 (2 H, d, *J* 8.2), 7.31 (2 H, d, *J* 8.0), 5.47 (1 H, ddt, *J* 16.0, 10.8, 7.3), 5.07 – 4.94 (2 H, m), 4.83 (1 H, d, *J* 7.1), 3.60 (1 H, dd, *J* 11.3, 4.1), 3.53 (1 H, dd, *J* 11.3, 5.2), 3.31 – 3.24 (1 H, m), 2.43 (3 H, s), 2.18 (2 H, hept, *J* 6.9), 2.03 (1 H, m). The identity of synthesized product was confirmed based on reported NMR spectra.[26]

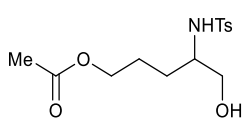

5-Hydroxy-4-((4-methylphenyl)sulfonamido)pentyl acetate (**3f'**)

δ_H (400 MHz, Chloroform-*d*) 7.77 (2 H, d, *J* 8.0), 7.30 (2 H, d, *J* 8.0), 5.15 (1 H, d, *J* 8.2), 3.92 (2 H, dt, *J* 6.6, 3.2), 3.50 (2 H, qd, *J* 11.2, 4.2), 3.26 (1 H, dq, *J* 7.9, 3.8), 2.42 (3 H, s), 2.30 (1 H, s), 2.01 (3 H, s), 1.64 – 1.36 (4 H, m). δ_C (101 MHz, Chloroform-*d*) 171.34, 143.77, 137.70, 129.90, 127.19, 64.63, 63.97, 55.22, 28.40, 24.92, 21.68, 21.07. HRMS (ESI): m/z $[M+Na]^+$ calcd for $C_{14}H_{21}NNaO_5S$: 338.1038, found: 338.1033

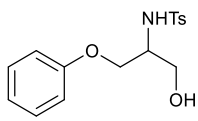

N-(1-Hydroxy-3-phenoxypropan-2-yl)-4-methylbenzenesulfonamide (**3g'**)

δ_H (500 MHz, Chloroform-*d*) 7.84 – 7.74 (2 H, m), 7.31 – 7.18 (4 H, m), 6.96 (1 H, t, *J* 7.5), 6.80 – 6.69 (2 H, m), 5.41 (1 H, d, *J* 7.8), 4.00 (1 H, dd, *J* 9.7, 4.7), 3.89 (1 H, dd, *J* 9.6, 5.6), 3.80 (1 H, dd, *J* 11.3, 4.5), 3.69 (1 H, dd, *J* 11.3, 4.8), 3.63 (1 H, dt, *J* 7.8, 4.8), 2.41 (3 H, s), 2.15 (1 H, s). δ_H (126 MHz, Chloroform-*d*) 157.98, 143.84, 137.40, 129.92, 129.64, 127.23, 121.55, 114.50, 66.89, 62.37, 54.10, 21.66. HRMS (ESI): m/z $[M+Na]^+$ calcd for $C_{16}H_{19}NNaO_4S$: 344.0932, found: 344.0927

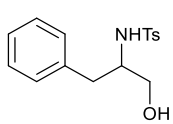

N-(1-Hydroxy-3-phenylpropan-2-yl)-4-methylbenzenesulfonamide (**3h'**)

δ_H (400 MHz, Chloroform-*d*) 7.59 (2 H, d, *J* 8.0), 7.23 – 7.14 (5 H, m), 6.97 (2 H, dd, *J* 6.1, 3.0), 5.12 (1 H, d, *J* 7.2), 3.63 (1 H, dd, *J* 11.3, 3.8), 3.52 (1 H, dd, *J* 11.2, 4.8), 3.44 (1 H, tt, *J* 7.5, 4.4), 2.77 (1 H, dd, *J* 13.8, 7.1), 2.67 (1 H, dd, *J* 13.8, 7.2),

2.48 (1 H, s), 2.40 (3 H, s). The identity of synthesized product was confirmed based on reported NMR spectra.[32]

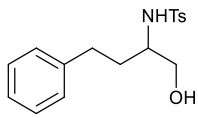

N-(1-Hydroxy-4-phenylbutan-2-yl)-4-methylbenzenesulfonamide (**3i'**)

δ_H (500 MHz, Chloroform-*d*) 7.79 – 7.71 (2 H, m), 7.30 (2 H, d, *J* 7.8), 7.25 – 7.20 (2 H, m), 7.16 (1 H, dd, *J* 8.3, 6.2), 6.99 (2 H, d, *J* 7.4), 4.95 (1 H, s), 3.58 (1 H, dt, *J* 11.0, 3.1), 3.51 (1 H, dt, *J* 11.3, 3.3), 3.28 (1 H, s), 2.54 (1 H, ddd, *J* 15.2, 9.3, 6.7), 2.48 – 2.40 (4 H, m), 1.93 (2 H, s), 1.84 – 1.60 (2 H, m). δ_H (101 MHz, Chloroform-*d*) 143.65, 141.11, 137.69, 129.87, 128.48, 128.35, 127.23, 126.06, 64.64, 55.25, 33.40, 31.85, 21.65. HRMS (ESI): m/z $[M+Na]^+$ calcd for $C_{17}H_{21}NNaO_3S$: 342.1140, found: 342.1134

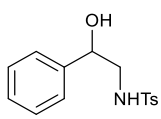

N-(2-Hydroxy-2-phenylethyl)-4-methylbenzenesulfonamide (**3j'-*b***)

3j'-*b* was prepared according to the general procedure E *with the following modifications*: The reaction was conducted without 1,2,3,5-tetrakis(carbazol-9-yl)-4,6-*d*icyanobenzene.

δ_H (400 MHz, Chloroform-*d*) 7.72 (2 H, d, *J* 8.1), 7.37 – 7.20 (7 H, m), 5.07 (1 H, dd, *J* 8.2, 4.6), 4.86 – 4.74 (1 H, m), 3.24 (1 H, ddd, *J* 12.3, 8.3, 3.6), 3.02 (1 H, ddd, *J* 13.2, 8.7, 4.5), 2.59 (1 H, d, *J* 3.6), 2.42 (3 H, s). The identity of synthesized product was confirmed based on reported NMR spectra.[33]

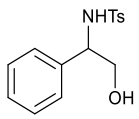

N-(2-Hydroxy-1-phenylethyl)-4-methylbenzenesulfonamide (**3j'-*l***)

3j'-*l* was prepared according to the general procedure E *with the following modifications*: The reaction was conducted without 1,2,3,5-tetrakis(carbazol-9-yl)-4,6-*d*icyanobenzene.

δ_H (400 MHz, Chloroform-*d*) 7.61 (2 H, d, *J* 8.0), 7.24 – 7.14 (5 H, m), 7.14 – 7.06 (2 H, m), 5.32 (1 H, d, *J* 6.6), 4.39 (1 H, q, *J* 5.9), 3.75 (2 H, q, *J* 6.3, 4.5), 2.38 (3 H, s). The identity of synthesized product was confirmed based on reported NMR spectra.[34]

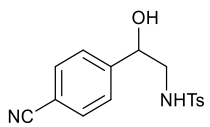

N-(2-(4-Cyanophenyl)-2-hydroxyethyl)-4-methylbenzenesulfonamide (**3k'-*b***)

3k'-*b* was prepared according to the general procedure E *with the following modifications*: The reaction was conducted without 1,2,3,5-tetrakis(carbazol-9-yl)-4,6-*d*icyanobenzene.

δ_H (400 MHz, Chloroform-*d*) 7.62 – 7.51 (2 H, m), 7.51 – 7.42 (2 H, m), 7.32 – 7.23 (2 H, m), 7.18 (2 H, d, *J* 7.9), 5.91 (1 H, s), 4.49 (1 H, t, *J* 5.3), 3.79 (1 H, dd, *J* 11.4, 4.2), 3.68 (1 H, dd, *J* 11.3, 6.6), 2.39 (3 H, s). δ_C (101 MHz, Chloroform-*d*) 144.06, 143.30, 138.64, 137.79, 136.84, 132.37, 129.75, 128.00, 127.25, 65.72, 59.02, 21.66. HRMS (ESI): m/z $[M-H]^-$ calcd for $C_{16}H_{15}N_2O_3$: 315.0809, found: 315.0807

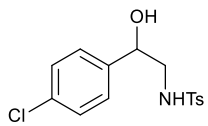

N-(2-(4-Chlorophenyl)-2-hydroxyethyl)-4-methylbenzenesulfonamide (**3l'-*b***)

3l'-*b* was prepared according to the general procedure E *with the following modifications*: The reaction was conducted without 1,2,3,5-tetrakis(carbazol-9-yl)-4,6-*d*icyanobenzene.

δ_H (400 MHz, Chloroform-*d*) 7.71 (2 H, d, *J* 8.0), 7.32 – 7.27 (4 H, m), 7.22 (2 H, d, *J* 8.2), 4.98 (1 H, t, *J* 6.3), 4.83 – 4.77 (1 H, m), 3.23 (1 H, ddd, *J* 12.1, 7.8, 3.5), 2.99 (1 H, ddd, *J* 13.2, 8.4, 4.5), 2.59 (1 H, s), 2.43 (3 H, s). The identity of synthesized product was confirmed based on reported NMR spectra.[32]

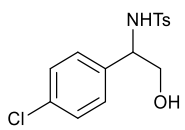

N-(1-(4-Chlorophenyl)-2-hydroxyethyl)-4-methylbenzenesulfonamide (**3l'-*l***)

3l'-*l* was prepared according to the general procedure E *with the following modifications*: The reaction was conducted without 1,2,3,5-tetrakis(carbazol-9-yl)-4,6-dicyanobenzene.

δ_H (400 MHz, Chloroform-*d*) 7.59 (2 H, d, *J* 8.0), 7.18 (4 H, dd, *J* 8.1, 5.3), 7.05 (2 H, d, *J* 8.2), 5.38 (1 H, d, *J* 6.3), 4.38 (1 H, q, *J* 5.8), 3.71 (2 H, dp, *J* 22.8, 5.8), 2.39 (3 H, s). The identity of synthesized product was confirmed based on reported NMR spectra.[35]

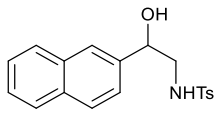

N-(2-Hydroxy-2-(naphthalen-2-yl)ethyl)-4-methylbenzenesulfonamide (**3m'-*b***)

3m'-*b* was prepared according to the general procedure E *with the following modifications*: The reaction was conducted without 1,2,3,5-tetrakis(carbazol-9-yl)-4,6-dicyanobenzene.

δ_H (400 MHz, Chloroform-*d*) 7.80 (4 H, d, *J* 8.2), 7.70 (2 H, dd, *J* 8.3, 1.9), 7.53 – 7.44 (2 H, m), 7.35 (1 H, d, *J* 8.5), 7.30 (1 H, d, *J* 7.8), 7.28 – 7.21 (2 H, m), 5.11 (1 H, t, *J* 6.3), 5.00 – 4.94 (1 H, m), 3.34 (1 H, ddd, *J* 12.2, 8.0, 3.6), 3.11 (1 H, ddd, *J* 12.9, 8.5, 4.4), 2.72 (1 H, s), 2.42 (3 H, s). The identity of synthesized product was confirmed based on reported NMR spectra.[32]

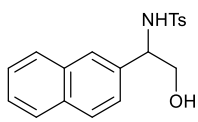

N-(2-Hydroxy-1-(naphthalen-2-yl)ethyl)-4-methylbenzenesulfonamide (**3m'-*l***)

3m'-*l* was prepared according to the general procedure E *with the following modifications*: The reaction was conducted without 1,2,3,5-tetrakis(carbazol-9-yl)-4,6-dicyanobenzene.

δ_H (400 MHz, Chloroform-*d*) 7.80 – 7.73 (1 H, m), 7.67 (2 H, dd, *J* 11.9, 7.5), 7.58 (2 H, d, *J* 7.9), 7.52 – 7.41 (3 H, m), 7.19 (1 H, dt, *J* 8.5, 1.4), 7.04 (2 H, d, *J* 7.9), 5.47 (1 H, d, *J* 6.7), 4.58 (1 H, q, *J* 5.9), 3.84 (2 H, s), 2.24 (3 H, s), 2.06 (1 H, s). δ_C (101 MHz, Chloroform-*d*) 143.58, 137.09, 134.72, 133.11, 129.87, 129.50, 128.67, 127.97, 127.68, 127.29, 126.44, 126.40, 126.35, 124.53, 66.22, 59.75, 21.46. HRMS

(ESI): m/z $[M+Na]^+$ calcd for $C_{19}H_{19}NNaO_3S$: 364.0978, found: 364.0976.

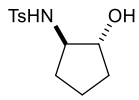

N-(2-Hydroxycyclopentyl)-4-methylbenzenesulfonamide (**3n'**)

δ_H (400 MHz, Chloroform-*d*) 7.78 (2 H, d, *J* 8.0), 7.32 (2 H, d, *J* 8.1), 4.99 (1 H, d, *J* 5.9), 4.04 (1 H, q, *J* 6.8), 3.22 (1 H, ddd, *J* 14.1, 8.2, 6.0), 2.89 (1 H, s), 2.43 (3 H, s), 2.04 – 1.82 (2 H, m), 1.69 – 1.26 (4 H, m). The identity of synthesized product was confirmed based on reported NMR spectra.[36]

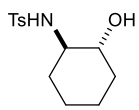

N-(2-Hydroxycyclohexyl)-4-methylbenzenesulfonamide (**3o'**)

δ_H (400 MHz, Chloroform-*d*) 7.78 (2 H, d, *J* 7.9), 7.32 (2 H, d, *J* 7.9), 4.76 (1 H, d, *J* 7.0), 3.29 (1 H, q, *J* 8.7, 7.4), 2.91 – 2.74 (1 H, m), 2.53 (1 H, s), 2.43 (3 H, s), 2.02 (1 H, dt, *J* 11.7, 3.8), 1.86 – 1.69 (1 H, m), 1.66 (1 H, dd, *J* 8.6, 3.0), 1.30 – 1.05 (4 H, m). The identity of synthesized product was confirmed based on reported NMR spectra.[32]

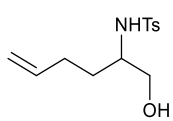

N-(1-Hydroxyhex-5-en-2-yl)-4-methylbenzenesulfonamide (**3u'**)

δ_H (500 MHz, Chloroform-*d*) 7.77 (2 H, d, *J* 8.3), 7.31 (3 H, d, *J* 8.0), 5.61 (1 H, ddt, *J* 17.0, 10.3, 6.6), 4.98 (1 H, d, *J* 8.2), 4.94 – 4.79 (2 H, m), 3.56 (1 H, dd, *J* 11.2,

3.8), 3.48 (1 H, dd, *J* 11.2, 4.9), 3.27 (1 H, tt, *J* 7.1, 3.9), 2.43 (3 H, s), 2.17 (0 H, d, *J* 5.8), 2.01 – 1.83 (2 H, m), 1.60 – 1.42 (2 H, m). δ_C (126 MHz, Chloroform-*d*) 143.58, 137.68, 137.22, 129.73, 127.13, 115.39, 64.55, 55.06, 31.00, 29.60, 21.51. HRMS (ESI): m/z $[M+Na]^+$ calcd for $C_{13}H_{19}NNaO_3S$: 292.0983, found: 292.0978

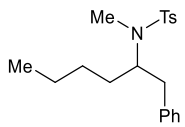

N,4-Dimethyl-*N*-(1-phenylhexan-2-yl)benzenesulfonamide (**4a**)

δ_H (400 MHz, Chloroform-*d*) 7.52 (2 H, d, *J* 7.7), 7.29 – 7.16 (5 H, m), 7.10 (2 H, d, *J* 6.7), 4.21 – 4.08 (1 H, m), 2.71 (3 H, s), 2.56 (2 H, t, *J* 7.2), 2.38 (3 H, s), 1.38 (2 H, d, *J* 5.2), 1.29 – 1.10 (4H, m), 0.80 (3 H, t, *J* 5.9). δ_C (101 MHz, Chloroform-*d*) 142.77, 138.48, 137.25, 129.45, 129.14, 128.46, 127.09, 126.33, 58.84, 39.17, 30.88, 28.45, 27.71, 22.33, 21.45, 13.90. HRMS (ESI): m/z $[M+H]^+$ calcd for $C_{20}H_{28}NO_2S$: 346.18353, found: 346.1824

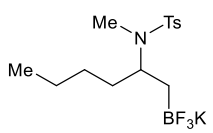

N,4-Dimethyl-*N*-(1-(trifluoro-4-boraneyl)hexan-2-yl)benzenesulfonamide, potassium salt (**5a**)

δ_H (500 MHz, Acetone-d_6) 7.70 (2 H, d, *J* 8.4), 7.32 (2 H, d, *J* 7.9), 4.09 (1 H, tt, *J* 10.4, 3.5), 2.87 (3 H, s), 2.53 (3 H, s), 2.38 (3 H, s), 1.68 (1 H, tdd, *J* 13.2, 6.3, 3.0), 1.36 – 1.27 (1 H, m), 1.26 – 1.09 (4 H, m), 0.83 (3 H, t, *J* 6.8), 0.23 – 0.13 (1 H, m), 0.05 – -0.06 (1 H, m). δ_c (126 MHz, Chloroform-*d*) 141.97, 138.51, 129.10, 127.31, 57.21, 57.19, 33.24, 26.53, 22.41, 20.47, 13.66.δ_B (161 MHz, Chloroform-*d*) 4.64.

δ_F (471 MHz, Acetone-d_6) -139.06 (d, *J* 80.6). HRMS (ESI): m/z $[M-K]^-$ calcd for $C_{14}H_{22}BF_3NO2S$: 336.14164, found: 336.1422

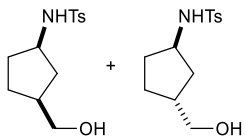

cis : **trans** = 1.2 : 1.0

N-(2-(Hydroxymethyl)cyclopentyl)-4-methylbenzenesulfonamide (**7u'**)

6u-*cis* δ_H (400 MHz, Chloroform-*d*) 7.75 (1 H, d, *J* 8.0), 7.28 (1 H, d, *J* 8.2), 5.51 (1 H, d, *J* 7.9), 3.62 (1 H, q, *J* 6.4), 3.52 (1 H, d, *J* 5.0), 2.42 (3 H, s), 2.09 (1 H, q, *J* 7.6, 5.4), 1.93 (1 H, ddd, *J* 13.4, 9.1, 6.7), 1.72 – 1.60 (2 H, m), 1.56 – 1.45 (2 H, m), 1.20 (1 H, tdd, *J* 10.9, 8.0, 3.7). δ_c (126 MHz, Chloroform-*d*) 143.26, 138.19, 129.76, 127.17, 65.95, 54.95, 38.99, 36.63, 33.63, 25.77, 21.65.

6u-*trans* δ_H (400 MHz, Chloroform-*d*) 7.75 (2 H, d, *J* 8.0), 7.35 – 7.23 (2 H, m), 4.87 (1 H, d, *J* 7.1), 3.62 (1 H, h, *J* 6.2), 3.43 (2 H, dd, *J* 6.7, 2.8), 2.42 (3 H, s), 2.26 – 1.11 (5 H, m). δ_c (126 MHz, Chloroform-*d*) 143.47, 137.81, 129.83, 127.20, 66.71, 54.71, 39.50, 36.36, 33.54, 26.77, 21.65.

HRMS (ESI): m/z $[M+Na]^+$ calcd for $C_{13}H_{19}NNaO_3S$: 292.0983, found: 292.0978.

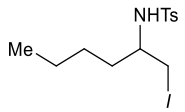

N-(1-Iodohexan-2-yl)-4-methylbenzenesulfonamide (**6a**)

δ_H (400 MHz, Chloroform-*d*) 7.77 (2 H, d, *J* 8.1), 7.31 (2 H, d, *J* 8.0), 4.65 (1 H, d, *J* 8.7), 3.22 (1 H, dd, *J* 10.3, 3.1), 3.15 (1 H, dd, *J* 10.3, 4.8), 2.94 (1 H, tq, *J* 7.7, 3.9),

2.43 (3 H, s), 1.76 (1 H, s), 1.43 (2 H, tt, *J* 7.5, 5.8), 1.30 – 1.03 (3 H, m), 0.80 (3 H, t, *J* 6.9). The identity of synthesized product was confirmed based on reported NMR spectra.[20]

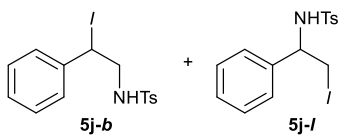

5j-*b* **5j-*l***

b* : *l = 2.0 : 1.0

N-(2-Iodo-2-phenylethyl)-4-methylbenzenesulfonamide (**6j-*b***) and *N*-(2-Iodo-1-phenylethyl)-4-methylbenzenesulfonamide (**6j-*l***)

6j-*b* δ_H (400 MHz, Chloroform-*d*) 7.71 (2 H, d, *J* 8.3), 7.32 (2 H, d, *J* 8.0), 7.30 – 7.17 (5 H, m), 5.01 (1 H, t, *J* 7.8), 4.88 (1 H, t, *J* 6.6), 3.69 (1 H, dt, *J* 14.3, 7.2), 3.51 (1 H, ddd, *J* 14.2, 8.2, 6.2), 2.45 (3 H, s).

6j-*l* δ_H (400 MHz, Chloroform-*d*) 7.62 (2 H, d, *J* 8.3), 7.25 – 7.17 (5 H, m), 7.08 (2 H, dd, *J* 6.6, 2.9), 5.31 (1 H, d, *J* 7.0), 4.40 (1 H, q, *J* 6.5), 3.47 – 3.36 (2 H, m), 2.39 (3 H, s).

The identity of synthesized products were confirmed based on reported NMR spectra.[37]

3.5 References

1. For selected reviews, see: (a) D. G. Hall, *Boronic Acids: Preparation and Applications in Organic Synthesis, Medicine and Materials*, ed. D. G. Hall, Wiley-VCH, Weinheim, 2nd edn, 2011; (b) J. Plescia and N. Moitessier, *Eur. J. Med. Chem.*, 2020, **195**, 112270.

2. For a review, see: C. Cabrele, T. A. Martinek, O. Reiser and Ł. Berlicki, *J. Med. Chem.*, 2014, **57**, 9718-9739.

3. For representative examples, see: (a) H. S. Soor, J. Hansen, D. B. Diaz, S. Appavoo and A. K. Yudin, *Pept Sci.*, 2019, **111**, e24072; (b) A. S. Gorovoy, O. Gozhina, J.-S. Svendsen, G. V. Tetz, A. Domorad, V. V. Tetz and T. Lejon, *J. Pept. Sci.*, 2013, **19**, 613-618; (c) A. S. Gorovoy, O. V. Gozhina, J. S. Svendsen, A. A. Domorad, G. V. Tetz, V. V. Tetz and T. Lejon, *Chem. Biol. Drug Des.*, 2013, **81**, 408-413.

4. For reviews, see: (a) X. Li and D. G. Hall, *Adv. Synth. Catal.*, 2021, **363**, 2209-2223; (b) A. Šterman, I. Sosič, S. Gobec and Z. Časar, *Org. Chem. Front.*, 2019, **6**, 2991-2998.

5. For homologation strategies for the synthesis of β-aminoboronates, see: (a) D. S. Matteson, K. M. Sadhu and M. L. Peterson, *J. Am. Chem. Soc.*, 1986, **108**, 810-819; (b) A. Fawcett, A. Murtaza, C. H. U. Gregson and V. K. Aggarwal, *J. Am. Chem. Soc.*, 2019, **141**, 4573-4578; (c) Q. Xie and G. Dong, *J. Am. Chem. Soc.*, 2021, **143**, 14422-14427.

6. For other synthetic approaches, see: (a) D. B. Diaz, C. C. G. Scully, S. K. Liew, S. Adachi, P. Trinchera, J. D. St. Denis and A. K. Yudin, *Angew. Chem.*

Int. Ed., 2016, **55**, 12659-12663; (b) J. D. St. Denis, C. F. Lee and A. K. Yudin, *Org. Lett.*, 2015, **17**, 5764-5767; (c) Z. X. Giustra, X. Yang, M. Chen, H. F. Bettinger and S.-Y. Liu, *Angew. Chem. Int. Ed.*, 2019, **58**, 18918-18922; (d) J. Li, H. Wang, Z. Qiu, C.-Y. Huang and C.-J. Li, *J. Am. Chem. Soc.*, 2020, **142**, 13011-13020.

7. For a review, see: E. C. Neeve, S. J. Geier, I. A. I. Mkhalid, S. A. Westcott and T. B. Marder, *Chem. Rev.*, 2016, **116**, 9091-9161.

8. For hydroborations of aminoalkenes, see: (a) Z.-T. He, Y.-S. Zhao, P. Tian, C.-C. Wang, H.-Q. Dong and G.-Q. Lin, *Org. Lett.*, 2014, **16**, 1426-1429; (b) J.-B. Xie, S. Lin, S. Qiao and G. Li, *Org. Lett.*, 2016, **18**, 3926-3929; (c) K. Kubota, Y. Watanabe, K. Hayama and H. Ito, *J. Am. Chem. Soc.*, 2016, **138**, 4338-4341; (d) D. Kong, S. Han, R. Wang, M. Li, G. Zi and `G. Hou, *Chem. Sci.*, 2017, **8**, 4558-4564; (e) H. Lee, B. Y. Lee and J. Yun, *Org. Lett.*, 2015, **17**, 764-766; (f) X.-Y. Bai, W. Zhao, X. Sun and B.-J. Li, *J. Am. Chem. Soc.*, 2019, **141**, 19870-19878; (g) K. Hayama, R. Kojima, K. Kubota and H. Ito, *Org. Lett.,* 2020, **22**, 739–744; (h) R. Nallagonda and R. R. Karimov**,** *ACS Catal.*, 2021, **11**, 248–254.

9. For aminoborations of alkenes, see: (a) R. Sakae, K. Hirano and M. Miura, *J. Am. Chem. Soc.*, **2015**, *137*, 6460-6463; (b) H.-C. Jiang, X.-Y. Tang and M. Shi, *Chem. Commun.*, 2016, **52**, 5273-5276; (c) A. Parra, L. Amenós, M. Guisán-Ceinos, A. López, J. L. García Ruano and M. Tortosa, *J. Am. Chem. Soc.*, 2014, **136**, 15833-15836; (d) L. Wu, O. Zatolochnaya, B. Q u, L. Wu, L. A. Wells, M. C. Kozlowski, C. H. Senanayake, J. J. Song and Y.

Zhang, *Org. Lett.*, 2019, **21**, 8952-8956; (e) Z. Liu, H.-Q. Ni, T. Zeng and K. M. Engle, *J. Am. Chem. Soc.*, 2018, **140**, 3223-3227; (f) C.-H. Yang, Y.-S. Zhang, W.-W. Fan, G.-Q. Liu and Y.-M. Li, *Angew. Chem. Int. Ed.*, 2015, **54**, 12636-12639.

10. For nulceophilic additions onto imines see: (a) J. Kim, K. Ko and S. H. Cho, *Angew. Chem. Int. Ed.*, 2017, **56**, 11584-11588; (b) X. Li and D. G. Hall, *J. Am. Chem. Soc.*, 2020, **142**, 9063-9069.

11. For a ring-opening borylation of aziridines, see: Y. Takeda, A. Kuroda, W. M. C. Sameera, K. Morokuma and S. Minakata, *Chem. Sci.*, 2016, **7**, 6141-6152.

12. For a review, see: (a) X. E. Hu, *Tetrahedron*, 2004, **60**, 2701-2743; For representative examples, see: (b) J. Wu, X. Sun and H.-G. Xia, *Eur. J. Org. Chem.*, 2005, 4769-4772; (c) M. Kumar, S. K. Pandey, S. Gandhi and V. K. Singh, *Tetrahedron Lett.*, 2009, **50**, 363-365; (d) S. Minakata, T. Hotta, Y. Oderaotoshi and M. Komatsu, *J. Org. Chem.*, 2006, **71**, 7471-7472.

13. For reviews, see: (a) F. W. Friese and A. Studer, *Chem. Sci.*, 2019, **10**, 8503-8518; (b) Y.-M. Tian, X.-N. Guo, H. Braunschweig, U. Radius, and T. B. Marder*, Chem. Rev.,* 2021, **121**, 3561−3597

14. For a photoinduced transition-metal-free radical borylations of alkyl halides, see: (a) Y. Cheng, C. Mück-Lichtenfeld and A. Studer, *Angew. Chem. Int. Ed.*, 2018, **57**, 16832-16836; (b) Q. Liu, J. Hong, B. Sun, G. Bai, F. Li, G. Liu, Y. Yang and F. Mo, *Org. Lett.*, 2019, **21**, 6597-6602; (c) D. Mazzarella, G. Magagnano, B. Schweitzer-Chaput and P. Melchiorre, *ACS Catal.*, 2019,

9, 5876-5880; (d) L. Zhang, Z.-Q. Wu and L. Jiao, *Angew. Chem. Int. Ed.*, 2020, **59**, 2095-2099.

15. Due to the instability of catechol boronic ester, the crude product was converted to the more stable pinacol ester prior to analysis. However, even the corresponding pinacol ester is not entirely free from stability problems and required careful handling during isolation. A purified sample of **3a** provides only 73% of the product remaining after a silica gel chromatography. In general, a significantly higher yield was obtained from NMR analysis of the crude mixture. Moreover, direct oxidation in the catechol boronate stage gave an even greater yield, indicating successful formation of the aminoboronate.

16. The yield of the desired product was significantly diminished under the photocatalytic system in the case of aromatic aziridines (**3j'**, 30%, 1.1:1.0 *b*:*l*). For the ring opening of aziridines with an aryl substituent (**1j**), the presence of the photocatalytic system not only prevented the generation of β-iodoamine intermediate, but also had a destructive effect on the entire system by decomposing the starting material We believe that this undesirable pathway explains the preferred reaction conditions for arene-substituted aziridines that does not use photocatalysts (Table 3.2, **3j'**–**3m'**).

17. For the stability and synthetic potency of trifluoroborate salt, see: S. Darses and J.-P. Genet, *Chem. Rev.*, 2008, **108**, 288-325

18. For related examples, see: (a) J. Wu, R. M. Bär, L. Guo, A. Noble and V. K. Aggarwal, *Angew. Chem. Int. Ed.*, 2019, **58**, 18830-18834; (b) F. Sandfort,

F. Strieth-Kalthoff, F. J. R. Klauck, M. J. James and F. Glorius, *Chem. Eur. J.*, 2018, **24**, 17210-17214.

19. For a related example of potent photoreductant activity, see: A. F. Chmiel, O. P. Williams, C. P. Chernowsky, C. S. Yeung and Z. K. Wickens, *J. Am. Chem. Soc.*, 2021, **143**, 10882-10889.

20. T. J. Steiman, J. Liu, A. Mengiste and A. G. Doyle, *J. Am. Chem. Soc.*, 2020, **142**, 7598-7605.

21. C.-Y. Huang and A. G. Doyle, *J. Am. Chem. Soc.*, 2015, **137**, 5638-5641.

22. B. P. Woods, M. Orlandi, C.-Y. Huang, M. S. Sigman and A. G. Doyle, *J. Am. Chem. Soc.*, 2017, **139**, 5688-5691.

23. B. K. Das, S. Pradhan and T. Punniyamurthy, *Org. Lett.*, 2018, **20**, 4444-4448.

24. J. Wu, R. M. Bär, L. Guo, A. Noble and V. K. Aggarwal, *Angew. Chem. Int. Ed.*, 2019, **58**, 18830-18834.

25. X. -F. Cai, G. -S. Feng, B. Wu, and Y. -G Zhou, *Org. Lett.*, 2014, **16**, 2680-2683.

26. D. J. Lapinsky and S. C. Bergmeier, *Tetrahedron*, 2002, **58**, 7109-7117.

27. D. Albanese, D. Landini, M. Penso and S. Petricci, *Tetrahedron*, 1999, **55**, 6387-6394.

28. J. Davies, D. Janssen-Müller, D. P. Zimin, C. S. Day, T. Yanagi, J. Elfert and R. Martin, *J. Am. Chem. Soc.*, 2021, **143**, 4949-4954.

29. C.-Y. Huang and A. G. Doyle, *J. Am. Chem. Soc.*, 2012, **134**, 9541-9544.

30. D. Craig, C. J. T. Hyland and S. E. Ward, *Chem. Commun.*, 2005, 3439-3441.

31. S. Gazzola, E. M. Beccalli, T. Borelli, C. Castellano, D. Diamante and G. Broggini, *Synlett*, 2018, **29**, 503-508.

32. H. Yang and W.-H. Zheng, *Angew. Chem. Int. Ed.*, 2019, **58**, 16177-16180.

33. B. Biletskyi, L. Kong, A. Tenaglia and H. Clavier, *Adv. Synth. Catal.*, 2021, **363**, 2578-2585.

34. K. Wen, Z. Wu, B. Chen, J. Chen and W. Zhang, *Org. Biomol. Chem.*, 2018, **16**, 5618-5625.

35. H. Sugimoto, A. Mikami, K. Kai, P. K. Sajith, Y. Shiota, K. Yoshizawa, K. Asano, T. Suzuki and S. Itoh, *Inorg. Chem.*, 2015, **54**, 7073-7082.

36. Z. Wang, Y.-T. Cui, Z.-B. Xu and J. Qu, *J. Org. Chem.*, 2008, **73**, 2270-2274.

37. A. Viceriat, I. Marchand, S. Carret and J.-F. Poisson, *Org. Lett.*, 2021, **23**, 2449-2454.

Chapter 4. Metal-free 1,2-arylboration for the synthesis of heterocyclic boronate esters via photoinduced C(sp^2)–I bond cleavage*

4.1 Introduction

Efficient methodologies for the synthesis of complex molecules are continuously being sought.[1] In this regard, the difunctionalization of simple alkenes presents a unique and noteworthy strategy as two chemical bonds are installed simultaneously.[2,3] Among the myriad of possible functional groups, the boron group is of great interest because its various bonding modes enable several well-known transformations (Scheme 4.1A).[4]

Since the recent advent of transition-metal-mediated cross-coupling, numerous highly efficient carboboration methods have been reported.[5,6] However, considering the aim of achieving sustainable chemical production, the development of greener, wasteless protocols is highly desirable. To our knowledge, the radical-based carboboration strategy, which avoids the use of transition metal catalysts and external additives, has been less developed.[7] Herein, we present a metal-catalyst-free 1,2-arylboration strategy and its application in the synthesis of indoline and coumaran boronate esters using blue LED light irradiation (Scheme 4.1B).

* The majority of this work contains unpublished results.

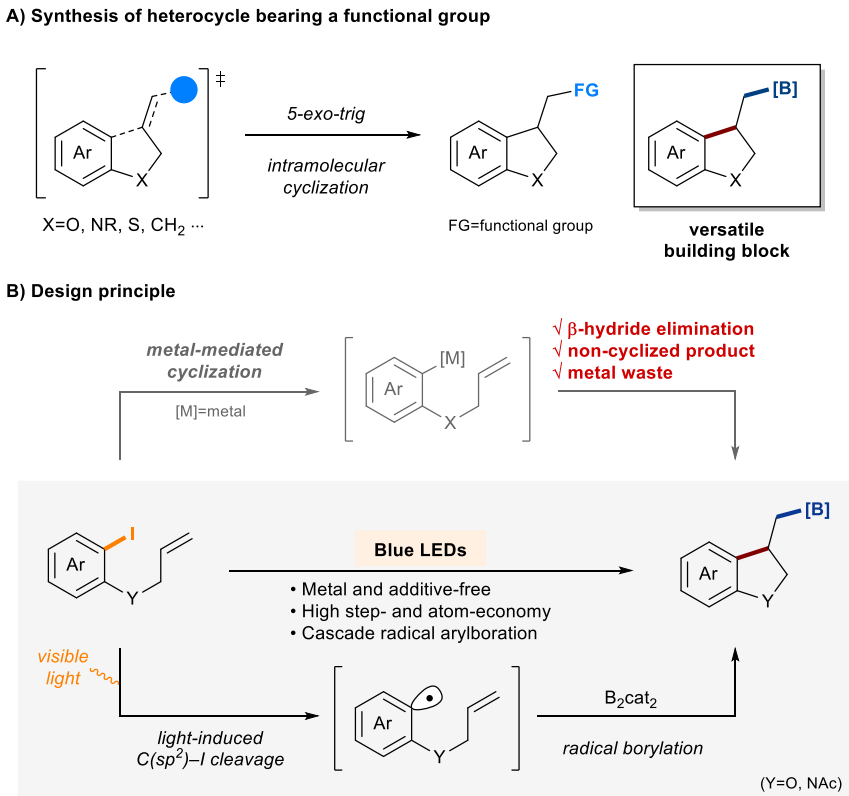

Scheme 4.1 Target strategy for the synthesis of heterocyclic boronate esters

In terms of developing a green and sustainable process, we attempt to minimize the reaction waste by using photons as the only energy. Moreover, this new single-step C–C and C–B bond-forming reaction enables rapid access to the target molecules with excellent step- and atom-economy. Ultimately, convenient preparation of heterocyclic compounds containing indoline or coumaran scaffolds,[8,9] common structural motifs with important bioactivity,[10] was realized (Figure 4.1).

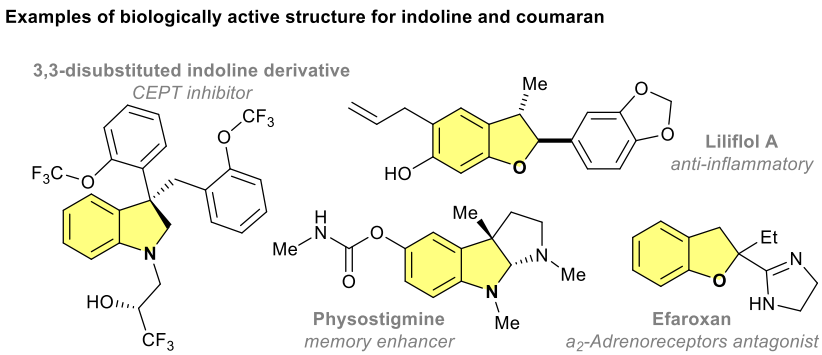

Figure 4.1 Potentially accessible bioactive compounds

4.2 Results and discussion

4.2.1 Evaluation of reaction parameters

To evaluate the hypothesis, we attempted the coupling of 1-allyloxy-2-iodobenzene (**1**) with bis(catecholato)diboron (B_2cat_2) in *N*,*N*-dimethylformamide (DMF) for 15 h under visible light with a wavelength of 390 nm (Table 4.1). Due to the instability of catechol alkylboronic esters, the crude product was transesterified using pinacol and triethylamine (TEA). The reaction proceeded efficiently to afford desired product **1a** in 93% yield (entry 1). In the absence of light, the reaction did not occur, indicating the necessity for photon energy (entry 2). However, when a light source with a wavelength of 456 nm was used, the desired product was formed in low yield (entry 3). In recent years, several examples of bis(pinacolato)diboron (B_2pin_2)-activated radical borylations have been published.[11] No conversion of starting material was observed with the use of B_2pin_2 under the optimized conditions (entry 4). When aryl bromide was used instead of **1**, the reaction did not proceed (entry 5). Decreasing the reaction time from 15 h to 3 h did not improve the yield of the desired

product (entry 6). The use of *N*,*N*-dimethylacetamide (DMAc) instead of DMF as the solvent led to inferior results (entry 7).

Table 4.1 Evaluation of reaction parameters[a]

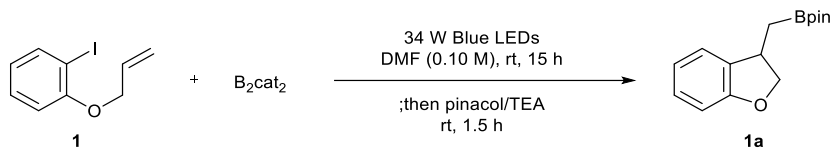

Entry	Conditions	Yields (%)
1	As shown	93
2	No light	0
3	Wavelength of 456 nm instead of 390 nm	15
4	B_2pin_2 instead of B_2cat_2	0
5	Ar–Br instead of Ar–I	0
6	3 h instead of 15 h	68
7	DMAc instead of DMF	0

[a] The reaction is set up with 1-allyloxy-2-iodobenzene (0.20 mmol), B_2cat_2 (2.0 equiv) in DMF (0.10 M), irradiated with the blue LEDs wavelength of 390 nm. Yields were determined by ^{1}H NMR analysis using 1,1,2,2,-tetrachloroethane as an internal standard. B_2pin_2=bis(pinacolato)diboron. B_2cat_2=bis(catecholato)diboron. DMAc=*N*,*N*-dimethylacetamide. DMF= *N*,*N*-dimethylformamide.

4.2.2 Expected reaction mechanism

Based on previous reports,[12] the reaction mechanism is proposed in Figure 4.2. An aryl radical (**Int-I**), generated photochemically from aryl iodide (**1**) via C–I bond homolysis, is trapped intramolecularly by the tethered alkene.[13] Following the formation of an sp^3-hybridized carbon radical intermediate (**Int-II**), complexation with DMF and B_2cat_2 occurs, delivering a B–B single electron σ-bond complex (**Int-III**).[14] Following B–B bond homolysis, the borylated compound (**Int-IV**) and DMF-complexed boryl radical (**Int-V**) are formed. Treatment with pinacol and triethyl-

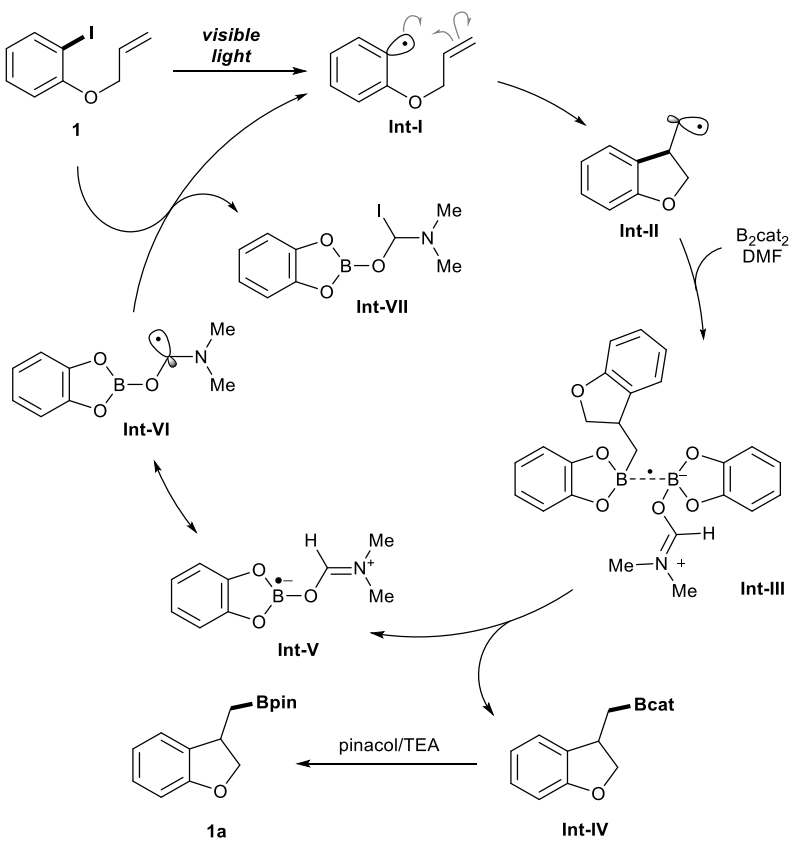

Figure 4.2 Expected reaction mechanism

amine (TEA) converted the unstable catechol boronic ester into a stable pinacol boronic ester as the desired product **1a**. The ensuing α-aminoalkyl radical intermediate (**Int-VI**), best described by resonance structures, abstracts an iodine atom or reduces the aryl halide providing an aryl radical (**Int-I**) and **Int-VII**.[15]

4.2.3 Preliminary 1,2-arylboration results (intra- and intermolecular reactions)

Table 4.2 Preliminary results of the 1,2-arylboration[a]

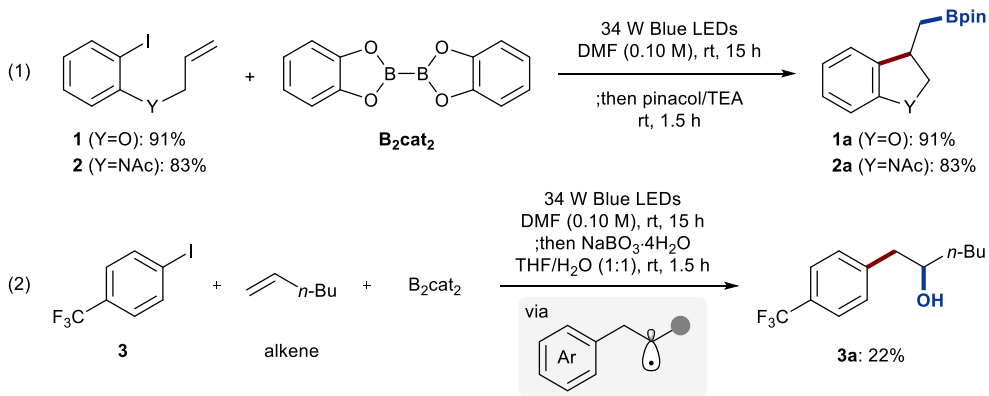

[a] The reaction is set up with aryl iodide (0.20 mmol), B_2cat_2 (2.0 equiv) in DMF (0.10 M), irradiated with the blue LEDs wavelength of 390 nm (10.0 equivalents of alkene were used in eq 2). B_2cat_2=bis(catecholato)diboron, DMF=*N*,*N*-dimethylformamide. rt=room temperature. TEA=triethylamine. Ac=acetyl.

With the optimized reaction conditions in hand, the developed intramolecular 1,2-arylboration reaction was evaluated for the preparation of heterocyclic boronate ester derivatives (Table 4.2, eq 1). Successful reactivity was observed in the cases of coumaran and indoline derivatives, and the corresponding products **1a** and **2a** were formed in 91% and 83% yield, respectively. Interestingly, when applied in a more

complicated system, sequential intermolecular 1,2-arylboration occurred between the aryl radical precursor (**3**) and alkene to afford the desired product **3a** with high selectivity.

4.3 Conclusion

In conclusion, we have developed an efficient 1,2-arylboration method for the synthesis of heterocyclic boronate esters using light as the only energy source. The developed method is advantageous as it does not require the use of transition metals or organocatalysts and provides ready access to target boronate esters via $C(sp^2)$–I activation and radical cascade cyclization. Moreover, the formation of $C(sp^2)$–$C(sp^3)$ and $C(sp^3)$–B bonds in a one-pot process contributes to both step- and atom-economy. Overall, an unprecedented catalyst-free synthesis of heterocyclic boronate esters was developed.

4.4 Experimental section

4.4.1 General experimental details

Unless otherwise noted, all reactions were performed under inert conditions. Analytical TLC was performed on a Merck 60 F254 silica gel plates (0.25mm thickness), and visualized either using UV light (254 nm) or by staining with potassium permanganate and heating. Column chromatography was performed on Merck 60 silica gel (230–400 mesh). NMR spectroscopy experiments were conducted with a Varian 400 and 500 MHz or a Bruker 300 MHz system. NMR spectra were processed with ACD NMR Processor or MestReNova. Chemical shifts are reported in ppm and referenced to residual solvent peaks ($CHCl_3$ in $CDCl_3$: 7.26 ppm for ^{1}H, 77.16 ppm for ^{13}C). ^{19}F NMR spectra were calibrated to an external standard of neat $CFCl_3$ (0.0 ppm for ^{19}F). Coupling constants are reported in Hertz. Deuterated compounds were purchased from Cambridge Isotope Laboratories, Inc. All anhydrous solvents and chemicals were purchased from commercial sources (Sigma-Aldrich, Acros, Alfa Aesar, TCI, or Strem) and used without further purification. 34 W Blue LED lamps purchased from Kessil (Kessil H150 Grow Light-Blue) were used for all the visible light photocatalytic reactions. High resolution mass spectroscopy (HRMS) analyses were performed by the ultrahigh resolution ESI Q-TOF mass spectrometer at the Mass Spectrometry Laboratory of National Instrumentation Center for Environmental Management (NICEM) in Seoul National University.

4.4.2 General procedure for the preparation of aryl iodide[16]

Synthesis of *O*-(allyloxy)-2-iodobenzene

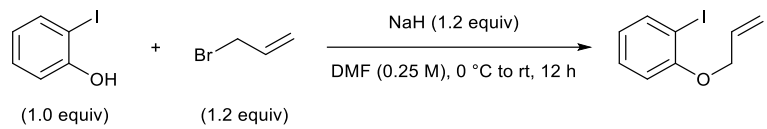

(1.0 equiv) (1.2 equiv)

To a solution of 2-iodophenol (1.0 mmol, 1.0 equiv) in DMF (3.0 mL) was slowly added NaH (60% in mineral oil, 1.2 mmol, 1.2 equiv) at 0 °C under N_2 atmosphere. The corresponding allyl bromide (1.2 mmol, 146 mg) was added dropwise and stirred at 0 °C for 20 min. After that, the resulting mixture was stirred at room temperature for 12 h. Upon completion, the reaction mixture was treated with a saturated aq. $Na_2S_2O_3$ (10 mL) and the aqueous layer was extracted with CH_2Cl_2 (20 mL, 3 times). The combined organic layer was dried over anhydrous Na_2SO_4 and concentrated to dryness. The crude mixture was purified by flash column chromatography on silica gel eluting with a mixture of EtOAc in hexanes to give the corresponding compounds.

Synthesis of *N*-allyl-*N*-(2-halophenyl)acetamides

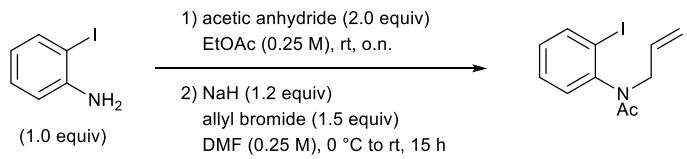

(1.0 equiv)

To a round bottom flask containing a solution of 2-iodoaniline (2.0 mmol, 1.0 equiv) in 8 mL ethyl acetate (EtOAc), acetic anhydride (4.0 mmol, 2.0 equiv) was added and the reaction mixture was stirred at room temperature overnight. The solvent was removed under reduced pressure and the crude solid was recrystallized from a

mixture of hexane and ethyl acetate to provide the *N*-(2-iodophenyl)acetamide as a white solid.

To a solution of *N*-(2-iodophenyl)acetamide (1.0 mmol, 1.0 equiv) in DMF (3.0 mL) was slowly added NaH (60% in mineral oil, 1.5 mmol, 1.5 equiv) at 0 °C under N_2 atmosphere. After vigorous evolution of hydrogen gas, the reaction mixture was treated with allyl bromide (1.5 mmol, 1.5 equiv) and warmed to room temperature. After stirring for 5 h, the reaction mixture was treated with a saturated aq. $Na_2S_2O_3$ (10 mL) and the aqueous layer was extracted with CH_2Cl_2 (20 mL, 3 times). The combined organic layer was dried over anhydrous Na_2SO_4 and concentrated to dryness. The crude mixture was purified by flash column chromatography on silica gel eluting with a mixture of EtOAc in hexanes to give the corresponding compounds.

4.4.3 General procedure for intramolecular 1,2-arylboration of unactivated alkenes

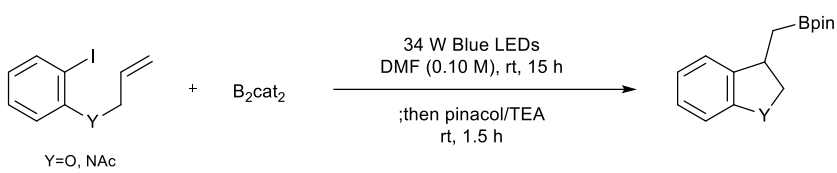

The reaction was set up in a nitrogen-filled glove box. To a 4 mL vial equipped with a PTFE-coated stirrer bar was added the corresponding aryl iodide (0.20 mmol, 1.0 equiv), B_2cat_2 (95 mg, 0.40 mmol, 2.0 equiv), and DMF (2.0 mL, 0.10 M). The reaction vial was removed from the glove box, stirred under 34 W blue LED irradiation. After 15 h, a solution of pinacol (0.40 mmol, 2.0 equiv) in triethylamine (1.0 M) was added to the mixture and stirred for an additional 1.5 h. The reaction

mixture was transferred to a separatory funnel and partitioned between water (7 mL) and Et_2O (20 mL). The organic layer was washed with water (7 mL x 3), dried over anhydrous Na_2SO_4 and concentrated to dryness. The crude mixture was purified by flash column chromatography on silica gel eluting with a mixture of EtOAc in hexanes to give the desired products.

4.4.4 General procedure for intermolecular 1,2-arylboration of unactivated alkenes

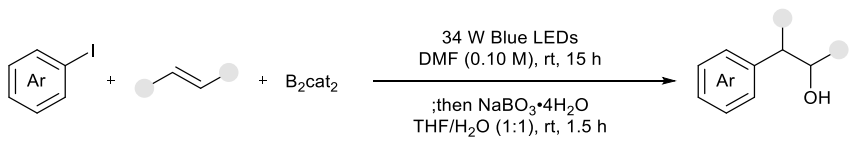

The reaction was set up in a nitrogen-filled glove box. To a 4 mL vial equipped with a PTFE-coated stirrer bar was added the corresponding aryl iodide (0.20 mmol, 1.0 equiv), alkene (2.0 mmol, 10.0 equiv), B_2cat_2 (95 mg, 0.40 mmol, 2.0 equiv), and DMF (2.0 mL, 0.10 M). The reaction vial was removed from the glove box, stirred under 34 W blue LED irradiation. After 15 h, $NaBO_3{\cdot}4H_2O$ in THF/H_2O (0.30M) was added to the mixture and stirred for an additional 1.5 h. The reaction mixture was transferred to a separatory funnel and partitioned between water (7 mL) and Et_2O (20 mL). The organic layer was washed with water (7 mL x 3), dried over anhydrous Na_2SO_4 and concentrated to dryness. The crude mixture was purified by flash column chromatography on silica gel eluting with a mixture of EtOAc in hexanes to give the desired products.

4.4.5 Characterization data of synthesized compounds

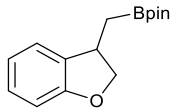

2-((2,3-Dihydrobenzofuran-3-yl)methyl)-4,4,5,5-tetramethyl-1,3,2-dioxaborolane (**1a**)

^{1}H NMR (499 MHz, $CDCl_3$) δ 7.20 (d, *J* = 7.3 Hz, 1H), 7.09 (t, *J* = 7.7 Hz, 1H), 6.84 (t, *J* = 7.4 Hz, 1H), 6.76 (d, *J* = 7.9 Hz, 1H), 4.70 (t, *J* = 8.8 Hz, 1H), 4.11 (t, *J* = 8.1 Hz, 1H), 3.71 – 3.57 (m, 1H), 1.33 (dd, *J* = 16.1, 5.8 Hz, 1H), 1.25 (d, *J* = 7.6 Hz, 12H), 1.10 (dd, *J* = 16.2, 8.8 Hz, 1H). ^{13}C NMR (126 MHz, $CDCl_3$) δ 168.71, 142.54, 136.84, 127.70, 123.73, 123.67, 116.99, 83.57, 56.98, 36.11, 25.00, 24.85, 24.31. HRMS (ESI): m/z $[M+Na]^+$ calcd for $C_{15}H_{21}BNaO_3$: 283.1476, found: 283.1479. The identity of synthesized product was confirmed based on reported NMR spectra.[17]

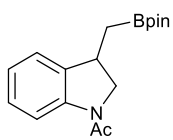

1-(3-((4,4,5,5-Tetramethyl-1,3,2-dioxaborolan-2-yl)methyl)indolin-1-yl)ethan-1-one (**2a**)

^{1}H NMR (499 MHz, $CDCl_3$) δ 8.16 (d, *J* = 7.9 Hz, 1H), 7.17 (t, *J* = 8.1 Hz, 2H), 7.01 (t, *J* = 7.4 Hz, 1H), 4.21 (t, *J* = 9.8 Hz, 1H), 3.67 (dd, *J* = 10.2, 6.6 Hz, 1H), 3.63 – 3.53 (m, 1H), 2.21 (s, 3H), 1.33 (dt, *J* = 10.8, 5.4 Hz, 1H), 1.20 (d, *J* = 6.9 Hz, 12H), 1.17 – 1.07 (m, 1H). ^{13}C NMR (126 MHz, $CDCl_3$) δ 168.71, 142.54, 136.83, 127.70, 123.73, 123.67, 116.99, 83.57, 56.98, 36.11, 25.00, 24.85, 24.32. HRMS (ESI): m/z $[M+H]^+$ calcd for $C_{17}H_{25}BNO_3$: 302.1922, found: 302.1919.

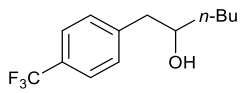

1-(4-(Trifluoromethyl)phenyl)hexan-2-ol (**3a**)

^{1}H NMR (400 MHz, $CDCl_3$) δ 7.57 (d, *J* = 7.9 Hz, 2H), 7.34 (d, *J* = 7.9 Hz, 2H), 4.02 – 3.59 (m, 1H), 2.88 (dd, *J* = 13.6, 4.0 Hz, 1H), 2.73 (dd, *J* = 13.6, 8.3 Hz, 1H), 1.58 – 1.28 (m, 7H), 0.92 (t, *J* = 6.9 Hz, 3H). ^{13}C NMR (101 MHz, $CDCl_3$) δ 143.13 (d, $^{5}J_{CF}$ = 1.2 Hz, C_q), 129.88, 128.90 (d, $^{2}J_{CF}$ = 32.4 Hz, C_q), 125.50 (q, $^{3}J_{CF}$ = 3.8 Hz), 124.43 (d, $^{1}J_{CF}$ = 271.8 Hz, C_q), 72.65, 43.90, 36.88, 28.02, 22.81, 14.20. ^{19}F NMR (376 MHz, $CDCl_3$) δ -62.85. HRMS (CI): m/z $[M–H]^+$ calcd for $C_{13}H_{16}F_3O$: 245.1148, found: 245.1154. The identity of synthesized product was confirmed based on reported NMR spectra.[18]

4.5 References

1. S. Zhi, X. Ma and W. Zhang, *Org. Biomol. Chem.*, 2019, **17**, 7632-7650.

2. (a) X. Chen, F. Xiao and W.-M. He, *Org. Chem. Front.*, 2021, **8**, 5206-5228; (b) H. Yao, W. Hu and W. Zhang, *Molecules*, 2021, **26**, 105; (c) K.-J. Bian, D. Nemoto, Jr., S.-C. Kao, Y. He, Y. Li, X.-S. Wang and J. G. West, *J. Am. Chem. Soc.*, 2022, **144**, 11810-11821.

3. (a) Y. Nakao, S. Ebata, A. Yada, T. Hiyama, M. Ikawa and S. Ogoshi, *J. Am. Chem. Soc.*, 2008, **130**, 12874-12875; (b) M. P. Watson and E. N. Jacobsen, *J. Am. Chem. Soc.*, 2008, **130**, 12594-12595; (c) H. Liu, C. Li, D. Qiu and X. Tong, *J. Am. Chem. Soc.*, 2011, **133**, 6187-6193; (d) S. G. Newman and M. Lautens, *J. Am. Chem. Soc.*, 2011, **133**, 1778-1780; (e) Y. Lan, P. Liu, S. G. Newman, M. Lautens and K. N. Houk, *Chem. Sci.*, 2012, **3**, 1987-1995; (f) D. A. Petrone, M. Lischka and M. Lautens, *Angew. Chem. Int. Ed.*, 2013, **52**, 10635-10638; (g) D. A. Petrone, H. Yoon, H. Weinstabl and M. Lautens, *Angew. Chem. Int. Ed.*, 2014, **53**, 7908-7912; (h) H. Yoon, A. D. Marchese and M. Lautens, *J. Am. Chem. Soc.*, 2018, **140**, 10950-10954; (i) T. Delcaillau, H. L. Schmitt, P. Boehm, E. Falk and B. Morandi, *ACS Catal.*, 2022, **12**, 6081-6091.

4. (a) M. Wang and Z. Shi, *Chem. Rev.*, 2020, **120**, 7348-7398; (b) Y.-M. Tian, X.-N. Guo, H. Braunschweig, U. Radius and T. B. Marder, *Chem. Rev.*, 2021, **121**, 3561-3597.

5. (a) K. M. Logan, S. R. Sardini, S. D. White and M. K. Brown, *J. Am. Chem. Soc.*, 2018, **140**, 159-162; (b) S. R. Sardini, A. L. Lambright, G. L. Trammel,

H. M. Omer, P. Liu and M. K. Brown, *J. Am. Chem. Soc.*, 2019, **141**, 9391-9400; (c) W. Wang, C. Ding, H. Pang and G. Yin, *Org. Lett.*, 2019, **21**, 3968-3971; (d) Z. Liu, Y. Gao, T. Zeng and K. M. Engle, *Isr. J. Chem.*, 2020, **60**, 219-229.

6. J. Qi, F.-L. Zhang, J.-K. Jin, Q. Zhao, B. Li, L.-X. Liu and Y.-F. Wang, *Angew. Chem. Int. Ed.*, 2020, **59**, 12876-12884.

7. Y. Cheng, C. Mück-Lichtenfeld and A. Studer, *J. Am. Chem. Soc.*, 2018, **140**, 6221-6225.

8. (a) A. S. Guram, R. A. Rennels and S. L. Buchwald, *Angew. Chem. Int. Ed.*, 1995, **34**, 1348-1350; (b) J. Zhu, B. A. Price, S. X. Zhao and P. M. Skonezny, *Tetrahedron Lett.*, 2000, **41**, 4011-4014; (c) K. Yamada, T. Kubo, H. Tokuyama and T. Fukuyama, *Synlett*, 2002, **2002**, 0231-0234.

9. (a) D.-S. Wang, Q.-A. Chen, W. Li, C.-B. Yu, Y.-G. Zhou and X. Zhang, *J. Am. Chem. Soc.*, 2010, **132**, 8909-8911; (b) A. Baeza and A. Pfaltz, *Chem. Eur. J.*, 2010, **16**, 2036-2039; (c) Z. Yang, F. Chen, Y. He, N. Yang and Q.-H. Fan, *Angew. Chem. Int. Ed.*, 2016, **55**, 13863-13866; (d) J. Wen, X. Fan, R. Tan, H.-C. Chien, Q. Zhou, L. W. Chung and X. Zhang, *Org. Lett.*, 2018, **20**, 2143-2147.

10. (a) D. Liu, G. Zhao and L. Xiang, *Eur. J. Org. Chem.*, 2010, 3975-3984; (b) T. S. Silva, M. T. Rodrigues, H. Santos, L. A. Zeoly, W. P. Almeida, R. C. Barcelos, R. C. Gomes, F. S. Fernandes and F. Coelho, *Tetrahedron*, 2019, **75**, 2063-2097.

11. (a) J. Zhang, H.-H. Wu and J. Zhang, *Eur. J. Org. Chem.*, 2013, 6263-6266;

(b) L. Zhang and L. Jiao, *J. Am. Chem. Soc.*, 2017, **139**, 607-610; (c) D. Hu, L. Wang and P. Li, *Org. Lett.*, 2017, **19**, 2770-2773; (d) L. Candish, M. Teders and F. Glorius, *J. Am. Chem. Soc.*, 2017, **139**, 7440-7443; (e) L. Zhang and L. Jiao, *Chem. Sci.*, 2018, **9**, 2711-2722; (f) L. Zhang and L. Jiao, *J. Am. Chem. Soc.*, 2019, **141**, 9124-9128; (g) Q. Liu, J. Hong, B. Sun, G. Bai, F. Li, G. Liu, Y. Yang and F. Mo, *Org. Lett.*, 2019, **21**, 6597-6602.

12. Y. Cheng, C. Mück-Lichtenfeld and A. Studer, *Angew. Chem. Int. Ed.*, 2018, **57**, 16832-16836.

13. A. N. Abeywickrema and A. L. J. Beckwith, *J. Chem. Soc., Chem. Commun.*, 1986, 464-465.

14. (a) R. L. Hudson and F. Williams, *J. Am. Chem. Soc.*, 1977, **99**, 7714-7716; (b) J. D. Hoefelmeyer and F. P. Gabbaï, *J. Am. Chem. Soc.*, 2000, **122**, 9054-9055; (c) A. Hübner, A. M. Diehl, M. Diefenbach, B. Endeward, M. Bolte, H.-W. Lerner, M. C. Holthausen and M. Wagner, *Angew. Chem. Int. Ed.*, 2014, **53**, 4832-4835.

15. T. Constantin, M. Zanini, A. Regni, N. S. Sheikh, F. Juliá and D. Leonori, *Science*, 2020, **367**, 1021-1026.

16. C. A. D. Caiuby, A. Ali, V. T. Santana, F. W. de S. Lucas, M. S. Santos, A. G. Corrêa, O. R. Nascimento, H. Jiang and M. W. Paixão, *RSC Adv.*, 2018, **8**, 12879-12886.

17. Y.-M. Tian, X.-N. Guo, I. Krummenacher, Z. Wu, J. Nitsch, H. Braunschweig, U. Radius and T. B. Marder, *J. Am. Chem. Soc.*, 2020, **142**, 18231-18242.

18. K. Donabauer, M. Maity, A. L. Berger, G. S. Huff, S. Crespi and B. König, *Chem. Sci.*, 2019, **10**, 5162-5166.

Chapter 5. Functionalization of the benzylic C(sp^3)–F bond driven by the excited state of boryl radicals*

5.1 Introduction

Organofluorine chemistry has attracted significant attention because fluorine incorporation often leads to improved properties of compounds investigated in pharmaceutical, agrochemical, and materials chemistry fields.[1] Fluorine is similar to hydrogen in size; however, its bond to carbon is the strongest of all carbon bonds due its high electronegativity.[2] Therefore, the development of C–F bond activation modes is challenging and has been recognized as a notable research objective.[3] Moreover, C–F bond functionalization leads to changes in the properties of the parent materials, allowing for new discoveries in industry.[4]

Classic approaches for cleavage of the C–F bond have been well studied, including nucleophilic aromatic substitution (S_NAr) or fluoride abstraction using a Lewis acid as an activator (Scheme 5.1A and B).[5,6] However, the above-mentioned strategies are limited by the requirement of activated and/or limited organofluorine compounds. With the recent advent of transition metal catalysis and improvements in the reaction setup, the introduction of various functional groups and expansion of the carbon skeleton has become feasible under mild conditions using simple fluorine compounds (Scheme 5.1C).[7,8] With the rapid development of this field, various

* The majority of this work contains unpublished results.

methodologies entailing C–F bond manipulation have been developed, disproving the existing prejudice that this bond is impossible to activate due to its exceptionally high bond dissociation energy.

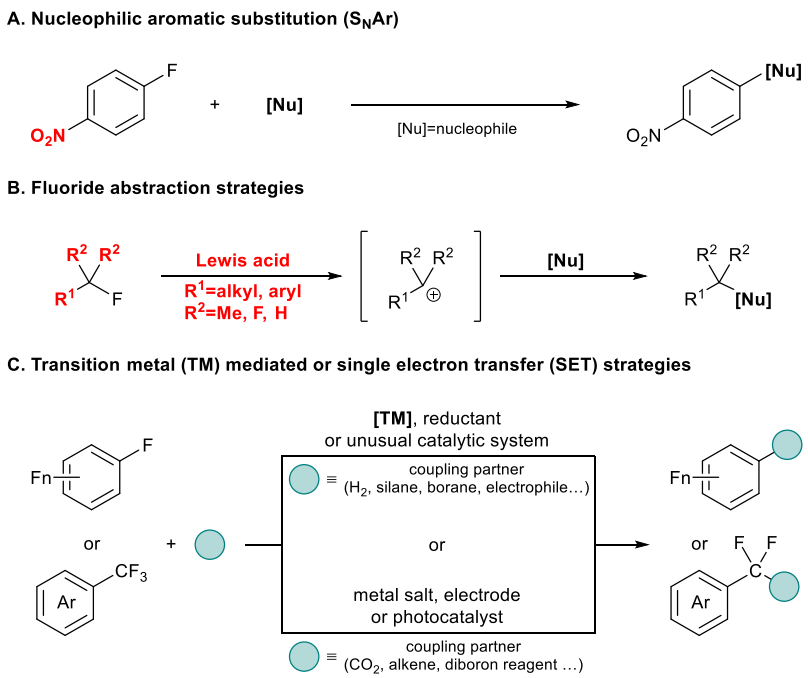

Scheme 5.1 Representative approaches for C–F bond activation in organic synthesis

Herein, we present an unprecedented C–F bond activation mode. Halogen atom transfer (XAT) is one of the most applied and significant protocols for the selective activation of carbon–halogen bonds and has been applied in numerous radical approaches.[9] The boryl radical can abstract a fluorine atom bonded to carbon, providing a thermodynamically favored equilibrium (Figure 5.1). The Lewis-base-ligated boryl radical, which is readily prepared via hydrogen atom transfer (HAT),

has been used in organic reactions and serves as a potential candidate for the boryl radical.[10] The simultaneously generated radical could be utilized as a reactive intermediate, thereby enabling subsequent functionalization.

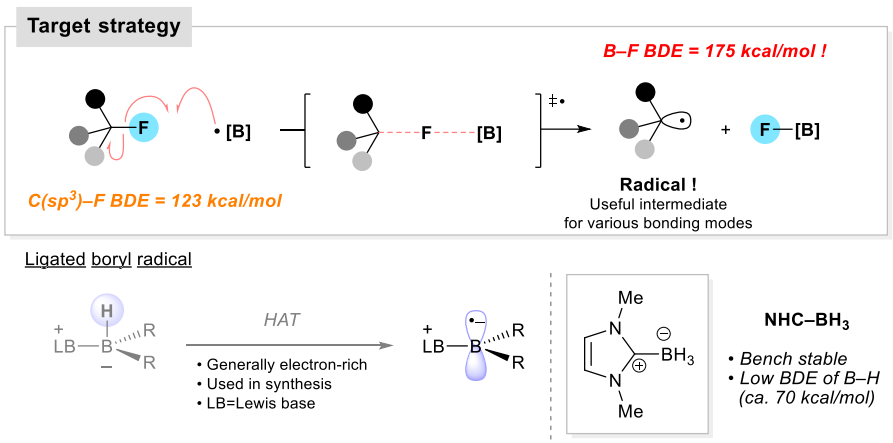

Figure 5.1 Design principle of fluorine atom transfer (FAT)

5.2 Results and discussion

5.2.1 Evaluation of reaction parameters

Table 5.1 Evaluation of reaction parameters[a]

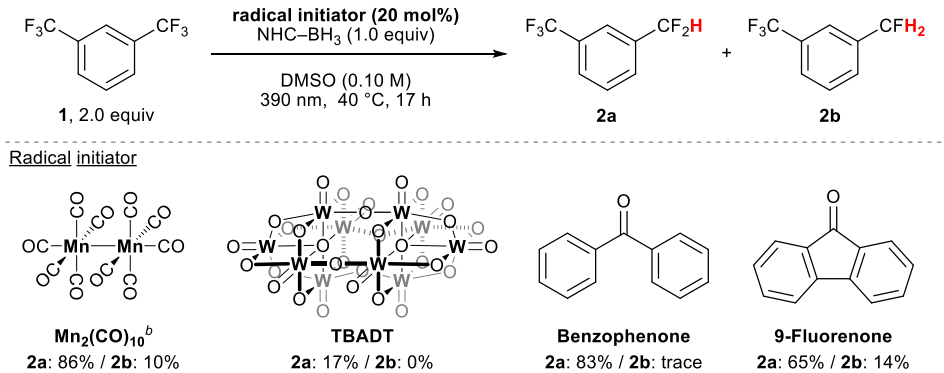

Entry	Conditions[c]	Yields (%) **2a** / **2b**
1	As shown	86 / 10
2	Wavelength of 456 nm instead of 390 nm	N.R.
3	No NHC–BH_3	N.R.
4	No $Mn_2(CO)_{10}$	2 / 0
5	Under air	2 / 0

[a] Reaction conditions: **1** (0.20 mmol), NHC–BH_3 (0.10 mmol), radical initiator (20 mol%), and DMSO (0.10 M) irradiated with 34 W blue LEDs. Yields were determined by ^{19}F NMR analysis using HFIP as an internal standard. [b] 10 mol% of the radical initiator was used. [c] 10 mol% of the Mn_2CO_{10} was used as radical initiator. DMSO = dimethyl sulfoxide. TBADT = tetra-*n*-butylammonium decatungstate. HFIP = 1,1,1,3,3,3-hexafluoro-2-propanol. N.R. = no reaction.

Initially, we explored the reactivity of NHC–BH_3 as a boryl radical precursor using 1,3-bis(trifluoromethyl)benzene (**1**) and radical initiators to promote C–F bond activation under light irradiation. To our delight, the hydrodefluorinated product (**2a**) was formed in 86% yield, along with the overreduction product **2b** in 10% yield, when manganese carbonyl ($Mn_2(CO)_{10}$) was used as the radical initiator (Table 5.1, entry 1). Furthermore, the application of commonly used visible light HAT catalysts, namely, tetra-*n*-butylammonium decatungstate (TBADT), benzophenone, and 9-fluorenone, was successful. It should be noted that the reactivity was determined by the wavelength of the light source (entry 2). Control experiments indicated that the presence of both NHC–BH_3 and the radical initiator, $Mn_2(CO)_{10}$, was crucial for a successful reaction (entries 3 and 4). For optimal results, the reaction was set up using a glove box (entry 5). Interestingly, when a silicon-based radical precursor was used instead of NHC–BH_3, the reactivity was maintained; further investigations in this area are ongoing in our research group.[11]

5.2.2 Plausible reaction mechansim

Based on our initial observation and previous literature, the proposed reaction mechanism is depicted in Figure 5.2. Light-induced radical initiation (RI) proceeded via HAT from NHC–BH_3 ($BDE_{B\text{-}H}$ = ca. 70 kcal/mol) to generate the boryl radical (**Int-1**). The corresponding radical intermediate (**Int-1**) can fully convert to the excited species (**Int-2**) in the reaction media based on our initial observation of wavelength-dependent reactivity (Table 5.1, entry 2) and the reported absorption spectra of **Int-1** at ~390 nm.[12] The excited boryl radical (**Int-2**) reacts with

trifluoromethyl arene ($ArCF_3$) leading to C–F bond cleavage to deliver the defluorinative benzylic radical, **Int-3**. Subsequent HAT from the radical initiator (RI–H) or NHC–BH_3 delivers the desired hydrodefluorination product, completing the catalytic cycle or radical propagation process.

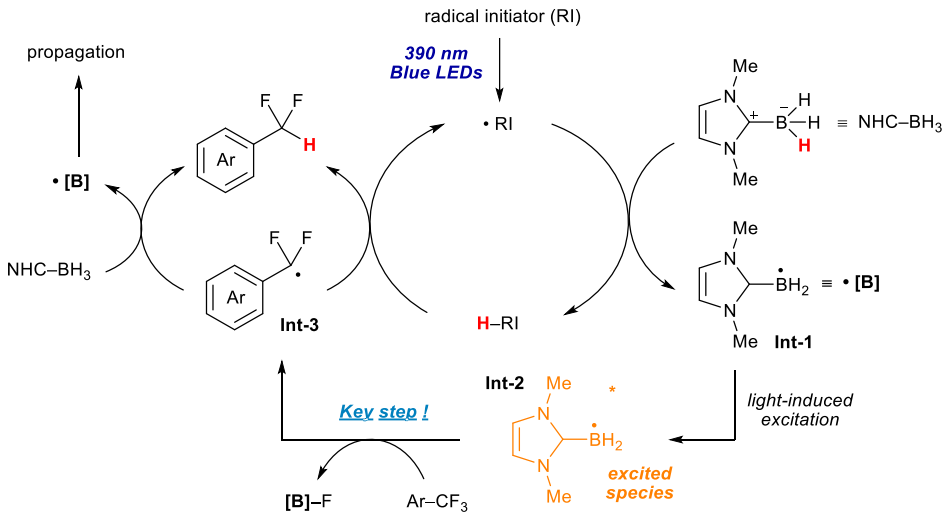

Figure 5.2 Proposed reaction mechanism of the hydrodefluorination reaction

At this point, two possible cleavage modes for the C–F bond to generate the benzylic radical intermediate (**Int-3**) were considered (Figure 5.3). In the first case, reduction of the excited boryl radical (**Int-2**) is favored due to the strong reducing character of the photoexcited radical species (path A), and a radical anion intermediate (**Int-2'**) is formed via single electron transfer ($E^0_{1/2}$ = −2.50 V vs. SCE in MeCN for trifluorotoluene). Resultant **Int-2'** could undergo mesolytic cleavage to expel the fluoride anion, delivering **Int-3**. However, in the case of path B, where

the radical reactivity of **Int-2** is dominant, C–F bond activation could occur via fluorine atom transfer (FAT).

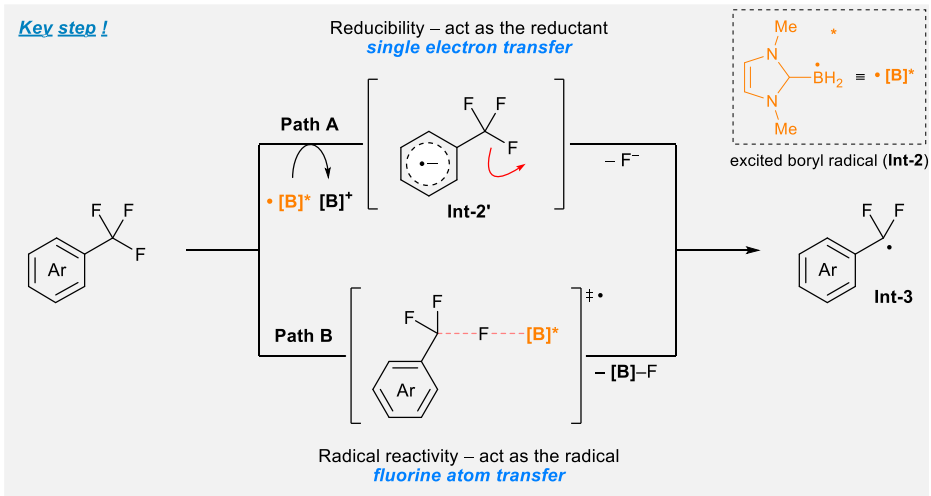

Figure 5.3 Two plausible reaction pathways by excited boryl radicals

5.2.3 Mechanistic studies

Next, we investigated the mechanistic aspects of the transformation to determine whether the reductive process (path A) could be excluded. First, to identify the radical anion intermediate (Figure 5.3, **Int-2'**) provided by the reductive process, an additional leaving group was installed at the benzylic position to observe the mesolytic cleavage (Scheme 5.2A). Under the optimized standard conditions (Table 5.1, entry 1), the prepared substrate **3** generated products wherein the pyridone was removed (**4–6**). Second, the contribution of the reducing process was examined using a redox indicator and spectroscopic analysis (Scheme 5.2B). When the optimized reaction was attempted in the presence of an electron acceptor (indigo), the hydrodefluorination efficiency was affected. Additionally, spectroscopic analysis of the reaction system following the addition of indigo indicated that a reduced form of indigo was detected ~380 nm, which is the similar absorption maximum of leuco-indigo.[13] Thus, these experimental results (Scheme 5.2A and B) were concluded that the reduction pathway is likely involved in the transformation. To gain further insight of the exact role of the excited boryl radical (**Int-2**), we used 1,1-diphenylacetylene **7** as a boryl radical acceptor,[14] which has a similar reduction potential ($E^0_{1/2}$ = −2.07 V vs. SCE in MeCN for 1,1-diphenylacetylene) to that of substrate **1** (Scheme 5.2C). As a result, only the hydrodefluorination product **2a** was obtained as a single product without any transformation of alkyne (**8** or **9**), suggesting that our methodology did not simply depend on the reduction potential. Thus, on the basis of our experimental observations, further mechanistic investigations and computational simulations to demonstrate the C–F bond cleavage step are currently underway in our group.

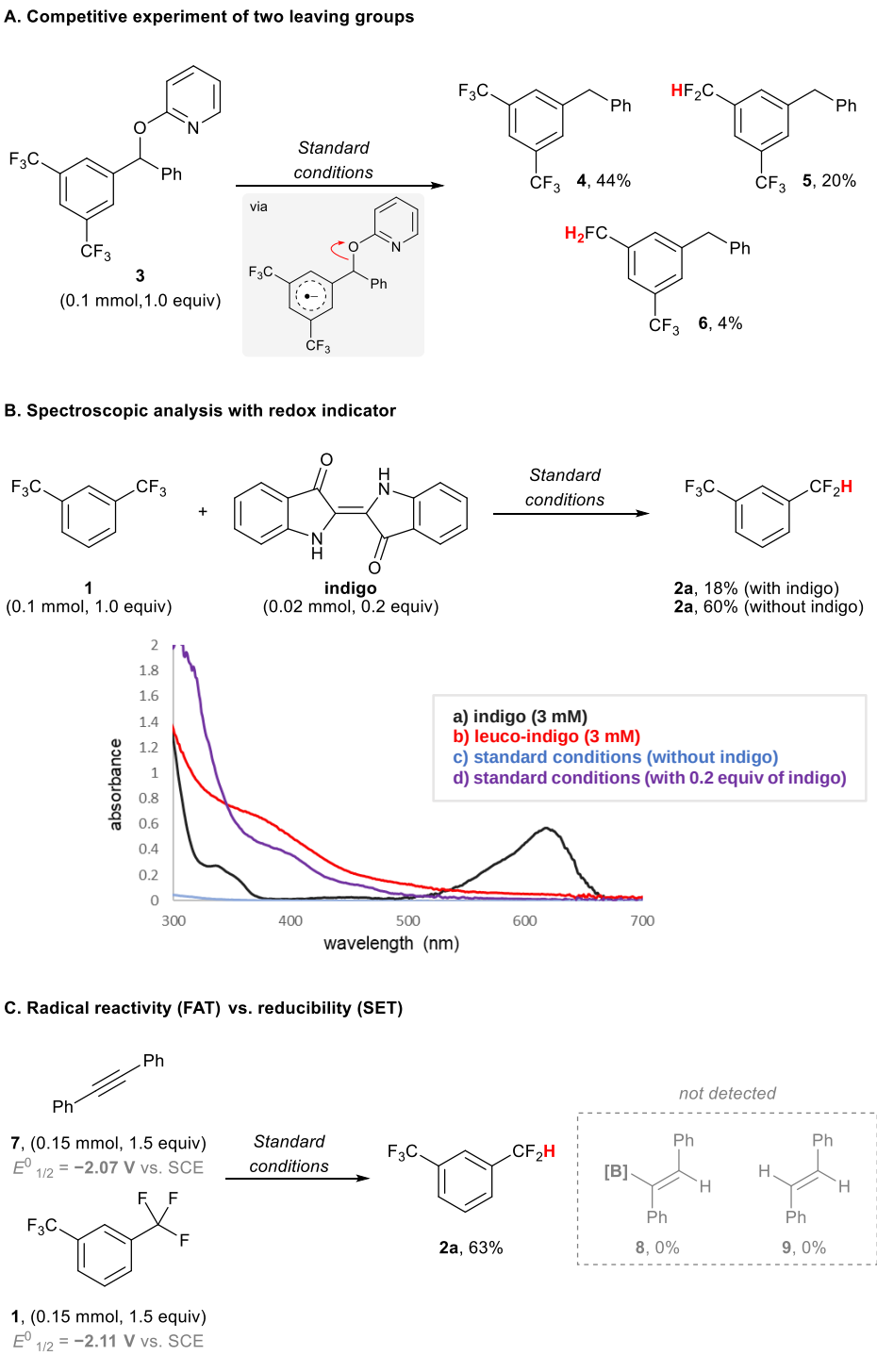

Scheme 5.2 Mechanistic studies

5.3 Experimental section

5.3.1 General experimental details

Unless otherwise noted, all reactions were performed under inert conditions. Analytical TLC was performed on a Merck 60 F254 silica gel plates (0.25mm thickness), and visualized either using UV light (254 nm) or by staining with potassium permanganate and heating. Column chromatography was performed on Merck 60 silica gel (230–400 mesh). NMR spectroscopy experiments were conducted with a Varian 400 and 500 MHz or a Bruker 300 MHz system. Gas chromatography (GC) was carried out using a GC-2030 (Shimadzu) equipped with an Rxi®-5Sil MS column and a flame ionization detector (FID). NMR spectra were processed with ACD NMR Processor or MestReNova. Chemical shifts are reported in ppm and referenced to residual solvent peaks ($CHCl_3$ in $CDCl_3$: 7.26 ppm for ^{1}H, 77.16 ppm for ^{13}C). ^{19}F NMR spectra were calibrated to an external standard of neat $CFCl_3$ (0.0 ppm for ^{19}F). Coupling constants are reported in Hertz. Deuterated compounds were purchased from Cambridge Isotope Laboratories, Inc. All anhydrous solvents and chemicals were purchased from commercial sources (Sigma-Aldrich, Acros, Alfa Aesar, TCI, or Strem) and used without further purification. 34 W Blue LED lamps purchased from Kessil (Kessil H150 Grow Light-Blue) were used for all the visible light photoreactions. UV–Vis spectra were recorded on an Agilent 8453 UV–Vis spectrophotometer with ChemStation software.

5.3.2 General procedure for hydrodefluorination reaction

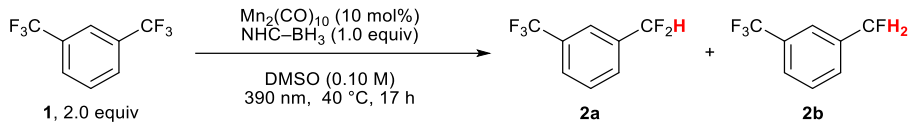

The reaction was set up in a nitrogen-filled glove box. To a 4 mL vial equipped with a PTFE-coated stirring bar was added the corresponding trifluoromethyl arene **1** (0.20 mmol, 2.0 equiv), NHC–BH_3 (0.10 mmol, 1.0 equiv), Mn_2CO_{10} (0.01 mmol, 10 mol%), and DMSO (1.0 mL). The reaction vial was removed from the glove box, stirred for 17 h under 34 W blue LED irradiation without fan cooling. At the end of the reaction, the crude residue was analyzed by ^{19}F NMR relative to 1,1,1,3,3,3-hexafluoro-2-propanol (HFIP) as an external standard.

5.3.3 Competitive experiments of two leaving groups

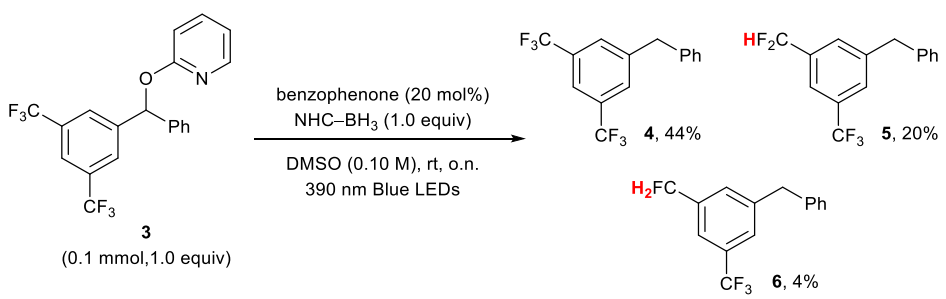

The reaction was set up in a nitrogen-filled glove box. To a 4 mL vial equipped with a PTFE-coated stirring bar was added the corresponding trifluoromethyl arene **3** (0.10 mmol, 1.0 equiv), NHC–BH_3 (0.10 mmol, 1.0 equiv), benzophenone (0.02 mmol, 20 mol%), and DMSO (1.0 mL). The reaction vial was removed from the glove box, stirred for 17 h under 34 W blue LED irradiation without fan cooling. At the end of the reaction, the resulting solution was transferred to a separatory funnel

and partitioned between water (7 mL) and Et_2O (20 mL). The organic extract was washed with water (7 mL x 2) and brine (7 mL), dried over $MgSO_4$, filtered, and concentrated under reduced pressure. The crude residue was analyzed by ^1H NMR relative to 1,1,2,2-tetrachloroethane (5.0 μL, 0.047 mmol) as an external standard to determine the existence of products **4–6** (Figure 5.4). The identity of synthesized products were confirmed based on reported NMR spectra.[15]

In GC-MS analysis, the selective ion chromatogram with peaks showing molecular weight values of products **4–6** (Figure 5.5). The elution peak at 14.796 min was determined to be product **4** with molecular weight values of 304. The elution peak at 16.676 min was determined to be product **5** with molecular weight values of 286. The elution peak at 17.665 min was determined to be product **6** with molecular weight values of 268.

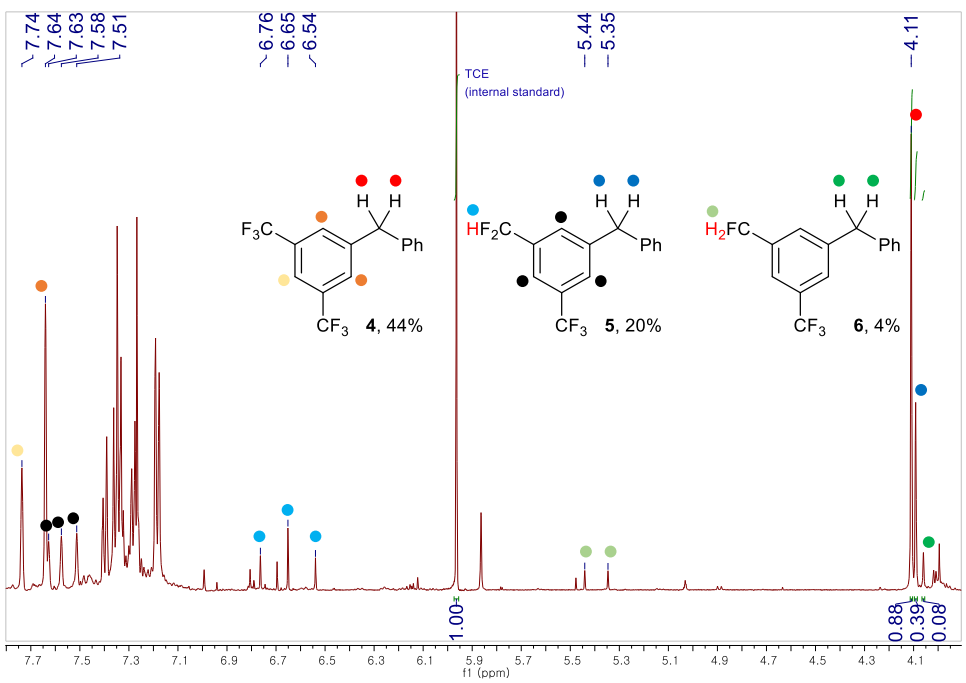

Figure 5.4 ^1H-NMR spectrum of the reaction mixture

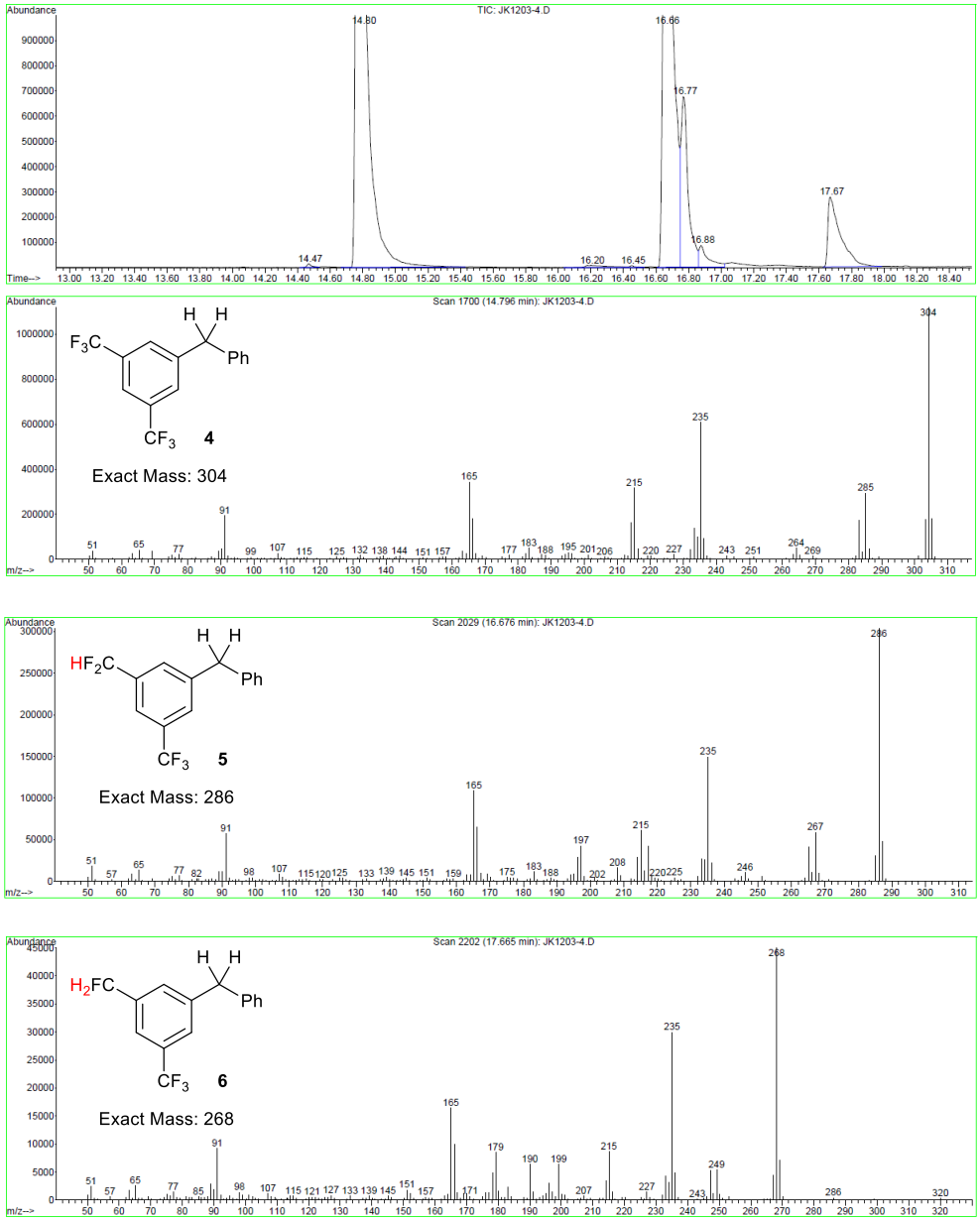

Figure 5.5 GC-MS spectrum of the reaction mixture

5.3.4 Characterization data of synthesized compounds

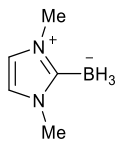

(1,3-Dimethyl-1H-imidazol-3-ium-2-yl)trihydroborate (**NHC–BH_3**)

It was synthesized by a previously reported procedure and the identity of the synthesized product was confirmed based on the reported NMR spectra.[16]

^{1}H NMR (400 MHz, $CDCl_3$) δ 6.79 (s, 2H), 3.73 (s, 6H), 1.01 (dd, *J* = 173.0, 86.0 Hz, 3H).

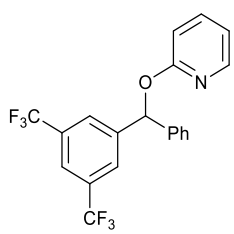

2-((3,5-Bis(trifluoromethyl)phenyl)(phenyl)methoxy)pyridine (**3**)

It was synthesized by a previously reported procedure and the identity of the synthesized product was confirmed based on the reported NMR spectra.[17]

^{1}H NMR (400 MHz, $CDCl_3$) δ 8.09 (dd, *J* = 4.3, 0.7 Hz, 1H), 7.90 (s, 2H), 7.76 (s, 1H), 7.61 (td, *J* = 8.3, 1.9 Hz, 1H), 7.43 (d, *J* = 7.7 Hz, 2H), 7.37 (dd, *J* = 8.8, 5.8 Hz, 3H), 7.31 (t, *J* = 7.2 Hz, 1H), 6.95 – 6.84 (m, 2H).

5.4 References

1. (a) H. Amii and K. Uneyama, *Chem. Rev.*, 2009, **109**, 2119-2183; (b) R. Britton, V. Gouverneur, J.-H. Lin, M. Meanwell, C. Ni, G. Pupo, J.-C. Xiao and J. Hu, *Nat. Rev. Methods Primers*, 2021, **1**, 47.

2. S. J. Blanksby and G. B. Ellison, *Acc. Chem. Res.*, 2003, **36**, 255-263.

3. J. L. Kiplinger, T. G. Richmond and C. E. Osterberg, *Chem. Rev.*, 1994, **94**, 373-431.

4. D. O'Hagan, *Chem. Soc. Rev.*, 2008, **37**, 308-319.

5. H.-G. Schmalz, O. Kiehl and B. Gotov, *Synlett*, 2002, **2002**, 1253-1256.

6. (a) K. Hirano, K. Fujita, H. Yorimitsu, H. Shinokubo and K. Oshima, *Tetrahedron Lett.*, 2004, **45**, 2555-2557; (b) P. A. Champagne, J. Pomarole, M.-È. Thérien, Y. Benhassine, S. Beaulieu, C. Y. Legault and J.-F. Paquin, *Org. Lett.*, 2013, **15**, 2210-2213.

7. (a) W. Huang and P. L. Diaconescu, *Organometallics*, 2017, **36**, 89-96; (b) H. Iwamoto, H. Imiya, M. Ohashi and S. Ogoshi, *J. Am. Chem. Soc.*, 2020, **142**, 19360-19367.

8. (a) Y. Yamauchi, T. Fukuhara, S. Hara and H. Senboku, *Synlett*, 2008, **2008**, 438-442; (b) S. B. Lang, R. J. Wiles, C. B. Kelly and G. A. Molander, *Angew. Chem. Int. Ed.*, 2017, **56**, 15073-15077; (c) S. Priya and J. D. Weaver, III, *J. Am. Chem. Soc.*, 2018, **140**, 16020-16025; (d) L. Zhang and L. Jiao, *J. Am. Chem. Soc.*, 2019, **141**, 9124-9128; (e) D. B. Vogt, C. P. Seath, H. Wang and N. T. Jui, *J. Am. Chem. Soc.*, 2019, **141**, 13203-13211; (f) Z. Wang, Y. Sun,

L.-Y. Shen, W.-C. Yang, F. Meng and P. Li, *Org. Chem. Front.*, 2022, **9**, 853-873.

9. F. Juliá, T. Constantin and D. Leonori, *Chem. Rev.*, 2022, **122**, 2292-2352.

10. (a) T. Taniguchi, *Eur. J. Org. Chem.*, 2019, 6308-6319; (b) T. Taniguchi, *Chem. Soc. Rev.*, 2021, **50**, 8995-9021.

11. In the developed method, both NHC–BH_3, a boryl radical precursor, as well as 1-hydrosilatrane, a silicon-centered radical precursor, provided the hydrodefluorination products. To understand this phenomenon, further mechanistic investigations are ongoing in our laboratory.

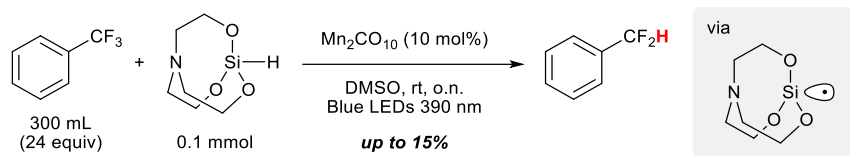

12. M.-A. Tehfe, J. Monot, M. M. Brahmi, H. Bonin-Dubarle, D. P. Curran, M. Malacria, L. Fensterbank, E. Lacôte, J. Lalevée and J.-P. Fouassier, *Polym. Chem.*, 2011, **2**, 625-631.

13. J. Wang, L. Lu and F. Feng, *Catalysts*, 2017, **7**, 275.

14. M. Shimoi, T. Watanabe, K. Maeda, D. P. Curran and T. Taniguchi, *Angew. Chem. Int. Ed.*, 2018, **57**, 9485-9490.

15. S. B. Munoz, C. Ni, Z. Zhang, F. Wang, N. Shao, T. Mathew, G. A. Olah and G. K. S. Prakash, *Eur. J. Org. Chem.*, 2017, 2322-2326.

16. M. M. Brahmi, J. Monot, M. Desage-El Murr, D. P. Curran, L. Fensterbank,

E. Lacôte and M. Malacria, *J. Org. Chem.*, 2010, **75**, 6983-6985.

17. J. Yang and G. B. Dudley, *J. Org. Chem.*, 2009, **74**, 7998-8000.

국문초록

탄소–수소 및 탄소–할로겐 결합 기능화에 기반한 새로운 합성 방법론의 개발

구장우

서울대학교 자연과학대학 화학부

화학적 다양성의 확장은 합성 유기 화학 분야에서 가장 깊게 생각해봐야 하는 주제 중 하나입니다. 라디칼을 활용하는 화학 반응은 앞선 논제에 핵심 해결책을 제공할 수 있습니다. 하지만 라디칼은 구조적으로 불안정한 화합물이기에, 가혹한 조건에서 만들어졌으며 통제하기 어려운 반응성을 가지고 있었습니다. 현대 유기 화학의 발전에 따라, 수많은 연구진은 온화한 조건에서 해당 화학종을 만들고자 하였으며 선택적이고 통제 가능한 반응 설계를 위해 오랜 시간 연구해왔습니다. 더불어 다양한 장비와 도구의 도입으로 새로운 반응 시스템을 확립하고자 하였습니다. 1장에서는 지난 십여 년 동안 탄소 중심 라디칼을 형성하는 대표적인 전략들과 이를 활용하여 새로운 화학 결합을 형성하는 방법을

소개합니다. 특히 탄소-수소(1부), 탄소-할로겐(2부) 결합의 활성화로 형성되는 라디칼에 대해 중점적으로 설명합니다.

1부에서는 탄소-수소 결합의 기능화를 중점적으로 다룹니다. 그 예시로 2장에서는, 광촉매와 니켈 촉매의 이중 촉매 전략을 활용하여 인돌의 벤질 자리 탄소-수소 결합 활성화를 소개합니다. 인돌의 산화되기 쉬운 성질에 착안하여, 순차적인 산화/탈 양성자화 과정을 거쳐 가장 산도가 낮은 벤질 자리의 수소를 활성화하게 됩니다. 다양한 아릴 및 아실 그룹은 니켈 촉매의 교차 짝지음 반응을 통해 도입되었습니다. 그뿐만 아니라 복잡한 기능성 기를 가지고 있는 생리활성 분자에도 개발된 반응을 적용할 수 있었습니다. 반응 기작 실험을 통해 라디칼 형성의 초기 단계를 밝힐 수 있었으며, 이는 분자 내에 유사한 결합 해리 에너지를 갖는 탄소-수소 결합 중 벤질 자리만 선택성이 높은 이유를 뒷받침합니다.

2부에서는 탄소-할로겐 결합 기능화를 중점적으로 다룹니다. 빛 에너지에 의해 요오드화 알킬(3장) 또는 요오드화 아릴(4장)으로부터 만들어지는 탄소 라디칼은 라디칼 보릴화 과정을 거쳐 새로운 탄소-붕소 결합을 형성합니다. 3장과 4장에서 형성된 생성물은 붕소기의 독특한 성질로 인해 약학적 활성을 갖게 됩니다. 개발된 반응은 금속촉매나 외부첨가제가 필요하지 않기 때문에 친환경적이고 원자 경제적인 반응이라고 할 수 있습니다. 개발된 반응의 핵심은 다양한 화학물질이 차례대로 반응하여서 한 용기 내에서 원하는 생성물을 제공한다는

것입니다. 또한, 5장에서는 예비 결과와 함께 라디칼 기반의 탄소–불소 결합 활성화를 간략하게 소개합니다. 반응 메커니즘 연구가 현재 연구실에서 진행 중이며, 탄소–불소 결합 절단 단계의 정확한 과정을 밝히고 발견한 반응성을 다양한 기질에 적용하고자 합니다.

주요어: 탄소, 수소, 할로겐, 라디칼, 광화학, 인돌, 아지리딘, 아미노붕소산, 헤테로 고리 화합물, 교차 짝지음 반응, 붕소화 반응, 탈수소불소화 반응, 불소 원자 이동

학번: 2017-21595